Type Synthesis and Static Balancing of a Class of Deployable Mechanisms

Jieyu Wang

Submitted for the degree of Doctor of Philosophy

Heriot-Watt University
Engineering and Physical Sciences

February 2019

ABSTRACT

This thesis addresses the type synthesis and static balancing of a class of deployable mechanisms, which can be applied in applications in many areas including aerospace and daily life.

Novel construction methods are proposed to obtain the deployable mechanisms. First, the type synthesis of the foldable 8-revolute joint (R) linkages with multiple modes is presented. Two types of linkages are constructed by connecting planar 4R linkages and spherical 4R linkages. The obtained linkages can be folded into two layers or four layers, and have multiple motion modes. A spatial triad is also adopted to build single-loop linkages, then the single-loop linkages are connected using spherical (S) joints or RRR chains to obtain deployable polyhedral mechanisms (DPMs). The DPMs have only 1-degree-of-freedom (DOF) when deployed, and several mechanisms with 8R linkages and 10R linkages have multiple motion modes and can switch modes through transition positions. In addition, when connecting single-loop linkages using half the number of the RRR chains, the prism mechanisms obtain an additional 1-DOF rotation mode.

Furthermore, the DPMs are developed into statically balanced mechanisms. The geometric static balancing approaches for the planar 4R parallelogram linkages, planar manipulators, spherical manipulators and spatial manipulators are developed so that the mechanisms can counter gravity while maintaining the positions of the mechanisms. Only springs are used to design the statically balanced system readily, with almost no calculation. A novel numerical optimization approach is also introduced which adopts the sum of squared differences of the potential energies as the objective function. Using the proposed static balancing approaches, the 8R linkages and the DPMs presented in this thesis can be statically balanced.

ACKNOWLEDGEMENTS

I really appreciate the support and help from my supervisor, Dr. Xianwen Kong. The results of my research rely on his inspirations and guidance. Apart from the knowledge, the most important thing I learned from him is the attitudes toward research and life.

Many thanks to my second supervisor, Dr Matthew W Dunnigan at Heriot-Watt University, who helped to revise my papers and thesis. I am also grateful to my colleagues, Dr. Ross Walker and Dr. Guochao Bai, who offered me numerous help in the process of my study. The visiting scholars from China, Prof. Jinjun Yu from Beihang University and Dr. Ziming Chen from Yanshan University also gave me lots of suggestions for my research.

Great appreciation goes to all my friends and the staffs in our institute, for their care and help.

Finally, I would like to give my best thanks to my parents. With their love and support, I can focus on my research and complete my PhD study.

ACADEMIC REGISTRY
Research Thesis Submission

Name*:*	Jieyu Wang		
School:	School of Engineering and Physical Sciences		
Version: *(i.e. First, Resubmission, Final)*	Final version	Degree Sought:	PhD in Mechanical Engineering

Declaration

In accordance with the appropriate regulations I hereby submit my thesis and I declare that:

1) the thesis embodies the results of my own work and has been composed by myself
2) where appropriate, I have made acknowledgement of the work of others and have made reference to work carried out in collaboration with other persons
3) the thesis is the correct version of the thesis for submission and is the same version as any electronic versions submitted*.
4) my thesis for the award referred to, deposited in the Heriot-Watt University Library, should be made available for loan or photocopying and be available via the Institutional Repository, subject to such conditions as the Librarian may require
5) I understand that as a student of the University I am required to abide by the Regulations of the University and to conform to its discipline.
6) I confirm that the thesis has been verified against plagiarism via an approved plagiarism detection application e.g. Turnitin.

* *Please note that it is the responsibility of the candidate to ensure that the correct version of the thesis is submitted.*

Signature of Candidate*:*	Jieyu Wang	Date:	

Submission

Submitted By *(name in capitals):*	
Signature of Individual Submitting:	
Date Submitted:	

For Completion in the Student Service Centre (SSC)

Received in the SSC by *(name in capitals):*			
Method of Submission *(Handed in to SSC; posted through internal/external mail):*			
E-thesis Submitted (mandatory for final theses)			
Signature:		Date:	

TABLE OF CONTENTS

LIST OF ABBREVIATIONS

Revolute joint: R joint

Universal joint: U joint

Spherical joint: S joint

Centre of mass: CM

Degree-of-freedom: DOF

Devavit-Hartenbergh: D-H

Parallel mechanism: PM

Deployable polyhedral mechanism: DPM

Remote centre of motion: RCM

LIST OF PUBLICATIONS

1. Wang, J. and Kong, X., 2019. A novel method for constructing multi-mode deployable polyhedron mechanisms using symmetric spatial compositional units. Journal of Mechanisms and Robotics, DOI: 10.1115/1.4042458.

2. Wang, J. and Kong, X., 2018. Deployable polyhedron mechanisms constructed by connecting spatial single-loop linkages of different types and/or in different sizes using S joints. Mechanism and Machine Theory, 124, pp.211-225.

3. Wang, J. and Kong, X., 2018. Deployable mechanisms constructed by connecting orthogonal Bricard linkages, 8R or 10R single-loop linkages using S joints. Mechanism and Machine Theory, 120, pp.178-191.

4. Wang, J. and Kong, X., A novel method for constructing multi-mode deployable polyhedron mechanisms using symmetric spatial RRR compositional units. Aug, 2018. ASME, International Design Engineering Technical Conference and Computers and Information in Engineering, DETC2018-85100.

5. Kong, X. and Wang, J., Reconfiguration analysis of a variable degrees-of-freedom multi-mode parallel manipulator. Jun, 2018. 4th IEEE/IFToMM International conference on Reconfigurable Mechanisms and Robots.

6. Chen, Z., Wei, X., Yang, Z., Zhao, C. and Wang, J., A 2-Dof deployable planar mechanism with continuous rotation characteristics. Jun, 2018. 4th IEEE/IFToMM International conference on Reconfigurable Mechanisms and Robots.

7. Wang, J., Yao, Y. and Kong, X., 2018. A reconfigurable tri-prism mobile robot with eight modes. Robotica, 36(10), pp.1454-1476.

8. Wang, J., Bai, G. and Kong, X., 2017. Single-loop foldable 8R mechanisms with multiple modes. In New Trends in Mechanism and Machine Science (pp. 503-510). Springer International Publishing.

9. Miao, Z., Wang, J. and Li, B., 2017. Mobile robot with multiple modes based on 4-URU parallel mechanism. In New Trends in Mechanism and Machine Science (pp. 399-407). Springer International Publishing.

10. Bai, G., Wang, J. and Kong, X., 2016. A Two-fingered anthropomorphic robotic hand with contact-aided cross four-bar mechanisms as finger joints. In Conference on Biomimetic and Biohybrid Systems (pp. 28-39). Springer International Publishing.

CHAPTER 1 – INTRODUCTION

Robotics is one of the key technologies being adopted worldwide. There is an increasing need for robots from food industries to the manufacturing sector. Mechanism design is an old subject and is still one of the most important aspects of robotics. With the development of advanced technologies, people pay less attention to it. However, mechanism design is indispensable to the industry. The developments of a number of technologies depend on the development of mechanical design which provides the essential machines.

Manipulators belong to mechanisms. Manipulators are composed of moving links and joints, and can be classified into serial manipulators and parallel mechanisms (PMs). Serial manipulators are composed of a series of links connected by joints and have simple structures and large workspaces, while PMs are consisted of two platforms and several limbs and have better stiffness, dynamic performances and can carry heavy loads. Two examples of serial manipulator and PM are respectively presented in Fig. 1.1. Serial manipulators are widely used in industry, for example, for painting, welding and assembly. PMs can be applied to flight simulators [1].

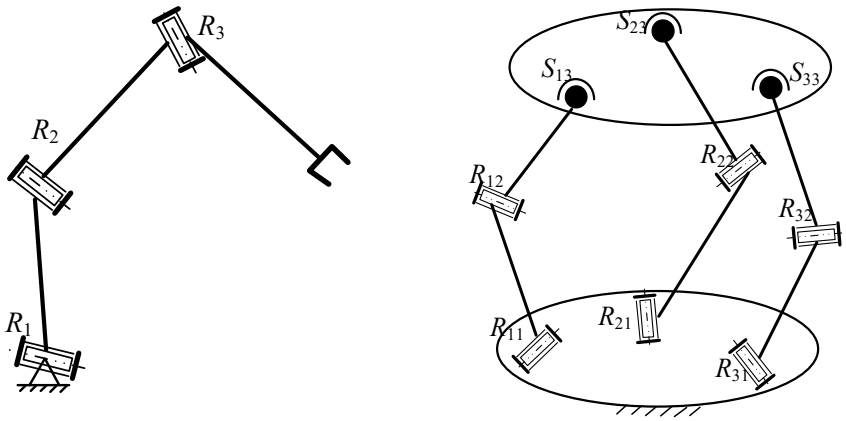

Fig. 1.1 Two types of manipulators: (a) serial manipulator; (b) PM.

The single-loop linkage is a special case of PM. In this thesis, only the loops with even numbers of links (which have symmetric structures) comprised of revolute (R) joints are discussed. 4R linkages include planar 4R linkage [Fig. 1.2(a)], spherical 4R linkage [Fig. 1.2(b)] and Bennett 4R linkage [Fig. 1.2(c)]. The axes of the R joints of the planar 4R linkage are parallel, and those of the spherical linkage intersect at a point. In the Bennett 4R linkage, the axes of the R joints are neither parallel nor intersected at a point. The

joints are designed in a particular way that makes this over-constrained linkage movable [2-3]. The Bennett 4R linkage is an important compositional mechanism, many linkages are based on Bennett 4R linkages, such as the Myard 5R linkage [4], Goldberg 5R linkage [5] and 7R linkages [6].

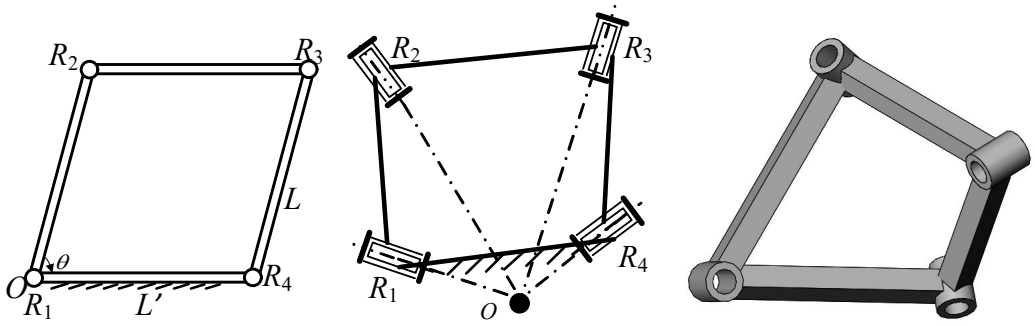

(a) (b) (c)

Fig. 1.2 4R linkages: (a) planar 4R linkage; (b) spherical 4R linkage; (c) Bennett 4R linkage.

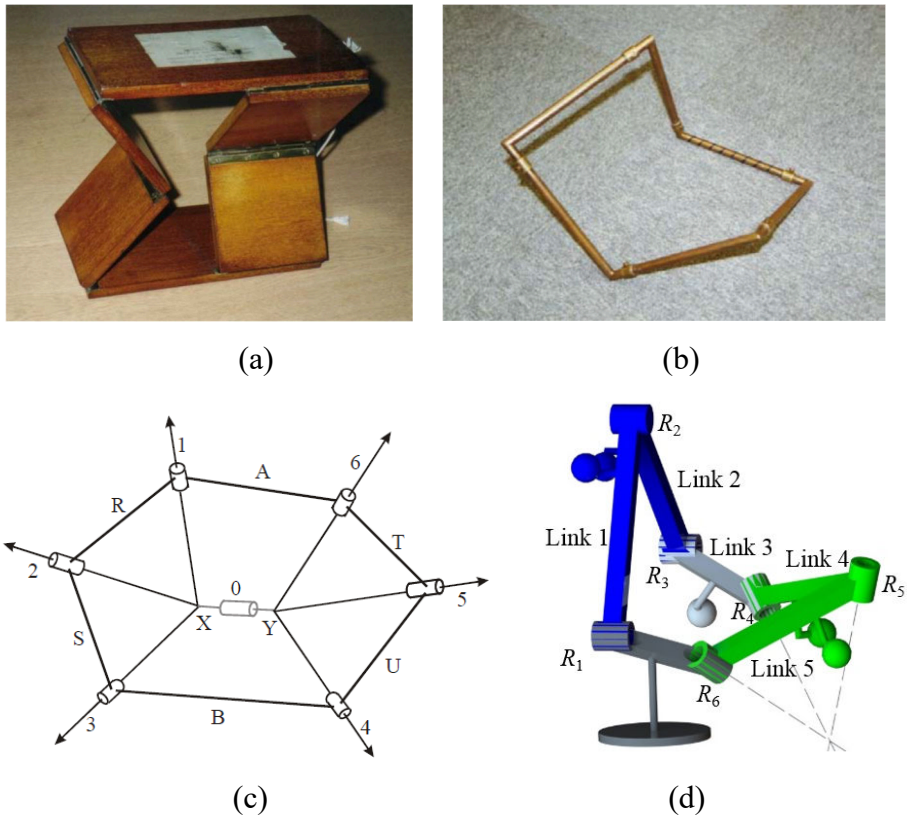

(a) (b) (c) (d)

Fig. 1.3 6R linkages: (a) Sarrus 6R linkage [7]; (b) Bricard 6R linkage [8]; (c) Bennett 6R hybrid linkage [10]; (d) Bennett plano-spherical hybrid linkage.

The first over-constrained 6R linkage is the Sarrus 6R linkage proposed by Sarrus [7], as shown in Fig. 1.3(a). The two platforms are always parallel and the three joint axes of

each limb are also parallel. Then the Bricard 6R linkage [Fig. 1.3(b)] was designed [8]. There are six types of Bricard linkages, categorized by the directions of the R joints, such as the line-symmetric Bricard linkage and the plane-symmetric Bricard linkage [9]. The Bennett 6R hybrid linkage in Fig. 1.3(c) was proposed by Bennett [10]. It is comprised of two spherical 4R linkages. The joints axes 1, 2 and 3 intersect at a point and the joint axes 4, 5 and 6 intersect at another point. The Bennett plano-spherical hybrid linkage, as shown in [Fig. 1.3(d)], has three joints with parallel axes and another three joints with intersecting axes. The other 6R linkages can be found in [11]. The 4R linkages and 6R linkages mentioned above all have single degree-of-freedom (DOF).

1.1 Foldable or Deployable Mechanisms

The foldable or deployable mechanisms refer to the mechanisms that can change their sizes or shapes to facilitate transportation and storage. Due to their characteristics, they are widely used in aerospace and daily life. Foldable mechanisms and deployable mechanisms sometimes intersect.

Foldable mechanisms are evolved from origami, by regarding the ceases as revolute joints and the panels as links. There are various methods that have been proposed for the structure of which the thickness of the panels cannot be neglected. Generally, we can offset the panels to facilitate folding. The foldable mechanisms are widely used on solar panels and roofs.

Chen et al. [12-13] developed a 1-DOF foldable mechanism base on the Bricard linkage. The mechanism can be spread onto a plane and be folded into a bundle (Fig. 1.4). In [14], another foldable 6R linkage was presented. It is a two-fold symmetric mechanism, and the axes of the joints intersect at two points, as shown in Fig. 1.5. Like the mechanism in [13], it can be spread onto a plane and be folded into a bundle.

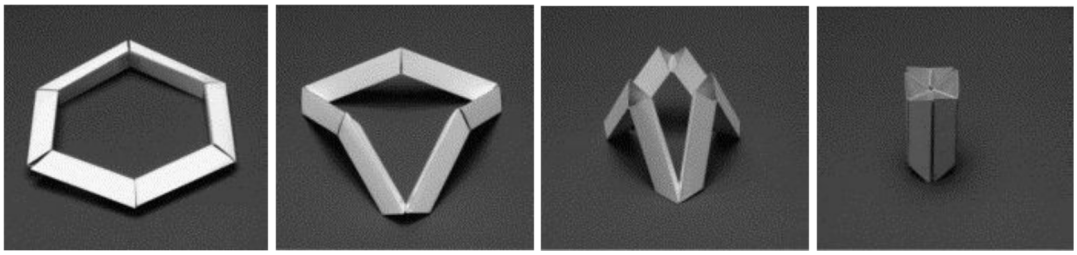

Fig. 1.4 Threefold-symmetric Bricard linkage [13]

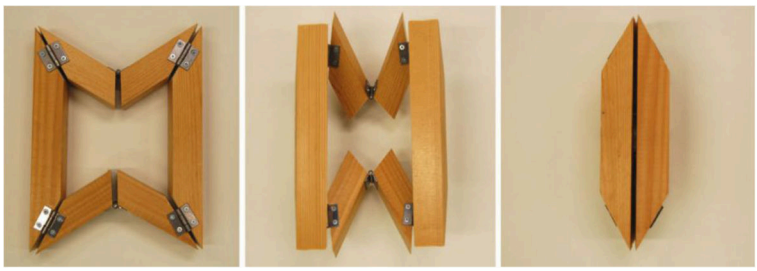

Fig. 1.5 Twofold-symmetric Bricard linkage [14]

Chen and You [15] also investigated a deployable mechanism consisted of four 6R linkages, as shown in Fig. 1.6. The mechanism can be spread onto a plane and be deployed into one dimension.

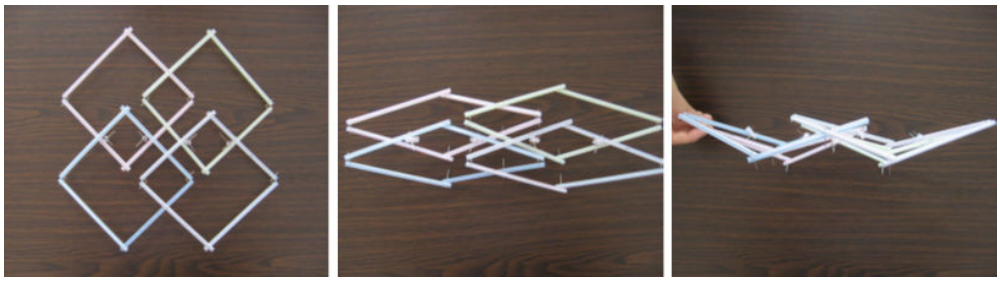

Fig. 1.6 Deployable mechanism consisted of four 6R linkages [15]

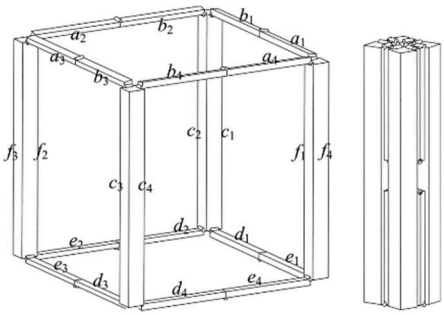

Fig. 1.7 Deployable cube mechanism based on 8R linkages [17]

Deng et al. [16] discussed a series of foldable single-loop linkages such as 4R, 5R, 6R, 7R and 8R linkages. The linkages can be spread onto a plane and be folded into a bundle. A deployable cube mechanism based on 8R linkages was introduced in [17], as shown in Fig. 1.7.

Li et al. [18] fabricated a deployable ring mechanism composed of many deployable modules. The mechanism is driven by torsion springs and controlled by cables. It has a high folding ratio, as shown in Fig. 1.8. Another deployable antenna was presented in [19]. Qi et al. [20] designed a novel double-layer truss deployable mechanism, which can be folded into a bundle or spread onto a large volume, as shown in Fig. 1.9. The DOFs of

the large-ratio mechanisms are all one. Single-layer deployable mechanisms that can be folded were also introduced in [21]. They are constructed by Myard linkages and have 1-DOF as well. Deployable mechanisms based on Bricard linkages were constructed in [22-23]. A family of deployable mechanisms was also presented in [24].

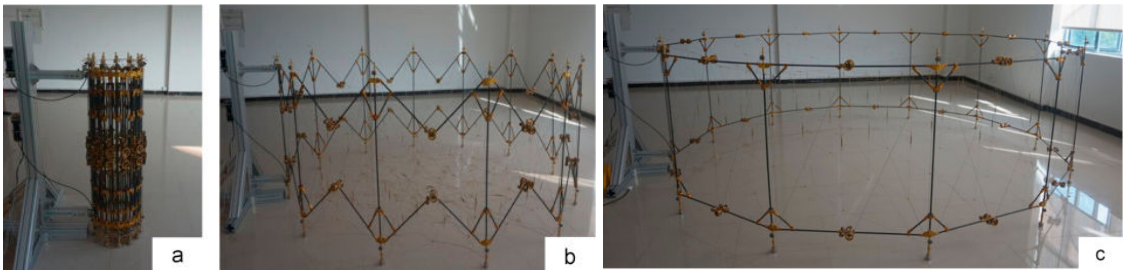

Fig. 1.8 Deployable ring mechanism in [18]

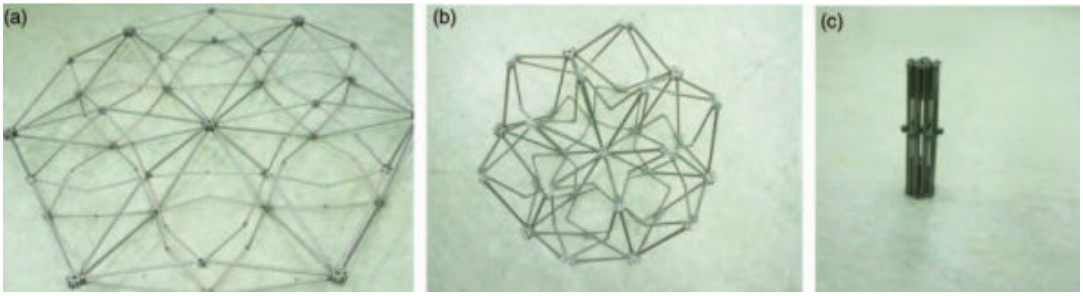

Fig. 1.9 The double-layer deployable mechanism in [20]

Lu et al. [25] proposed a family of deployable prism mechanisms, which can be folded and stretched in a single dimension, as shown in Fig. 1.10. The 1-DOF mechanisms with similar folding characteristics were also discussed in [26-27]. Lu et al. [28] also connected a 2-DOF deployable mechanism which can be deployed in two directions independently, as shown in Fig. 1.11. The mechanism is obtained by combining the units that are assembled by scissor linkages and Sarrus linkages.

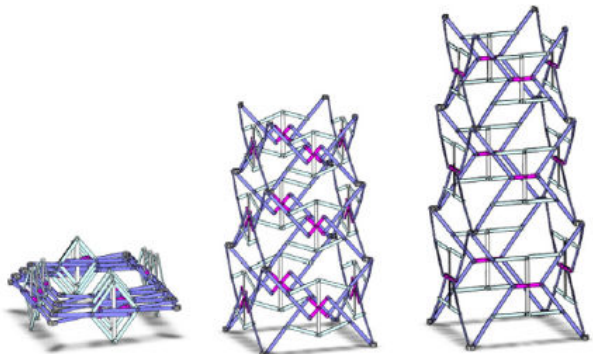

Fig. 1.10. 1-DOF deployable prism mechanism in [25]

Fig. 1.11 2-DOF deployable mechanism in [28]

A novel class of rigid-panel deployable antennas was introduced in [29], as shown in Fig. 1.12. The antenna surface is divided into several panels which are connected by R joints. The mechanism can be folded and spread around the centre line of the mechanism.

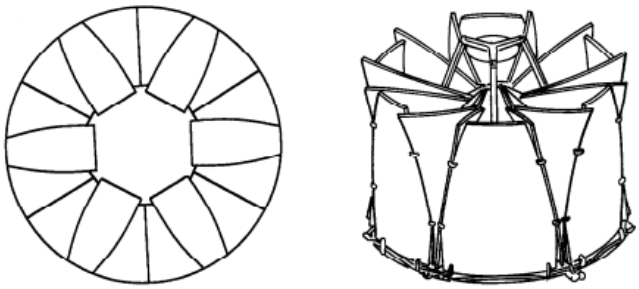

Fig. 1.12 Rigid-panel deployable antennas in [29]

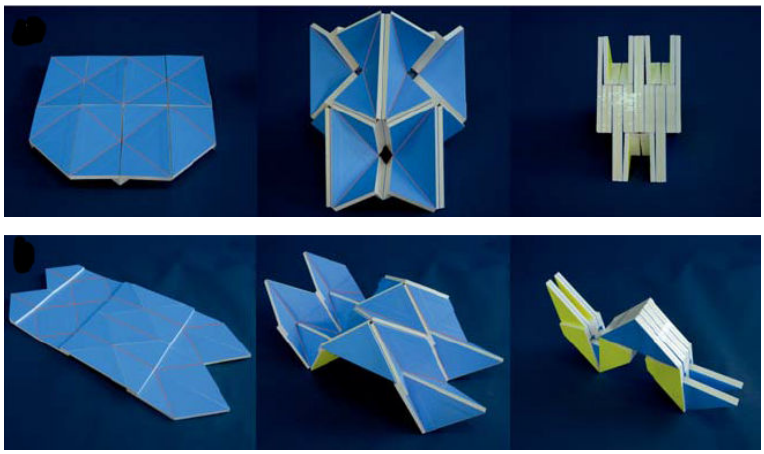

Fig. 1.13 Foldable mechanisms with thick panels in [30]

In [30], the folding process of mechanisms with thick panels was presented, as shown in Fig. 1.13. The method of offsetting panels away from the plane that is defined by two joints on the panels was used. The mechanisms are spread onto a plane in the initial state and can be folded into several layers.

Hoberman [31] designed the foldable panels comprised of four, six or nine links, by offsetting the axes of the hinges. A panel with nine links is shown in Fig. 1.14, the panel can be spread onto a plane and folded into a compact cuboid.

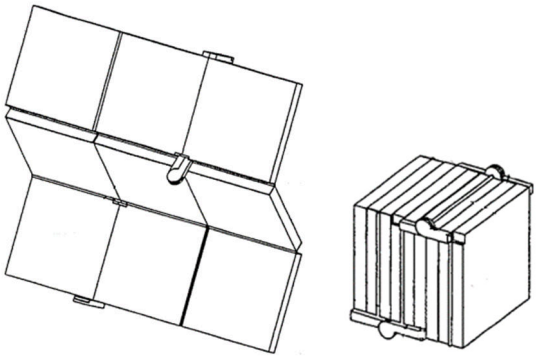

Fig. 1.14 Foldable panel made of thick panels in [31]

Fig. 1.15 Foldable habitat in [32]

An approach for accommodating for the thickness of the panels was also investigated in [32]. A foldable habitat was integrated, of which the folding ratio between the stowed and deployed configurations is 85% (Fig. 1.15).

Kang and Yi [33] provided the design and analysis of two new foldable mechanisms without parasitic motion. The two mechanisms can be folded to save space, as shown in Fig. 1.16. They can be applied to flat panel TV mounting.

A 6-DOF foldable PM for the ship-based stabilized platform, which is driven by four-bar linkages was designed in [34]. Specific R joints are replaced by four-bar linkages to facilitate folding. The limbs of the mechanism can be folded onto parallel planes, as shown in Fig. 1.17.

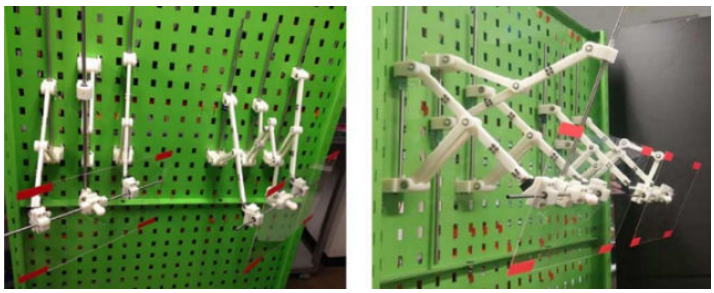

Fig. 1.16 Two foldable mechanisms in [33]

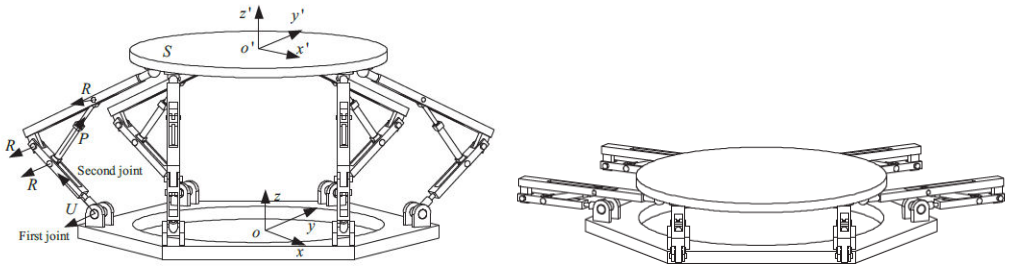

Fig. 1.17 Foldable PM in [34]

Jacobsen et al. [35] introduced the Lamina emergent mechanisms that can be fabricated using planar materials (laminae) and have motions out of the plane (Fig. 1.18). The mechanisms belong to the compliant mechanisms. The advantage of these type of mechanisms is that they can be manufactured one time and can work directly off the machine tools. After finishing work, they can be folded into the initial state. Several credit-card-sized products were fabricated based on lamina emergent mechanisms [36]. Some other applications such as board games were presented in [37].

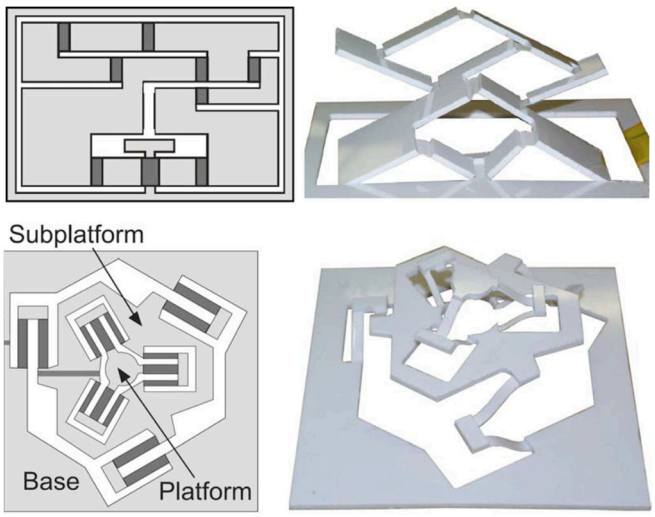

Fig.1.18 Lamina emergent mechanisms [35]

In [38], a design method was proposed to create foldable quadrilateral meshes. The obtained foldable structures have only 1-DOF and one of them is given in Fig. 1.19. Wood was cut to fabricate the mechanism with rigid panels and flexible joints.

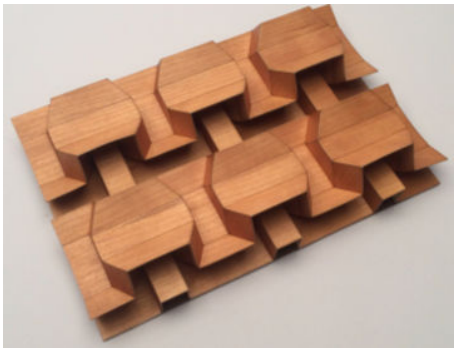

Fig. 1.19 A foldable wooden structure in [38]

Fig. 1.20 A foldable cut origami flasher [39]

Lang et al. also created a family of 1-DOF deployable cut origami flashers, as shown in Fig. 1.20. These mechanisms can be spread on a plane and be folded into a bunch. Examples of 4-fold, 5-fold and 6-fold mechanisms were presented in [39]. A cut is necessary in the process of folding and the panels are regarded as zero-thickness.

Nelson et al. [40] utilized the lamina emergent arrays (networks of lamina emergent joints) to design deployable structures. One example is given in Fig. 1.21. The mechanism can be spread onto a plane and deployed into a spatial structure.

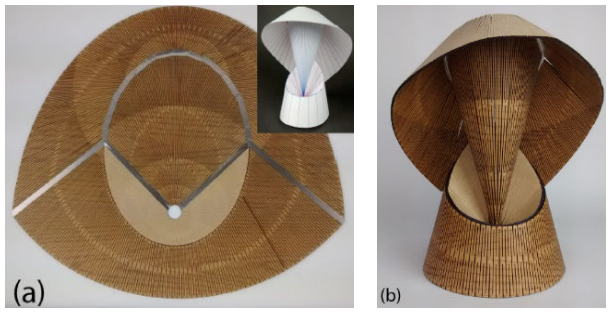

Fig. 1.21 A deployable structure using lamina emergent arrays [40]

An origami waterbomb base, which is a single-loop 8R compliant mechanism, was proposed by Hanna et al. [41], as shown in Fig. 1.22. Since the joints are flexible, the mechanism can be folded and has two stable states. In [42], membrane-enhanced lamina emergent torsional joints were designed, and the novel joints were also applied to the waterbomb base.

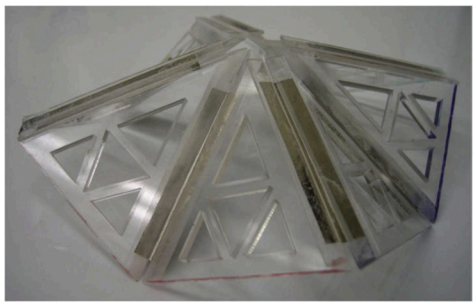

Fig. 1.22 A prototype of the waterbomb base [41]

Hoberman [43] assembled a family of deployable structures using loop assemblies, which are comprised of polygonal links. One mechanism with triangle links is presented in Fig. 1.23.

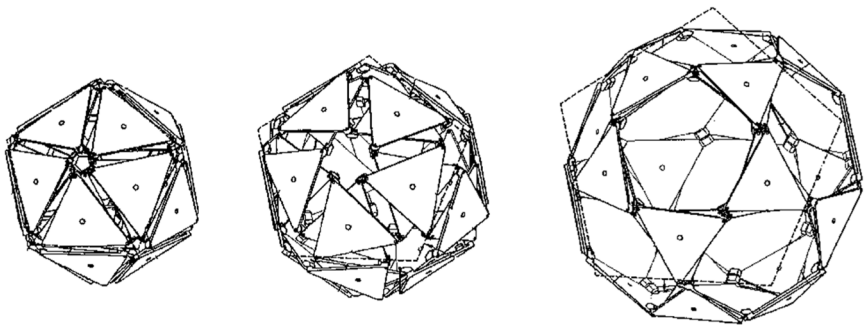

Fig. 1.23 Deployable structures with polygon links [43]

In [44], Hoberman used angulated strut elements to form scissors-pairs. Then the scissors-pairs were joined to form a closed-loop, comprised of which sphere structures such as the one in Fig. 1.24 were constructed. A geared expanding structure was also designed in [45].

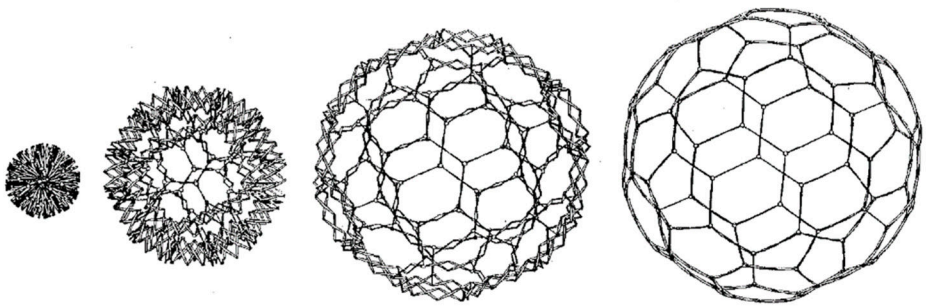

Fig. 1.24 Deployable structure constructed using strut elements [44]

Wei and Dai [46] investigated the geometry and kinematics of the Hoberman switch-pitch ball. The ball is equivalent to a multiple-loop mechanism composed of single-loop eight-bar linkages, as shown in Fig. 1.25.

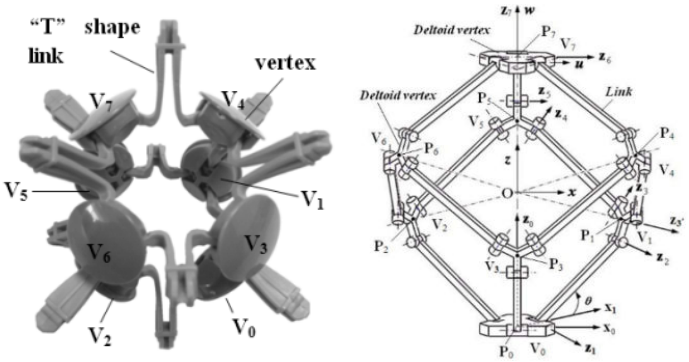

Fig. 1.25 Equivalent mechanism of the Hoberman sphere [46]

In [47], a dual-plane-symmetric spatial eight-bar linkage was proposed, and gears were added to convert the 8R linkage into a 1-DOF mechanism. Then the mechanisms are inserted into faces of the polyhedron to obtain deployable Platonic mechanism, as shown in Fig. 1. 26.

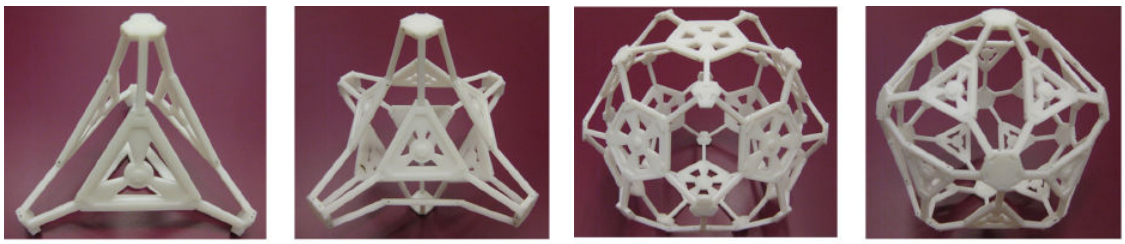

a) Tetrahedral mechanism b) Octahedral mechanism c) Dodecahedral mechanism d) Icosahedral mechanism

Fig. 1.26 Deployable Platonic mechanisms in [47]

By embedding planar linkages into faces of the polyhedron, 1-DOF deployable polyhedral mechanisms were obtained in [48], as shown in Fig. 1.27. The same approach

was also adopted in [49]. The cube mechanism obtained is presented in Fig. 1.28 and the icosahedron mechanism is shown in Fig. 1.29.

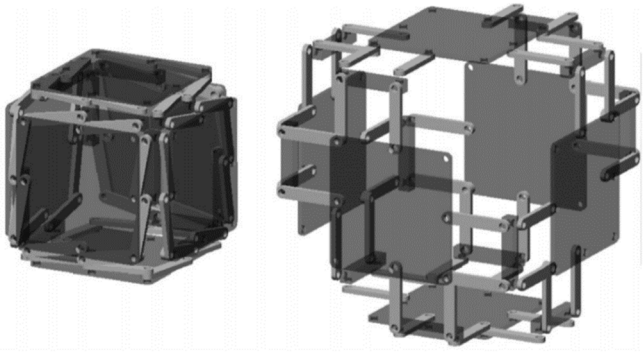

Fig. 1.27 Deployable cube mechanism in [48]

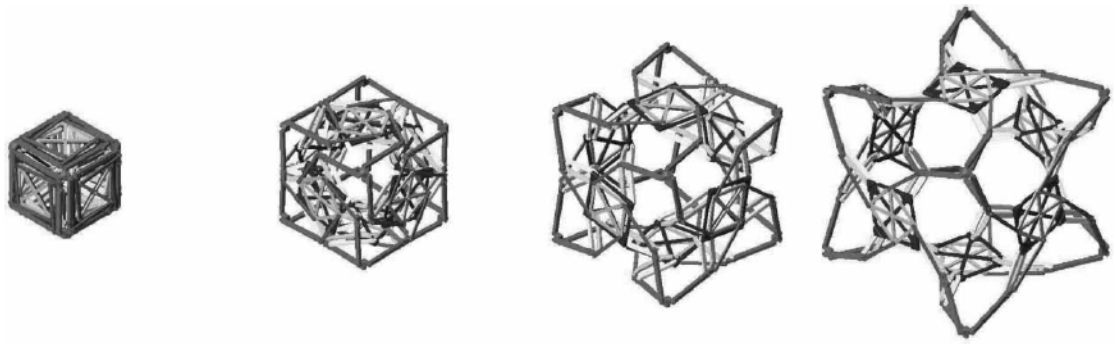

Fig. 1.28 Deployable cube mechanism in [49]

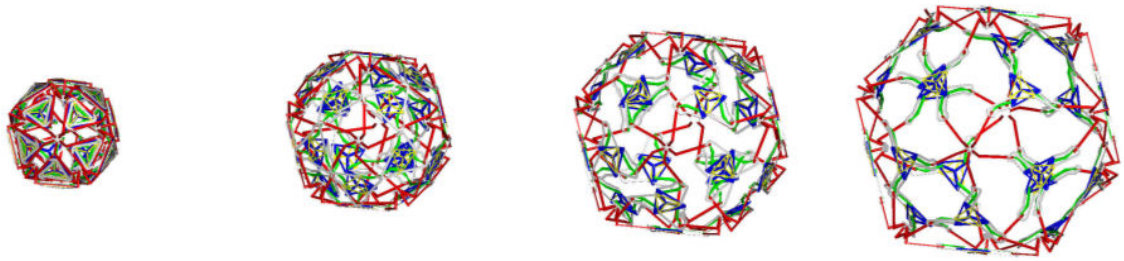

Fig. 1.29 Deployable icosahedron mechanism in [49]

In [50], a family of deployable mechanisms was also designed. Chen et al. [51] proposed a kinematic method to design DPMs with 1-DOF. The obtained mechanisms can achieve transitions between a truncated octahedron and cube, as shown in Fig. 1.30.

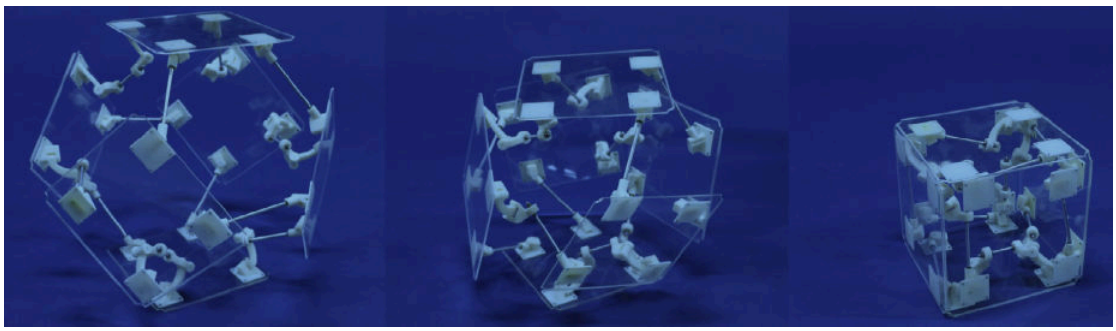

Fig. 1.30 A mechanism that can switch between a truncated octahedron and a cube [51]

1.2 Mechanisms with Multiple Modes

A mechanism with multiple modes refers to the mechanism that can change its configuration according to the tasks or the environments, to achieve the optimal choice of the movement and the highest efficiency. The self-reconfigurable robots that change configurations by disconnecting and reassembling the modules are flexible but have too large DOFs [52-53]. In [54], a metamorphic robotic system composed of hexagonal or square modules was proposed, as shown in Fig. 1.31.

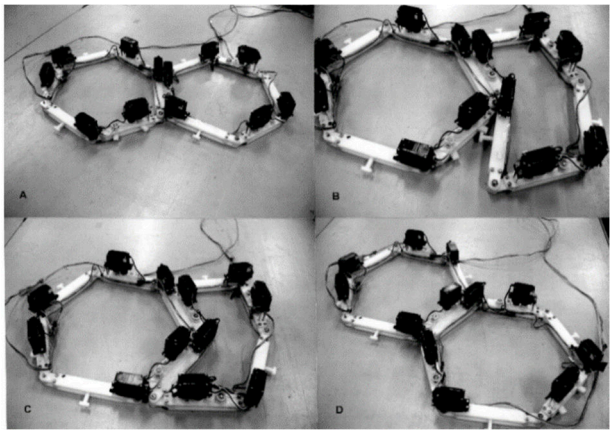

Fig. 1.31 A metamorphic robotic system [54]

During the past decades, more and more researchers were attracted by mechanisms that can change modes without disassembling the mechanisms. The mechanisms have fewer DOFs and switch motion modes through singular positions. The present research is mainly divided into: metamorphic mechanisms, kinematotropic mechanisms, discontinuity moveable mechanisms and the mechanisms with multiple modes.

1.2.1 Metamorphic Mechanisms

Metamorphic mechanisms in which 'the total number of effective links changes as they move from one configuration to another' were put forward by Dai and Jones [55]. This kind of mechanisms can change structure when spread or folded. The basic principle is the origami and decorative gifts boxes which comprise of flat cards and creases. A metamorphic robotic hand was designed in [56-57], as shown in Fig. 1.32. Several metamorphic PMs were then introduced, such as in [58-59]. A reconfigurable PM with planar five-bar metamorphic linkages was analysed in [60].

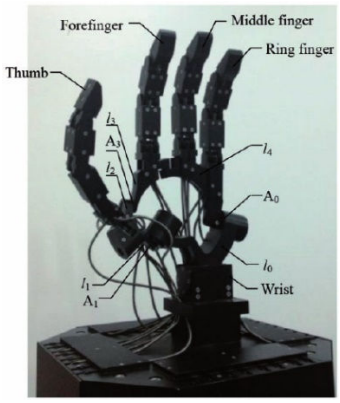

Fig. 1.32 Metamorphic robotic hand [57]

1.2.2 Discontinuously Movable Mechanisms

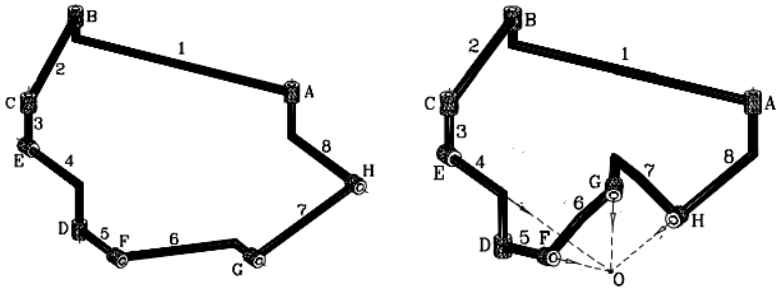

Fig. 1.33 Two discontinuously movable mechanisms [61]: (a) planar-planar 8R mechanism (b) planar-spherical 8R mechanism

Two novel discontinuously movable 8R mechanisms were proposed by Lee and Hervé [61]. One of them is constructed using two planar 4R linkages while the other one is connected by one planar linkage and one spherical linkage. They both have two modes (two planar 4R linkage modes, or a planar 4R linkage mode and a spherical linkage mode)

with discontinuous DOFs (Fig. 1.33]. Discontinuously 6R and seven-bar mechanisms were also introduced in [62-63].

1.2.3 Kinematotropic Mechanisms

Parikian introduced the first known single-loop kinematotropic mechanism, which is comprised of eight links and eight R joints (see Fig. 1.34), at the Sixth International Symposium on Advances in Robot Kinematics in 1996. The DOF of the mechanism is two. The mechanism behaves as a spatial mechanism and turns into the planar six-bar linkage, in which the DOF is three, through a singular position. Galletti and Fanghella [64] gave the detailed analysis for kinematotropic chains with DOFs range from one to three. Multi-loop kinematotropic mechanisms were provided in [65]. One example is shown in Fig. 1.35. The difference between the kinematotropic and discontinuously mechanisms is the DOF of the former changes after transforming while the latter doesn't.

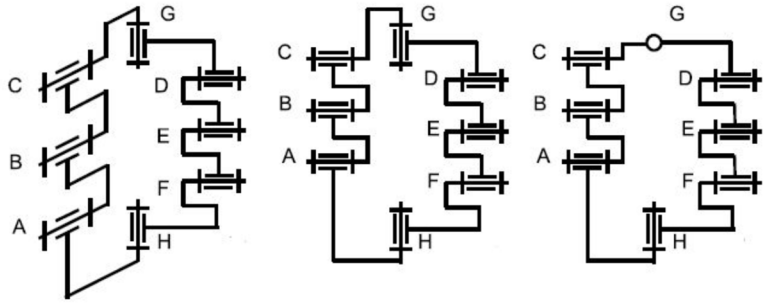

Fig. 1.34 Single-loop 8R kinematotropic mechanism [64]

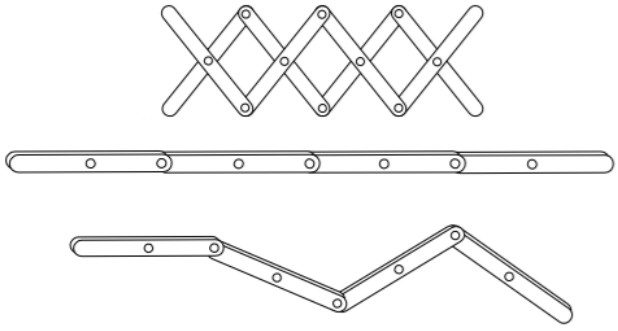

Fig. 1.35 Multiple-loop kinematotropic mechanism [65]

Wohlhart [66] also presented a kinematotropic linkage which changes its mode through specific positions. The mechanism is a spatial mechanism whose DOF can be changed between one and two, as shown in Fig. 1.36.

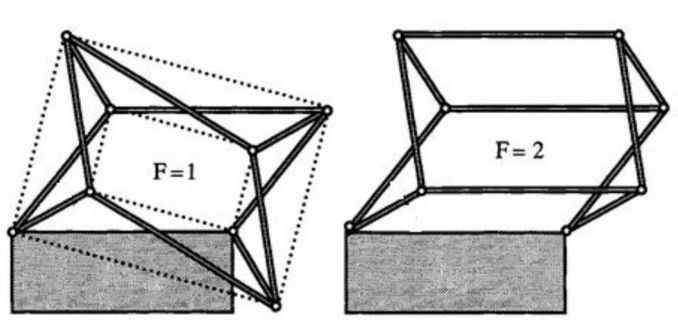

Fig. 1.36 Kinematotropic mechanism with one or two DOFs [66]

Ye et al. [67] introduced a family of reconfigurable PMs with diamond kinematotropic chains. The chain is constructed by three links and a 4-bar parallelogram, as shown in Fig. 1.37. The mechanism acts in different modes such as 3T, 2T1R, 2R1T and 3R when the 4-bar linkage is in specific postures (general position or singular position).

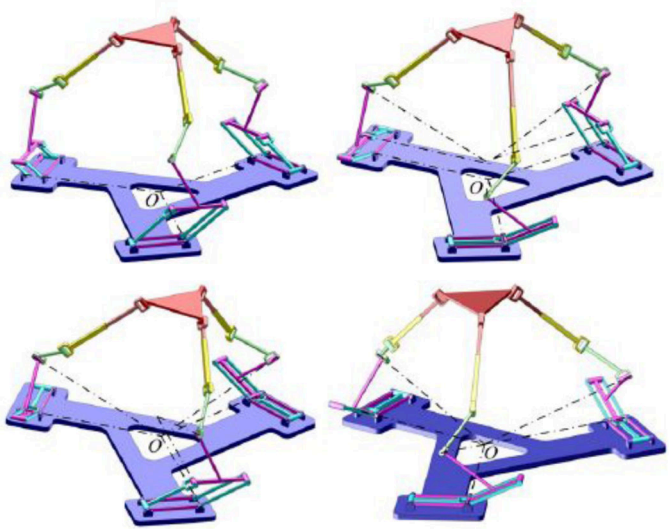

Fig. 1.37 Reconfigurable PM with diamond kinematotropic chains [67]

1.2.4 Mechanisms with Multiple Modes

Kong [68-76] investigated the type synthesis of the mechanisms with multiple motion modes, by utilizing the transition (singular) positions. The single-loop 7R mechanism in Fig. 1.38 was proposed by Kong [68]. The mechanism has variable DOFs and has five motion modes, including a 2-DOF planar 5R mode, two 1-DOF spatial 6R modes, and two 1-DOF spatial 7R modes.

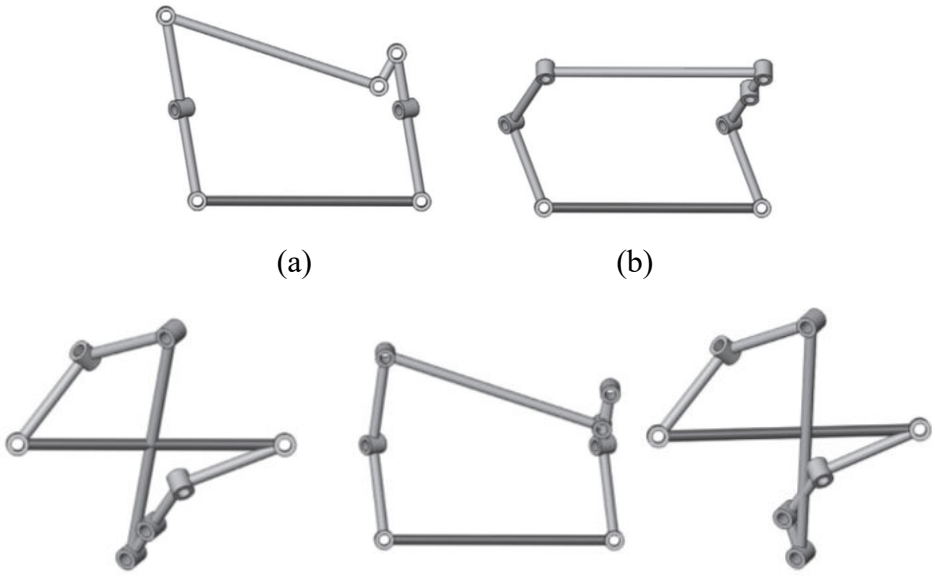

(a) (b)

(c) (d) (e)

Fig. 1.38 A variable-DOF 7R mechanism with multiple modes [68]: (a) 5R mode; (b-c) 6R modes; (d-e) 7R modes.

The type synthesis of single-DOF single-loop mechanisms with multiple operation modes was given in [69]. Huang et al. [70] further analysed a 1-DOF 7R linkage obtained by combining two Bennett linkages with a common joint. Removing the common joint, disconnecting both Bennett linkages and reassembling the linkages, a 7R linkage can be obtained. Since the mechanism is composed of two Bennett linkages, it has the motion modes of two Bennett linkages, as well as the 7R linkage mode. The linkage can deform between different motion modes through transition configurations.

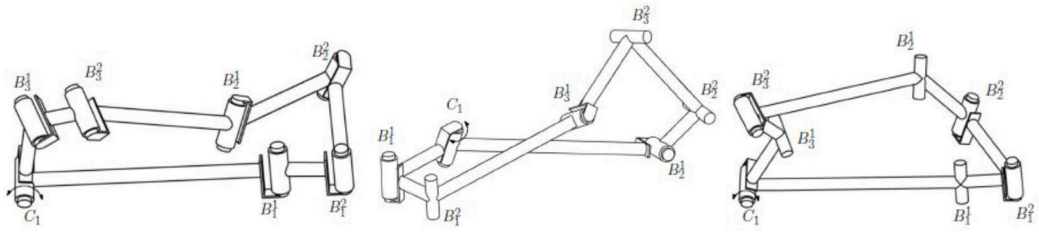

(a) (b) (c)

Fig. 1.39 7R spatial linkage in [70]: (a) transition configuration; (b-c) two Bennett linkage modes

Kong and Wang [71] analysed a variable-DOF 8R mechanism with four modes, including two 3-DOF modes and two 2-DOF modes, as shown in Fig. 1. 40. The work is based on the mechanism proposed by Parikian in 1996, additional modes were found through the reconfiguration analysis.

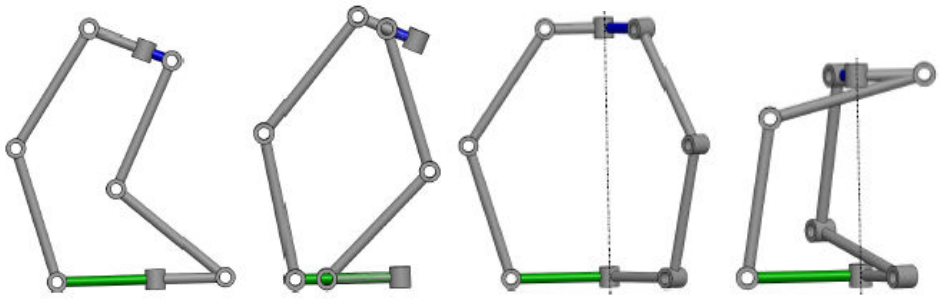

Fig. 1. 40 Variable-DOF 8R mechanism with multiple modes [71]

In [72-73], a novel method for the type synthesis for PMs with multiple modes was proposed. Type synthesis is to find all the possibility of the types of mechanisms. The definition of the PM with multiple modes is:

PM with multiple modes is referred to the PM with the same DOF but different motion modes. For example, planar motion, spherical motion, and spatial translation are all 3-DOF motions. f-DOF PMs with multiple modes have several motion modes with f-DOF.

-Kong [72], 2007

In [72], a 3-DOF PM that can switch between the 3-DOF spherical operation mode and the 3-DOF spatial translational operation mode through transition configurations was discussed as an example to illustrate the type synthesis method, as shown in Fig. 1.41. The transition configuration is when the intersection of the axes of the joints on the upper platform is coincident with those on the lower platform.

Replacing the upper platform in [72] with a Bricard linkage, another PM with multiple modes can be obtained, which was analysed in [74]. The axis of the joints within the chains can be adjusted by changing the posture of the Bricard linkage and locking specific joints. The mechanism can undergo several 3-DOF motion modes, including the planar mode, spherical mode, spatial mode, zero-torsion mode and general 3-DOF mode.

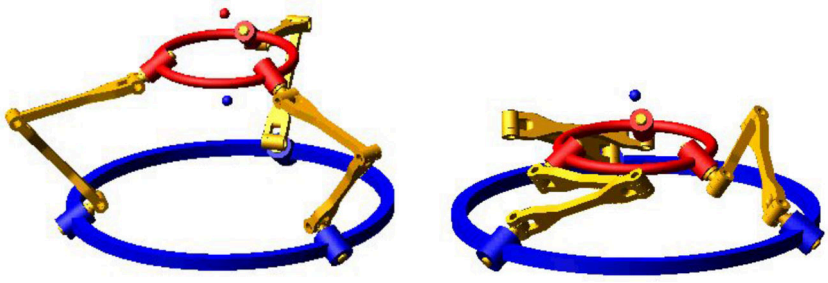

(a) (b)

Fig. 1.41 3-DOF PM with two modes by Kong [72]: (a) translational mode; (b) spherical mode

In [75], the modes analysis of a 3-DOF PM with multiple modes (Fig. 1.42) was carried out, using the Euler parameter quaternions and algebraic geometry approach. Using the proposed method, it is obtained that the mechanism has fifteen modes in total, including four translational modes, six planar modes, four zero-torsion-rate motion modes and one spherical mode. A 4-DOF 3-RER PM with two modes was also put forward in [76].

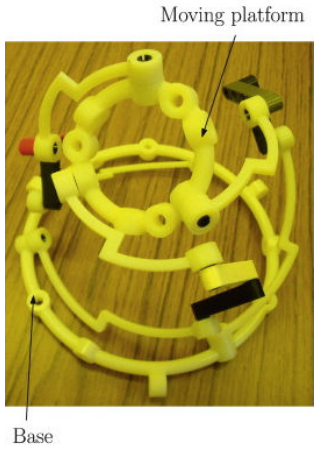

Fig. 1.42 Prototype of the 3-RER PM by Kong [76]

1.2.5 Deployable/Foldable Mechanisms with Multiple Modes

Combining the merits of deployable mechanisms and mechanisms with multiple modes, deployable mechanisms with multiple modes were proposed. 1-DOF deployable mechanisms which have four assembly modes were discussed in [77]. Using variable R joints, a group of reconfigurable and deployable mechanisms was designed by Wei and Dai [78].

A reconfigurable lift mechanism, composed of many planar linkages with R joints, which can be spread onto a plane and further folded to a bundle was fabricated in [79], as shown in Fig. 1.43.

Fig. 1.43 A reconfigurable lift mechanism by Zhao et al. [79]

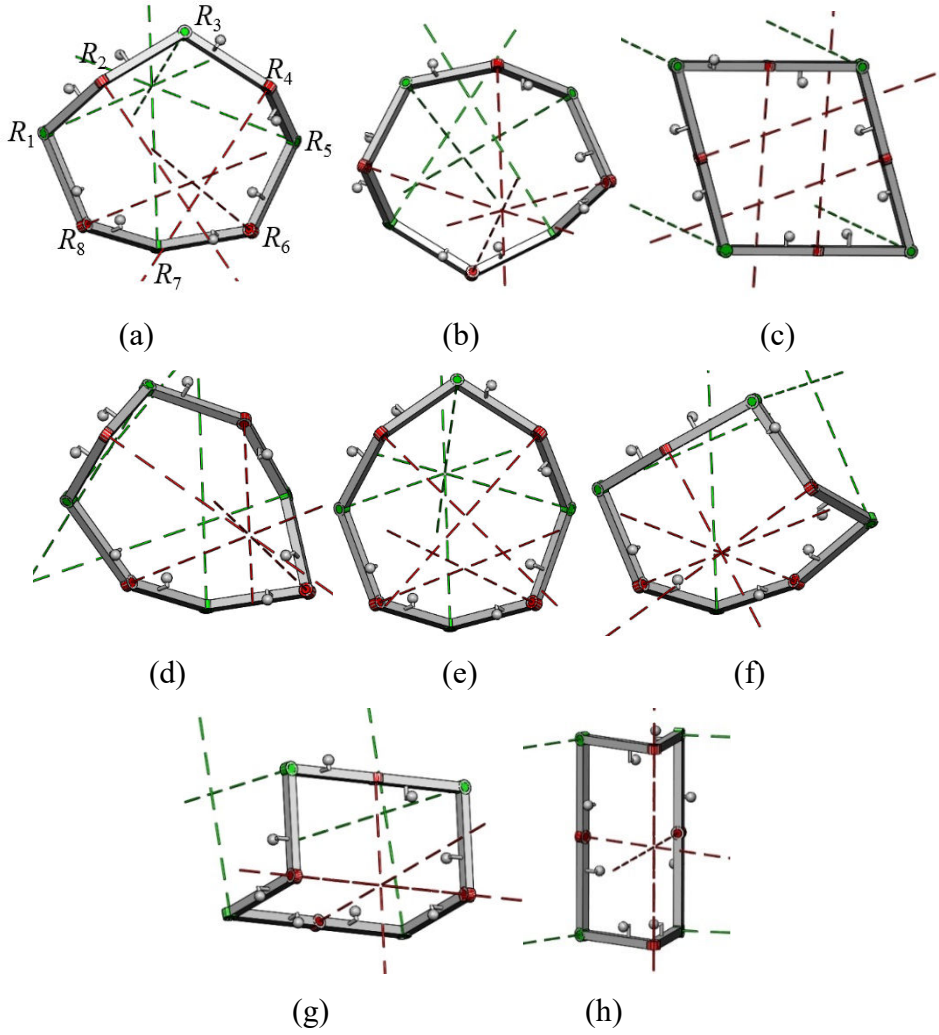

Fig. 1.44 Motion modes of the 8R linkage: (a-b) spherical 4R linkage modes; (c) planar 4R linkage mode; (d) spatial 8R linkage mode; (e-f) spatial 6R linkage modes; (g-h) folding modes

A rolling mechanism based on a deployable spatial 8R linkage was built in [80]. The linkage is composed of eight links and eight R joints, whose axes are perpendicular to

those of the adjacent R joints. It has multiple motion modes, including two 1-DOF spherical 4R linkage modes in which R_1, R_3, R_5 and R_7 (or R_2, R_4, R_6 and R_8) intersect at a point while R_2, R_4, R_6 and R_8 (or R_1, R_3, R_5 and R_7) are locked [Figs. 1.44(a-b)]; a 1-DOF planar 4R linkage mode, by locking R_2, R_4, R_6 and R_8 when R_1, R_3, R_5 and R_7 are parallel [Fig. 1.44(c)]; a 2-DOF spatial 8R linkage mode [Fig. 1.44(d)], two 1-DOF spatial 6R linkage modes, in which R_4 and R_8, or R_1 and R_5 are immobile [Figs. 1.44(e-f)]; and two 1-DOF 2R folding modes, in which R_1, R_3, R_4, R_5, R_7 and R_8, or R_1, R_2, R_3, R_5, R_6 and R_7 are immobile [Figs. 1.44(g-h)].

Wang et al. [81] designed a 16-bar mechanism with two motion modes, including a spherical linkage mode and a planar linkage mode, as shown in Fig. 1.45. When deployed, the mechanism works in the spherical 4R linkage mode and when folded, it turns into the planar 4R linkage mode.

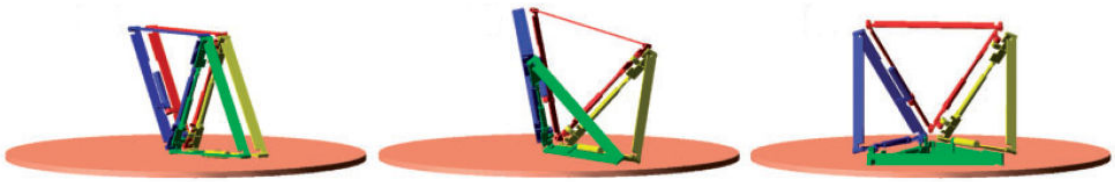

(a) (b) (c)

Fig. 1.45 The 16-bar mechanism with two modes [81]: (a) planar linkage configuration; (b) planar linkage mode to spherical linkage mode; (c) spherical linkage configuration

Li et al. [82] constructed a family of reconfigurable DPMs using parallelogram mechanisms. In [83], a reconfigurable angulated element and reconfigurable generalized angulated elements were designed and then used as modules to connect deployable mechanisms. The mechanisms can switch between the Hoberman sphere motion mode [Figs. 1.46(a-b)] and the radially reciprocating motion mode [Figs. 1.46(c-d)].

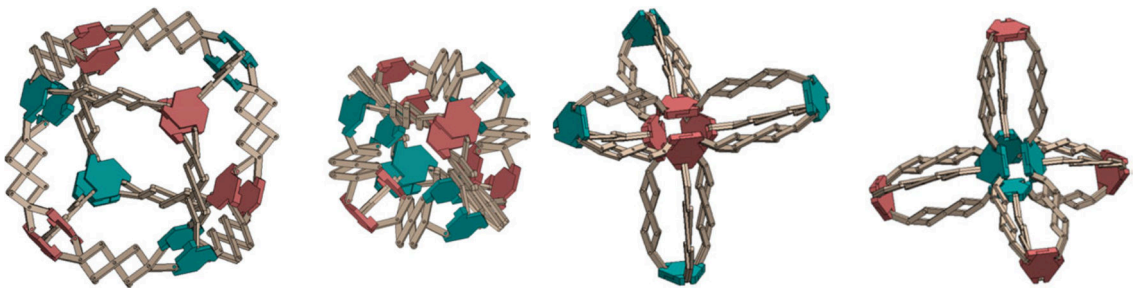

(a) (b) (c) (d)

Fig. 1.46 Reconfigurable and deployable mechanism by Li [83]: (a-b) Hoberman sphere motion modes; (c-d) radially reciprocating motion modes

However, the structures of most of the deployable mechanisms with multiple modes in the literature are very complicated. Mechanisms with simple structures will be proposed in this thesis.

1.3 Statically Balanced Mechanisms

Energy is one of the important topics all over the world. As we are consuming more and more resources, energy-saving becomes an important issue. Energy-efficient means reducing the energy that is used in the products or services. In the field of robotics, there are many approaches to save energy of the robots. One of the approaches to achieve energy-efficiency is to apply the principle of static balancing and to reduce the energy used to eliminate the effect of gravity or inertia force and moment.

To achieve the balance of the biped human-like robots [84-85], force control methods can be used. The forces and torques can be computed for the robot, according to the CM (centre of mass) and external forces. Then the robots can adjust their postures according to their current states.

The balanced robots using the control method are flexible, but the robots are high-cost, compared with using the method of structure design. Counterweights and springs can be adopted to compensate for the gravity. A system is statically balanced if the total potential energy or torque of the system is constant. Static balancing leads to low actuation forces required to move the devices, and therefore helps improve the efficiency of the mechanism.

(a) (b)

Fig. 1.47 Applications of balanced devices using counterweight [87]: (a) crane; (b) bridge

The principle of force-balance has been applied to our daily life. For example, in the elevators, a heavy counterweight is used to balance the load of the elevator carriage. As

a result, the actuator lifts much less of the weight of the carriage [86]. As shown in Fig. 1.47, counterweights are used on crane or bridge to counterbalance the payload [87].

The Anglepoise lamp is a balanced-arm lamp designed in 1932 by George Carwardine [88], as shown in Fig. 1.48(a). Springs are used to balance the lamp and make sure the lamp head can keep its positions in any postures. Detailed analysis of the design was given in [89]. Another balanced lamp was proposed in [90] by Carwardine. Scissors fork mechanism and springs are adopted to counterbalance the weight of the lamp head, as shown in Fig. 1.48(b).

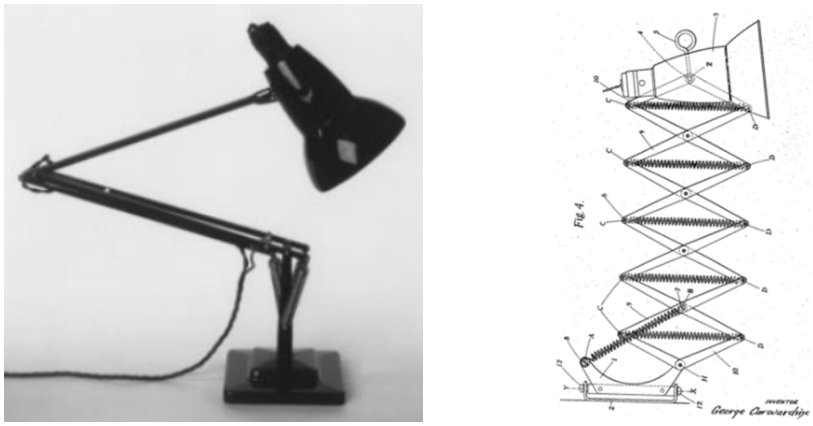

(a) (b)

Fig. 1.48 Statically balanced lamps: (a) type I [89]; (b) type II [90]

Bell et al. [91] proposed a statically balanced device that can support the surgical light-head of a surgical light apparatus. The force balanced surgical light was also discussed in [92-93].

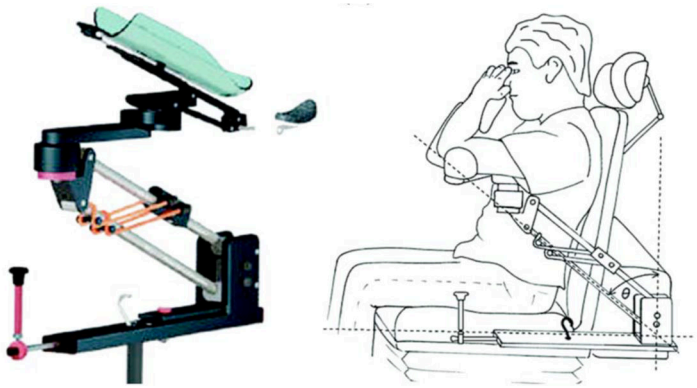

Fig. 1.49 Arm support using the statically balanced mechanism [95]

In [94], the statically balanced mechanism was applied to arm support for the people suffering from the problems of lifting their arms (Fig. 1.49). The arm support can adjust

the balancer to another payload without external force or energy. The same application can also be found in [95-96].

In [97], a gravity-balanced sit-to-stand assist device was designed using the principle of static balancing (Fig. 1.50). Banala et al. [98] built a device assisting people to walk by reducing or eliminating the effects of gravity using springs, as shown in Fig. 1.51.

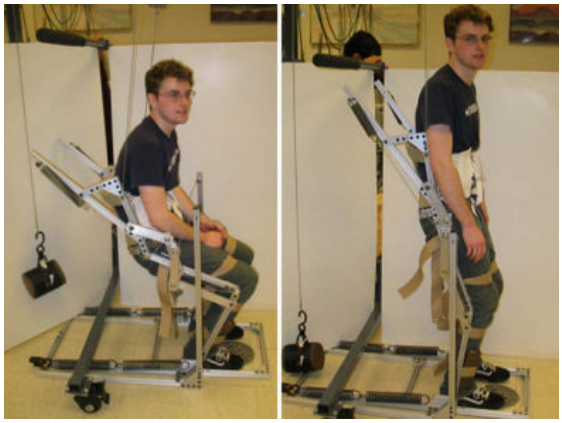

Fig. 1.50 A gravity-balanced sit-to-stand assist device [97]

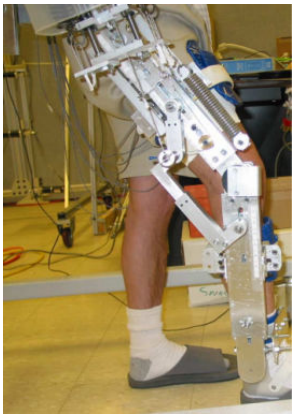

Fig. 1.51 A force-balanced walking assist device [98]

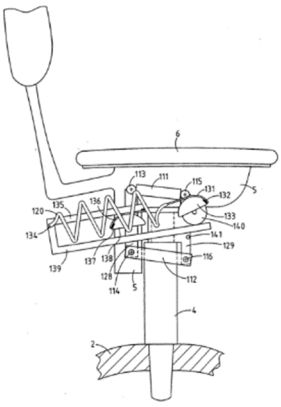

Fig. 1.52 A seating unit with a spring compensation mechanism [99]

In [99], the balancing mechanism with springs is used as a supporting part for a seating unit to support a body, as shown in Fig. 1.52.

Kuo and Lai [100] proposed a novel laparoscope holder used for minimally invasive surgery, as shown in Fig. 1.53. The mechanism is constructed using a parallelogram linkage (positioning arm) and a PM (orientating wrist). The device has a remote centre of motion (RCM) characteristics.

Fig. 1.53 Statically balanced laparoscope holder in [100]

There are various methods can be adopted to design the force balance mechanisms, such as using mass and lever, zero-free-length springs and torsion beam [101].

1.3.1 Statically Balanced Mechanisms Using Zero-free-length Springs

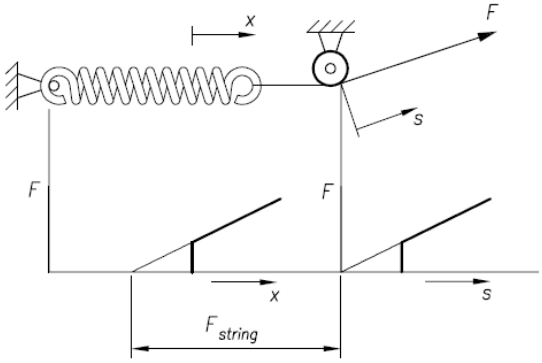

Fig. 1.54 Design of the zero-free-length spring using pulley and strings [104]

The zero-free-length springs can be used to design statically balanced mechanisms. The total potential energy of the system is constant when statically balanced. The zero-free-length spring can be achieved using the pulley and strings [102], as shown in Fig. 1.54.

Wongratanaphisan and Cole [103] analysed the gravity-compensated 4R linkage with two springs. The result also shows that there are two stable and two unstable states for the four-bar linkage with springs, as shown in Fig. 1.55.

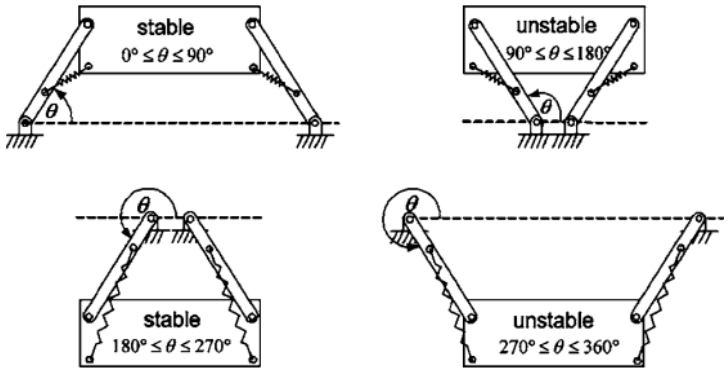

Fig. 1.55 Stable and unstable configurations of 4R linkage [103]

Several statically balanced 1-DOF planar linkages were presented in [105], such as the Stephenson mechanism and Watt mechanism, using only springs. Lin [106] designed the statically balanced SSS (spherical joint) arm and RSR arm using springs, as shown in Fig. 1.56. Dunning and Herder [107] assembled three springs for the gravity balancing of the 2-link arm.

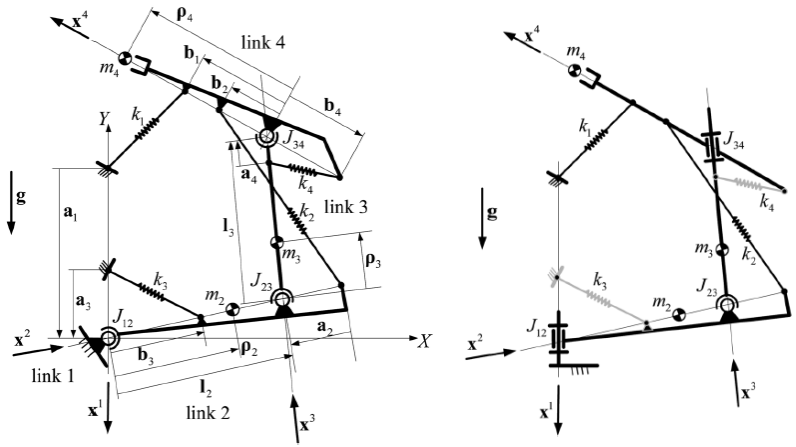

(a) (b)

Fig. 1.56 Statically balanced SSS and RSR manipulators: (a) SSS manipulator; (b) RSR manipulator [106]

Lustig et al. [108] analysed the statically balanced serial planar linkage using a stiffness matrix approach. Walsh et al. [109] put forward a general methodology to design *n*-spring balancers for the 2-DOF manipulator with yaw-pitch rotation. Robertson et al. [110] investigated the static balancing of a single-loop linkage with two modes using one spring, by attaching the spring right above the intersection of rotation lines in the two modes.

The systems mentioned above are all balanced using only springs. In other literature, to facilitate identifying the CM of the system or attaching the springs, auxiliary parallelograms were added. Rahman et al. (Fig. 1.57) [102] and Herder [104] introduced the statically balanced planar serial manipulators or spatial manipulators composed of planar linkages using auxiliary parallelograms and springs.

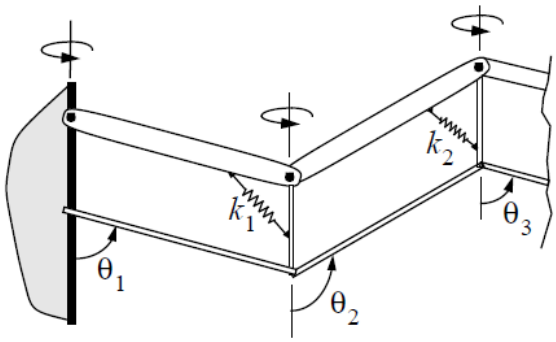

Fig. 1.57 Statically balanced planar mechanism with multiple DOFs [104]

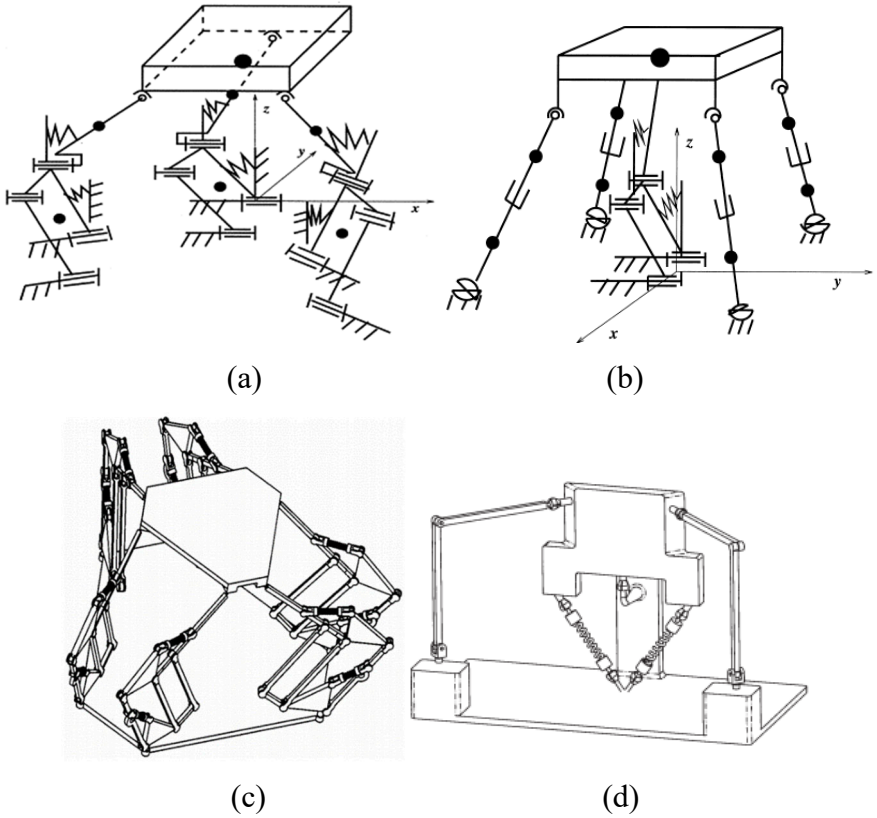

Fig. 1.58 Statically balanced PMs with springs: (a) spatial 3-DOF PM [114]; (b) spatial 4-DOF PM [115]; (c) spatial 6-DOF PM [116]; (d) spherical 3-DOF PM [117]

Agrawal [112] designed the gravity-balanced 2-link and 3-link leg orthoses using auxiliary parallelograms and non-zero-free-length springs. The static balancing of planar

3-DOF PMs was addressed in [113]. Gosselin and Wang [114-117] proposed a series of statically balanced mechanisms, including spatial 3-DOF PMs [Fig. 1.58(a)], spatial 4-DOF PMs [Fig. 1.58(b)], spatial 6-DOF PMs [Fig. 1.58(c)] and spherical 3-DOF PMs [Fig. 1.58(d)]. Auxiliary parallelograms were adopted to attach the springs.

In [118], the CM of the system was identified by using auxiliary parallelograms, then springs were used to connect the CM of the manipulator and to balance the spatial manipulators, as shown in Fig. 1.59.

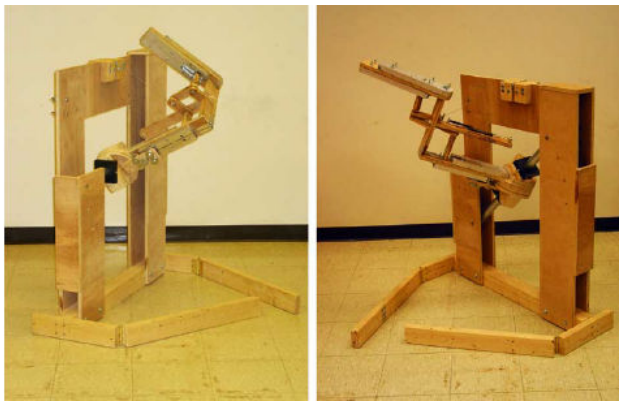

Fig. 1.59 Gravity-balanced spatial manipulator using auxiliary parallelograms [118]

1.3.2 Statically Balanced Mechanisms Using Counterweights

In [119-120], planar 4R linkages were balanced using counterweights. Van der Wijk [121] investigated the statically balanced manipulators, including the 4R linkage and PMs composed of RRR chains, using counterweights. Laliberté discussed the statically balanced 3-DOF planar PM with counterweights in [113]. In [114-117], a family of spatial PMs was designed and balanced using counterweights, including spatial 6-DOF PMs, spatial 3-DOF PMs, and spatial 4-DOF UPS/RUS PMs, as shown in Fig. 1.60.

Russo et al. [122] studied the static balancing of the 6-DOF PM using counterweights or pantograph counterweight. The force balancing of spatial metamorphic 6R linkage was investigated in [123]. Kuo et al. [124] presented the statically balanced design of the reconfigurable mechanism with variable DOFs, using only one counterweight.

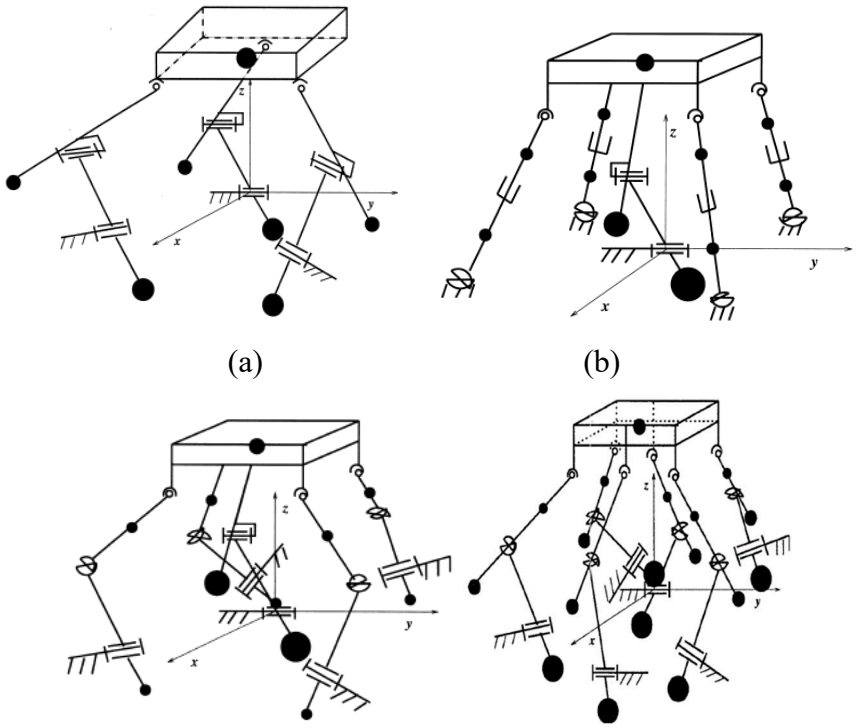

Fig. 1.60 Statically balanced PMs with counterweights: (a) spatial 3-DOF PM [114]; (b-c) spatial 4-DOF PMs [115]; (d) spatial 6-DOF PM [116]

Fig. 1.61 Statically balanced 6-DOF PM using pantograph counterweight [122]

1.3.3 Statically Balanced Mechanisms Using Other Methods

Except for balancing the mechanisms using springs or counterweights, there are other methods to balance the mechanisms, such as using gears or cams. In [121], the mechanism was balanced by identifying the CM of the manipulator based on the method of principal vectors proposed by Fischer [125]. Then the CM of the manipulator was mounted on the base. As a result, the mechanism is balanced at any positions since the heights of the CM

of the manipulator keeps constant, as shown in Fig. 1.62. The similar method was also adopted in [126].

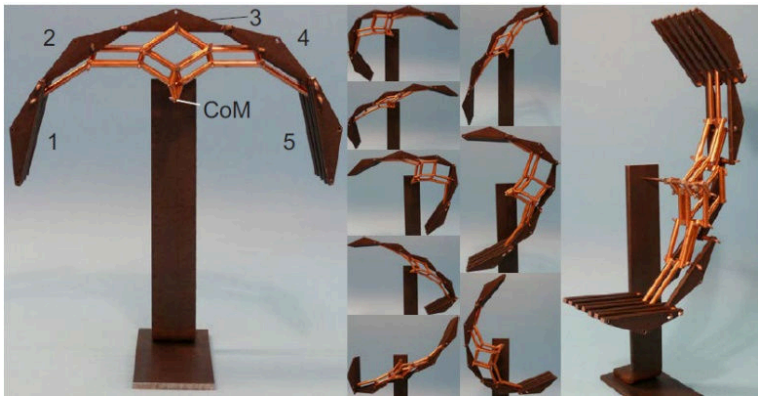

Fig. 1.62 Statically balanced 5R manipulator in [121]

In [127], a balancing method was proposed for the 4R linkage using non-circular gears. Gallego and Herder [128], Rijff et al. [129] and Radaelli et al. [130] adopted the torsion springs to develop the gravity-balanced mechanisms. Boisclair et al. [131] addressed the gravity compensation of robotic manipulators using cylindrical Halbach arrays.

1.3.4 Statically Balanced Mechanisms Using Combined Methods

The balancing approaches mentioned above can also be combined to design the statically balanced system. The static balancing of the planar 3-DOF PM was addressed in [113], using a combination of both counterweights and springs (Fig. 1.63).

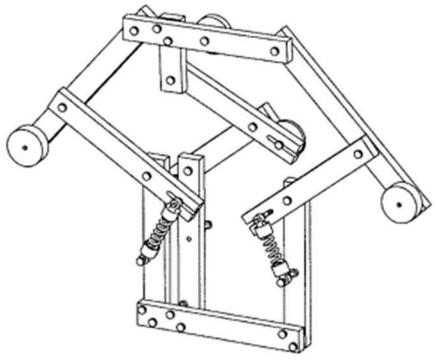

Fig. 1.63 Static balancing of the planar 3-DOF PM using both counterweights and springs [113]

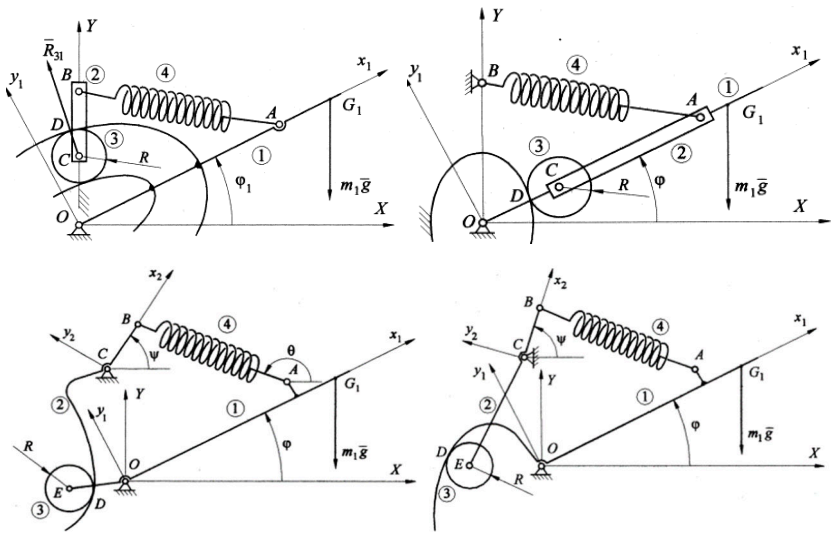

Fig. 1.64 Statically balanced 1-link manipulators with spring and cam [132-133]

In [132-133], both cams and springs were adopted to balance the 1-link manipulator. Four solutions were provided, as shown in Fig. 1.64. Koser [134] also achieved the static balancing of a 1-DOF manipulator by using cam and spring.

Van der Wijk and Herder [135] presented the reactionless 4R linkage by using counter-rotary counter-masses, which were also adopted in [136]. Arakelian and Smith [137] dealt with the balancing of the 4R linkage using the counterweight formed by gears.

Cho et al. [138] designed a gravity compensator for the arm with roll-pitch rotation. The system is comprised of two 1-DOF gravity compensators (with springs) and a bevel differential (using gears), as shown in Fig. 1.65. Based on the work in [138], a 4-DOF incomplete balanced manipulator was developed in [139]. Bijlsma et al. [140] designed a gravity equilibrator using geared transmission and torsion bars, as shown in Fig. 1.66.

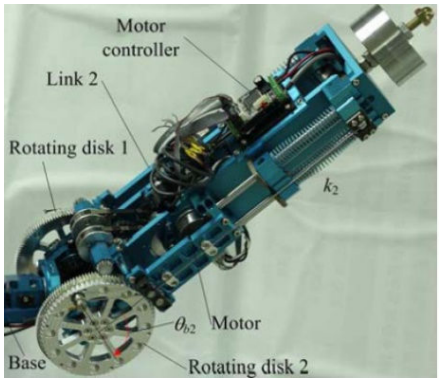

Fig. 1.65 A gravity compensator for the arm with roll-pitch rotation [138]

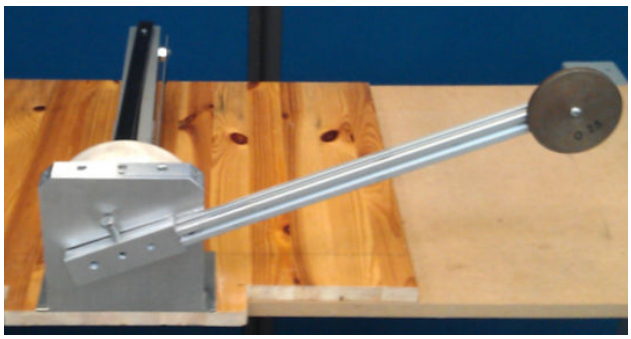

Fig. 1.66 Statically balanced mechanism using geared transmission and torsion bars [140]

1.3.5 Statically Balanced Mechanisms with Variable Payloads

In the cases that the weights of the payloads change, for example for the arm support, the weight of the support changes when picking up or dropping objects. Hence, various static balancing methodologies for the mechanisms with variable payloads were proposed.

In [141], five strategies are described to adapt the balancing under varying payload conditions (Fig. 1.67): (a) changing the positions of the counterweights; (b) changing the joint locations; (c) changing the amount of counterweights; (d) adding additional linkages; (e) adding redundant joints.

Chu and Kuo [142] built a statically balanced 1-DOF manipulator, in which the change of the payload can be sensed by the spring. Cam was adopted to adjust the system to adapt to variable payloads, as shown in Fig. 1.68(a).

Van Dorsser et al. [94] designed an adjustable arm support, based on the method of rearranging the springs without changing their lengths. In [143], the system was adjusted by changing the stiffness of the spring, as shown in Fig. 1.68(b). Wisse et al. [144] utilized the virtual spring concept to design the system with variable payloads. Barents et al. [145] designed a statically balanced cabinet using the spring to spring balancing, as shown in Fig. 1.68(c). In [146-148], the statically balanced mechanisms with variable payloads were also proposed.

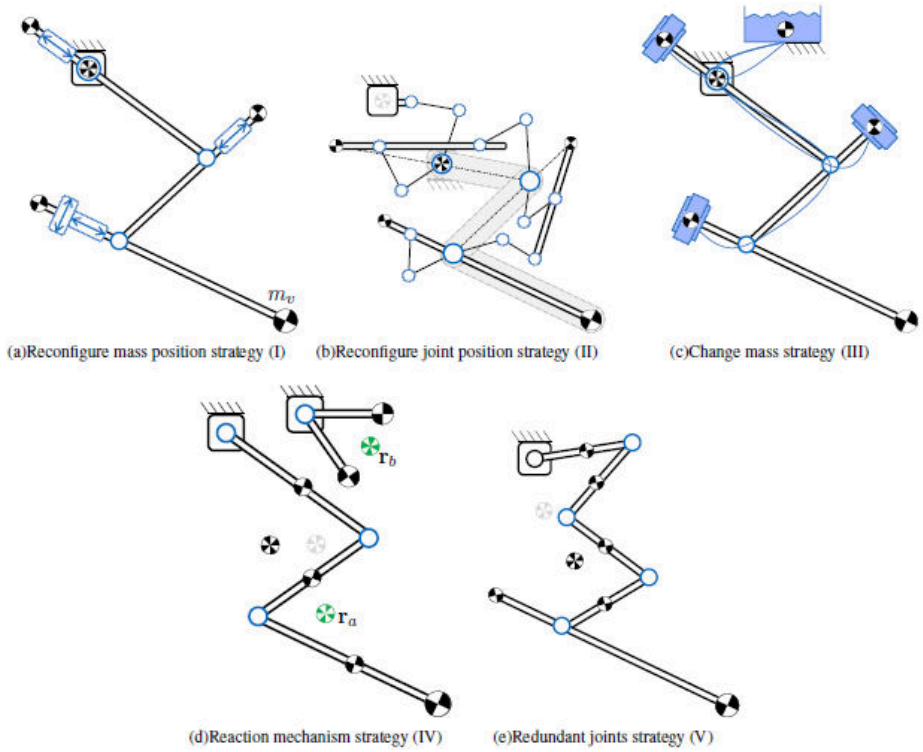

Fig. 1.67 Five strategies applied to planar 3-DOF mechanisms [141]

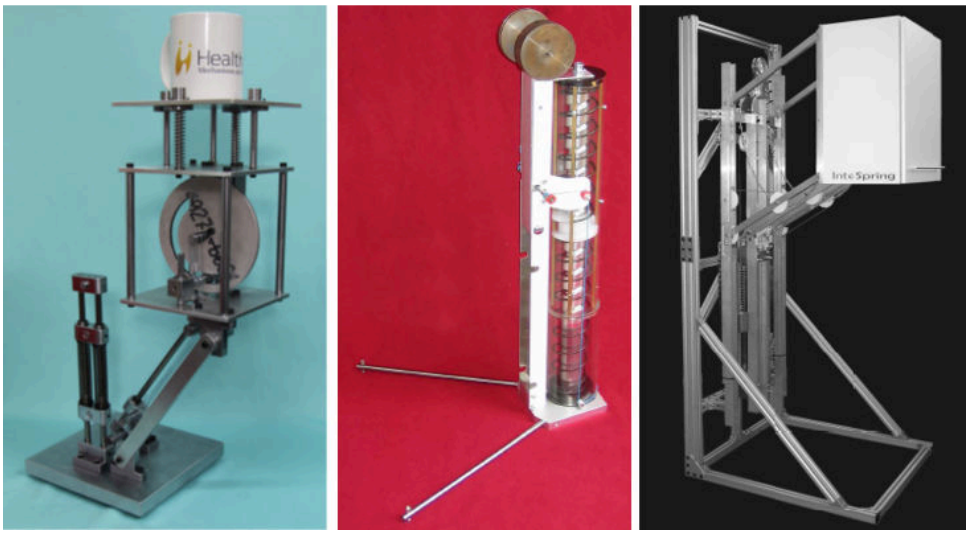

(a) (b) (c)

Fig. 1.68 Statically balanced systems with variable payloads: (a) using cam [142]; (b) by adjusting the spring stiffness [143]; (c) using spring to spring balancing [145]

1.3.6 Methods of Calculating Positions of Springs or Counterweights

When calculating the positions of the attachment points of springs or counterweights, different methods can be adopted, such as using the algebraic method, geometric method or numerical method. Lin et al. [149] demonstrated several statically balanced spatial

manipulators, whose design parameters were obtained by diagonalizing the stiffness matrix. This method was also applied in [108]. In [150], a screw-based balancing methodology was introduced to derive the balancing conditions for 4R linkages. In [151], two methods, including the algebraic method and the geometric method, were presented for the balancing of Bennett linkage. Meanwhile, several optimization methods were used to obtain the positions of springs and counterweights. In [152], the static balancing of a medical parallel robot with tension spring, torsion spring or counterweight was achieved by minimizing the 'motor torque root-mean-square value'. Haines [153] put forward a method for optimizing the 'root-mean-square shaking moment and/or driving torque'. In [154-155], the 'linear combination of the resultant bearing force and the input-torque required to drive the linkage' was set as the objective function to optimize the 4R linkage. The same objective function was also adopted in [156-157]. In [158], a planar PM was optimized by minimizing the 'sum-squared values of the elements of the position or velocity or acceleration sensitivity matrix'. A 'mean-square root of the sum squared discrete values of all the reaction forces in the manipulator' was adopted as the objective function in [159]. The average force was minimized to design the statically balanced mechanism in [160]. Schwarzfischer et al. [161] minimized the difference of the output motion compared with the desired output motion, to design an energy-efficient six bar Watt-II-Mechanism.

Nevertheless, the static balancing method for general spatial mechanisms, especially the ones with multiple modes is still an open issue. The approach proposed in the literature for the mechanisms with multiple modes can only be applied to specific mechanisms, and the masses of the links were neglected and only the mass of the end-effector was considered in most of the references. The optimization methods, however, are more suitable for the systems using counterweights.

1.4 Objectives and Layout of the Thesis

This thesis focuses on the type synthesis and static balancing of a class of deployable mechanisms with multiple modes. A construction approach to the foldable 8R linkages with multiple modes will be introduced first. Then a novel construction method will be proposed to design deployable mechanisms using a symmetric triad. Several mechanisms obtained have multiple motion modes and can switch modes through transition configurations. The mechanisms have simpler structures and fewer DOFs, compared with the mechanisms in the literature. Finally, the deployable mechanisms will be developed

into statically balanced mechanisms. Novel static balancing approaches will be proposed, including the algebraic method, the geometric method and the optimization method. Using the proposed geometric approaches, the planar mechanisms, spherical mechanisms, the variations of spherical mechanisms and spatial mechanisms will be balanced, with almost no calculation. The mechanisms in this thesis are all composed of links whose weights cannot be neglected, while only the weights of the payloads on the end effectors were considered in the literature. A numerical optimization method will also be introduced, which is suitable for the system with springs. Based on the proposed static balancing methods, the deployable mechanisms with multiple modes can be developed into statically balanced mechanisms.

The thesis is organized as follows. Chapter 2 summarizes the theoretical tools and the fundamentals used in this thesis. The construction method for the single closed-loop foldable mechanisms is described in Chapter 3. Chapter 4 focuses on the design of multi-loop deployable mechanisms constructed using S joints. The S joints in Chapter 4 are replaced by RRR chains in Chapter 5. Chapter 6 describes the statically balanced methods for planar mechanisms, spherical mechanisms and spatial mechanisms using springs, and develops the deployable mechanisms obtained in Chapters 3, 4 and 5 into the statically balanced mechanisms. Finally, conclusions are drawn.

CHAPTER 2 – THEORETICAL TOOLS AND FUNDAMENTALS

In this chapter, the theoretical tools used in this thesis will be introduced. The fundamentals of the static balancing of the mechanisms will also be discussed.

2.1 Mathematical Basis

2.1.1 Distance Between a Point and a Plane Defined by Three Points

Suppose there are three points P_1, P_2 and P_3 that define a plane, P_4 is a point out of the plane. The normal vector of the plane $\boldsymbol{N} = \{l\ m\ n\}^T$ can be calculated by

$$\boldsymbol{N} = (\boldsymbol{P_1} - \boldsymbol{P_2}) \times (\boldsymbol{P_2} - \boldsymbol{P_3}) \tag{2.1}$$

The plane equation can be obtained as

$$l(x - P_{1x}) + m(y - P_{1y}) + n(z - P_{1z}) = 0 \tag{2.2}$$

The distance between P_4 and the plane is

$$H = \frac{\left|l(P_{4x} - P_{1x}) + m(P_{4y} - P_{1y}) + n(P_{4z} - P_{1z})\right|}{\sqrt{l^2 + m^2 + n^2}} \tag{2.3}$$

The distance equation will be used in Chapter 4 to calculate the deploying ratio of the deployable mechanism.

2.1.2 DOF Analysis

The DOF is the mobility of the mechanism which is constrained by joints. DOF analysis is the basic problem in the process of mechanism design. The DOF of the serial manipulator is the sum of the mobility of all the joints:

$$M = \sum_{i=1}^{p} f_i \tag{2.4}$$

The DOF of the closed-loop spatial mechanism can be calculated using the conventional formula for DOF. There are several types of formulas, and this thesis will use the formula proposed by Hunt [162-163].

$$M = d(q - p) + \sum_{i=1}^{p} f_i \tag{2.5}$$

For the single-loop linkages, the formula is simplified as $M = \sum_{i=1}^{p} f_i - 6 + \lambda$. q, p, and f_i respectively represent the number of mobile links, the number of joints and the freedom of the i^{th} joint. d is the rank of the mechanism, and is equal to 6 - λ, where λ is the number of common constraints. For a general spatial mechanism, d = 6, and for planar

mechanisms and spherical mechanisms, d = 3. In some special cases, the rank of the system can be obtained using screw theory.

Suppose that $\boldsymbol{s}$ is a unit vector along the screw axis and $\boldsymbol{r}$ is the position vector of a point on the screw axis [164]. The unit screw of an R joint or a force [Fig. 2.1(a)] is in the format of

$$\$_{\mathbf{0}} = (\boldsymbol{s}; \boldsymbol{r} \times \boldsymbol{s}) = (l \quad m \quad n; a \quad b \quad c) \tag{2.6}$$

The unit screw of a prismatic (P) joint or a couple [Fig. 2.1(b)] is in the format of

$$\$_{\infty} = (0; \boldsymbol{s}) = (0 \quad 0 \quad 0; l \quad m \quad n) \tag{2.7}$$

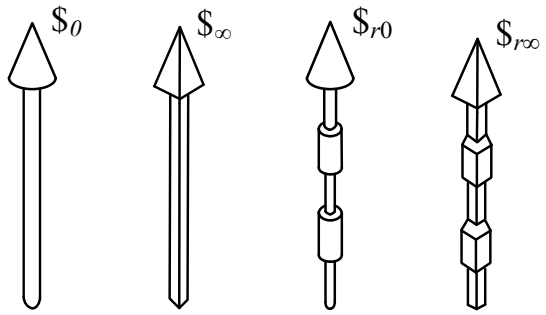

Fig. 2.1 Screws: (a) the screw of an R joint or a force; (b) the screw of a P joint or a wrench; (c-d) reciprocal screws

The joint twist and the constraint wrench [Fig. 2.1(c-d)] of a system are reciprocal.

$$\$_1 \cdot \$_2 = 0 \tag{2.8}$$

The relationship between twist system and its wrench system is [73]:

a) *The axis of $\$_0$ is coplanar with the axis of any $\$_{r0}$.*
b) *The axis of $\$_\infty$ is perpendicular to the axis of any $\$_{r0}$.*
c) *The axis of $\$_0$ is perpendicular to the axis of any $\$_{r\infty}$.*

Hence, when given a mechanism, the twist system can be presented, then the constraint system can be obtained. The number of the common constraints of the mechanism is equal to the rank of the constraint system. Finally, the mobility of the mechanism is obtained.

2.1.3 Notations of D-H Convention

To obtain the positions of the links of the mechanism, the Denavit-Hartenberg (D-H) notation [165] will be introduced. In the D-H convention, the local coordinate frames (Fig. 2.2) are defined as:

a) *The z_i axis is along the i^{th} joint axis.*

b) *The x_i axis points to the $(i+1)^{th}$ joint. If the axes of the i^{th} joint and the $(i+1)^{th}$ joint intersect, x_i is perpendicular to the plane defined by the two joint axes.*

c) *The y_i axis can be obtained using the right-hand rule.*

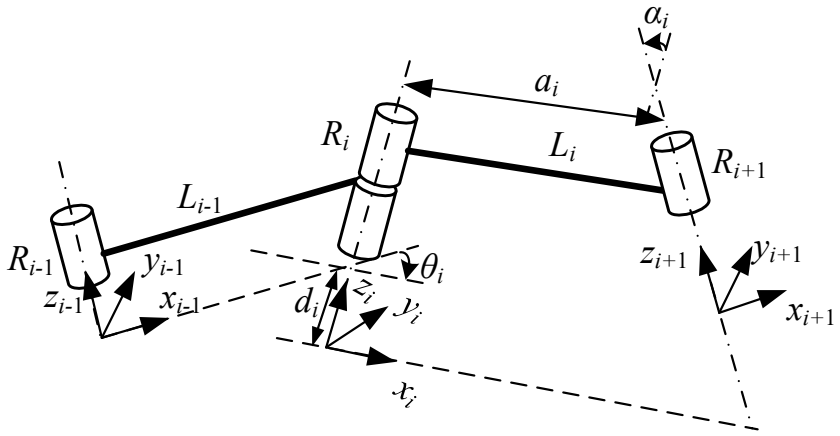

Fig. 2.2 D-H parameters

Four D-H parameters below are used to describe each link of the mechanism:

a) *a_i = the distance from z_i to z_{i+1} measured along x_i.*

b) *α_i = the angle between z_i and z_{i+1} measured about x_i.*

c) *d_i = the distance from x_{i-1} to x_i measured along z_i.*

d) *θ_i = the angle between x_{i-1} to x_i measured about z_i .*

The transfer matrix ${}^{i-1}_{i}T$ from $(i\text{-}1)^{\text{th}}$ local frame to i^{th} local frame can be obtained by moving d_i along z_i, rotating θ_i about z_i, moving a_{i-1} along x_i and rotating α_{i-1} about x_i.

$$ {}^{i-1}_{i}T = T_x(a_{i-1})R_x(\alpha_{i-1})R_z(\theta_i)T_z(d_i) \tag{2.9} $$

where

$$ T_x(a_{i-1}) = \begin{bmatrix} 1 & 0 & 0 & a_{i-1} \\ 0 & 1 & 0 & 0 \\ 0 & 0 & 1 & 0 \\ 0 & 0 & 0 & 1 \end{bmatrix} $$

$$ R_x(\alpha_{i-1}) = \begin{bmatrix} 1 & 0 & 0 & 0 \\ 0 & C\alpha_{i-1} & -S\alpha_{i-1} & 0 \\ 0 & S\alpha_{i-1} & C\alpha_{i-1} & 0 \\ 0 & 0 & 0 & 1 \end{bmatrix} $$

$$ R_z(\theta_i) = \begin{bmatrix} C\theta_i & -S\theta_i & 0 & 0 \\ S\theta_i & C\theta_i & 0 & 0 \\ 0 & 0 & 1 & 0 \\ 0 & 0 & 0 & 1 \end{bmatrix} $$

$$T_z(d_i) = \begin{bmatrix} 1 & 0 & 0 & 0 \\ 0 & 1 & 0 & 0 \\ 0 & 0 & 1 & d_i \\ 0 & 0 & 0 & 1 \end{bmatrix}$$

where *C* and *S* stand, respectively, for the cosine and the sine of the angles. The transfer matrix is obtained as:

$$T = \begin{bmatrix} C\theta_i & -S\theta_i & 0 & a_{i-1} \\ C\alpha_{i-1}S\theta_i & C\alpha_{i-1}C\theta_i & -S\alpha_{i-1} & -d_iS\alpha_{i-1} \\ S\alpha_{i-1}S\theta_i & S\alpha_{i-1}C\theta_i & C\alpha_{i-1} & d_iC\alpha_{i-1} \\ 0 & 0 & 0 & 1 \end{bmatrix} \tag{2.10}$$

The position vector of the i^{th} link in the $(i\text{-}1)^{th}$ local coordinate frame ${}^{i-1}\boldsymbol{P_i}$ can be obtained by multiplying the position vector of the i^{th} link in the i^{th} local coordinate frame ${}^{i}\boldsymbol{P_i}$ and the transfer matrix ${}^{i-1}_{i}T$ in homogeneous form as

$$\begin{Bmatrix} {}^{i-1}\boldsymbol{P_i} \\ 1 \end{Bmatrix} = {}^{i-1}_{i}T \begin{Bmatrix} {}^{i}\boldsymbol{P_i} \\ 1 \end{Bmatrix} \tag{2.11}$$

The position vector of the i^{th} link in the global coordinate frame can be calculated as

$$\begin{Bmatrix} \boldsymbol{P_i} \\ 1 \end{Bmatrix} = {}^{0}_{1}T\,{}^{1}_{2}T\,{}^{2}_{3}T\,{}^{3}_{4}T \cdots {}^{i-1}_{i}T \begin{Bmatrix} {}^{i}\boldsymbol{P_i} \\ 1 \end{Bmatrix} \tag{2.12}$$

It is noted that in a closed-loop mechanism, the product of the transfer matrices equals the identity matrix, which means

$${}^{i}_{1}T\,{}^{1}_{2}T\,{}^{2}_{3}T\,{}^{3}_{4}T \cdots {}^{i-1}_{i}T = I \tag{2.13}$$

2.1.4 Optimization Toolbox of MATLAB

To obtain the minimum value of a constrained nonlinear function with multiple variables, the optimization toolbox 'fmincon' of MATLAB is adopted. The objective function is in the format of *fun* = *f*(*x*(1), *x*(2)…*x*(*n*)). The optimization results can be yielded by using the programming solver of

$$[x, fval] = fmincon(fun, x0, [], [], [], [], lb, ub, nonlcon, options)$$

where *x* starts from *x*0 and attempts to find a minimizer *x* of the function. *lb* and *ub* are a set of lower and upper bounds on the design variable. The obtained result is a set of variables that satisfies the constraints, and the minimum value of the objective function.

2.2 Mass Moment Substitution

In the process of balancing mechanisms using the geometric method, the mass of certain links can be replaced by several equivalent masses located on the axes of the joints. As a consequence, the mass of the link is distributed onto its adjacent links. Using the mass

moment substitution methods, one can reduce the static balancing of mechanisms to that of several serial or tree-like kinematic chains. Three cases in which the link has two R joints with parallel axes, intersecting axes or skew axes will be presented respectively.

2.2.1 Mass Moment Substitution of an RR Link with Parallel Joint Axes

The mass moment substitution of an RR link with two parallel joint axes is shown in Fig. 2.3. The joint axes of R_i and R_{i+1} are parallel. The i^{th} local coordinate frame is set at O, which is a point on the axis of R_i. z_i is along the joint axis of R_i and x_i is perpendicular to the plane defined by R_i and R_{i+1}. Suppose that the distance between R_i and R_{i+1} is t_0, the position vectors of the two point-masses expressed in the i^{th} local frame are [166]

$$\begin{cases} {}^{i}\boldsymbol{P}_{i1} = \{0 \quad 0 \quad t_1\}^T \\ {}^{i}\boldsymbol{P}_{i2} = \{0 \quad t_0 \quad t_2\}^T \end{cases} \tag{2.14}$$

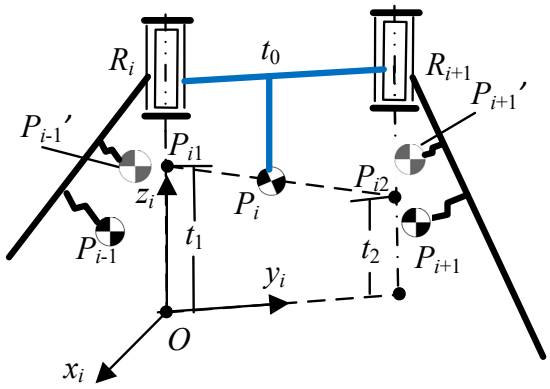

Fig. 2.3 Mass moment substitution of an RR link with parallel joint axes

The mass and mass moment (about O) of link i should be equal to those of the two point-masses. Therefore

$$\begin{cases} m_i = m_{i1} + m_{i2} \\ m_i g \ {}^{i}\boldsymbol{P}_{i} = m_{i1} g \ {}^{i}\boldsymbol{P}_{i1} + m_{i2} g \ {}^{i}\boldsymbol{P}_{i2} \end{cases} \tag{2.15}$$

The following conditions can be obtained by solving Eq. (2.15).

$$\begin{cases} a_i = 0 \\ t_1 = (c_i t_0 - b_i t_2)/(t_0 - b_i) \\ m_{i2} = m_i b_i / t_0 \\ m_{i1} = (m_i c_i - m_{i2} t_2)/t_1 \end{cases} \tag{2.16}$$

where $\{a_i \quad b_i \quad c_i\}^T$ represents the position of the CM of the i^{th} link with respect to the i^{th} local coordinate frame.

The mass of an RR link with parallel joint axes can be replaced by two equivalent masses on the two R joints when the CM of the link is on the plane defined by the two

axes of the *R* joints. Besides, the CM of the link and the two equivalent masses should be collinear. The position of the CM of the augmented $(i\text{-}1)^{th}$ link in the $(i\text{-}1)^{th}$ local frame can be obtained by combining the mass moment of the $(i\text{-}1)^{th}$ link and the first mass-point.

$$^{i-1}\boldsymbol{P}_{i-1}{}' = (m_{i-1}g^{i-1}\boldsymbol{P}_{i-1} + m_{i1}g^{i-1}\boldsymbol{P}_{i1})/(m_{i-1} + m_{i1})g \tag{2.17}$$

Similarly, the CM of the augmented $(i+1)^{th}$ link in the $(i+1)^{th}$ local frame can be calculated by

$$^{i+1}\boldsymbol{P}_{i+1}{}' = (m_{i+1}g^{i+1}\boldsymbol{P}_{i+1} + m_{i2}g^{i+1}\boldsymbol{P}_{i2})/(m_{i+1} + m_{i2})g \tag{2.18}$$

The positions of the CMs of the augmented links in the local frames are then obtained.

2.2.2 Mass Moment Substitution of an RR Link with Intersecting Joint Axes

The RR link with intersecting joint axes is shown in Fig. 2.4, the joint axes of R_i and R_{i+1} intersect at *O*. The angles between R_i and R_{i+1} are noted as α, the position vectors of the two mass-points in the i^{th} local frame can be yielded as [167]

$$\begin{cases} {}^{i}\boldsymbol{P}_{i1} = \{0 \quad 0 \quad t_1\}^T \\ {}^{i}\boldsymbol{P}_{i2} = \{0 \quad t_2S\alpha \quad t_2C\alpha\}^T \end{cases} \tag{2.19}$$

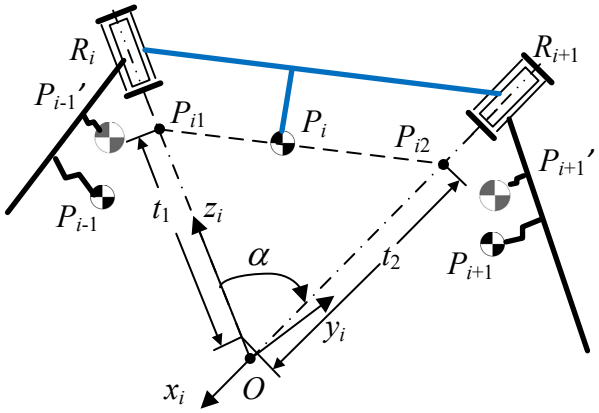

Fig. 2.4 Mass moment substitution of an RR link with intersecting joint axes

The following conditions are obtained by substituting Eq. (2.19) into Eq. (2.15).

$$\begin{cases} a_i = 0 \\ t_1 = t_2C\alpha(c_i tan\alpha - b_i)/(t_2S\alpha - b_i) \\ m_{i2} = m_i b_i / t_2 S\alpha \\ m_{i1} = (m_i c_i - m_{i2}t_2C\alpha)/t_1 \end{cases} \tag{2.20}$$

It is observed that the mass moment substitution conditions are: the CM of the link and the two R joints are coplanar and the CM of the link is on the line defined by the two mass-points.

2.2.3 Mass Moment Substitution of an RR Link with Skew Joint Axes

Moving R_{i+1} by t_0 along x_n in Section 2.2.2, the link with two skew R joints is obtained, as shown in Fig. 2.5. The angle and distance between R_i and R_{i+1} are denoted as α and t_0 respectively. O_{2P}, P_{i2P} and R_{ip} are the projections of O_2, P_{i2} and R_i on the z_iy_i plane.

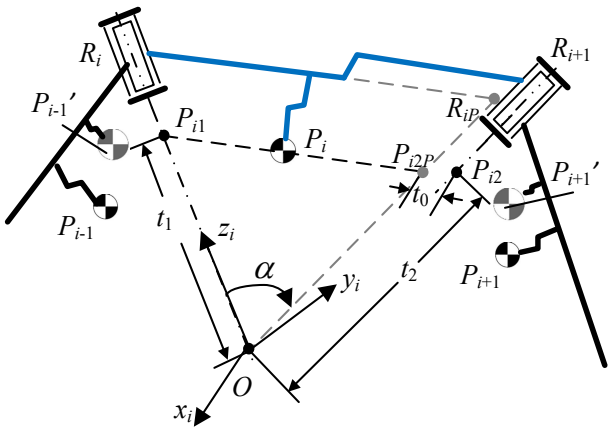

Fig. 2.5 Mass moment substitution of an RR link with skew joint axes

The position vectors of the two mass-points relative to the i^{th} local coordinate frame are represented by [168-169]

$$\begin{cases} {}^{i}\boldsymbol{P_{i1}} = \{0 \quad 0 \quad t_1\}^T \\ {}^{i}\boldsymbol{P_{i2}} = \{t_0 \quad t_2 S\alpha \quad t_2 C\alpha\}^T \end{cases} \tag{2.21}$$

The masses and the positions of the two point-masses are obtained as

$$\begin{cases} m_{i2} = m_i a_i / t_0 \\ m_{i1} = (m_i c_{ni} - m_{i2} t_2 C\alpha)/t_1 \\ t_2 = b_i t_0 / a_i S\alpha \\ t_1 = t_0(c_i tan\alpha - b_i)/tan\alpha(t_0 - a_i) \end{cases} \tag{2.22}$$

The CM of the link and the two masses point should be collinear.

2.3 Static Balancing Method and Its Extensions

In this section, the basic principle of static balancing will be introduced. The statically balanced 1-link manipulator will be presented and then the static balancing method will be extended to apply to the manipulators with multi-link and multi-DOF.

2.3.1 One-link Manipulator

According to [117], a link manipulator mounted to the base using an S joint can be statically balanced using only one zero-free-length spring. The spring connecting point $\boldsymbol{H}$ on the base is right above the S joint and the height is assumed to be h. $\boldsymbol{b}$ is the position vector of the spring connecting point on the manipulator and $\boldsymbol{r}$ is the position vector of the CM of the manipulator. Vectors $\boldsymbol{b}$ and $\boldsymbol{r}$ must be proportional [117], i.e.,

$$\boldsymbol{r} = (kh/mg)\boldsymbol{b} \tag{2.23}$$

where m, g and k represent the mass of the manipulator, the gravitational acceleration, and the stiffness of spring respectively. The spring connecting point on the manipulator should be on the line defined by the CM of the manipulator and the centre of the S joint [Fig. 2.6(a)]. $h = mg/k$ when attaching the spring to the CM of the manipulator directly, for the sake of convenience of calculation and description [Fig. 2.6(b)]. This condition can also apply to one-link manipulators with an R joint [104] or a universal (U) joint.

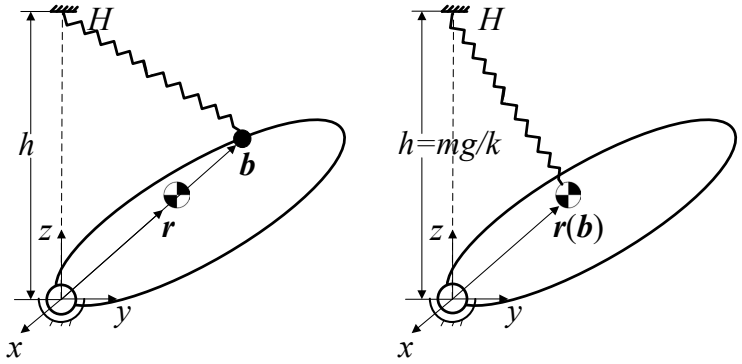

(a) (b)

Fig. 2.6 Statically balanced 3-DOF 1-link manipulator: (a) conditions in [117]; (b) attaching the spring to the CM of the manipulator

For the 1-link manipulator mounted to the base using an R joint, the spring can be attached to an arbitrary point right above the axis of the R joint. As shown in Fig. 2.7(a), the angle between the axis of the R joint and the vertical axis is denoted by α (with constant value), and the position of the CM of the manipulator in the local coordinate frame is $\{a\ b\ c\}^T$. $\boldsymbol{T}$ is a point on the axis of the R joint, $OT = t$. $\boldsymbol{H}$ is right above $\boldsymbol{T}$, with a distance of h. Now the special cases that no spring is required to balance the manipulator will be discussed.

The position of $\boldsymbol{T}$, $\boldsymbol{H}$ and the CM of the manipulator $\boldsymbol{P}$ are computed as

$$\boldsymbol{T} = \{0 \quad -tS\alpha \quad tC\alpha\}^T \tag{2.24}$$

$$\boldsymbol{H} = \{0 \quad -tS\alpha \quad tC\alpha + h\}^T \tag{2.25}$$

$$\boldsymbol{P} = \{aC\theta - bS\theta \quad bC\theta C\alpha - cS\alpha + aC\alpha S\theta \quad cC\alpha + bC\theta S\alpha + aS\theta S\alpha\}^T \tag{2.26}$$

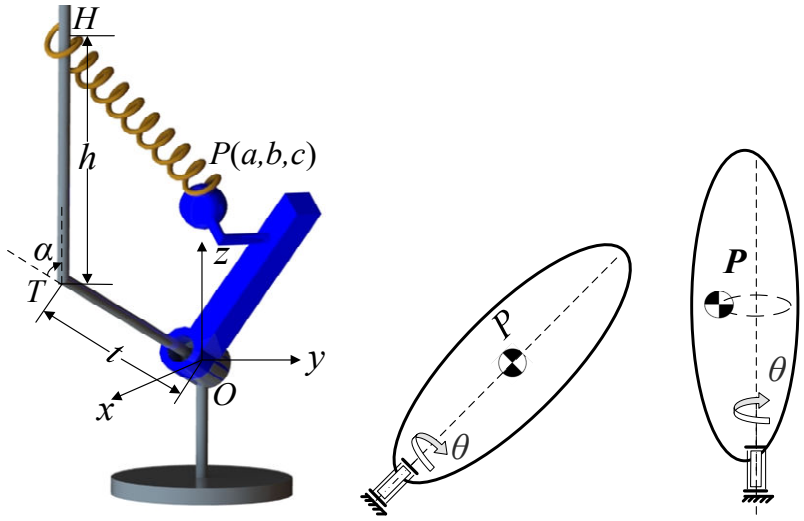

(a) (b) (c)

Fig. 2.7 Statically balanced 1-DOF 1-link manipulator: (a) the 3D model of the manipulator; (b) the CM of the link is on the joint axis; (c) the axis of the R joint is vertical

One spring is adopted, with one end attached to $\boldsymbol{H}$, and the other end to the CM of the manipulator. The potential energy of the link consists of two parts, including the potential energy associated with gravity (V_{mi}) and the elastic potential energy stored in the springs (V_{si}). The total potential energy of the manipulator is

$$V = \frac{1}{2}k|\boldsymbol{P}-\boldsymbol{H}|^2 + mgP_z = \frac{1}{2}k[a^2+b^2+h^2+(c-t)^2] + (-chk+cmg+hkt)C\alpha \\ -(hk-mg)S\alpha(bC\theta+aS\theta) \tag{2.27}$$

When the manipulator is statically balanced, the total potential energy should be constant. One can obtain that

$$h = mg/k \quad or \tag{2.28}$$

$$a = 0 \text{ and } b = 0 \text{ } or \text{ } \alpha = 0° \tag{2.29}$$

Eq. (2.29) indicates that the system is balanced if the CM of the link is on the joint axis [Fig. 2.7(b)], or the axis of the first R joint is vertical [Fig. 2.7(c)].

2.3.2 Two-link Manipulators with 2-DOF

Based on the static balancing method of the 1-link manipulator above, the multi-link manipulator with multiple DOFs constructed using the 1-link manipulator can also be balanced. In this section, the static balancing approach of several 2-link manipulators with 2-DOF will be introduced.

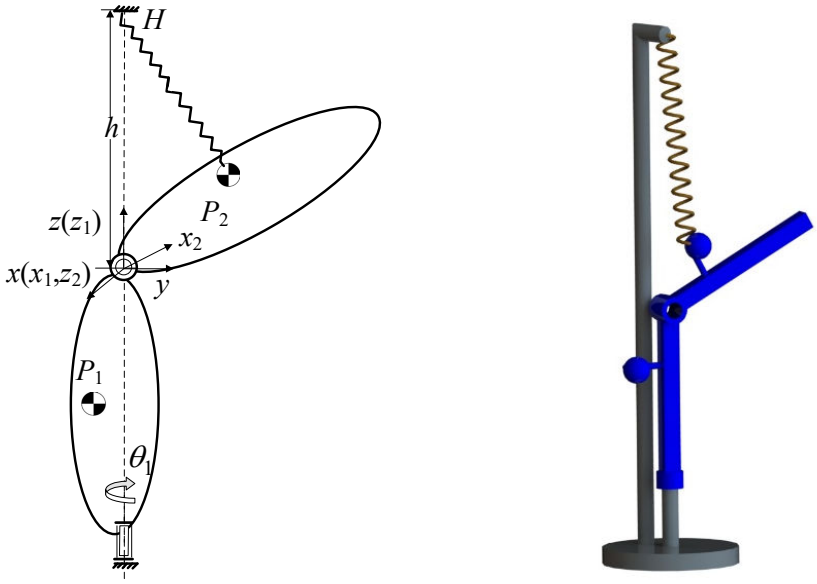

(a) (b)

Fig. 2.8 Statically balanced 2-link manipulator with yaw-roll rotation: (a) the sketch of the manipulator; (b) the 3D model of the manipulator

The 2-link manipulator with yaw-roll rotation is presented in Fig. 2.8. The manipulator is constructed using the two 1-link manipulators in Fig. 2.7(a) and Fig. 2.7(c) respectively. It has been proved that the manipulator in Fig. 2.7(c) has no need to balance, so only one spring is used to balance the 2-link manipulator with yaw-roll rotation. One end of the spring is attached to H, which is fixed on link 1 and is right above R_2 with a height of h ($h = m_2g/k$), the other end is attached to P_2.

A fixed coordinate frame is attached to the base, with its origin at the intersection of the axes of the two R joints, and the z-axis is pointing vertically upward. Suppose the position vector of the CM of the i^{th} link in the local frame i is represented by

$$^{i}\boldsymbol{P_i} = \{a_i \quad b_i \quad c_i\}^T \tag{2.30}$$

The position vectors of the global CMs of the two links are calculated using the D-H approach as

$$\boldsymbol{P_1} = \{a_1C\theta_1 - b_1S\theta_1 \quad b_1C\theta_1 + a_1S\theta_1 \quad c_1\}^T \tag{2.31}$$

$$\boldsymbol{P_2} = \{P_{2x} \quad P_{2y} \quad -b_2C\theta_2 - a_2S\theta_2\}^T \tag{2.32}$$

where

$$P_{2x} = a_2C\theta_1C\theta_2 - b_2C\theta_1S\theta_2 - c_2S\theta_1$$

$$P_{2y} = a_2C\theta_2S\theta_1 - b_2S\theta_1S\theta_2 + c_2C\theta_1$$

The spring connecting point H on the base is given by

$$\boldsymbol{H} = \{0 \quad 0 \quad m_2g/k\}^T \tag{2.33}$$

The total potential energy of the manipulator is obtained as

$$V = V_s + V_m = \frac{1}{2}k|\boldsymbol{P_2} - \boldsymbol{H}|^2 + m_2 g P_{2z} + m_1 g P_{1z}$$
$$= (a_2^2 k^2 + b_2^2 k^2 + c_2^2 k^2 + m_2^2 g^2)/2k + m_1 g c_1 \quad (2.34)$$

Eq. (2.34) verifies the system is constant in any configurations. Similarly, the manipulator in Fig. 2.9 in which the first link is horizontal is balanced. Instead of attaching the spring to the CM of the link, the attachment point B_2 can be any point on the line defined by P_2 and R_2.

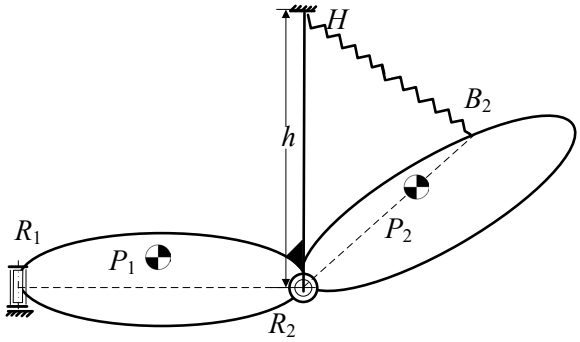

Fig. 2.9 Statically balanced 2-link manipulator with yaw-roll rotation II

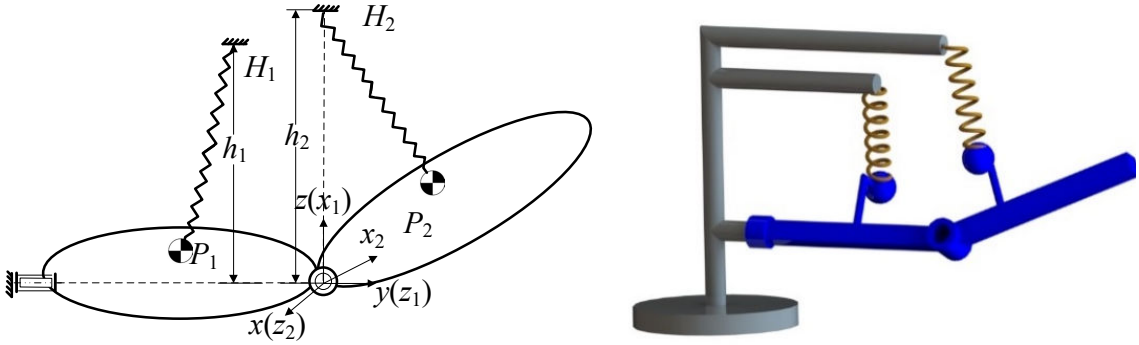

(a) (b)

Fig. 2.10 Statically balanced 2-link manipulator with pitch-roll rotation: (a) the sketch of the manipulator; (b) the 3D model of the manipulator

The manipulator with pitch-roll rotation is shown in Fig. 2.10. It consists of two moving links connected by two R joints with intersecting and orthogonal axes. The first link rotates around the *y*-axis which is horizontal and the axis of the second R joint is perpendicular to the axis of the first R joint.

Two springs are used to balance the two links of the manipulator respectively. The spring connecting point on the base $\boldsymbol{H}_1$ for balancing of the first link can be any point right above the axis of first R joint. The other end is attached to the CM of the first link. One end of the second spring $\boldsymbol{H}_2$ is located on the vertical axis passing through the intersection of the two R joints, the other end is fixed on the CM of the second link.

The position vectors of the CMs of the links in the global coordinate frame can be obtained as

$$\boldsymbol{P_1} = \{-b_1 S\theta_1 + a_1 C\theta_1 \quad c_1 \quad -a_1 S\theta_1 - b_1 C\theta_1\}^T \tag{2.35}$$

$$\boldsymbol{P_2} = \{P_{2x} \quad -b_2 C\theta_2 - a_2 S\theta_2 \quad P_{2z}\}^T \tag{2.36}$$

where

$$P_{2x} = a_2 C\theta_2 C\theta_1 - b_2 C\theta_1 S\theta_2 - c_2 S\theta_1$$

$$P_{2z} = -a_2 S\theta_1 C\theta_2 + b_2 S\theta_1 S\theta_2 - c_2 C\theta_1$$

The springs connecting points $\boldsymbol{H_1}$ and $\boldsymbol{H_2}$ on the base are given by

$$\boldsymbol{H_1} = \{0 \quad -s \quad m_1 g/k\}^T \tag{2.37}$$

$$\boldsymbol{H_2} = \{0 \quad 0 \quad m_2 g/k\}^T \tag{2.38}$$

The total potential energies of both links are expressed as

$$V_1 = V_{s1} + V_{m1} = \frac{1}{2} k|\boldsymbol{P_1} - \boldsymbol{H_1}|^2 + mgP_{1z} = (a_1^2 k^2 + b_1^2 k^2 + c_1^2 k^2 + m_1^2 g^2 + 2c_1 s k^2 + s^2 k^2)/2k \tag{2.39}$$

$$V_2 = V_{s2} + V_{m2} = \frac{1}{2} k|\boldsymbol{P_2} - \boldsymbol{H_2}|^2 + mgP_{2z} = (a_2^2 k^2 + b_2^2 k^2 + c_2^2 k^2 + m_2^2 g^2)/2k \tag{2.40}$$

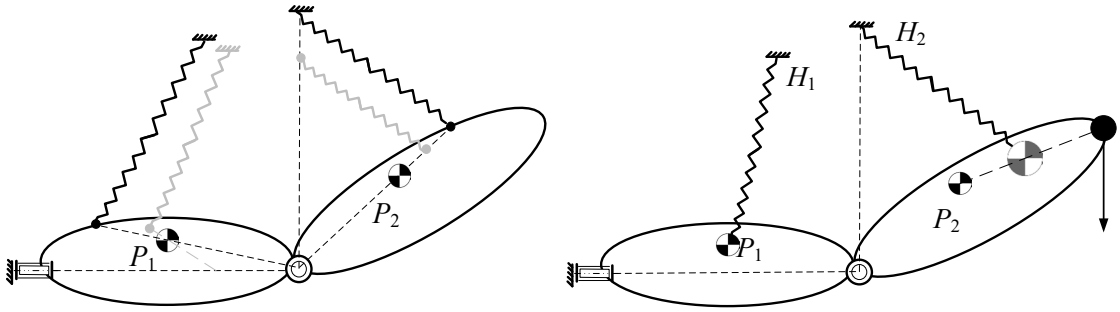

(a) (b)

Fig. 2.11 Extensions of the statically balanced 2-link manipulator with pitch-roll rotation: (a) attaching the spring to the point that is on the line defined by the joint and the CM of the link (two solutions); (b) with additional payload

Eqs. (2.39-2.40) verify the feasibility of the balancing method for the 2-link manipulators with pitch-roll rotation. It is noteworthy that the spring connecting point on the link can be any point on the line defined by the joint and the CM of the link, as shown in Fig. 2.11(a). If an additional payload is added, as shown in Fig. 2.11(b), the method still works by identifying the combined CM of the second link.

2.3.3 Multi-link Manipulators with 3-DOF

Based on the results in Section 2.3.1 and 2.3.2, multi-link manipulators with 3-DOF can also be balanced. In this section, statically balanced manipulators with two links assembled on one R joint and one universal (U) joint, and those with three links connected using three R joints are presented. The axes of the R joints, including the ones within the U joint, are always perpendicular to each other in the initial state.

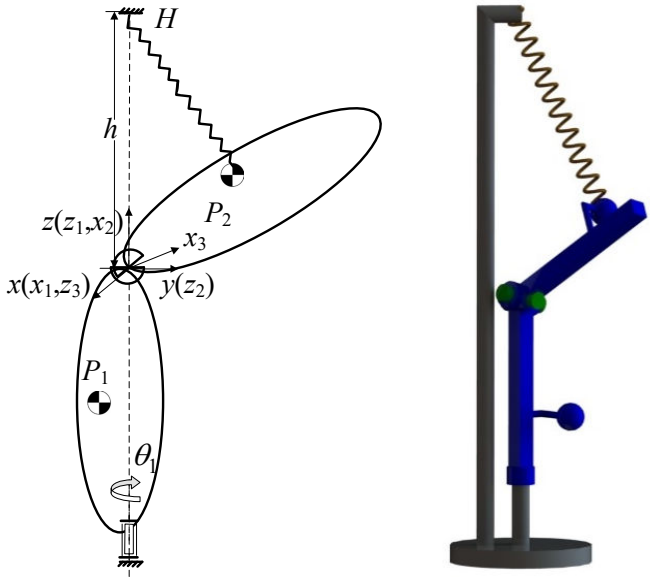

(a) (b)

Fig. 2.12 Statically balanced 2-link manipulator with yaw-pitch-roll rotation: (a) the sketch of the manipulator; (b) the 3D model of the manipulator

The manipulator with yaw-pitch-roll rotation is constructed using a 1-link manipulator in Fig. 2.7(c) and a 1-link manipulator mounted on a U joint, as shown in Fig. 2.12. The first R joint is along z-axis which is pointing vertically upward and the two axes of the U joint are on the plane that perpendicular to the R joint in the initial state. The position vectors of the global CMs of the links are

$$\boldsymbol{P_1} = \{a_1C\theta_1 - b_1S\theta_1 \quad b_1C\theta_1 + a_1S\theta_1 \quad c_1\}^T \tag{2.41}$$

$$\boldsymbol{P_2} = \{P_{2x} \quad P_{2y} \quad -a_2C\theta_2C\theta_3 + b_2C\theta_2S\theta_3 - c_2S\theta_2\}^T \tag{2.42}$$

where

$$P_{2x} = S\theta_1(b_2C\theta_3 + a_2S\theta_3) + C\theta_1[-c_2C\theta_2 + S\theta_2(a_2C\theta_3 - b_2S\theta_3)]$$

$$P_{2y} = -C\theta_1(b_2C\theta_3 + a_2S\theta_3) + S\theta_1[-c_2C\theta_2 + S\theta_2(-a_2C\theta_3 + b_2S\theta_3)]$$

The springs connecting point $\boldsymbol{H}$ on the base is

$$\boldsymbol{H} = \{0 \quad 0 \quad m_2g/k\}^T \tag{2.43}$$

Only one spring is needed to balance the manipulator. The total potential energy of the system is expressed as

$$V = V_s + V_m = \frac{1}{2}k|\boldsymbol{P_2} - \boldsymbol{H}|^2 + m_2 g P_{2z} + m_1 g P_{1z} \\ = (a_2^2k^2 + b_2^2k^2 + c_2^2k^2 + m_2^2g^2)/2k + m_1 g c_1 \tag{2.44}$$

which is a constant. Similarly, the manipulator in Fig. 2.13 is balanced.

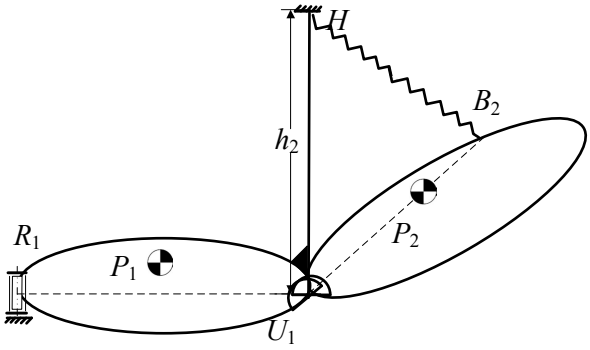

Fig. 2.13 Statically balanced 2-link manipulator with yaw-pitch-roll rotation

The manipulator with pitch-yaw-roll rotation is shown in Fig. 2.14. The axis of the R joint is on the horizontal plane and the two axes of the U joint are on the plane that is perpendicular to the axis of the R joint in the initial state.

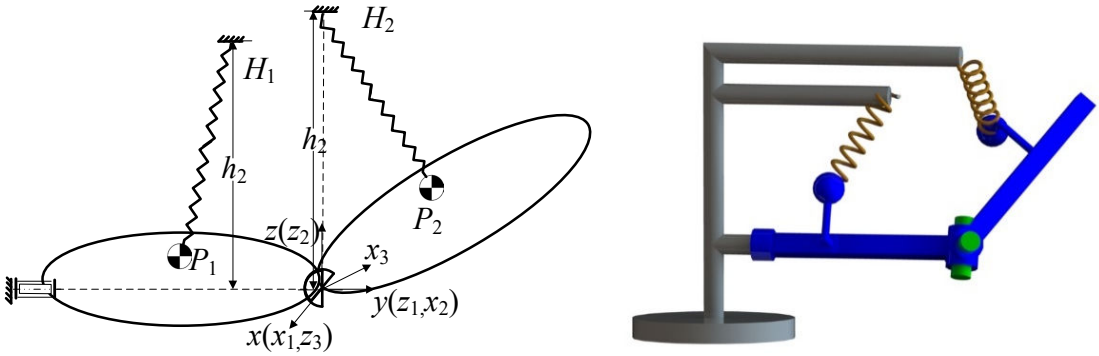

(a) (b)

Fig. 2.14 Statically balanced 2-link manipulator with pitch-yaw-roll rotation: (a) the sketch of the manipulator; (b) the 3D model of the manipulator

Two springs are used to balance the two links of the manipulator respectively. Like the 2-DOF 2-link manipulator, one end of each spring is attached right above the joint, while the other end is fixed on the CM of the link.

The position vectors of the CMs of the two links are obtained as

$$\boldsymbol{P_1} = \{a_1C\theta_1 - b_1S\theta_1 \quad c_1 \quad -a_1S\theta_1 - b_1C\theta_1\}^T \tag{2.45}$$

$$\boldsymbol{P_2} = \{P_{2x} \quad b_2C\theta_2S\theta_3 - a_2C\theta_2C\theta_3 - c_2S\theta_2 \quad P_{2z}\}^T \tag{2.46}$$

where

$$P_{2x} = S\theta_1(b_2C\theta_3 + a_2S\theta_3) + C\theta_1[-c_2C\theta_2 + S\theta_2(a_2C\theta_3 - b_2S\theta_3)]$$
$$P_{2z} = C\theta_1(b_2C\theta_3 + a_2S\theta_3) + S\theta_1[c_2C\theta_2 + S\theta_2(-a_2C\theta_3 + b_2S\theta_3)]$$

The spring connecting points $\boldsymbol{H_1}$ and $\boldsymbol{H_2}$ on the base are

$$\boldsymbol{H_1} = \{0 \quad -s \quad m_1g/k\}^T \tag{2.47}$$

$$\boldsymbol{H_2} = \{0 \quad 0 \quad m_2g/k\}^T \tag{2.48}$$

The potential energies of the two links are

$$\begin{aligned} V_1 = V_{s1} + V_{m1} = \tfrac{1}{2}k|\boldsymbol{P_1} - \boldsymbol{H_1}|^2 + mgP_{1z} \\ = (a_1^2k^2 + b_1^2k^2 + c_1^2k^2 + m_1^2g^2 + 2c_1sk^2 + s^2k^2)/2k \end{aligned} \tag{2.49}$$

$$V_2 = V_{s2} + V_{m2} = \tfrac{1}{2}k|\boldsymbol{P_2} - \boldsymbol{H_2}|^2 + mgP_{2z} = (a_2^2k^2 + b_2^2k^2 + c_2^2k^2 + m_2^2g^2)/2k \tag{2.50}$$

The results imply that the manipulator with pitch-yaw-roll rotation is statically balanced through its range of motion.

The manipulators in Figs. 2.15 and 2.16 are constructed using the 1-link manipulator in Fig. 2.7 (c) and the 2-link manipulator in Fig. 2.10. Similarly, the first link has no need to balance, and the second link and the third link can be balanced using two springs.

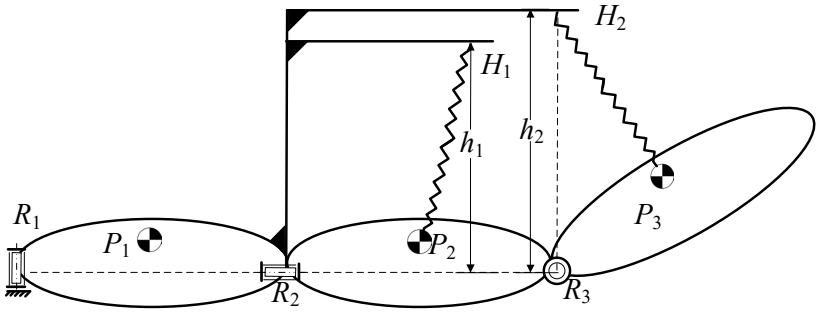

Fig. 2.15 Statically balanced 3-link manipulator with yaw-roll-pitch rotation I

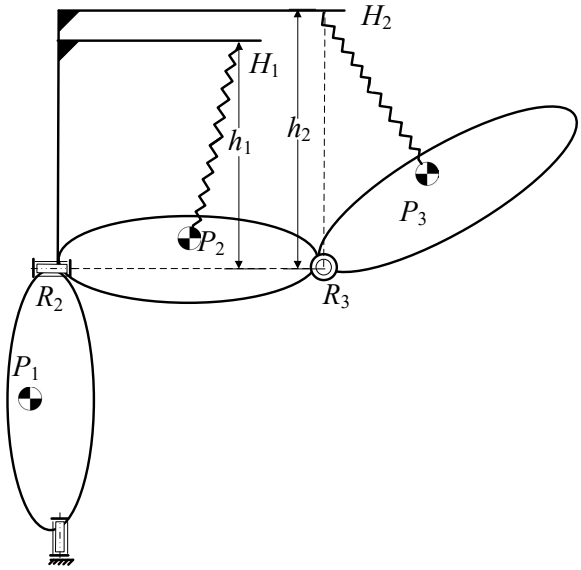

Fig. 2.16 Sketch of the 3-link manipulator with yaw-roll-pitch rotation II

2.4 Summary

In this chapter, the theoretical tools, including the calculation of the distance, DOF and kinematic analysis and the optimization tools, have been introduced. The optimization tools will be used on the calculations of the minimum of the potential energy variance to obtain the positions of the attachment of the springs. The fundamentals of static balancing of the manipulators, including the 1-link, 2-link and 3-link manipulators, have been discussed. The static balancing approaches proposed in this thesis will be based on the above statically balanced manipulators.

CHAPTER 3 – TYPE SYNTHESIS OF DEPLOYABLE SINGLE-LOOP 8R LINKAGES WITH MULTIPLE MODES

In this section, a novel construction method for the single-loop foldable mechanisms with multiple modes will be introduced. Two types of 8R mechanisms can be obtained using the proposed method.

3.1 Construction Method

The mechanisms can be fully folded by offsetting the panels away from the planes defined by the joints (offset distance d is equal to one half of the thickness of the panel). The modified planar 4R linkage and spherical 4R linkage are presented in Fig. 3.1.

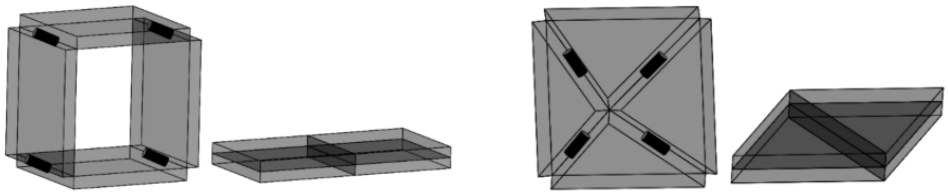

(a) (b)

Fig. 3.1 Mono-mode foldable mechanisms: (a) planar 4R linkage; (b) spherical 4R linkage

A spatial foldable 8R mechanism 1-5-2-6-3-7-4-8 can be obtained by connecting two foldable 4R linkages 1-2-3-4 and 5-6-7-8. The first type of 8R mechanisms is constructed by combining two spherical 4R linkages, as shown in Fig. 3.2(a). The second type of 8R mechanisms is designed by connecting a planar 4R linkage and a spherical 4R linkage, as shown in Fig. 3.2(b). The two 4R linkages are staggered rather than connecting consecutively for two reasons: the former configuration is symmetric and the latter one cannot be spread onto a plane.

The two types of 8R mechanisms are listed in Table 3.1. The orders of wrench systems and the DOF analysis are also given, using the formula described in Section 2.1.2. It is noted that the DOF obtained is the instantaneous DOF. The singular positions will be identified.

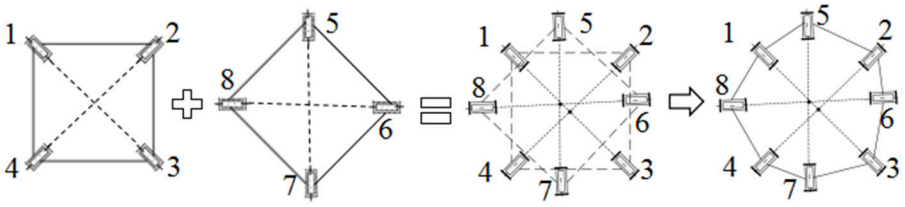

(a)

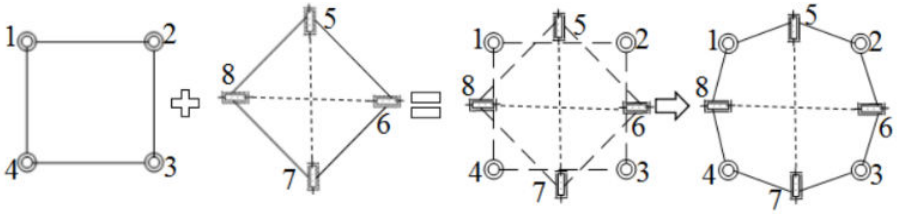

(b)

Fig. 3.2 Spatial 8R mechanisms: (a) type I; (b) type II

Table 3.1. The obtained foldable 8R mechanisms

Type	*Mechanism*	*Order of wrench system*	*M*
Spherical 4R -spherical 4R mechanism	(1)	*λ=4 (singular positions)*	*M=6*
		λ=3 (general positions)	*M=5*
	(2)	*λ=2 (singular positions)*	*M=4*
		λ=1 (general positions)	*M=3*
Spherical 4R -planar 4R mechanism	(3)	*λ=1 (singular positions)*	*M=3*
		λ=0 (general positions)	*M=2*
	(4) (5) (6)	*λ=0*	*M=2*

3.2 Double-centred 8R Mechanism

Figure 3.3 shows an origami that we see frequently. We regard the panels as rigid bodies and the creases as revolute joints, then the origami turns into a 16-bar linkage. An 8R mechanism which is the first mechanism in Table 3.1 can be achieved by removing the outer eight links. All the revolute joints of the mechanism are on the same plane and intersect at one point when spread. The instantaneous DOF of the mechanism is 5 and is 6 when spread.

(a) (b)

Fig. 3.3 Design process of the mechanism: (a) 16-link origami; (b) single-centred 8R mechanism evolved from origami

To have better foldability, several approaches can be adopted, such as offsetting the R joints or using flexible joints. A prototype of the single-centred 8R mechanism of which the revolute joints are designed with soft materials is shown in Fig. 3.4. It can be seen from Figs. 3.4(b-c) that the mechanism can be fully folded. Another merit of the prototype with flexible joints is that they can recover to the initial state after working. The structure is the same as the waterbomb base in [41].

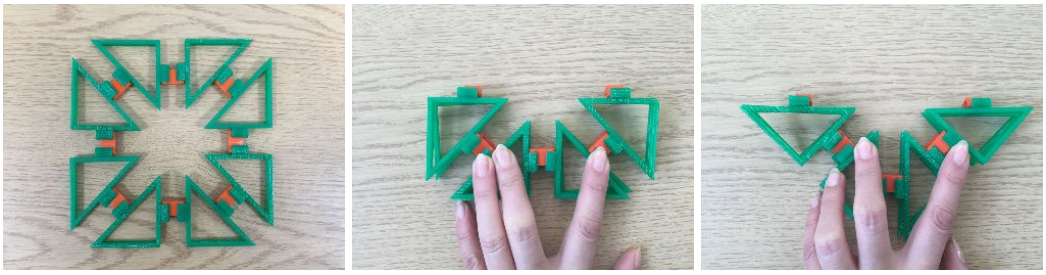

(a) (b) (c)

Fig. 3.4 Single-centred 8R mechanism with compliant joints: (a) spread state; (b-c) folded states

Another method is to offset the R joints. The resulting mechanism is a double-centred 8R mechanism. As shown in Fig. 3.5, the panels are designed in a shape of the isosceles right triangle and are connected to another two panels by two joints that are mounted at the base and the hypotenuse of the triangle. The angle between the two joints is 45 degrees and the distance between them is equal to the thickness of the panels. As a consequence, the axes of joints 1, 2, 3 and 4 intersect at a point, while those of 5, 6, 7 and 8 intersect at another point. The projections of all the joints onto the ground plane intersect at a point. The initial state of the mechanism, which is a singular configuration is referred to the position when spread onto a plane. In the initial state, the two planes that are generated by the axes of the joints of the two spherical 4R linkages respectively are parallel with

the plane defined by the panels. The line defined by the two centres of the two spherical 4R linkages are perpendicular to the plane defined by the joint axes of each spherical 4R linkage.

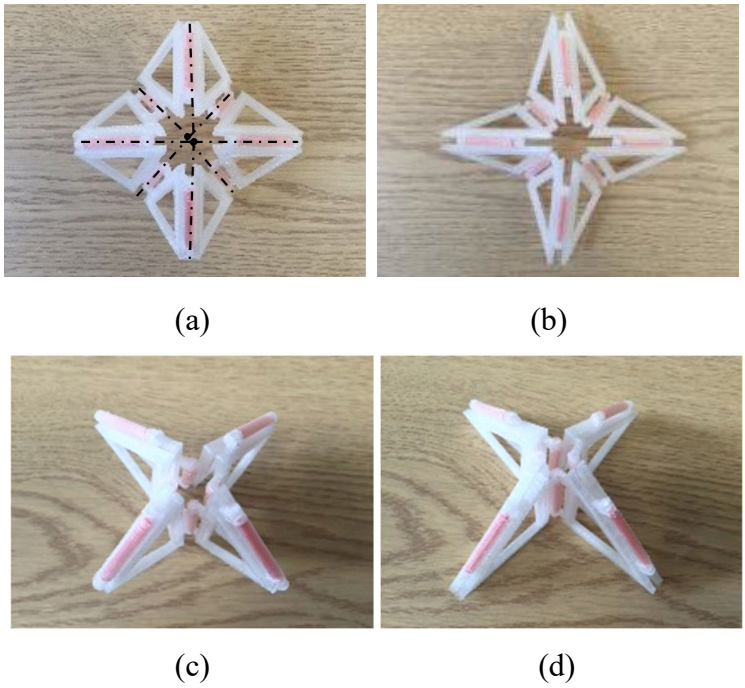

(a) (b)

(c) (d)

Fig. 3.5 Double-centred 8R mechanism: (a-b) spherical 4R linkage modes; (c-d) planar 4R linkage modes

The mechanism can behave as: (a) spherical 4R linkages when driving joints 5, 6, 7 and 8 (or 1, 2, 3 and 4) synchronously and then locking the joints of one of the spherical 4R linkages [Figs. 3.5(a-b)]; (b) planar 4R linkages when actuating joints 5, 6, 7 and 8 (1, 2, 3 and 4) to be parallel and locking joints 1, 2, 3 and 4 (5, 6, 7 and 8), as shown in Figs. 3.5(c-d); and (c) spatial 8R linkage. The DOF of the mechanism is 4 in the initial state (singular position) and reduces to 3 in other positions. The mechanism can be folded into two layers as shown in Fig. 3.6(b) when rotating joints 6 and 8 (or 5 and 7). In this position, $R_1//R_4$ (the axes of R joint 1 and 4 are parallel), $R_5//R_7$ and $R_2//R_3$. It can also be folded into four layers as shown in Fig. 3.6(c) in which state $R_5//R_6//R_7//R_8$. Following a similar procedure, when folding along axes of joints 1 and 3 (or 2 and 4), the mechanism deforms into the position in Fig. 3.6(d) and can be deployed into the posture in Fig. 3.6(e). The pins for the axes of the revolute joints are manufactured with soft material in order to easily assemble and disassemble the mechanism without breaking the rigid part. This flexible pin provides a novel method to design easy-assemble revolute joints without changing the kinematic characteristics of the mechanism, considering the pins barely have deformation along the directions that are perpendicular to the axis of the pin.

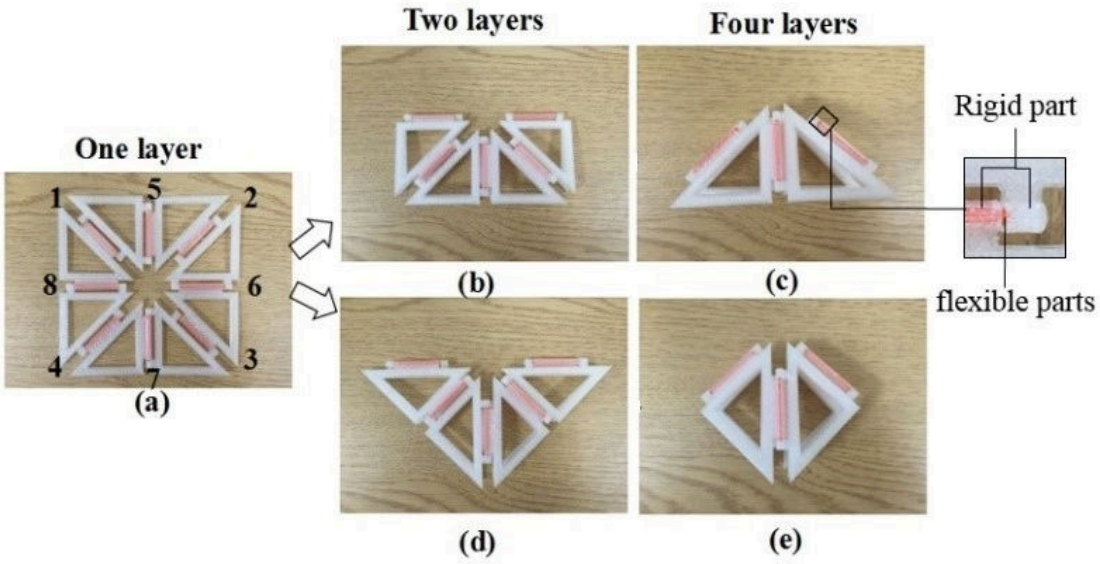

Fig. 3.6 Folding process of the double-centred 8R mechanism

3.3 Perpendicular-axis 8R Mechanism

Combining a spherical 4R linkage and a planar 4R linkage, a perpendicular-axis 8R mechanism shown in Fig. 3.7(a) can be obtained. This mechanism has been discussed in [80]. The two joints on the same panels are designed at the base and the vertex of the triangle links and are perpendicular to each other. In the initial configuration, $R_1//R_2//R_3//R_4$, joints 5, 6, 7 and 8 lie on the same plane and intersect at a point. The axes of joints 5 and 7 are collinear, those of 6 and 8 are also collinear, and R_5 is perpendicular to R_6. The instantaneous DOF of the mechanism is three in this position.

To improve the foldability, a novel mechanism which is a variation of the perpendicular-axis 8R mechanism is designed as follows. Starting from the configuration when the mechanism is spread onto a plane [Fig. 3.7(a)], lift modules A and C by a distance h, which is the thickness of the panels, apart from B and D along the direction that is perpendicular to the panels [Fig. 3.7(b)]. As a consequence, the axes of joints 5, 6, 7 and 8 are on the same plane and intersect at two points in the initial configuration, $R_5//R_7$, and $R_6//R_8$. The order of the wrench system in this configuration is zero and the DOF of the mechanism is two. The configuration can be further modified into the one shown in Fig. 3.8(a), in which joints 1, 2, 3 and 4 are offset away from the central planes of the panels and the panels are cut to enable the links connected by R_5 to be embedded into the links connected by R_7 in the folding process. An additional part is assembled to assure concentric of joint R_7.

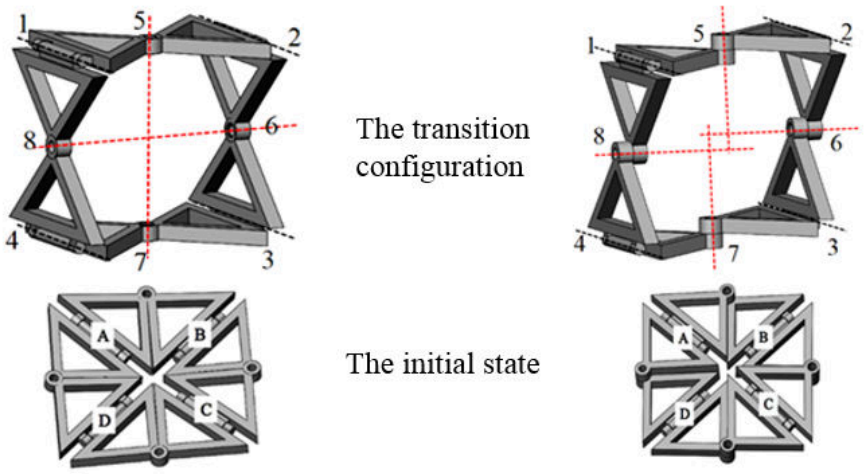

Fig. 3.7 Perpendicular-axis 8R mechanism: (a) the mechanism in [80]; (b) the variation of the mechanism

The mechanism has three modes: (a) planar 4R linkage mode [Fig. 3.8(a)] when locking joints 5, 6, 7 and 8 in the initial configuration, (b) spherical 4R linkage mode when the axes of joints 5, 6, 7 and 8 intersect at a point and joints 1, 2, 3 and 4 are locked [Fig. 3.8(f)], (c) spatial 8R linkage mode. In the spherical linkage mode, the axes of joints 1, 2, 3 and 4 of the mechanism in [80] have a common point, so do joints 5, 6, 7 and 8. While only the axes of joints 5, 6, 7 and 8 intersect at a point in the proposed mechanism.

When rotating R_6 and R_8 in the initial configuration, the mechanism turns into the position in which $R_1 \perp R_4$ (the axes of R joints 1 and 4 are perpendicular to each other), $R_2 \perp R_3$ and $R_5 \perp R_7$, as shown in Fig. 3.8(b). Then locking R_6 and R_8, the mechanism deforms into a 1-DOF triple-centred six-bar linkage. By rotating R_5 clockwise or anticlockwise, the 6R linkage can be spread into one layer, when $R_5//R_6//R_7//R_8$, joints 1, 2, 3 and 4 are on two parallel planes and their projections on any one of planes that are perpendicular to joints 5, 6, 7 and 8 intersect in a point, as shown in Fig. 3.8(g), or be folded into two layers in which the projections of joints 1, 2, 3 and 4 on the ground plane generate a square, joints 5, 6, 7 and 8 are parallel without the consideration of interference [see Fig. 3.8(c)].

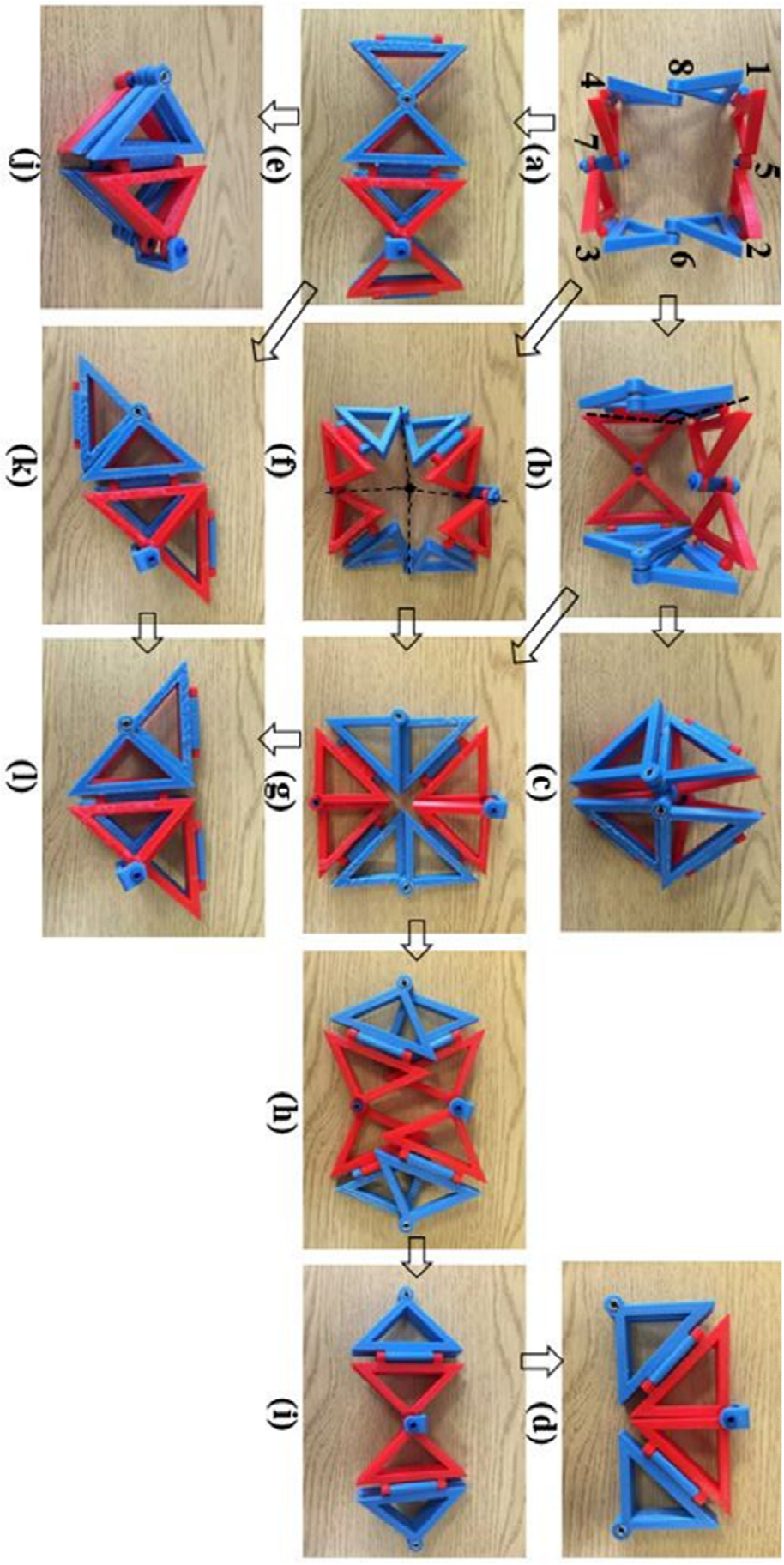

Fig. 3.8 Folding process of variation of perpendicular-axis 8R mechanism

The mechanism can be folded into two layers through two approaches by alternatively fixing joints 5, 6, 7 and 8 and rotating any one of joints 1, 2, 3 and 4 in the initial configuration [Fig. 3.8(e)] or rotating any one of joints 5, 6, 7 and 8 when the mechanism is in its spread state [Figs. 3.8(h) and (i)]. In the two folded states, joints 1, 2, 3 and 4 are parallel with each other, joints 5, 6, 7 and 8 are also parallel. The configuration in Fig. 3.8(i) deforms to the posture in Fig. 3.8(d) by driving R_5 and R_7 90 degrees. Then the configuration in Fig. 3.8(e) can be turned into the ones in Figs. 3.8(k) and (l) and further be folded into four layers which is shown in Fig. 3.8(j) by actuating joints 5, 6, 7 and 8. In this state, joints 1, 2, 3 and 4 are on a plane that is perpendicular to the planes of the panels, as well as the plane defined by the axes of joints 5, 6, 7 and 8.

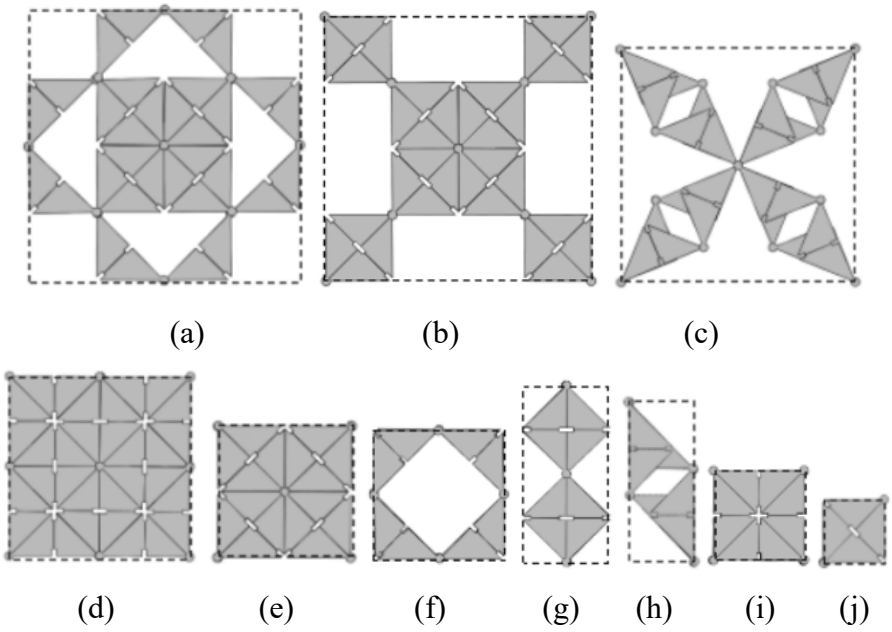

Fig. 3.9 32-bar mechanism

Since the side of the triangle is longer than its height, the process of folding into four layers of this prototype is achieved using clearance. If we change the shapes of the panels, for example rounding the base angle of the triangles, the mechanism can be folded into four layers without utilizing the clearance. The folding radio between the maximum volume [the cube into which the mechanism would exactly fit, shown in Fig. 3.8(a)] and the minimum volume [shown in Fig. 3.8(j)] is $r \approx 9.54$. This shows that the mechanism has excellent folding performance.

Cutting the links of the mechanism in Fig. 3.7(a) in half, reassembling the mechanism, and overlapping four mechanisms, then the 32-bar mechanism in Fig. 3.9 is obtained. The

folding ratio between the maximum area [shown in Fig. 3.9(a)] and the minimum area [shown in Fig. 3.9(j)] of the mechanism $r = 32$.

3.4 Summary

Two types of single-loop foldable 8R mechanisms with multiple modes have been presented. The mechanisms are composed of eight thick triangle panels and eight R joints that are mounted on the side or vertex of the triangles. The first type is constructed by connecting two spherical 4R linkages; the second type is the mechanisms combining a planar 4R linkage and a spherical 4R linkage. The mechanisms have the modes that inherited from the two original 4R linkages and an additional spatial 8R linkage mode.

The mechanisms can spread onto a plane and emerge out of the plane. In addition, they can be folded onto two planes and four planes in different ways to facilitate storage and transportation. The mechanisms have the potential to be applied to roofs [Fig. 3.10(a)], solar panels [Fig. 3.10(b)] and space mirrors, and are suitable for 3D-printing. This characteristic also provides an opportunity to develop 4D printing mechanisms, which can transform from one state to another directly off the build plate.

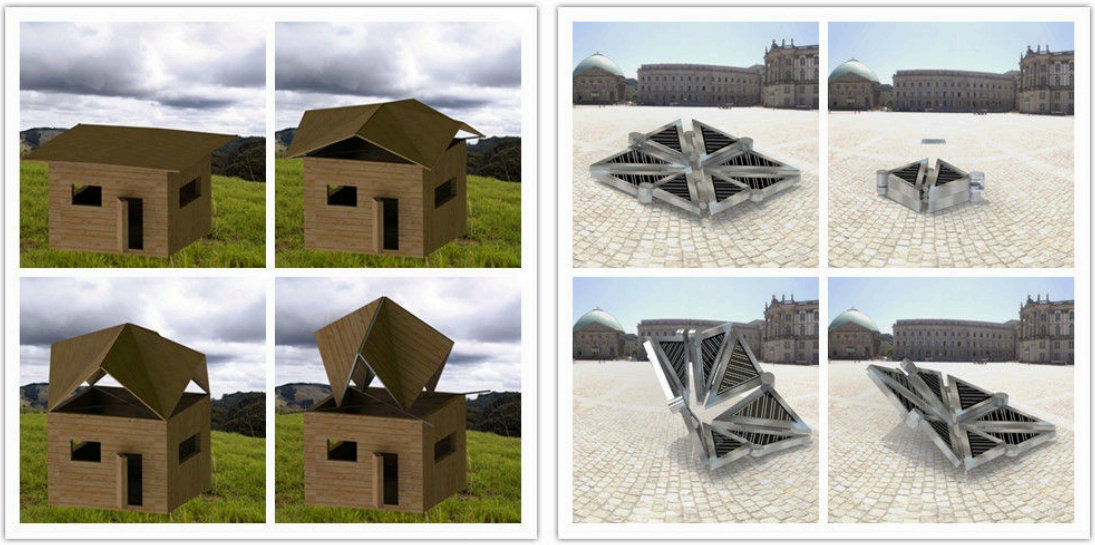

(a) (b)

Fig. 3.10 The applications of the 8R mechanisms: (a) roofs; (b) solar panels

Table 3.2. Comparisons of the two types of mechanisms

	One layer	*Two layers*	*Two layers*
Spherical-Spherical	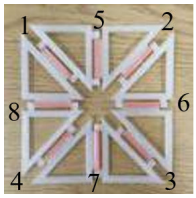		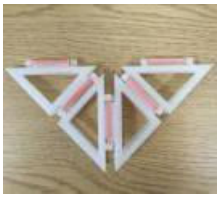
Spherical-Planar	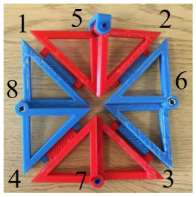	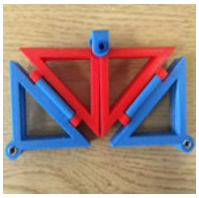	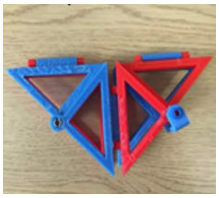
	Four layers	*Planar mode*	*Spherical mode*
Spherical-Spherical	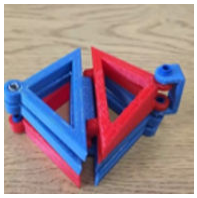	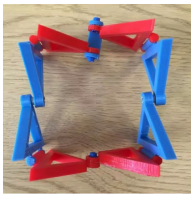	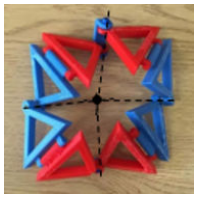
Spherical-Planar	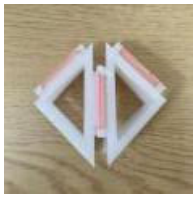		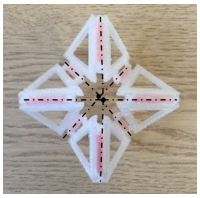

Even though the two types of mechanisms have different configurations, they have common motion modes and similar folded states, as shown in Table 3.2. Both of them can be spread onto a plane. In addition, they can be folded into two layers in which posture $R_1//R_4$, $R_2//R_3$ or $R_1//R_3$, R_2 and R_4 are collinear and then further folded into four layers in which the axes of joints 1, 2, 3 and 4 are on the same plane and parallel with each other. Both of the mechanisms have multiple modes, including planar 4R modes when joints 1, 2, 3 and 4 are parallel with each other, spherical 4R modes when joints 5, 6, 7 and 8 intersect and spatial 8R modes.

CHAPTER 4 – TYPE SYNTHESIS OF DEPLOYABLE POLYHEDRAL MECHANISMS WITH MULTIPLE MODES CONNECTED USING S JOINT

In the previous chapter, single-loop 8R linkages have been constructed. This chapter is to design deployable multiple-loop mechanisms by connecting orthogonal single-loop linkages. An orthogonal single-loop linkage refers to a linkage with an even number of identical links with orthogonal R joint axes and no offset. A novel construction method will be proposed to obtain DPMs using S joints.

4.1 DPMs Based on Identical Bricard Linkages

In this section, deployable mechanisms based on identical orthogonal Bricard linkages will be designed.

4.1.1 Analysis of Bricard Linkage

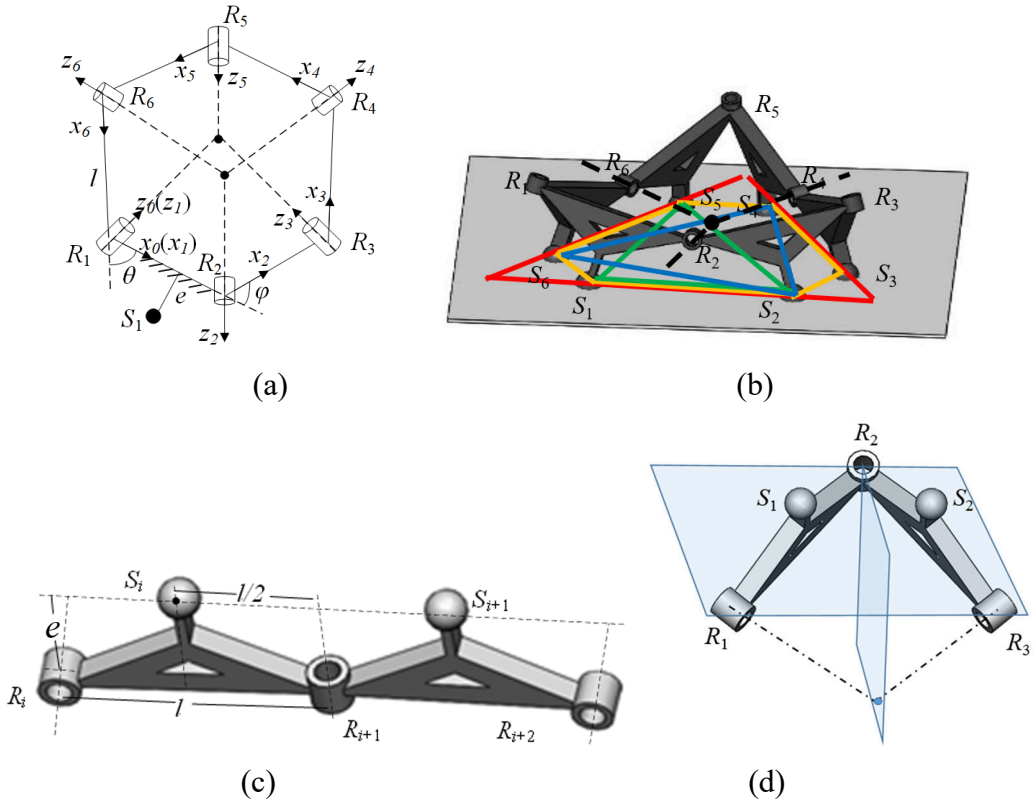

Fig. 4.1 Orthogonal Bricard linkage: (a) the sketch of the Bricard linkage; (b) the 3D model of the Bricard linkage; (c-d) the spatial triads

Kong et al. introduced the plane-symmetric spatial triad shown in Figs. 4.1 (c-d) in [71]. In this triad, the axes of R joints 1 and 3 are symmetric about a plane passing through the axis of R_2 and so are the centres of S joints 1 and 2. A single-loop composed of three such units is called the three-fold plane-symmetric Bricard linkage [13]. The analysis of the orthogonal Bricard linkage has been given in several references [12-13] using the D-H approach. The links of the orthogonal Bricard linkage are all identical and the adjacent joints are perpendicular to each other (Fig. 4.1). Let l represent the link length of the Bricard linkage. The D-H parameters are given as

Table 4.1 D-H parameters of the Bricard linkage

i	a_{i-1}	α_{i-1}	d_i	θ_i
1	l	270^o	0	θ
2	l	90^o	0	φ
3	l	270^o	0	θ
4	l	90^o	0	φ
5	l	270^o	0	θ
6	l	90^o	0	φ

According to Ref. [13], the output angle φ can be represented by input angle θ

$$\varphi = arccos\left(-\frac{C\theta}{C\theta+1}\right) \tag{4.1}$$

Let frame 1 be the reference frame, the positions of R_1 and R_2 are

$$\boldsymbol{P_1} = \{0 \quad 0 \quad 0\}^T \tag{4.2}$$

$$\boldsymbol{P_2} = \{l \quad 0 \quad 0\}^T \tag{4.3}$$

Suppose the position vector of joint (i+1) in frame i (O_i-$x_iy_iz_i$) is represented by $^{\boldsymbol{i}}\boldsymbol{P_{i+1}}$. We have

$$^{\boldsymbol{2}}\boldsymbol{P_3} = {}^{\boldsymbol{3}}\boldsymbol{P_4} = {}^{\boldsymbol{4}}\boldsymbol{P_5} = {}^{\boldsymbol{5}}\boldsymbol{P_6} = \{l \quad 0 \quad 0\}^T \tag{4.4}$$

The positions of R_3, R_4, R_5 and R_6 in the global frame can be calculated as

$$\begin{Bmatrix}\boldsymbol{P_3}\\1\end{Bmatrix} = {}_2^1T\begin{Bmatrix}^{\boldsymbol{2}}\boldsymbol{P_3}\\1\end{Bmatrix} = \left\{\frac{l}{C\theta+1} \quad 0 \quad l\sqrt{\frac{2C\theta+1}{(C\theta+1)^2}} \quad 1\right\}^T \tag{4.5a}$$

$$\begin{Bmatrix}\boldsymbol{P_4}\\1\end{Bmatrix} = {}_2^1T{}_3^2T\begin{Bmatrix}^{\boldsymbol{3}}\boldsymbol{P_4}\\1\end{Bmatrix} = \left\{-l(C\theta-1) \quad lS\theta \quad l(C\theta+1)\sqrt{\frac{2C\theta+1}{(C\theta+1)^2}} \quad 1\right\}^T \tag{4.5b}$$

$$\begin{Bmatrix}\boldsymbol{P_5}\\1\end{Bmatrix} = {}_2^1T{}_3^2T{}_4^3T\begin{Bmatrix}^{\boldsymbol{4}}\boldsymbol{P_5}\\1\end{Bmatrix} = \left\{-\frac{lC\theta}{C\theta+1} \quad \frac{lS\theta}{C\theta+1} \quad l\sqrt{\frac{2C\theta+1}{(C\theta+1)^2}} \quad 1\right\}^T \tag{4.5c}$$

$$\begin{Bmatrix}\boldsymbol{P_6}\\1\end{Bmatrix} = {}_2^1T{}_3^2T{}_4^3T{}_5^4T\begin{Bmatrix}^{\boldsymbol{5}}\boldsymbol{P_6}\\1\end{Bmatrix} = \{-lC\theta \quad lS\theta \quad 0 \quad 1\}^T \tag{4.5d}$$

where ${}^{i-1}_{i}T$ are given in Appendix (A). Now the characteristics of the orthogonal Bricard linkage will be revealed in order to construct DPMs. Define S_i (i = 1, 2, …6) on link i with its position vector ${}^{i}\boldsymbol{S_i}$ in the coordinate frame O_i-$x_iy_iz_i$ as (Fig. 4.1(b))

$$ {}^{i}\boldsymbol{S_i} = \begin{cases} \{l/2 \quad 0 \quad e\}^T & \text{for } i = 1,\ 3 \text{ and } 5 \\ \{l/2 \quad e \quad 0\}^T & \text{for } i = 2,\ 4 \text{ and } 6 \end{cases} \tag{4.6} $$

where e is called the offset of point S_i.

The positions of the S_2, S_3, S_4, S_5 and S_6 in the global frame can be calculated as

$$ \begin{Bmatrix} \boldsymbol{S_2} \\ 1 \end{Bmatrix} = {}^{1}_{2}T \begin{Bmatrix} {}^{\boldsymbol{2}}\boldsymbol{S_2} \\ 1 \end{Bmatrix} = \{ l - e\sqrt{\tfrac{2C\theta+1}{(C\theta+1)^2}} - \tfrac{lC\theta}{2(C\theta+1)} \quad 0 \quad \tfrac{l}{2}\sqrt{\tfrac{2C\theta+1}{(C\theta+1)^2}} - \tfrac{eC\theta}{C\theta+1} \quad 1 \}^T \tag{4.7a} $$

$$ \begin{Bmatrix} \boldsymbol{S_3} \\ 1 \end{Bmatrix} = {}^{1}_{2}T\,{}^{2}_{3}T \begin{Bmatrix} {}^{\boldsymbol{3}}\boldsymbol{S_3} \\ 1 \end{Bmatrix} = \{ l - e\sqrt{\tfrac{2C\theta+1}{(C\theta+1)^2}} - \tfrac{lC\theta}{C\theta+1} - \tfrac{lC\theta^2}{2(C\theta+1)} \quad \tfrac{lS\theta}{2} \quad S_{3z} \quad 1 \}^T \tag{4.7b} $$

where

$$ \boldsymbol{S_{3z}} = l\sqrt{\tfrac{2C\theta+1}{(C\theta+1)^2}} - \tfrac{eC\theta}{C\theta+1} + \tfrac{lC\theta}{2}\sqrt{\tfrac{2C\theta+1}{(C\theta+1)^2}} $$

$$ \begin{Bmatrix} \boldsymbol{S_4} \\ 1 \end{Bmatrix} = {}^{1}_{2}T\,{}^{2}_{3}T\,{}^{3}_{4}T \begin{Bmatrix} {}^{\boldsymbol{4}}\boldsymbol{S_4} \\ 1 \end{Bmatrix} = \{ S_{4x} \quad lS\theta - eS\theta\sqrt{\tfrac{2C\theta+1}{(C\theta+1)^2}} - \tfrac{lC\theta S\theta}{2(C\theta+1)} \quad S_{4z} \quad 1 \}^T \tag{4.7c} $$

where

$$ \boldsymbol{S_{4x}} = (l - lC\theta - lC\theta^2 + 2eC\theta\sqrt{\tfrac{2C\theta+1}{(C\theta+1)^2}} + 2eC\theta^2\sqrt{\tfrac{2C\theta+1}{(C\theta+1)^2}})/[2(C\theta+1)] $$

$$ \boldsymbol{S_{4z}} = (2l\sqrt{\tfrac{2C\theta+1}{(C\theta+1)^2}} - 2eC\theta + 3lC\theta\sqrt{\tfrac{2C\theta+1}{(C\theta+1)^2}} + lC\theta^2\sqrt{\tfrac{2C\theta+1}{(C\theta+1)^2}})/[2(C\theta+1)] $$

$$ \begin{Bmatrix} \boldsymbol{S_5} \\ 1 \end{Bmatrix} = {}^{1}_{2}T\,{}^{2}_{3}T\,{}^{3}_{4}T\,{}^{4}_{5}T \begin{Bmatrix} {}^{\boldsymbol{5}}\boldsymbol{S_5} \\ 1 \end{Bmatrix} = \{ S_{5x} \quad lS\theta - eS\theta\sqrt{\tfrac{2C\theta+1}{(C\theta+1)^2}} - \tfrac{lC\theta S\theta}{2(C\theta+1)} \quad S_{5z} \quad 1 \}^T \tag{4.7d} $$

where

$$ S_{5x} = -\left[C\theta\left(2l + lC\theta - 2e\sqrt{\tfrac{2C\theta+1}{(C\theta+1)^2}} - 2eC\theta\sqrt{\tfrac{2C\theta+1}{(C\theta+1)^2}}\right)\right]/[2(C\theta+1)] $$

$$ S_{5z} = (l\sqrt{\tfrac{2C\theta+1}{(C\theta+1)^2}} - 2eC\theta + lC\theta\sqrt{\tfrac{2C\theta+1}{(C\theta+1)^2}})/[2(C\theta+1)] $$

$$ \begin{Bmatrix} \boldsymbol{S_6} \\ 1 \end{Bmatrix} = {}^{1}_{2}T\,{}^{2}_{3}T\,{}^{3}_{4}T\,{}^{4}_{5}T\,{}^{5}_{6}T \begin{Bmatrix} {}^{\boldsymbol{6}}\boldsymbol{S_6} \\ 1 \end{Bmatrix} = \{ -\tfrac{lC\theta}{2} \quad \tfrac{lS\theta}{2} \quad e \quad 1 \}^T \tag{4.7e} $$

The normal vector to the plane defined by S_1, S_2 and S_3 can be obtained by $\boldsymbol{N} = (\boldsymbol{S_2} - \boldsymbol{S_1}) \times (\boldsymbol{S_3} - \boldsymbol{S_2})$

$$ N = \left\{ \tfrac{lS\theta(2e+4eC\theta-l\sqrt{2C\theta+1})}{4(C\theta+1)} \quad \tfrac{l(2e+4eC\theta-l\sqrt{2C\theta+1})}{4} \quad \tfrac{lS\theta(l-2e\sqrt{2C\theta+1})}{4(C\theta+1)} \right\}^T \tag{4.8} $$

The plane defined by S_i (i = 1, 2, 3) is calculated as

$$ N_x(x - l/2) + N_y y + N_z(z - e) = 0 \tag{4.9} $$

Substituting the positions of S_4, S_5 and S_6 into Eq. (4.9), it can be verified that S_i (i = 1, 2, …6) are always on the same plane, which is referred to the mirror plane in the following

sections. As shown in Fig. 4.1(b), the lines defined by S_1 and S_2, S_3 and S_4, and S_5 and S_6 respectively form a regular triangle. $S_1S_2S_3S_4S_5S_6$ is a semi-regular hexagon. The edges of the hexagon vary with the deformation of the Bricard linkage. In addition, both triangles $S_1S_3S_5$ and $S_2S_4S_6$ are regular triangles.

Based on the above characteristics of the orthogonal Bricard linkage, DPMs will be constructed by connecting orthogonal Bricard linkages through S joints located at S_i on each link.

4.1.2 DPMs Based on Bricard Linkages

By connecting two orthogonal Bricard linkages, which are mirrored versions of each other about the mirror plane, using six S joints located at S_i (i = 1, 2, …6), a DPM in the shape of a triangular prism can be obtained (Fig. 4.2). Since S_i (i = 1, 2, …6) of each orthogonal Bricard linkage remain on the same plane, the prism DPM has the same DOF of each orthogonal Bricard linkage, i.e., 1-DOF.

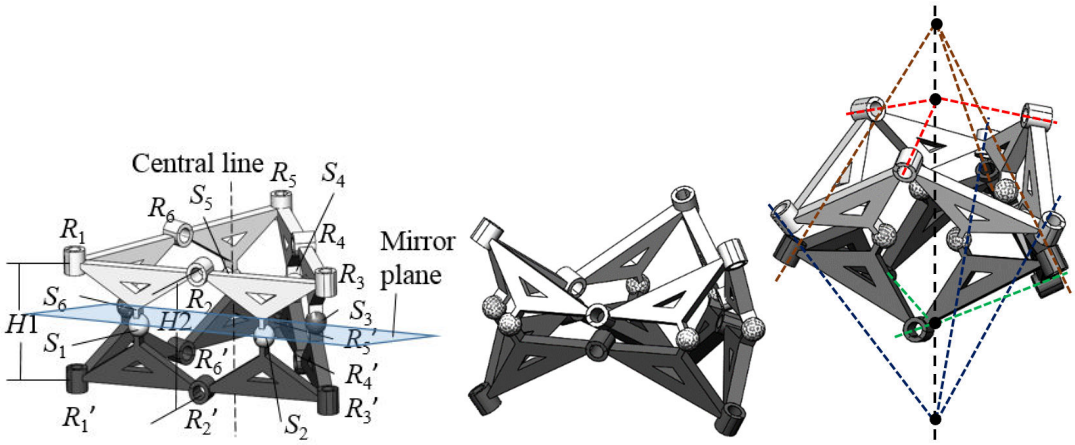

(a) (b) (c)

Fig. 4.2 Prism DPM based on orthogonal Bricard linkages: (a) initial posture; (b) outward deploying; (c) inward deploying

The prism DPM is axisymmetric about the line defined by the intersection of R_2, R_4 and R_6 and the intersection of R_2', R_4' and R_6' and plane-symmetric about three planes defined by joints R_i, $R_{(i+3)}$, R_i' and $R_{(i+3)}'$ (i = 1, 2 and 3). In the initial state [Fig. 4.2(a)], R_1, R_3 and R_5 of the two Bricard linkages are parallel with each other and R_2, R_4 and R_6 lie on the same plane and intersect at a point. R_1 and R_1' are collinear, and so are R_3 and R_3' and R_5 and R_5'. $R_2//R_2'$, $R_4//R_4'$ and $R_6//R_6'$. When deployed, the two Bricard linkages deform

synchronously and are always symmetrical about the mirror plane. The axes of the R joints of each Bricard linkage intersect at two points, and these four intersection points are always collinear. The mechanism has two deploying states, which are referred to as the outward state [Fig. 4.2(b)] and the inward state [Fig. 4.2(c)]. In the outward state, the distance between joints R_1 and R_1' increases with the distance between joints R_2 and R_2' decreasing, while in the inward state, the distance between joints R_1 and R_1' decreases with the distance between joints R_2 and R_2' increasing.

To define the ratio of the stowed-to-deployed diameter of the prism PM, the circumscribed cylinder is used to represent the volume of the DPM (Fig. 4.3).

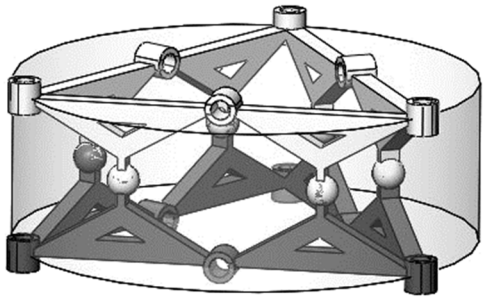

Fig. 4.3 Circumscribed cylinder of the mechanism

The side lengths of the equilateral triangles defined by joints R_1, R_3 and R_5 as well as R_2, R_4 and R_6 can be calculated, respectively, as:

$$D1=|\boldsymbol{P_3} - \boldsymbol{P_1}| \tag{4.10}$$

$$D2=|\boldsymbol{P_4} - \boldsymbol{P_2}| \tag{4.11}$$

The plots of $D1$ and $D2$ with respect to the variation of input angle (R_1) $\theta \in [0°, 120°]$ are displayed in Fig. 4.4 for the case when the link length $l = 0.05m$. D1 and D2 vary from $0.05m$ to $0.1m$. D1 obeys to monotonic decreasing, while D2 obeys monotonic increasing. It can be seen that when $\theta = 90^o$, $D1 = D2$; when $\theta > 90^o$, $D1 > D2$; and when $\theta < 90^o$, $D1 < D2$.

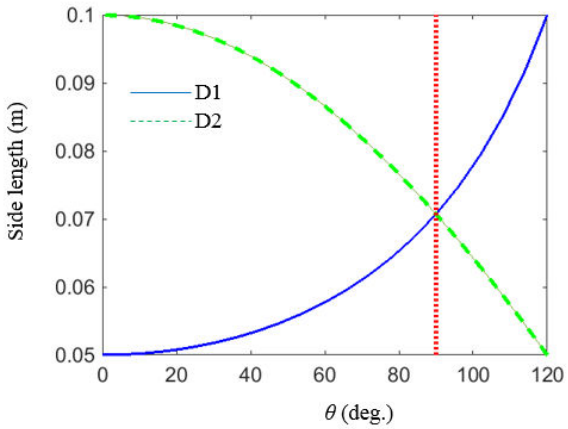

Fig. 4.4 Plots of D1 and D2 with respect to θ

The distance, H1, between joints R_1 and R_1' is twice the distance between R_1 and the mirror plane (Fig. 4.2). We have

$$H1 = \frac{2\left|-\frac{l}{2}t - ne\right|}{\sqrt{t^2+m^2+n^2}} \tag{4.12}$$

Similarly, the distance, H2, between R_2 and R_2' is (shown in Fig. 4.2)

$$H2 = \frac{2\left|t\left(l-\frac{l}{2}\right) - ne\right|}{\sqrt{t^2+m^2+n^2}} \tag{4.13}$$

When deployed inward, H1 < H2, and when deployed outward, H1 > H2. The volume of the circumscribed cylinder of the mechanism V can be described by

$$V = \begin{cases} \theta \geq 90° \begin{cases} \pi\left(\frac{D1}{3}\right)^2 \times H1 & outward\ deploying \\ \pi\left(\frac{D1}{3}\right)^2 \times H2 & inward\ deploying \end{cases} \\ \theta < 90° \begin{cases} \pi\left(\frac{D2}{3}\right)^2 \times H1 & outward\ deploying \\ \pi\left(\frac{D2}{3}\right)^2 \times H2 & inward\ deploying \end{cases} \end{cases} \tag{4.14}$$

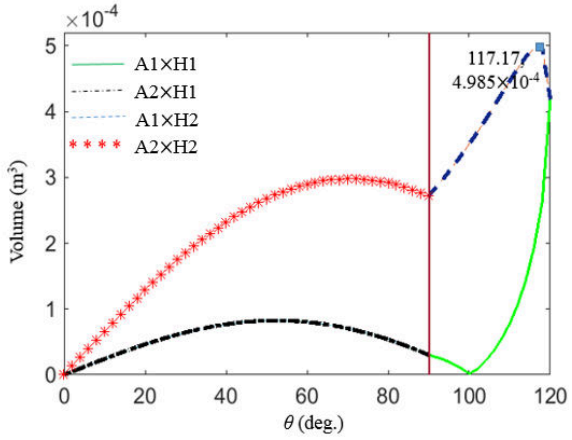

Fig. 4.5 The volume of the circumscribed cylinder of the DPM

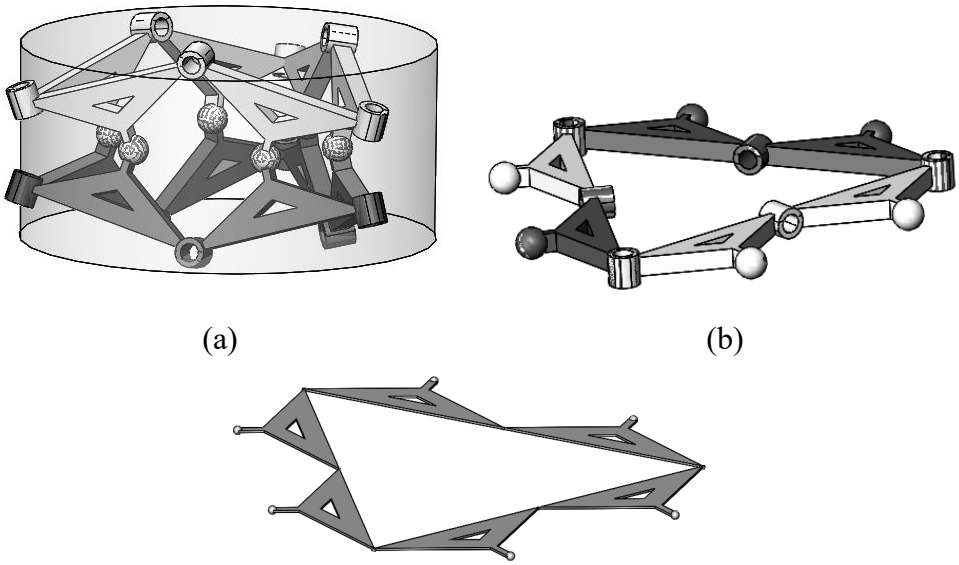

(a) (b)

(c)

Fig. 4.6 The maximum and minimum volume positions of the circumscribed cylinder of the DPM: (a) maximum volume position; (b) minimum volume position; (c) minimum volume position of the origami model.

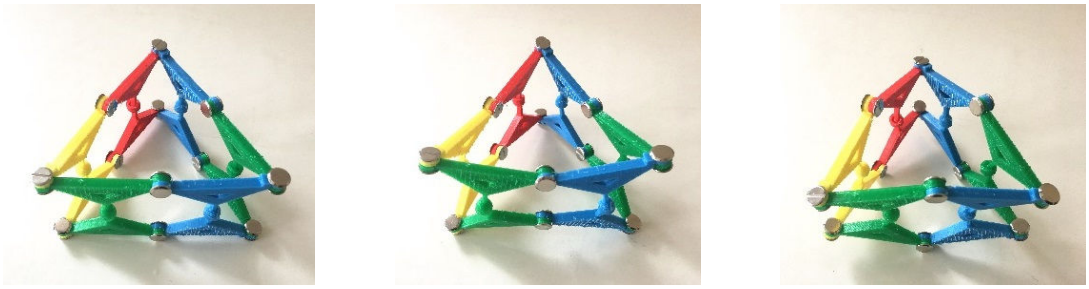

(a) (b) (c)

Fig. 4.7 Rigid-joint prototype of the prism DPM based on orthogonal Bricard linkages: (a) initial posture; (b) outward deploying; (c) inward deploying

Let $e = 0.02mm$, the variation of the volume of the circumscribed cylinder of the DPM with respect to the input angle θ within the range from 0° to 120° is depicted in Fig. 4.5. It can be observed that the volume reaches the maximum value of $4.985\times10^{-4}m^3$ when θ = 117.17°, as shown in Fig. 4.6(a). For an ideal zero-thickness model, the minimum volume of the circumscribed cylinder is zero when $\theta = 0^o$ [Fig. 4.6(c), when the two Bricard linkages overlap].

A 3D printed prototype (Fig. 4.7) is fabricated to verify the feasibility of the mechanism. A compliant prototype is also built with its links printed using rigid material and its joints with soft material (Fig. 4.8). Since the initial state is a stable state, the mechanism can

recover to the initial state after deploying. In the initial state, the mechanism is in the shape of a regular prism. When deployed, it can be spread onto parallel planes through two ways shown in Figs. 4.8(b) and (c) respectively. Suppose the thickness of the links is $h = 0.005m$, the minimum volume of the mechanism [Fig. 4.8(c)] is $2\sqrt{3}l^2h = 4.33 \times 10^{-5}m^3$. The ratio between the maximum volume and the minimum volume is $r = 11.5$.

(a) (b) (c)

Fig. 4.8 Compliant prototype of the prism DPM based on orthogonal Bricard linkages: (a) initial posture; (b) outward deploying; (c) inward deploying

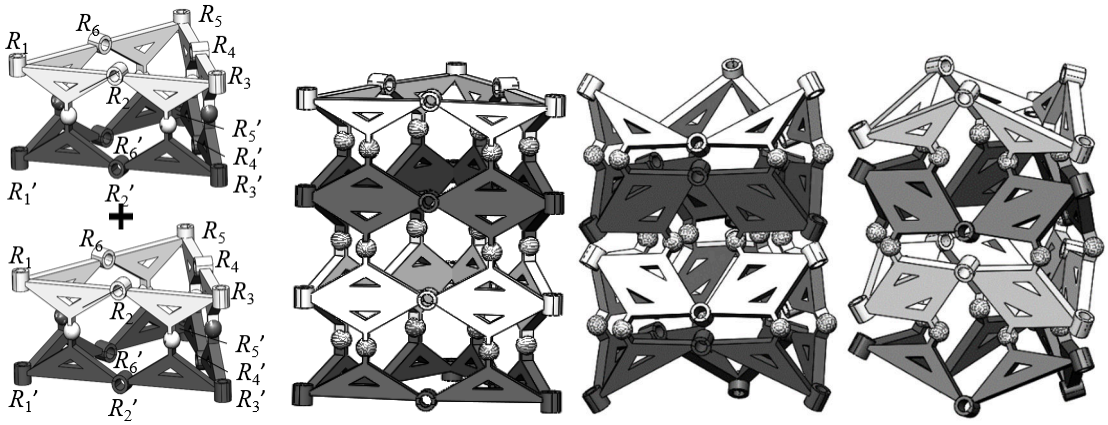

(a) (b) (c) (d)

Fig. 4.9 The multiple-layer prism DPM constructed using Bricard linkages: (a) the construction method; (b) initial posture; (c) outward deploying; (d) inward deploying

By overlaying the prism DPMs, the mechanism can be extended along the axial direction. The 1-DOF *n*-layer prism DPM in Fig. 4.9 is connected using *n* prism DPM proposed above. Let R_1', R_2', R_3', R_4', R_5' and R_6' of the first DPM be coincident with R_1, R_2, R_3, R_4, R_5 and R_6 of the second DPM respectively, a double layers DPM is obtained. Using the construction method, multiple-layer DPM can be constructed. The mechanisms can be deployed outward [Fig. 4.9(b)] and inward [Fig. 4.9(c)]. It can be applied to sun

shield, or other aerospace mechanisms.

A three-layer prototype is 3D printed with rigid links and flexible joints. The compliant prototype has a higher folding ratio than the rigid mechanism in Fig. 4.9. The mechanism is in the shape of a prism in its stable position [refers to the initial state in Fig. 4.10(a)] and can be folded into four layers through two approaches [Figs. 4.10(b) and (c) respectively]. The flexible joints also provide a method to develop origami mechanisms into think panel foldable mechanisms. It is noted that the mechanisms with offset rigid joints can also be folded into several layers. The folding ratio can be expressed as

$$r = 2en/(n+1)h \tag{4.15}$$

The folding ratio of the prototype is 6. The ratio will be larger when increasing the value of e and decreasing the value of h, and the ratio can reach to infinity when h tends towards 0.

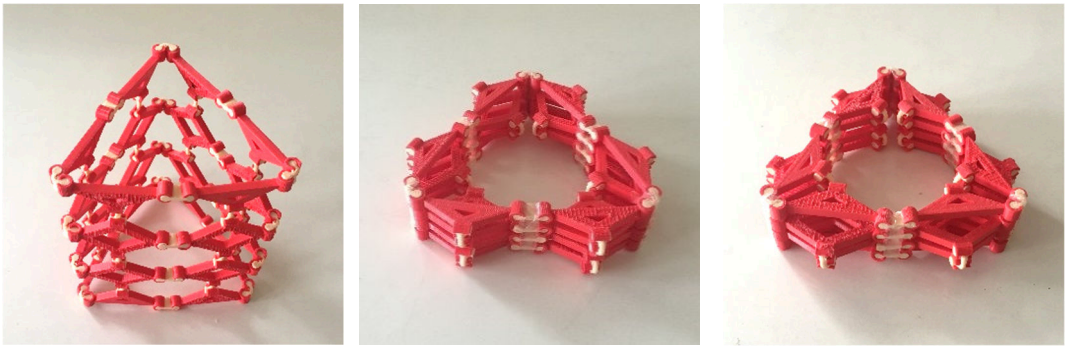

(a) (b) (c)

Fig. 4.10 The prototype of the multi-layer prism DPM constructed using Bricard linkages: (a) initial posture; (b) outward deploying; (c) inward deploying

A 1-DOF DPM in the shape of a tetrahedron can also be obtained (Fig. 4.11) by connecting four orthogonal Bricard linkages using twelve S joints. Each Bricard linkage is connected with another Bricard linkage by two S joints. In the initial state [Fig. 4.11(a)], R_1, R_3 and R_5 of each Bricard linkages are parallel with each other and R_2, R_4 and R_6 lie on the same plane and intersect at a point. The planes defined by joints R_2, R_4 and R_6 of each Bricard linkage generate a regular tetrahedron and the planes defined by the six S joints of each Bricard linkage generate a similar tetrahedron.

The DOF of the mechanism is one and the tetrahedron DPM can be deployed outward [Fig. 4.11(b)], which refers to the case that the distance between R_5 and R_5' increases from the initial configuration, or inward [Fig. 4.11(c)], which refers to the case that the distance between R_5 and R_5' decreases from the initial configuration.

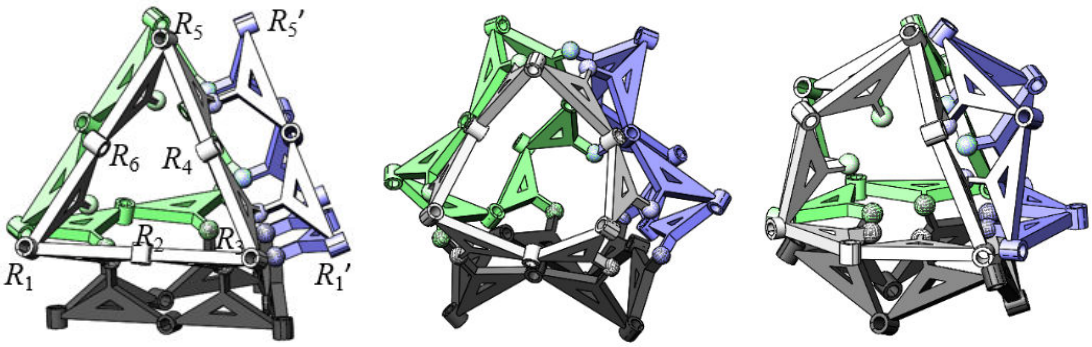

(a) (b) (c)

Fig. 4.11 Tetrahedron DPM based on orthogonal Bricard linkages: (a) initial posture; (b) outward deploying; (c) inward deploying

A tetrahedron DPM with compliant joints is fabricated with a high ratio of stowed-to-deployed diameter. In the initial state as presented in Fig. 4.12(a), the mechanism is in a shape of a regular tetrahedron and the angle τ between the plane defined by R_3 and R_5 in the first Bricard linkage and the plane defined by R_1' and R_5' in the adjacent Bricard linkage $\tau = \pi - \arccos(1/3) \approx 109.5°$. The angle τ becomes zero when deployed inward or π when deployed outward. The mechanism is stable in its initial state, so it will return to the initial state after the deploying process.

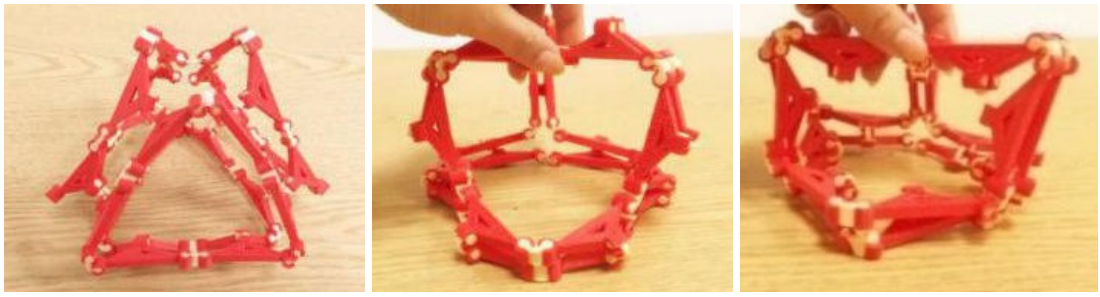

(a) (b) (c)

Fig. 4.12 Compliant Prototype of tetrahedron DPM based on orthogonal Bricard linkages: (a) initial posture; (b) outward deploying; (c) inward deploying

Similarly, a 1-DOF DPM in the shape of an octahedron is constructed by connecting eight orthogonal Bricard linkages with twenty-four S joints (Fig. 4.13). The mechanism can be deployed outward or inward, as shown in Figs. 4.13(b) and (c). When connecting twenty orthogonal Bricard linkages with sixty S joints, a deployable 1-DOF DPM in the shape of an icosahedron is obtained (Fig. 4.14).

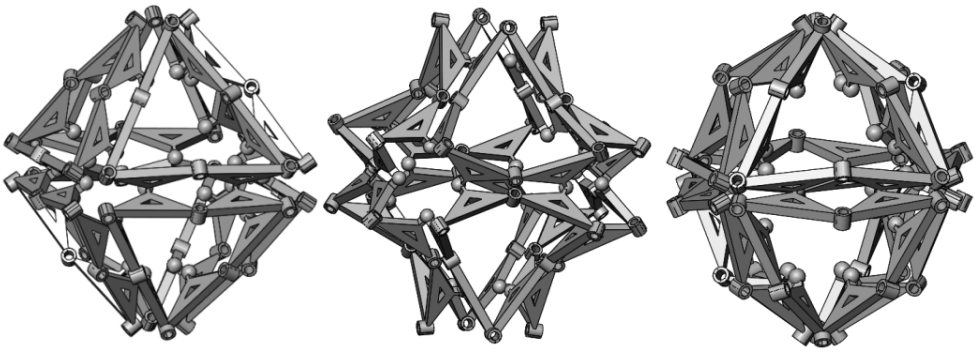

(a) (b) (c)

Fig. 4.14 Octahedron DPM based on orthogonal Bricard linkages: (a) initial posture; (b) outward deploying; (c) inward deploying

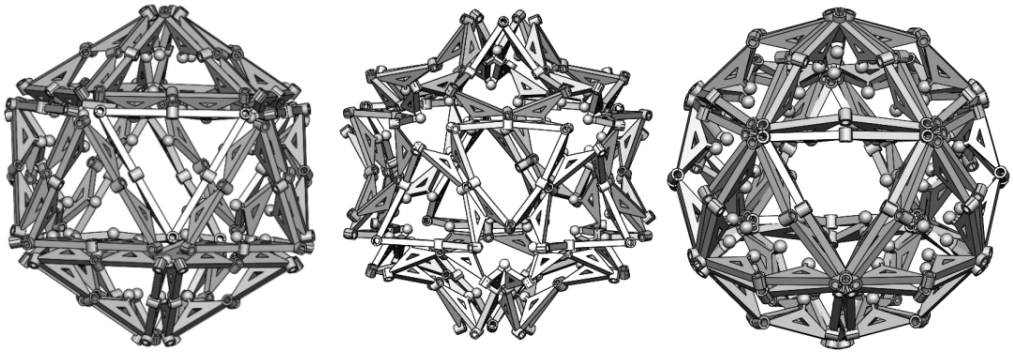

(a) (b) (c)

Fig. 4.14 Icosahedron DPM based on orthogonal Bricard linkages: (a) initial posture; (b) outward deploying; (c) inward deploying

4.1.3 Variations of the Mechanisms Based on Bricard Linkages

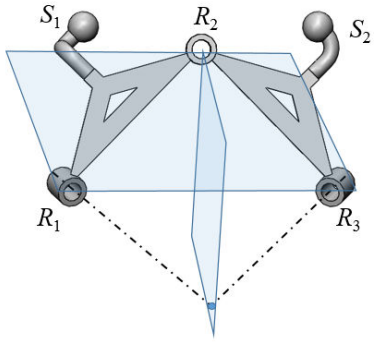

Fig. 4.15 The triad unit of the single-loop linkages

Using the above approach for constructing DPMs using orthogonal single-loop linkages, we can also construct similar DPMs by connecting single-loop linkages in which the axes

of two adjacent joints are not perpendicular. Such single-loop mechanisms are composed of three to five identical spatial plane-symmetric triad as shown in Fig. 4.15.

However, these DPMs may not be as practical as the mechanisms based on orthogonal single-loop mechanisms. For example, the prism DPM based on the three-fold plane-symmetric Bricard linkage with a twist angle of 60° is either not a regular prism in the initial position [configuration I in Figs. 4.16(a-b)] or cannot be folded onto two planes when using flexible joints [configuration II in Figs. 4.16(c-d)].

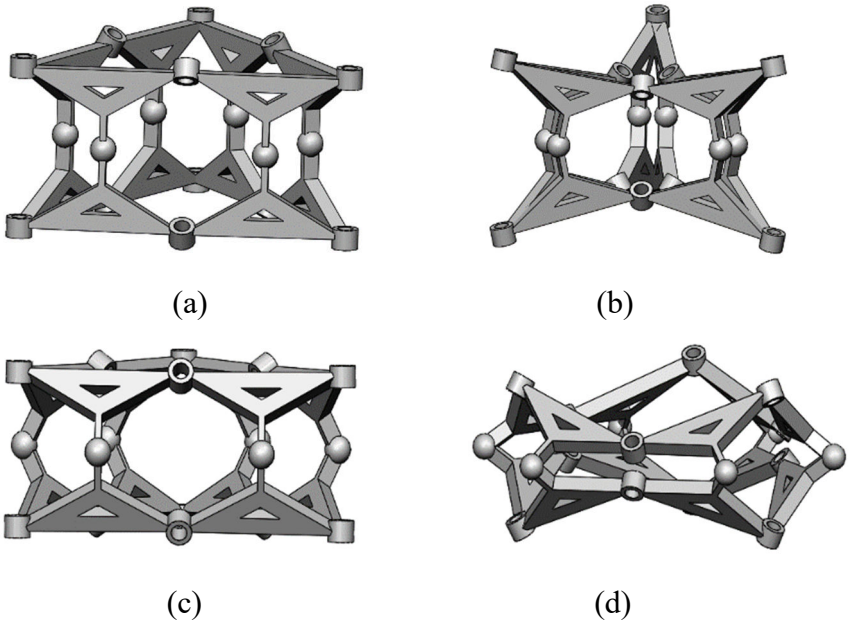

(a) (b)

(c) (d)

Fig. 4.16 Prism DPMs based on Bricard linkages with a twist angle of 60°: (a-b) configuration I; (c-d) configuration II

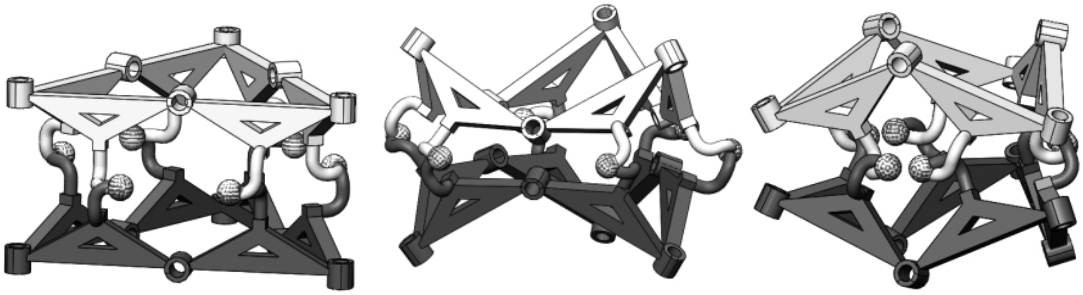

(a) (b) (c)

Fig. 4.17 Variation of prism DPM based on Bricard linkages: (a) initial posture; (b) outward deploying; (c) inward deploying

It is noted that the S joints can be set at arbitrary positions on the links as long as the mechanism is symmetric about the mirror plane. As shown in Fig. 4.17 and Fig. 4.18, the S joint has an offset from the plane defined by the triangle link, as well as the median of

the triangle, since the hexagons formed by the S joints of the two Bricard linkages respectively always coincide. The DOFs of these mechanisms are also one.

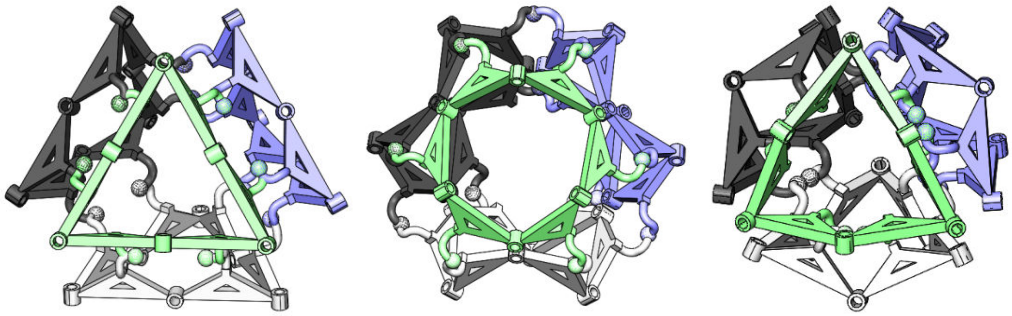

(a) (b) (c)

Fig. 4.18 Variation of tetrahedron DPM based on Bricard linkages: (a) initial posture; (b) outward deploying; (c) inward deploying

4.2 DPMs Based on Identical 8R/10R Linkages

In this section, 8R and 10R linkages will be adopted to connect DPMs, using the proposed construction method.

4.2.1 Analysis of 8R Linkage

By connecting four spatial triads [Fig. 4.19(a)], an orthogonal 8R linkage is obtained, as shown in Figs. 4.19(b-c). The 8R linkage is composed of eight identical links and eight R joints and has two DOF in a general position [80]. The adjacent joint axes of the 8R linkages are perpendicular to each other.

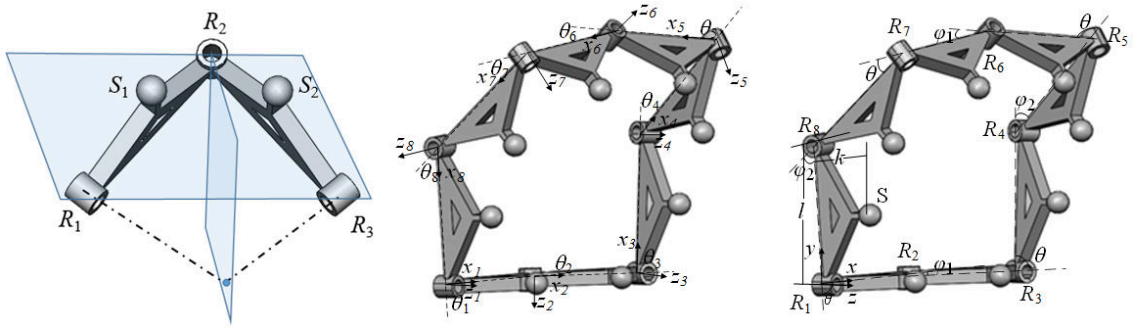

(a) (b) (c)

Fig. 4.19 Construction of orthogonal 8R linkage: (a) the triad; (b-c) the orthogonal 8R linkage

In a general position, the S joints of the 8R linkage are not on the same plane, as shown in Fig. 4.20(a). To construct DPMs using 8R linkages, the S joints should be coplanar [Fig. 4.20(b)]. Now it will be verified that the DOF of the 8R linkage reduces to one when the S joints are constrained to be coplanar.

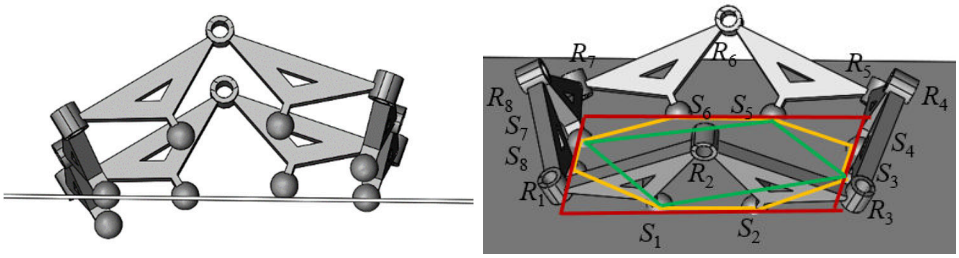

(a) (b)

Fig. 4.20 Variation of orthogonal 8R linkage: (a) the general configuration; (b) the virtual-plane-constrained configuration

The D-H parameters of the 8R linkage are given in Table 4.2. In the deployable mode, suppose that $\theta' = \theta$, for the sake of conciseness. $\varphi_1 = \varphi_2$ if the DOF of the virtual-plane-constrained 8R linkage is one, similar to the Bricard linkage. Otherwise, the DOF is still two. The position vectors of the centers of the S joints with respect to the local coordinate are

$$^{i}\boldsymbol{S_i} = \{l/2 \quad 0 \quad e\}^T \quad \text{for } i = 1,\ 3,\ 5 \text{ and } 7 \tag{4.16}$$

$$^{i}\boldsymbol{S_i} = \{l/2 \quad e \quad 0\}^T \quad \text{for } i = 2,\ 4,\ 6 \text{ and } 8 \tag{4.17}$$

Table 4.2 The D-H parameters of the 8R linkage

i	a_{i-1}	α_{i-1}	d_i	θ_i
1	l	270^o	0	θ
2	l	90^o	0	φ_1
3	l	270^o	0	θ'
4	l	90^o	0	φ_2
5	l	270^o	0	θ
6	l	90^o	0	φ_1
7	l	270^o	0	θ'
8	l	90^o	0	φ_2

Link 1 is fixed on the ground, and the global coordinate frame is attached to R_1. The position vectors of the centres of the S joints in the global coordinate frame can be calculated as

$$\begin{Bmatrix} \boldsymbol{S_2} \\ 1 \end{Bmatrix} = {}_2^1T \begin{Bmatrix} {}^{\boldsymbol{2}}\boldsymbol{S_2} \\ 1 \end{Bmatrix} = \{l + lC\varphi_1/2 - eS\varphi_1 \quad 0 \quad eC\varphi_1 + lS\varphi_1/2 \quad 1\}^T \tag{4.18a}$$

$$\begin{Bmatrix} \boldsymbol{S_3} \\ 1 \end{Bmatrix} = {}_2^1T\,{}_3^2T \begin{Bmatrix} {}^{\boldsymbol{3}}\boldsymbol{S_3} \\ 1 \end{Bmatrix} = \{S_{3x} \quad lS\theta/2 \quad eC\varphi_1 + lS\varphi_1 + lC\theta S\varphi_1/2 \quad 1\}^T \tag{4.18b}$$

where

$$S_{3x} = l + lC\varphi_1 - eS\varphi_1 + lC\theta C\varphi_1/2$$

$$\begin{Bmatrix} \boldsymbol{S_4} \\ 1 \end{Bmatrix} = {}_2^1T\,{}_3^2T\,{}_4^3T \begin{Bmatrix} {}^{\boldsymbol{4}}\boldsymbol{S_4} \\ 1 \end{Bmatrix} = \{S_{4x} \quad S\theta[l(2 + C\varphi_2) - 2eS\varphi_2]/2 \quad S_{4z} \quad 1\}^T \tag{4.18c}$$

where

$$S_{4x} = l - S\varphi_1(2eC\varphi_2 + lS\varphi_2)/2 + C\varphi_1[l + C\theta(l + lC\varphi_2/2 - eS\varphi_2)]$$

$$S_{4z} = C\varphi_1(eC\varphi_2 + lS\varphi_2/2) + S\varphi_1\{2l + C\theta[l(2 + C\varphi_2) - 2eS\varphi_2]\}/2$$

$$\begin{Bmatrix} \boldsymbol{S_5} \\ 1 \end{Bmatrix} = {}_2^1T\,{}_3^2T\,{}_4^3T\,{}_5^4T \begin{Bmatrix} {}^{\boldsymbol{5}}\boldsymbol{S_5} \\ 1 \end{Bmatrix} = \{S_{5x} \quad S\theta[l(2 + C\theta)(1 + C\varphi_2) - 2eS\varphi_2]/2 \quad S_{5z} \quad 1\}^T \tag{4.18d}$$

where

$$S_{5x} = l + 2lC^4(\theta/2)C\varphi_1 + \{C\varphi_2[lC\theta(2 + C\theta)C\varphi_1 - 2eS\varphi_1] - [2eC\theta C\varphi_1 + l(2 + C\theta)S\varphi_1]S\varphi_2\}/2$$

$$S_{5z} = \{C\varphi_1[2eC\varphi_2 + l(2 + C\theta)S\varphi_2] + S\varphi_1\{4lC^4(\theta/2) + C\theta[l(2 + C\theta)C\varphi_2 - 2eS\varphi_2]\}\}/2$$

${}_i^{i-1}T$ are given in Appendix (B). The normal vector to the mirror plane defined by joint centres of S_1, S_2 and S_3 is obtained as

$$\boldsymbol{N} = \begin{Bmatrix} -lS\theta[2e(-1 + C\varphi_1) + lS\varphi_1]/4 \\ -l(1 + C\theta)[2e(-1 + C\varphi_1) + lS\varphi_1]/4 \\ lS\theta(l + lC\varphi_1 - 2eS\varphi_1)/4 \end{Bmatrix} \tag{4.19}$$

The equation of the plane can be expressed as

$$N_x(x - l/2) + N_y y + N_z(z - e) = 0 \tag{4.20}$$

The condition that the joint centre of S_4 is on the plane defined by S_1, S_2 and S_3 is

$$N_x(S_{4x} - l/2) + N_y S_{4y} + N_z(S_{4z} - e) = -\frac{1}{2}lS\theta[lC(\tfrac{\varphi_1}{2}) - 2eS(\tfrac{\varphi_1}{2})]S(\tfrac{\varphi_1 - \varphi_2}{2})[lC(\tfrac{\varphi_2}{2}) - 2eS(\tfrac{\varphi_2}{2})] = 0 \tag{4.21}$$

which leads to

$$\varphi_2 = \varphi_1 \qquad \text{or} \tag{4.22}$$

$$\varphi_2 = 2\tan^{-1}(2e/l) \tag{4.23}$$

When $\varphi_2 = 2\tan^{-1}(2e/l)$, S_3 and S_4 are concentric, in which position S_5 is not on the mirror plane unless S_1 and S_2 are also concentric. In this case, φ_1 is also equal to

$2\tan^{-1}(2e/l)$ and the linkage is in spherical 4R linkage mode (discussed in the following section). Substituting the position vectors of S_5, S_6, S_7 and S_8 into Eq. (4.20), it is verified that all the S joints are on the same plane when $\varphi_2 = \varphi_1$. Hence, $\varphi_2 = \varphi_1$ is the unique solution.

The 8R linkage is a single closed-loop, the product of the transfer matrices equals the identity matrix, which means

$$ {}^1_2T\,{}^2_3T\,{}^3_4T\,{}^4_5T\,{}^5_6T\,{}^6_7T\,{}^7_8T\,{}^8_1T = I \tag{4.24} $$

φ_1 ($\varphi_1 = \varphi_2$) can be represented by θ as

$$ \varphi_2 = \varphi_1 = arccos\left(\frac{1-C\theta}{C\theta+1}\right) \tag{4.25} $$

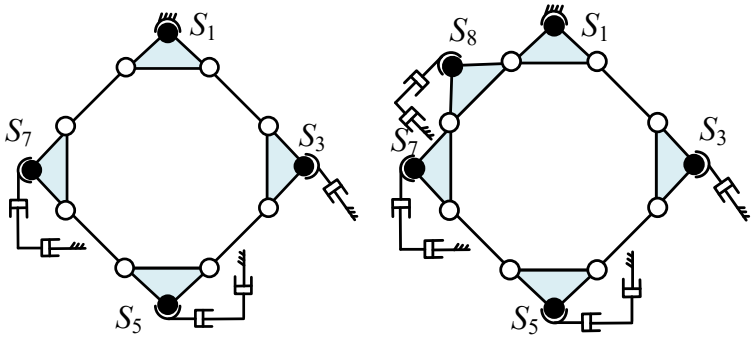

(a) (b)

Fig. 4.21 Sketch of the virtual-plane-constrained orthogonal 8R linkage: (a) four spheres are constrained on the plane; (b) five spheres are constrained on the plane

Then the DOF of the virtual-plane-constrained orthogonal 8R linkage will be verified using the conventional formula. When four spheres are constrained on the same plane, assume that the center of S_1 is fixed on the plane, S_3 has a translational DOF on the plane and S_5 and S_7 have two translational DOFs on the plane [Fig. 4.21(a)]. The DOF of the linkage can also be computed by

$$ M = 6(q-p) + \sum_{i=1}^{p} f_i = 6(8-12) + 8 + 3 + 4 + 5 \times 2 = 1 \tag{4.26} $$

When s additional spheres are constrained to be on the plane, the 8R linkage is over-constrained [Fig. 4.21(b)].

$$ M = 6(q-p) + \sum_{i=1}^{p} f_i = 6 \times (8-12-s) + 8 + 3 + 4 + 5 \times (2+s) = 1 - s \tag{4.27} $$

The DOF of the linkage is still one, due to the symmetry characteristics of the linkage. It can be readily proved that the virtual-plane-constrained 10R/12R linkages also have one DOF when deployed.

The virtual-plane-constrained orthogonal 8R linkage has three 1-DOF modes: spatial

mode [Fig. 4.22(a)], planar 4R mode [Fig. 4.22(b)], and spherical 4R mode [Fig. 4.22(c)]. In the spatial mode, the lines defined by S_1 and S_2, S_3 and S_4, S_5 and S_6 and S_7 and S_8 respectively form a square [red one in Fig. 20(b)], $S_1S_3S_5S_7$ is a square [green one in Fig. 20(b)] too. $S_1S_2S_3S_4S_5S_6S_7S_8$ is a semi-regular octagon. $S_1S_2 = S_3S_4 = S_5S_6 = S_7S_8$ and $S_2S_3 = S_4S_5 = S_6S_7 = S_8S_1$. In the planar 4R mode, the mechanism moves like a 4-bar mechanism composed of joints R_1, R_3, R_5 and R_7, whose joint axes are perpendicular to the plane defined by S_i (i = 1, 2, …8). In the spherical 4R mode, the mechanism moves like a 4-bar mechanism composed of joints R_1, R_3, R_5 and R_7, whose joint axes intersect at a point.

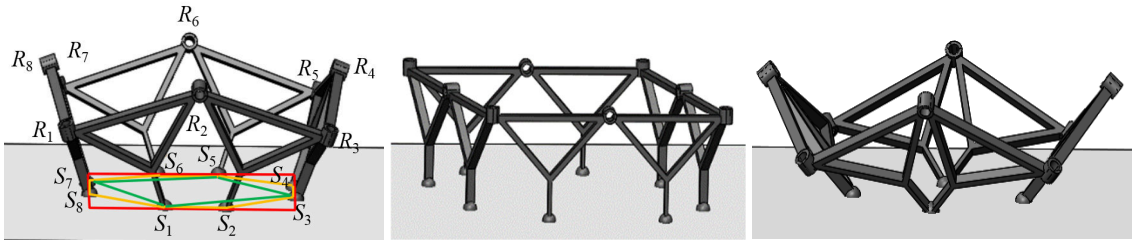

(a) (b) (c)

Fig. 4.22 The virtual-plane-constrained orthogonal 8R linkage: (a) spatial mode; (b) planar 4R linkage mode; (d) spherical 4R linkage mode.

4.2.2 DPMs Based on 8R/10R Linkages

By connecting two 8R orthogonal linkages, which are mirrored versions of each other about the mirror plane, using eight S joints located at S_i (i = 1, 2, …8), a quadrangular DPM can be obtained (Fig. 4.23). Since S_i (i = 1, 2, …8) of each orthogonal 8R linkage remain on the same plane, the DPM has the same DOF of each constrained orthogonal 8R linkage, i.e., 1-DOF.

The DPM based on 8R orthogonal linkages has three modes: deployable mode; planar 4R mode and spherical 4R mode. In the deployable mode, the mechanism can be deployed outward or inward, when all the eight S joints move backwards or towards, as shown in Figs. 4.23(b) and (c). In the planar 4R mode [Fig. 4.23(d)], the two 8R linkages deform synchronously and each moves as a planar 4R linkage composed of joints R_1, R_3, R_5 and R_7. In the spherical 4R mode [Fig. 4.23(f)], the two 8R linkages also deform synchronously and each moves as a spherical 4R linkage composed of joints R_1, R_3, R_5 and R_7 as well.

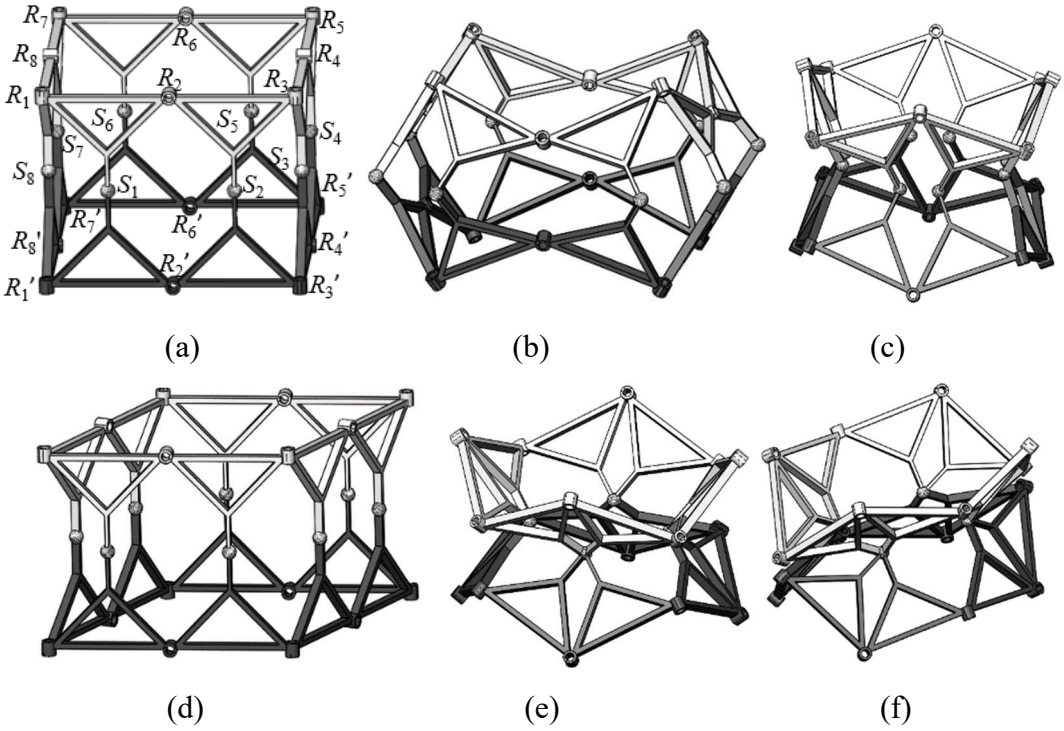

Fig. 4.23 Quadrangular DPM based on orthogonal 8R linkages: (a) deployable mode↔planar 4R mode; (b) outward deploying; (c) inward deploying (e) deployable mode↔spherical 4R mode; and (f) spherical 4R mode

The deployable mode and the planar 4R mode can be switched through the transition configuration I (singular configuration) [Fig. 4.23(a)]. In this transition configuration, the axes of joints R_1, R_3, R_5 and R_7 are parallel, and R_2 and R_4 are collinear, as well as R_4 and R_8. The deployable mode and the spherical 4R mode can be transformed through the transition configuration II, which is shown in Fig. 4.23(e). S_1 and S_2 are adjusted to be concentric, as well as S_3 and S_4, S_5 and S_6, S_7 and S_8, and $S_1S_3S_5S_7$ is a square. Compared with the multi-mode deployable mechanisms in the references, the mechanism has a very simple structure and is lightweight.

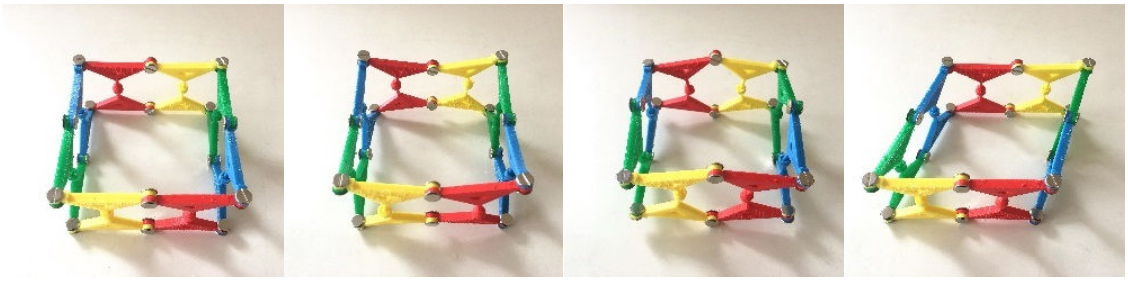

Fig. 4.24 Rigid prototype of the quadrangular DPM based on orthogonal 8R linkages: (a) initial posture; (b) outward deploying; (c) inward deploying; (d) planar 4R mode

A rigid prototype is fabricated to verify the DOF of the mechanism, as shown in Fig. 4.24. It is noted that the spherical 4R mode can only be achieved if there is no interference between the S joints. The mechanism has one DOF in each mode.

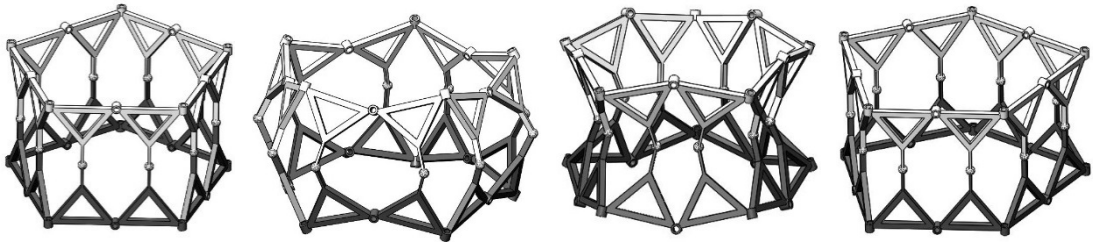

(a) (b) (c) (d)

Fig. 4.25 Pentagonal prism DPM based on orthogonal 10R linkages: (a) initial posture; (b) outward deploying; (c) inward deploying; (d) planar 5R linkage mode

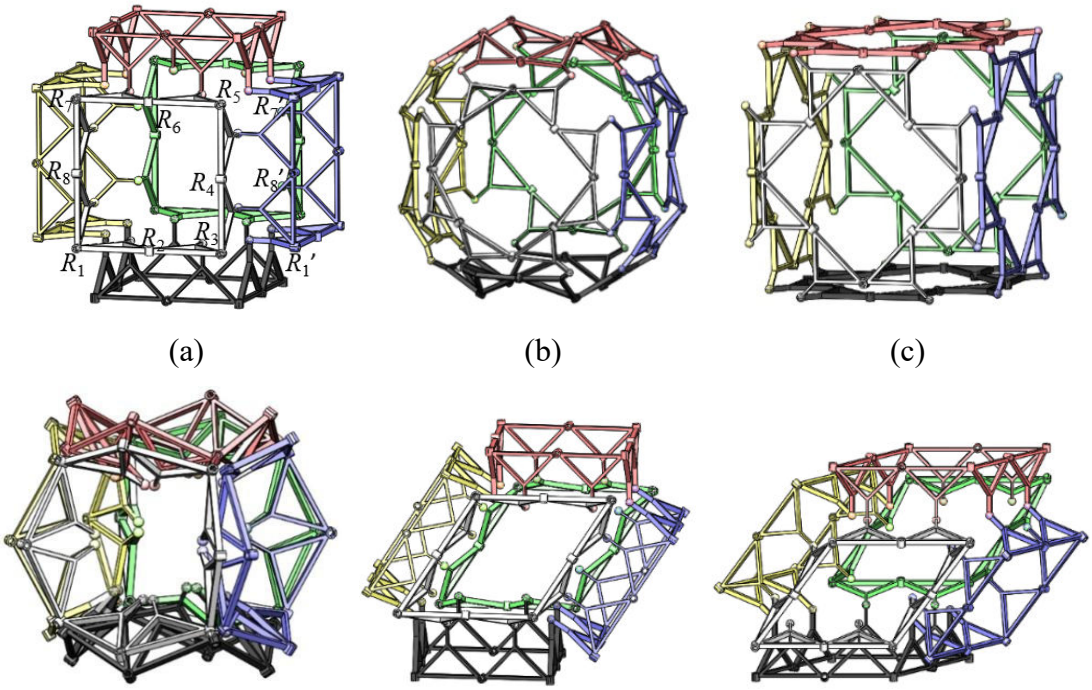

(a) (b) (c)

(d) (e) (f)

Fig. 4.26 Rhombohedron DPM based on orthogonal 8R linkages: (a) initial posture; (b)-(c) outward deploying; (d) inward deploying; (e)-(f) 3-DOF parallelepiped mechanism mode.

Using the construction method proposed, mechanisms based on other orthogonal single-loop linkages can be obtained as well. Figure 4.25 illustrates the pentagonal prism DPM constructed by two orthogonal 10R linkages using ten S joints. The mechanism has

two modes, including a 1-DOF deployable mode [Fig. 4.25(b-c)] and a 2-DOF planar 5R linkage mode [Fig. 4.25(d), in which the mechanism behaves as a planar 5R linkage and has two DOFs]. Unlike the DPM based on orthogonal 8R linkages, this DPM has no spherical mode. This DPM is a new variable-DOF mechanism and therefore enriches the types of variable-DOF mechanisms.

Connecting six orthogonal 8R linkages, leads to the construction of a DPM in the shape of a rhombohedron in the initial state (Fig. 4.26). Each 8R linkage connects with four 8R linkages using two S joints between each pair of 8R linkages. In the initial state, the planes defined by R_2, R_4, R_6 and R_8 in each 8R linkage generate a rhombohedron and the planes defined by the centers of S joints in each 8R linkage generate a smaller rhombohedron. The angle τ' between the plane defined by R_3 and R_5 in the first 8R linkage and the plane defined by R_1' and R_7' in the adjacent 8R linkage is 90°.

The mechanism has two modes. In the first mode, it can be deployed outward and inward, as shown in Figs. 4.26(b-d). When deployed outward, τ' ranges from 90° [Fig. 4.26(a)] to 270° [Fig. 4.26(c)]; when deployed inward [Fig. 4.26(d)], τ' ranges from 90° to 10°, considering the link interference. In the second mode, R_2, R_4, R_6 and R_8 in each 8R linkage lose their DOFs, and the mechanism behaves as parallelepiped mechanism [170]. The mechanism in this mode has three DOFs, as shown in Figs. 4.26(e) and (f).

A 1-DOF DPM in the shape of a dodecahedron is also designed as shown in Fig. 4.27. It is constructed using twelve 10R orthogonal linkages and sixty S joints. The mechanism can also be deployed outward [Fig. 4.27(b)] and inward [Fig. 4.27(c)]. It is noted the deploying ratio depends on the shape of the links which affects the interference between the links.

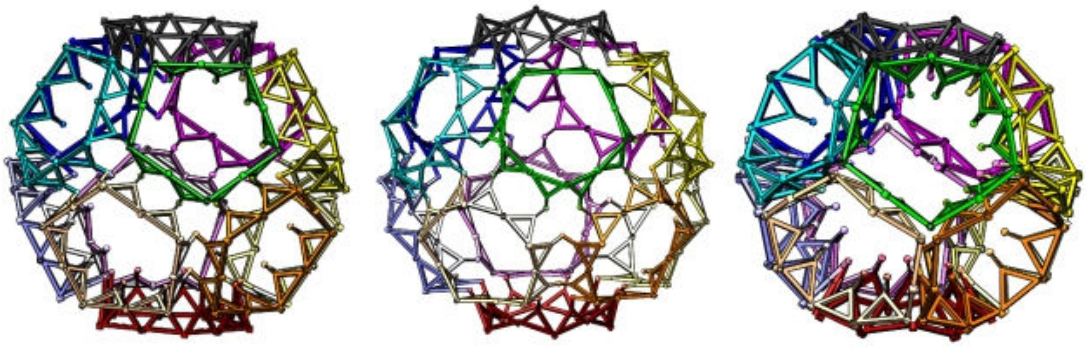

(a) (b) (c)

Fig. 4.27 Dodecahedron DPM based on orthogonal 10R linkages: (a) initial posture; (b) outward deploying; (c) inward deploying

4.3 DPMs Based on Different Loops

Instead of constructing DPMs using identical loops, the same type of loops with different sizes or different types of loops can be adopted to connect DPMs.

4.3.1 DPMs Based on the Same Type of Linkages with Different Sizes

By connecting two single-loop linkages with the same type but different sizes, frustum DPMs are constructed. The deployable triangular frustum mechanism based on two Bricard linkages will be addressed as an example to illustrate the construction method. As shown in Fig. 4.28, the S joints of the bigger Bricard linkage are on the medians of the triangle links, while the S joints of the smaller one have offset from the medians.

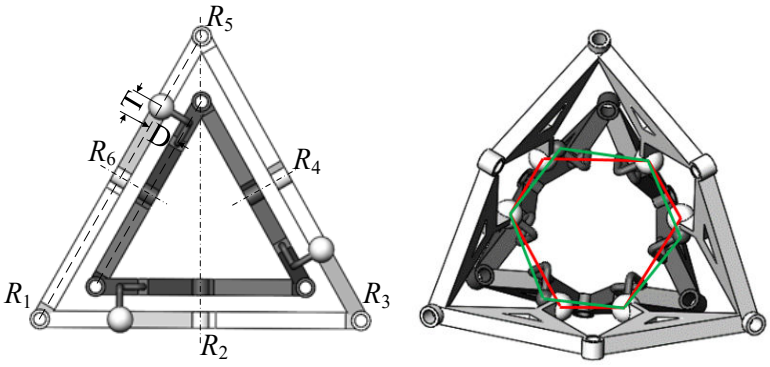

(a) (b)

Fig. 4.28 The relationship between the two Bricard linkages with different sizes: (a) the positions of the S joints; (b) semi-regular hexagons defined by the S joints

Let l and l' represent the link lengths of the two triads respectively. The distances between the medians of the triangles within the two loops along the direction of the joint axis of R_2 (or R_4, R_6) and R_1R_3 (or R_3R_5, R_5R_1) are noted as D and T respectively [Fig. 4.28(a)]. D and T are calculated as

$$D = l/\sqrt{3} - l'/\sqrt{3} \tag{4.28}$$

$$T = l/2 - l'/2 \tag{4.29}$$

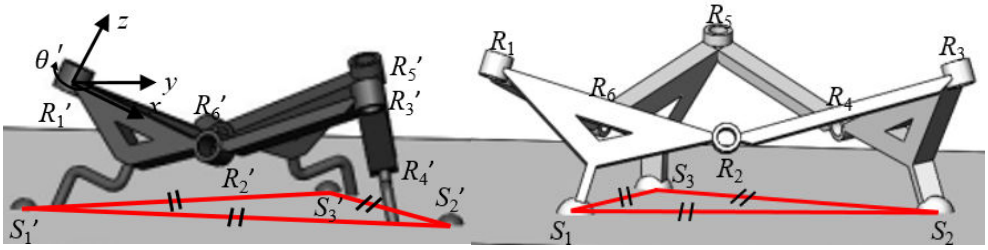

(a) (b)

Fig. 4.29 The two Bricard linkages with different sizes: (a) the smaller one; (b) the bigger one

Unlike the DPM constructed by *n*R orthogonal linkages with the same size using *n* S joints, the loop can only be connected to the other loop with different size by *n*/2 S joints. As shown in Fig. 4.28(a), only three S joints are used to connect the two Bricard linkages with different sizes. The ratio of one side length and the adjacent side length of the semi-regular hexagons defined by the S joints of the two Bricard linkages respectively are distinct. The smaller loop rotates when deploying [Fig. 4.28(b)].

Now it will be verified that the three spheres of the bigger Bricard linkage and those of the smaller Bricard linkage form two regular triangles respectively during the deploying process (Fig. 4.29). The position vectors of the spheres of the bigger Bricard linkage have been given in Eq. (4.7), and those of the smaller Bricard linkage are to be calculated.

The joint centre of first S joint of the smaller Bricard linkage is obtained as

$$\boldsymbol{S_1'} = \left\{ \frac{l'}{2} - T \quad -D \quad e \right\}^T \tag{4.30a}$$

The position vectors of the other two S joints are calculated as

$$\begin{Bmatrix} \boldsymbol{S_2'} \\ \mathbf{1} \end{Bmatrix} = {}_1^2T\,{}_3^2T \begin{Bmatrix} \boldsymbol{S_1'} \\ 1 \end{Bmatrix} = \{S_{2x}' \quad (l'-l)C\theta'/\sqrt{3} - (l-2l')S\theta'/2 \quad S_{2z}' \quad 1\}^T \tag{4.30b}$$

where

$$S_{2x}' = -3l'C\theta' + 3(l-2l')C^2\theta'/2 + 3l'b - 3eab - \sqrt{3}(l-l')C\theta'S\theta']/3b$$

$$a = \sqrt{\frac{2C\theta'+1}{(C\theta'+1)^2}}$$

$$b = 1 + C\theta'$$

$$S_{2z}' = C\theta'\{-e/b - (l-2l')a/2\} + a[3l' + \sqrt{3}(l-l')S\theta']/3$$

$$\begin{Bmatrix} \boldsymbol{S_3'} \\ \mathbf{1} \end{Bmatrix} = {}_1^2T\,{}_3^2T\,{}_4^3T\,{}_5^4T \begin{Bmatrix} \boldsymbol{S_1'} \\ 1 \end{Bmatrix} = \{S_{3x}' \quad S_{3y}' \quad la/2 + e(1/c-1) \quad 1\}^T \tag{4.30c}$$

where

$$S_{3x}' = \{3C\theta'[-2l' + (lC\theta')/c + 2ea] + 2\sqrt{3}(l'-l)S\theta'\}/6$$

$$S_{3y}' = (l'-ea)S\theta' + C\theta'[(l'-l)/\sqrt{3} - l\tan(\theta'/2)/2]$$

$$c = \sqrt{\frac{S^2\,\theta'}{(C\,\theta'+1)^2}}$$

The three spheres form a triangle, whose squared side lengths are

$$\begin{aligned}|\boldsymbol{S_2'} - \boldsymbol{S_1'}|^2 = |\boldsymbol{S_3'} - \boldsymbol{S_2'}|^2 = |\boldsymbol{S_1'} - \boldsymbol{S_3'}|^2 = \left[C\,\theta'\,D - D + S\,\theta'\left(\frac{l}{2} - l'\right)\right]^2 \\ + \left\{\frac{l'}{2} + T - ea - \frac{C\,\theta'}{2b}\left[\left(l' - \frac{l}{2}\right)C\,\theta' + 2(l' + S\,\theta'\,D)\right]\right\}^2 \\ + \left[e - l'a + \frac{e\,C\,\theta'}{b} + S\,\theta'\,aD + C\,\theta'\,a\left(\frac{l}{2} - l'\right)\right]^2\end{aligned} \tag{4.31}$$

Equation (4.31) indicates that the triangle formed by the three spheres of the smaller Bricard linkage is a regular triangle. The squared side lengths of the triangle defined by the spheres of the bigger Bricard linkage are yielded as

$$\begin{aligned}|\boldsymbol{S_2} - \boldsymbol{S_1}|^2 = |\boldsymbol{S_3} - \boldsymbol{S_2}|^2 = |\boldsymbol{S_1} - \boldsymbol{S_3}|^2 \\ = \{-6el\sqrt{d} - 2elC\theta\sqrt{d} + 4e^2d + l^2[3 + C\theta(3 + C\theta)]\}/[2(1 + C\theta)]\end{aligned} \tag{4.32}$$

where

$$d = 1 + 2C\theta$$

The triangle defined by the three spheres of the bigger Bricard linkage also keeps as a regular triangle. There always exist θ and θ' to equalise the two side lengths. Let $l = 0.05m$, $e = 0.02m$ and $l' = 0.03m$, $|\boldsymbol{S_2} - \boldsymbol{S_1}|^2 = |\boldsymbol{S_2'} - \boldsymbol{S_1'}|^2 = 0.0044m^2$ in the initial position, when $\theta = 120°$.

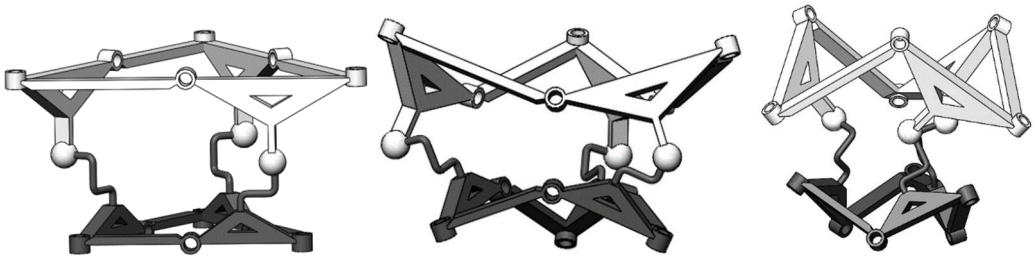

(a) (b) (c)

Fig. 4.30 Prism mechanism constructed using two Bricard linkages with different sizes: (a) initial posture; (b) outward deploying; (c) inward deploying

Based on the results, a triangular frustum mechanism is constructed using the two Bricard linkages with different sizes, as shown in Fig. 4.30. The mechanism can be deployed outward [Fig. 4.30(b)] and inward [Fig. 4.30(c)].

A prototype of the triangular frustum mechanism is fabricated to verify the feasibility of the mechanism (Fig. 4.31). The links are 3D printed with magnet disc inside, and the S joints are designed using steel balls.

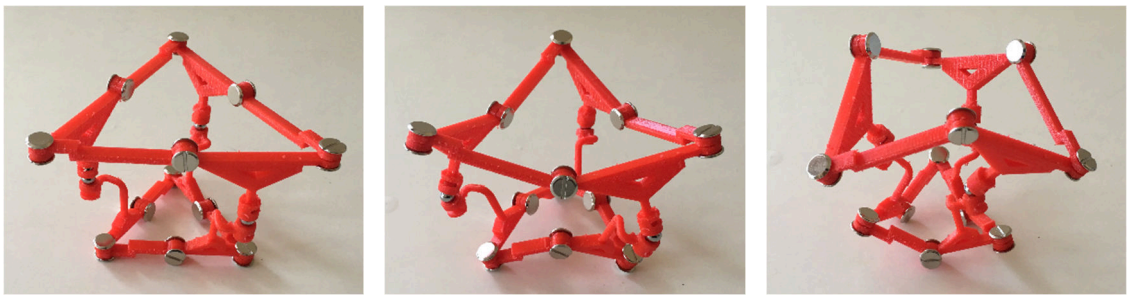

(a) (b) (c)

Fig. 4.31 Prototype of the triangular frustum mechanism constructed using two Bricard linkages with different sizes: (a) initial posture; (b) outward deploying; (c) inward deploying

A 1-DOF three-layer triangular frustum DPM based on Bricard linkages with different sizes is also constructed with a high stowed-to-deployed ratio (Fig. 4.32). It is measured in the CAD software that the height of the DPM is 143.87*mm* in the initial state [Fig. 4.32(a)] and can reach 74.99*mm* [Fig. 4.32(c)] when deployed inward. The deploying ratio is 1.92.

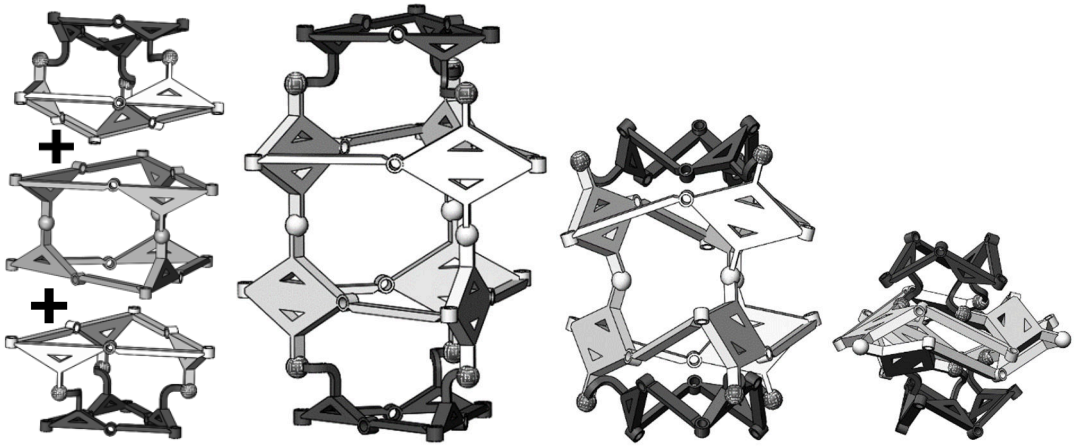

(a) (b) (c) (d)

Fig. 4.32 The multiple-layer DPM constructed using Bricard linkages with different sizes: (a) the construction method; (b) initial posture; (c) outward deploying; (d) inward deploying

Similarly, a quadrilateral frustum mechanism based on two 8R linkages with different sizes is built, as shown in Fig. 4.33. Unlike the DPM with identical loops, the mechanism has no planar 4R linkage mode or spherical 4R linkage mode. The distances between the medians of the triangles within the two loops along the direction of the joint axis of R_4R_8 and R_1R_7 are noted as D and T respectively. D and T (shown in Fig. 4.34) are calculated

as

$$D = l - l' \tag{4.33}$$

$$T = l/2 - l'/2 \tag{4.34}$$

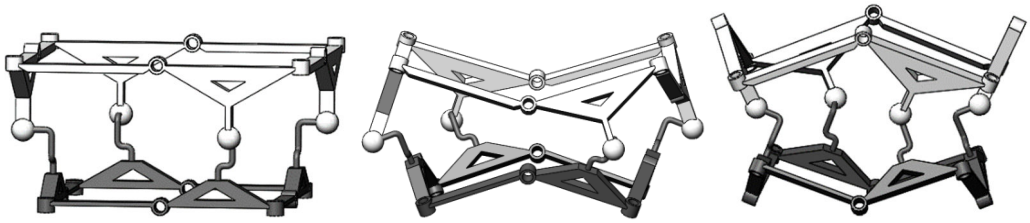

(a) (b) (c)

Fig. 4.33 Quadrilateral frustum mechanism constructed using two 8R linkages with different sizes: (a) initial posture; (b) outward deploying; (c) inward deploying

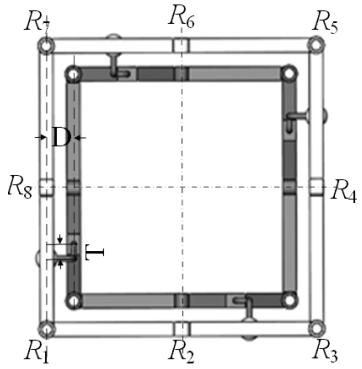

Fig. 4.34 Parameters of the two 8R linkages with different sizes

4.3.2 DPMs with Double Layers

Extending the mechanisms along the radial direction refers to constructing polyhedrons whose faces have double layers. First, a 1-DOF double-layer unit is designed, as shown in Fig. 4.35. The unit is obtained by deforming the triangular frustum mechanism in Fig. 9, through the deforming process presented in Fig. 4.36. The bigger Bricard linkage deploys while rotating. In the initial state, $R_1 // R_1'$ and R_2 and R_2' are collinear [Fig. 4.35(a)].

A double-layer prism mechanism is obtained by connecting two double-layer units, as shown in Fig. 4.37. The two units are symmetric about the mirror plane defined by the S joints. The DPM has one DOF and can be deployed outward [Fig. 4.37(b)] and inward [Fig. 4.37(c)]. The interference problem of the S joints can be solved by using steel balls and links with magnet disc.

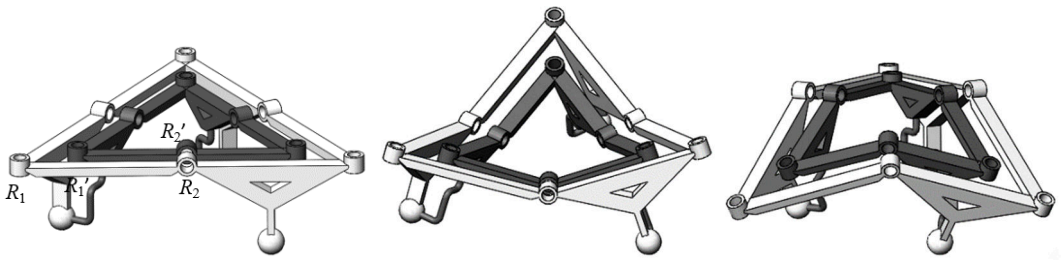

(a) (b) (c)

Fig. 4.35 The double-layer deployable unit constructed using Bricard linkages: (a) initial posture; (b) outward deploying; (c) inward deploying

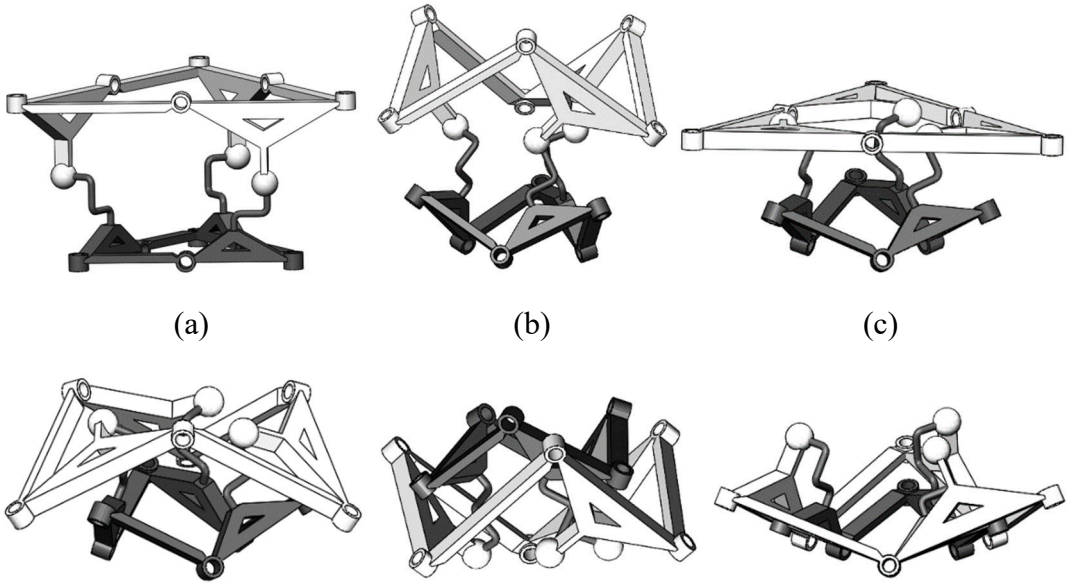

(a) (b) (c)

(d) (e) (f)

Fig. 4.36 The deforming process: (a) triangular frustum mechanism configuration; (b-e) deforming process; (f) double-layer configuration

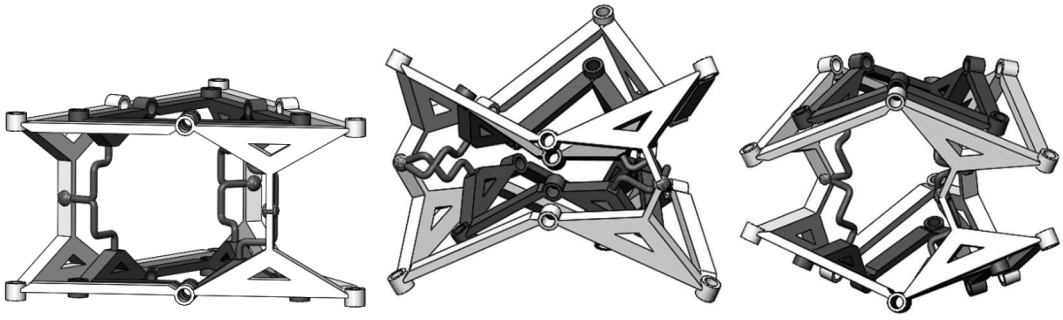

(a) (b) (c)

Fig. 4.37 The double-layer prism mechanism constructed using Bricard linkages: (a) initial posture; (b) outward deploying; (c) inward deploying

To construct DPMs using the double-layer units, three additional S joints are inserted on the bigger Bricard linkage, as shown in Fig. 4.38. Based on the modified units, 1-DOF double-layer tetrahedron DPM and octahedron DPM are obtained, as shown in Figs. 4.39 and 4.40 respectively.

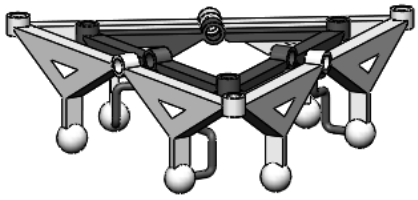

Fig. 4.38 Variation of the double-layer deployable unit

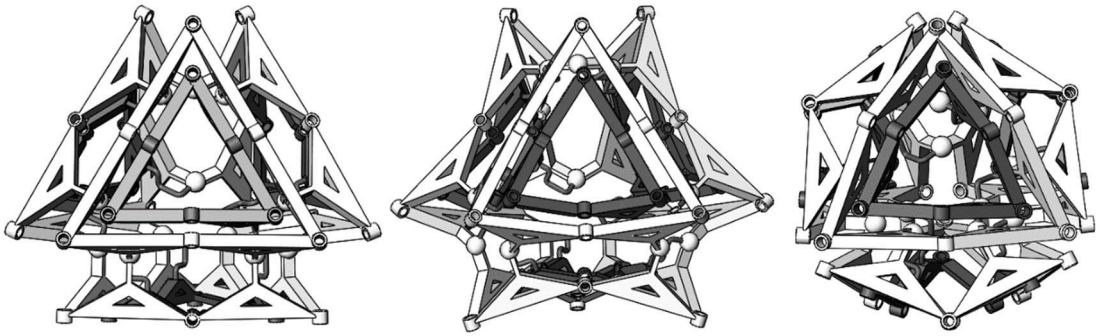

(a) (b) (c)

Fig. 4.39 Double-layer tetrahedron DPM constructed using Bricard linkages: (a) initial posture; (b) outward deploying; (c) inward deploying

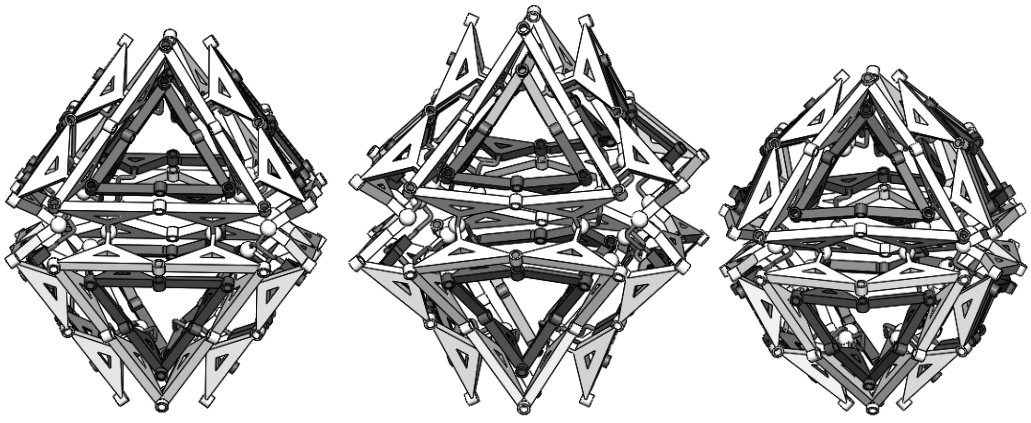

(a) (b) (c)

Fig. 4.40 Double-layer octahedron DPM constructed using Bricard linkages: (a) initial posture; (b) outward deploying; (c) inward deploying

DPMs constructed using 8R/10R-based double-layer units can also be built, which can

be deployed but have no planar or spherical 4R/5R linkage mode.

4.3.3 DPMs Based on Different Types of Linkages

In this section, different types of loops will be used to connect DPMs. 1-DOF DPMs can be obtained by connecting the virtual-plane-constrained 8R/10R linkages and Bricard linkages. When connecting additional loops, the degree of over-constraint increases but the mechanism still has 1-DOF [49]. As shown in Fig. 4.41, a 1-DOF rectangular pyramid mechanism is built by connecting four Bricard linkages and one 8R linkage. In the initial position, the Bricard linkages and the 8R linkage are in the shapes of regular triangles and square respectively, and the joint axis of R_1 in the 8R linkage and R_1' in the Bricard linkage are on the same plane. The mechanism can be deployed outward, which refers to the case that the distance between R_1 and R_1' increases [Fig. 4.41(b)], and inward, which refers to the case in which the distance between R_1 and R_1' decreases [Fig. 4.41(c)].

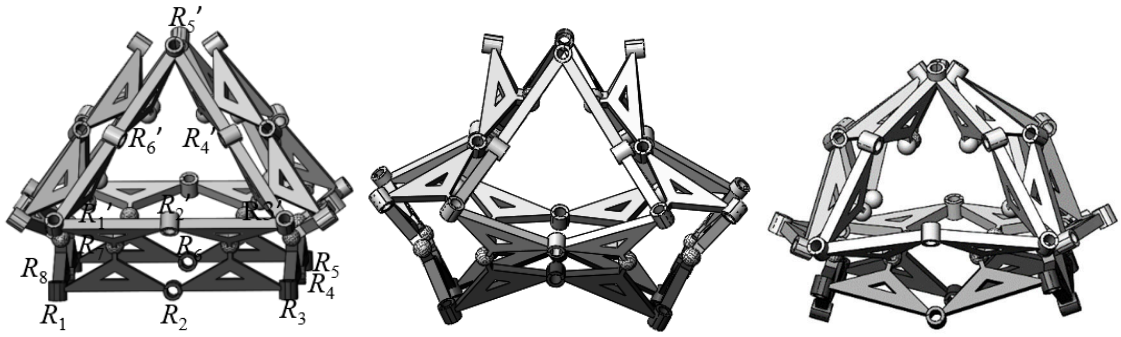

(a) (b) (c)

Fig. 4.41 The rectangular pyramid mechanism: (a) initial posture; (b) outward deploying; (c) inward deploying

A triangular prism mechanism is constructed using two Bricard linkages and three 8R linkages, as shown in Fig. 4.42. The mechanism can also be deployed outward [Fig. 4.42(b)] and inward [Fig. 4.42(c)]. Apart from the 1-DOF deployable mode, the mechanism has an additional 2-DOF translation mode, in which the Bricard linkages are immobile and the 8R linkages move as planar 4R linkages [Fig. 4.42(d)]. The mechanism in the translation mode is equal to the 14-bar mechanism in Fig. 4.42(e), and can translate along the direction that is perpendicular to R_2R_6. It can switch modes from deployable mode to translation mode through transition configuration, which is referred to the initial position shown in Fig. 4.42(a). In this transition configuration, the Bricard linkages and

8R linkages are in the shapes of regular triangles and squares respectively. The joint axis of R_1' in the upper Bricard linkage and that in the lower Bricard linkage are collinear, and perpendicular to the joint axes of R_1 and R_7 of the 8R linkage.

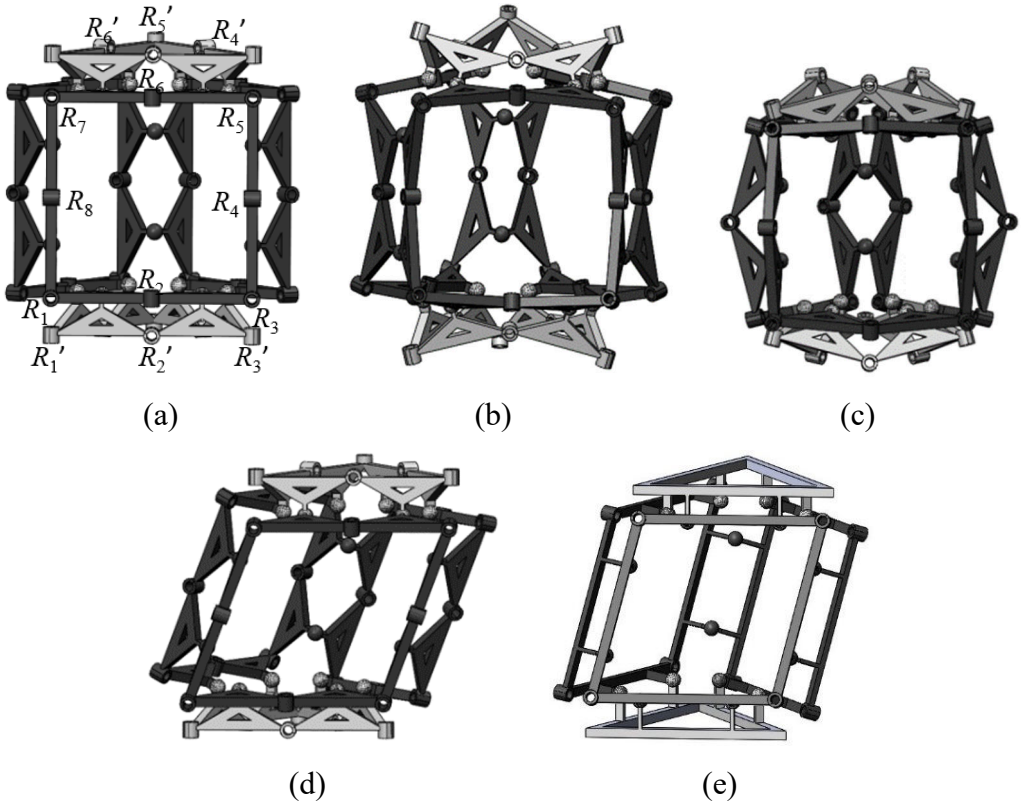

Fig. 4.42 The triangular prism mechanism: (a) initial posture; (b) outward deploying; (c) inward deploying; (d) 2-DOF translation mode; (e) the equilateral 2-DOF mechanism

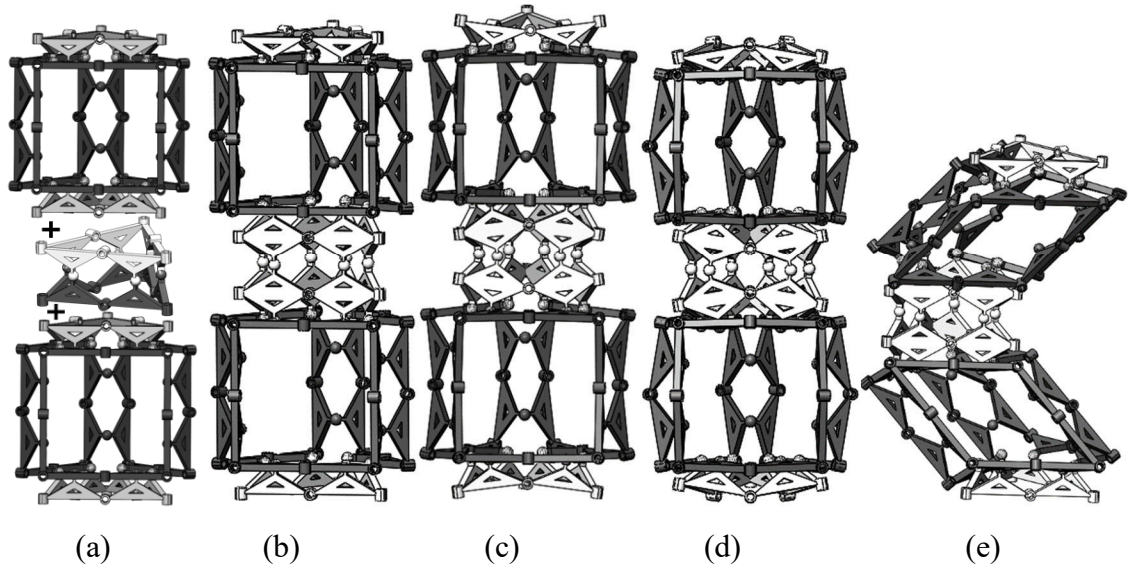

Fig. 4.43 The multiple-layer DPM constructed using Bricard linkages and 8R linkages: (a) the construction method; (b) initial posture; (c) outward deploying; (d) inward deploying; (e) 4-DOF translation mode

By joining n DPMs in Fig. 4.42 and n-1 DPMs in Fig. 4.2 along the axial direction, multiple-layer DPMs are obtained. The DPM has one DOF when deployed and the DOF is $2n$ in the translation mode. For example, the two-layer DPM in Fig. 4.43 has four DOFs in the translation mode. The mechanisms have the potential to be applied to robot arms.

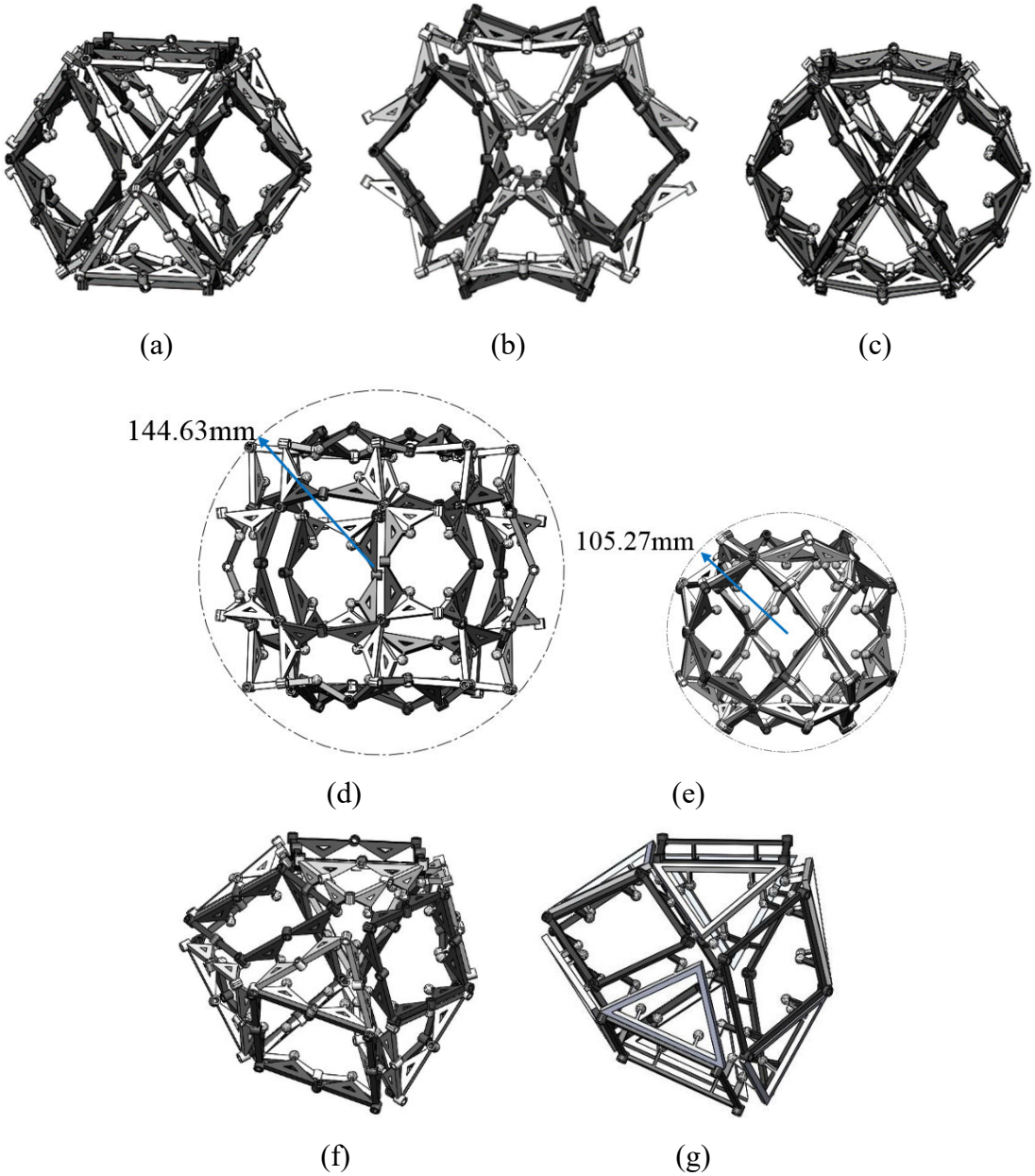

Fig. 4.44 The cuboctahedron mechanism: (a) initial posture; (b, d) outward deploying; (c, e) inward deploying; (f) 3-DOF cuboctahedron mechanism mode; (g) the equilateral 3-DOF mechanism

A cuboctahedron mechanism is also constructed, using six 8R linkages and eight Bricard linkages, as shown in Fig. 4.44. The mechanism has 1-DOF when deployed and

can switch to 3-DOF cuboctahedron mechanism [171] mode [Fig. 4.44(f)] through the transition configuration (initial position). The mechanism in the cuboctahedron mechanism mode is equal to the mechanism shown in Fig. 4.44(g). As observed from the 3D model in CAD, the radius of the sphere generated by the mechanism reaches 144.63*mm* when deployed outward [Fig. 4.44(d)] and can be 105.27*mm* when deployed inward [Fig. 4.44(e)]. The deploying ratio of the mechanism is $r = \pi r_o^3/\pi r_i^3 = 144.63^3/105.27^3 = 2.59$. It is noted the deploying ratio will increase if the structure is optimized to avoid interference.

A 1-DOF icosidodecahedron mechanism is built based on twelve 10R linkages and twenty Bricard linkages, as shown in Fig. 4.45. The deploying ratio of the mechanism is $r = \pi r_o^3/\pi r_i^3 = 221.85^3/156.65^3 = 2.84$.

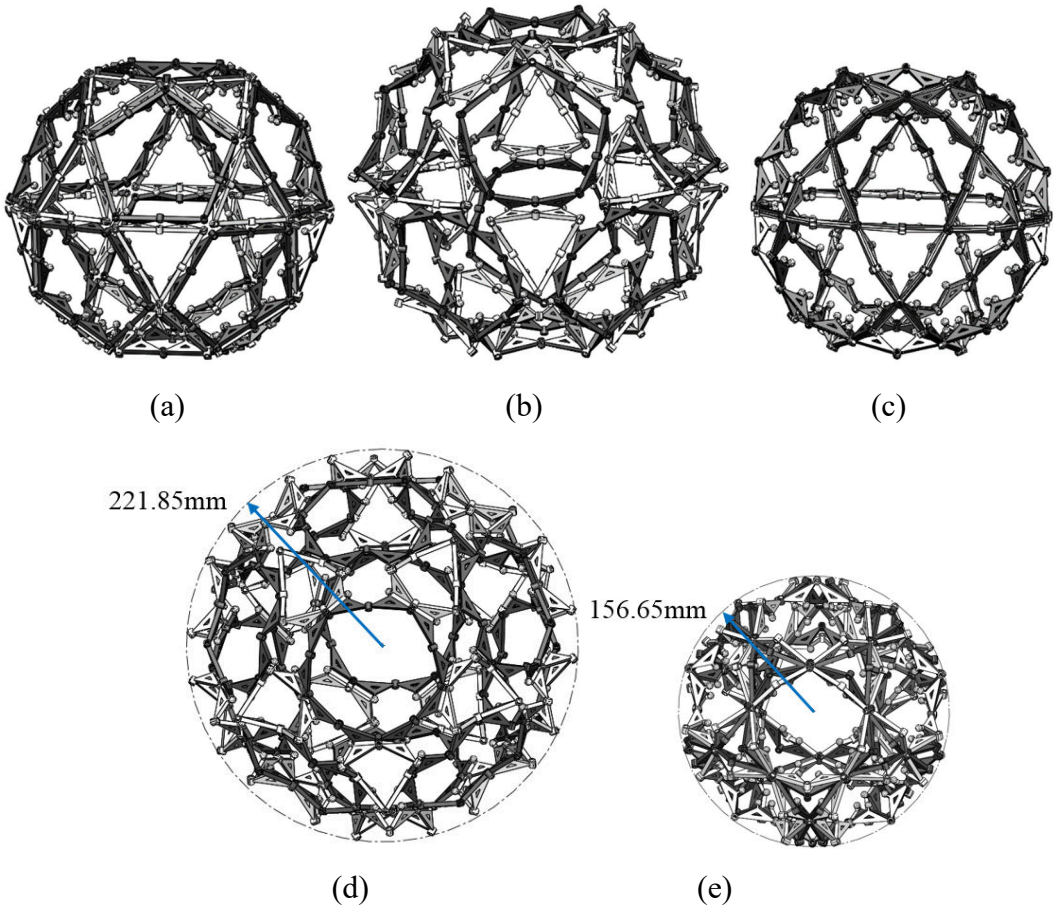

Fig. 4.45 The icosidodecahedron mechanism: (a) initial posture; (b, d) outward deploying; (c, e) inward deploying

Similarly, we can construct the following 15 DPMs (shown in Table 4.3): rhombicuboctahedron, truncated tetrahedron, truncated octahedron, truncated cube, snub cube, great rhombicuboctahedron, truncated icosahedron, truncated dodecahedron,

rhombicosidodecahedron, snub dodecahedron, pentagonal pyramid, triangular cupola, square cupola, pentagonal cupola, and pentagonal rotunda. It is noted that the DPMs based on the rhombicuboctahedron, truncated octahedron, great rhombicuboctahedron, rhombicosidodecahedron, triangular cupola, square cupola, pentagonal cupola have an additional motion mode with 6-DOF, 5-DOF, 5-DOF, 3-DOF, 1-DOF, 2-DOF and 3-DOF [171] respectively.

Table 4.3 DPMs

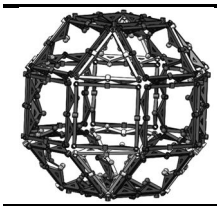	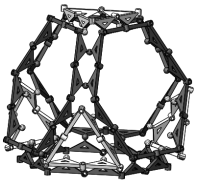	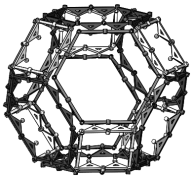	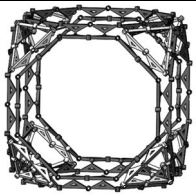	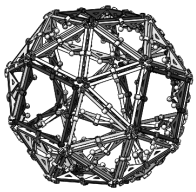
Rhombicuboc-tahedron	Truncated tetrahedron	Truncated octahedron	Truncated cube	Snub cube
6-DOF[a]		5-DOF		
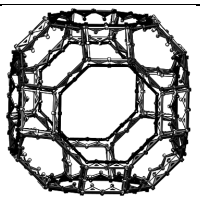	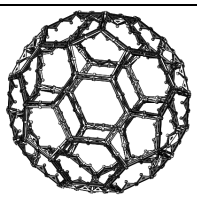	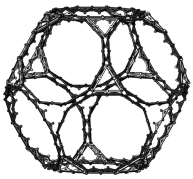	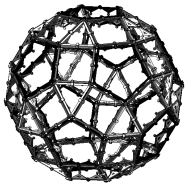	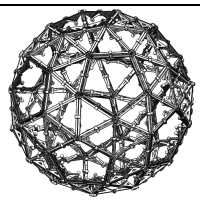
Great rhombicuboct-ahedron	Truncated icosahedron	Truncated dodecahedron	Rhombicosid-odecahedron	Snub dodecahedron
5-DOF			3-DOF	
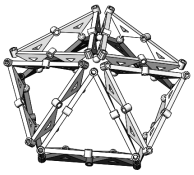	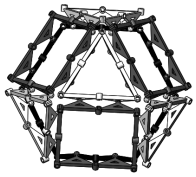	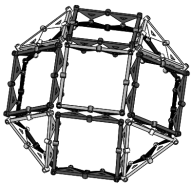	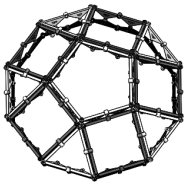	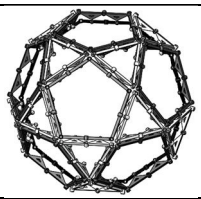
Pentagonal pyramid	Triangular cupola	Square cupola	Pentagonal cupola	Pentagonal rotunda
	1-DOF	2-DOF	3-DOF	

a. The DOFs are those of the mechanisms in the polyhedral mechanism modes, when the two links of the triads are on the same plane.

4.4 Summary

In this chapter, a construction method for designing DPMs has been addressed. Spatial single-loop linkages, such as Bricard linkages, 8R linkages and 10R linkages composed of several symmetric spatial triad units are connected using S joints. There are two types of DPMs, including the prism mechanisms and polyhedral mechanisms. The DPMs have

only one DOF when deployed and can be deployed inward and outward. Several mechanisms involving 8R/10R/12R linkages have multiple modes and can switch modes through transition positions. The variations of the DPMs, in which the S joints have offset, and the DPMs with different types of loops, the same type of loops but different sizes, double-layer and multiple-layer DPMs have been discussed respectively.

The single-layer DPMs have potential applications for education, entertainment and decorations and the multiple-layer DPMs can be used in applications that require a large folding ratio, such as sunshield or other aerospace mechanisms.

CHAPTER 5 – TYPE SYNTHESIS OF DEPLOYABLE POLYHEDRAL MECHANISMS WITH MULTIPLE MODES CONNECTED USING RRR CHAINS

DPMs connected using S joints have been described in Chapter 4. However, S joints are not as practical as R joints. They are expensive and are not easy to assemble. Hence, in this chapter, RRR chains with perpendicular joints will be used to replace the S joint.

5.1 Single-loop Linkages

In this chapter, there are two types of triad units adopted, including unit I with triangle links which are used to construct single-loop linkages, and unit II with straight links to connect the single-loop linkages [Figs. 5.1(a) and (b) respectively]. As described in the previous chapter, the adjacent R joints can be with arbitrary twist angles. The orthogonal unit, which is the most practical one, is just an example to illustrate the construction method.

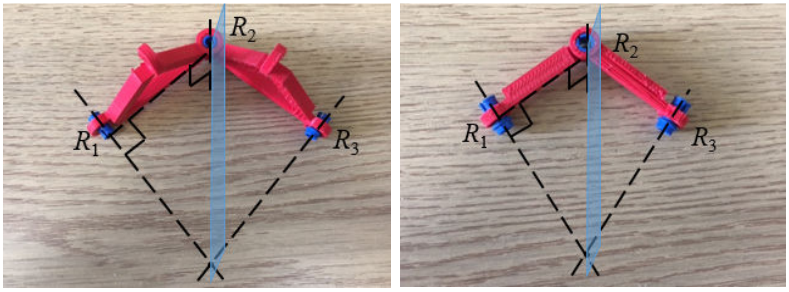

(a) (b)

Fig. 5.1 RRR triad: (a) unit I with triangle links; (b) unit II with straight links

Figure 5.2 shows one case of Bricard linkages obtained by connecting three units I. The linkage is axisymmetric about the line that passes through the intersection of the axes of R_2, R_4 and R_6 and is perpendicular to the plane defined by the three R joints in the initial posture. The mechanism has 1-DOF and can be deployed outward [Fig. 5.2(b)] and inward [Fig. 5.2(c)].

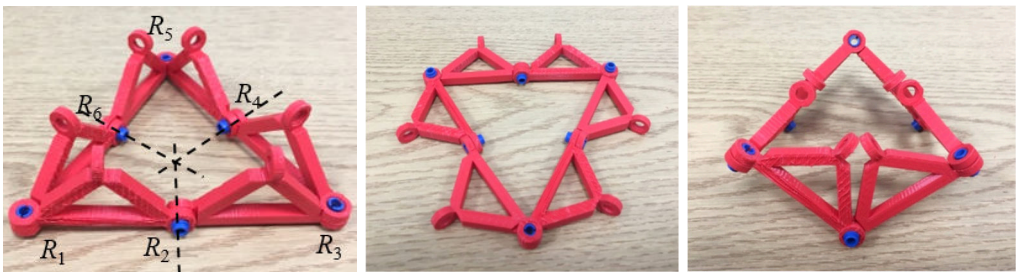

(a) (b) (c)

Fig. 5.2 Orthogonal Bricard linkage constructed using RRR units: (a) initial posture; (b) outward deploying; (c) inward deploying

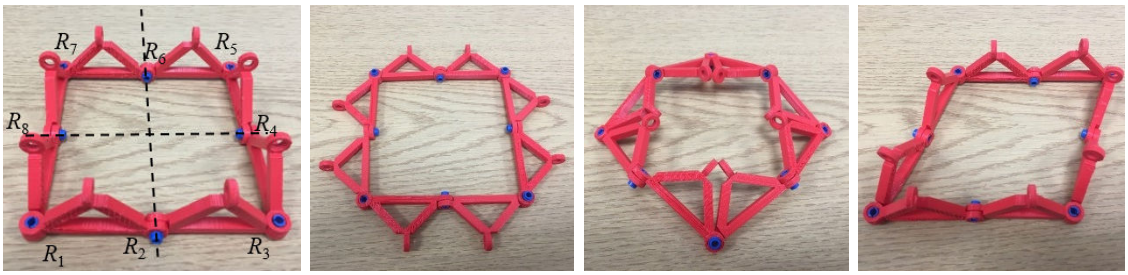

(a) (b) (c) (d)

Fig. 5.3 Orthogonal 8R linkage constructed using RRR units: (a) initial posture; (b) outward deploying; (c) inward deploying; (d) planar 4R linkage mode

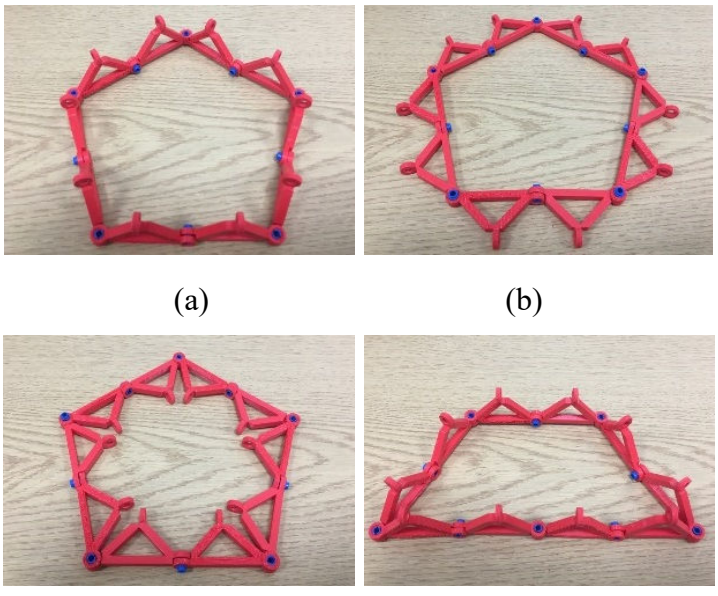

(a) (b)

(c) (d)

Fig. 5.4 Orthogonal 10R linkage constructed using RRR units: (a) initial posture; (b) outward deploying; (c) inward deploying; (d) planar 5R linkage mode

When connecting four units I, an 8R linkage can be obtained (Fig. 5.3). In the rest of this chapter, additional constraints are imposed on the linkage. In a deployable

mechanism composed of the 8R kinematic chain, there only exists a 1-DOF deploying mode [Figs. 5.3(b-c)], a 1-DOF planar 4R linkage mode [Fig. 5.3(d)] and a 1-DOF spherical 4R linkage mode (see Section 5.3 for details) due to the constraints imposed on the 8R kinematic chain by the deployable mechanism.

Similarly, the 10R kinematic chain in a deployable mechanism has only a 1-DOF deployable mode [Figs. 5.4(b-c)] and a 2-DOF 5R linkage mode [Fig. 5.4(d)]. In the next section, DPMs will be constructed using the above single-loop linkage chains.

5.2 DPMs Based on Bricard Linkages

The prism mechanism in Fig. 5.5 is constructed by connecting two identical Bricard linkages using six RRR kinematic chains (unit II, represented by C_i in Fig. 5.5). The construction process is shown in Fig. 5.6(a). In the initial state [Fig. 5.5(a)], the joint axes of R_1 and R'_1 coincide and all the chains are parallel. The mechanism has 1-DOF and can be deployed outward and inward, as shown in Figs. 5.5(b-c). R_2, R_2' and the three R joints in chain 1 and those in chain 2 form a spatial 8R linkage, so do R_1, R_1', the three joints of chain 1 and those in chain 6. The joint axes of R_{11}, R_{22}, R_{33}, R_{44}, R_{55} and R_{66} (the second R joints within the chains) are always on the same plane (refers to the mirror plane) and the six R joints form a semi-regular hexagon, as shown in Fig. 5.6(b). Among the six R joints, R_{22}, R_{44} and R_{66} form an equilateral triangle, whose side length varies when deploying the mechanism.

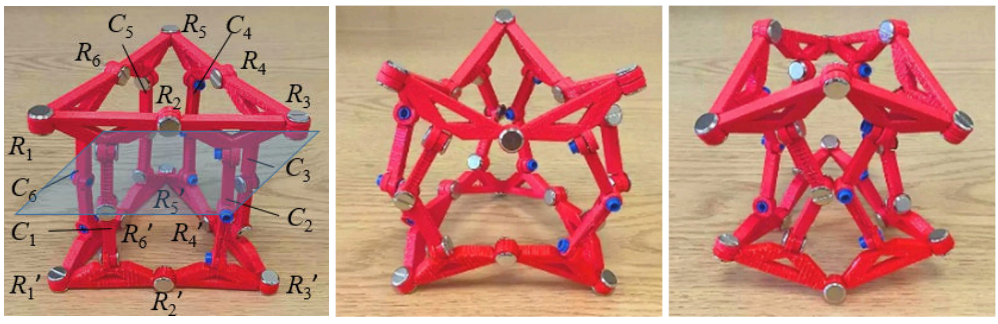

(a) (b) (c)

Fig. 5.5 Prism mechanism connected by Bricard linkages using six RRR chains: (a) initial posture; (b) outward deploying; (c) inward deploying

A double-layer prism mechanism is also constructed using two prism mechanisms in Fig. 5.5(a), as shown in Fig. 5.7. The upper prism mechanism deploys outward with the lower prism mechanism deploying inward [Fig. 5.7(b)] and the upper prism mechanism

deploys inward with the lower prism mechanism deploying outward [Fig. 5.7(c)]. A four-layer prism mechanism is also assembled, as shown in Fig. 5.8.

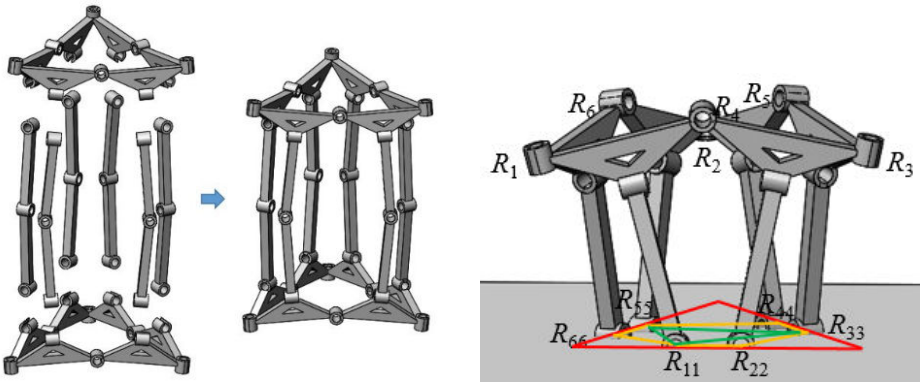

(a) (b)

Fig. 5.6 Prism mechanism connected by Bricard linkages using six RRR chains: (a) construction process; (b) the symmetry of the mechanism

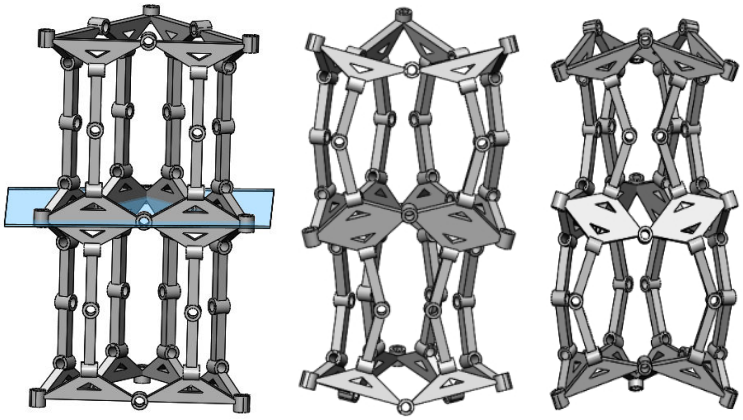

(a) (b) (c)

Fig. 5.7 Double-layer prism mechanism based on Bricard linkages: (a) initial posture; (b) outward deploying; (c) inward deploying

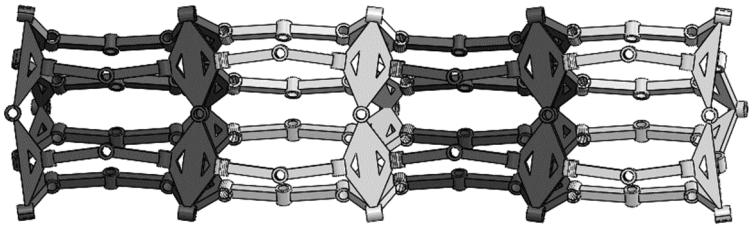

Fig. 5.8 Four-layer prism mechanism

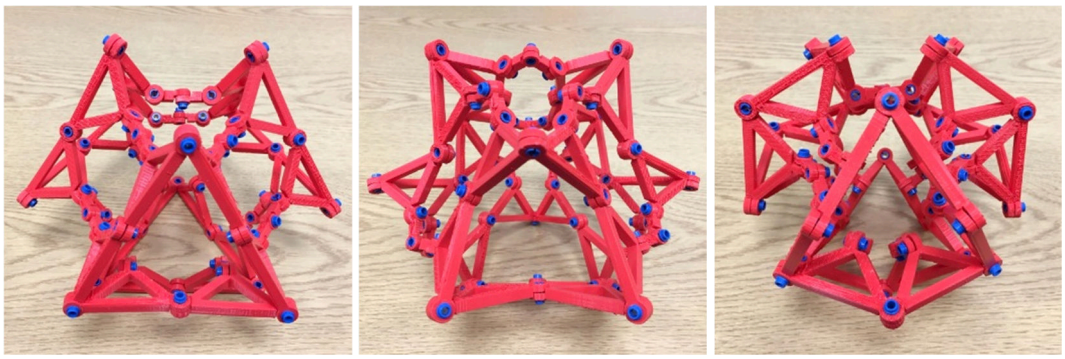

(a) (b) (c)

Fig. 5.9 Tetrahedron DPM based on Bricard linkages: (a) initial posture; (b) outward deploying; (c) inward deploying

By inserting the Bricard linkages into the faces of the tetrahedron, a tetrahedron mechanism constructed using four Bricard linkages and twelve RRR chains is obtained, as presented in Fig. 5.9(a). The mechanism can deploy inward and outward, as shown in Figs. 5.9(b-c).

5.3 DPMs Based on 8R/10R Linkages

Joining two 8R linkages using eight RRR chains, leads to a quadrangular prism mechanism, as shown in Fig. 5.10. In the initial state, the mechanism is in the shape of a regular quadrangular prism, the joint axes of R_1, R_3, R_5 and R_7 of the upper 8R linkage and the corresponding R joints of the lower 8R linkage are collinear, and all the RRR chains are parallel.

The mechanism has a 1-DOF deployable mode, as shown in Figs. 5.10(b-c). Through the singular position (the initial posture), the mechanism can switch into the 1-DOF planar 4R linkage mode, as shown in Fig. 5.10(d).

Now it will be verified that the quadrangular prism mechanism has only 1-DOF. Since the mechanism is always symmetric about the mirror plane, the mechanism is cut in half to facilitate analysis (Fig. 5.11). The cut mechanism is called the virtual-plane constrained 8R linkage. First, the joint axes of R_{11} and R_{33} are constrained to be on the mirror plane, the linkage is equivalent to the mechanism in Fig. 5.12(a). Assume that R_{11} is fixed on the plane, R_{33} has a translational DOF on the plane. The DOF of the linkage can be calculated using the conventional formula for DOF.

$$M = 6(q - p) + \sum_{i=1}^{p} f_i = 6 \times (11 - 13) + 8 + 2 + 3 = 1 \tag{5.1}$$

When s additional R_{ii} are constrained to be on the plane, the 8R linkage is over-constrained. Figure 5.12(b) shows the configuration in which R_{55} and R_{77} are also

constrained to be on the mirror plane ($s = 2$). The two joints have two translational DOFs on the plane respectively. The DOF of the virtual-plane-constrained orthogonal 8R linkage is still one, due to the symmetry characteristics of the linkage.

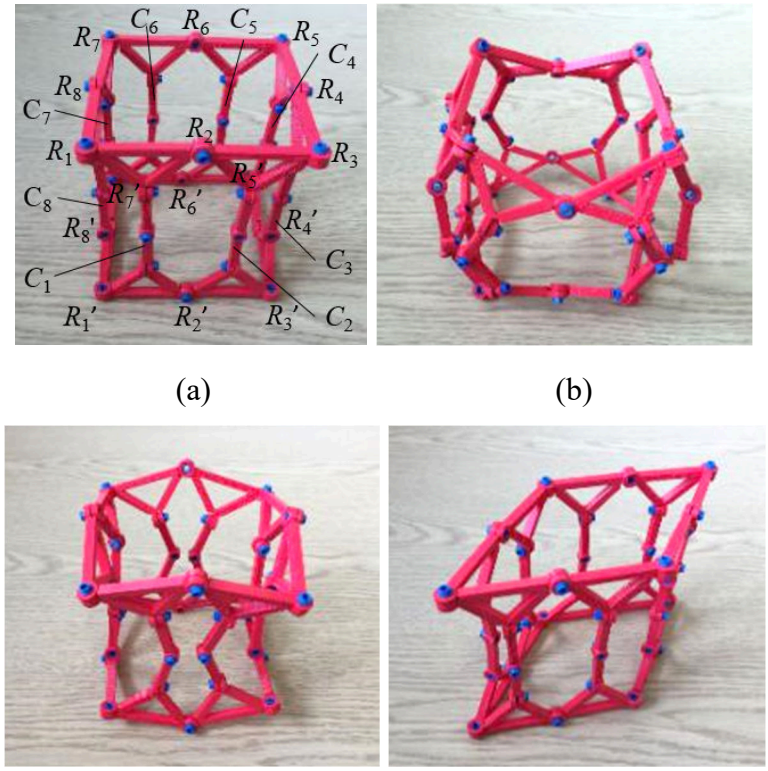

Fig. 5.10 Quadrangular prism mechanism connected by 8R linkages using eight RRR chains: (a) initial posture; (b) outward deploying; (c) inward deploying; (d) planar 4R linkage mode

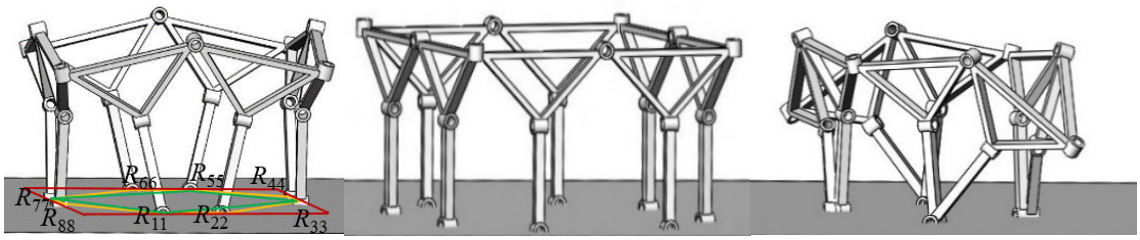

Fig. 5.11 The virtual-plane constrained 8R linkage: (a) spatial mode; (b) planar 4R linkage mode; (c) spherical 4R linkage mode

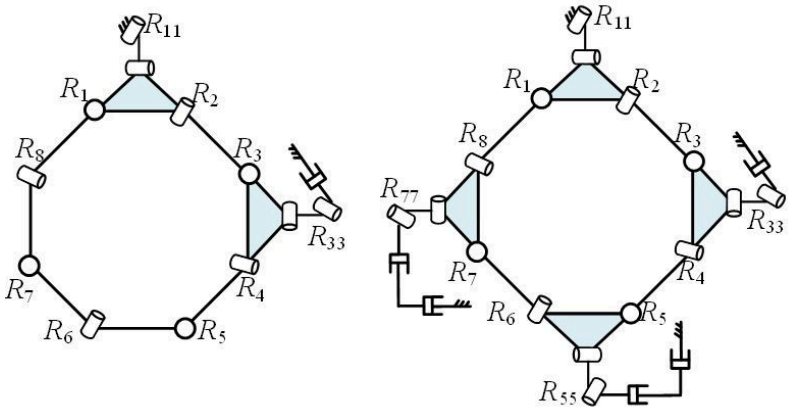

(a) (b)

Fig. 5.12 Sketch of the virtual-plane-constrained orthogonal 8R linkage: (a) two R joints are constrained on the plane; (b) four R joints are constrained on the plane

The virtual-plane-constrained orthogonal 8R linkage has three 1-DOF modes, including 1) spatial mode [deployable mode, as shown in Fig. 5.11(a)], in which R_{11}, R_{22}, R_{33}, R_{44}, R_{55}, R_{66}, R_{77} and R_{88} form a semi-regular octagon, and R_{11}, R_{33}, R_{55} and R_{77} form a square, 2) planar 4R linkage mode [Fig. 5.11(b)], when $R_{11}//R_{22}//R_{55}//R_{66}$, and 3) spherical 4R linkage mode [Fig. 5.11(c), discussed in Section 5.4].

Similar to constrained 8R linkages, it can be readily proved that the virtual-plane-constrained 10R/12R linkages also have one DOF when deployed. The sketch of the virtual-plane-constrained orthogonal 10R/12R linkages with five and six R joints constrained on the plane respectively are shown in Fig. 5.13. The virtual-plane-constrained orthogonal 10R and 12R linkages are both over-constrained.

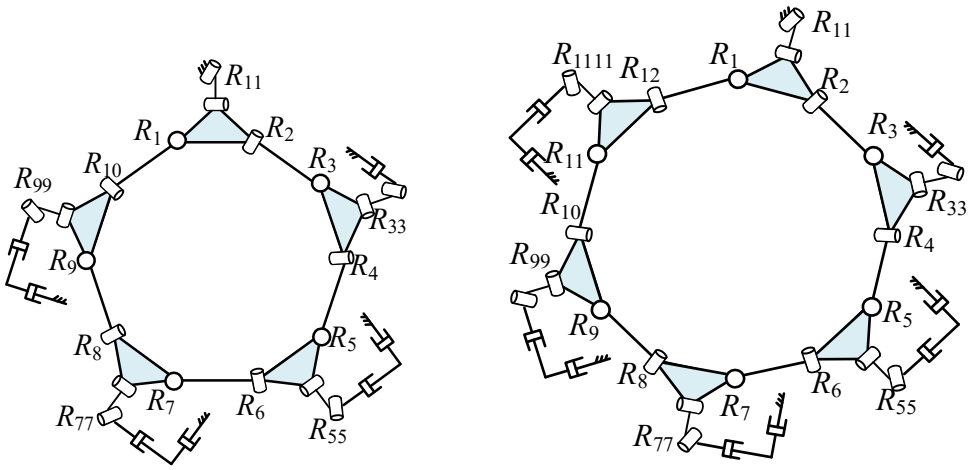

(a) (b)

Fig. 5.13 Sketch of the virtual-plane-constrained orthogonal 10R/12R linkages: (a) 10R linkage; (b) 12R linkage

Using the construction method, countless prism mechanisms can be obtained by connecting single-loop linkages using RRR chains. Figure 5.14 shows the pentagonal prism mechanism constructed by two 10R linkages using ten RRR chains. The mechanism has two modes, including a 1-DOF deployable mode [Figs. 5.14(b-c)] and a 2-DOF planar 5R mode [Fig. 5.14(d)].

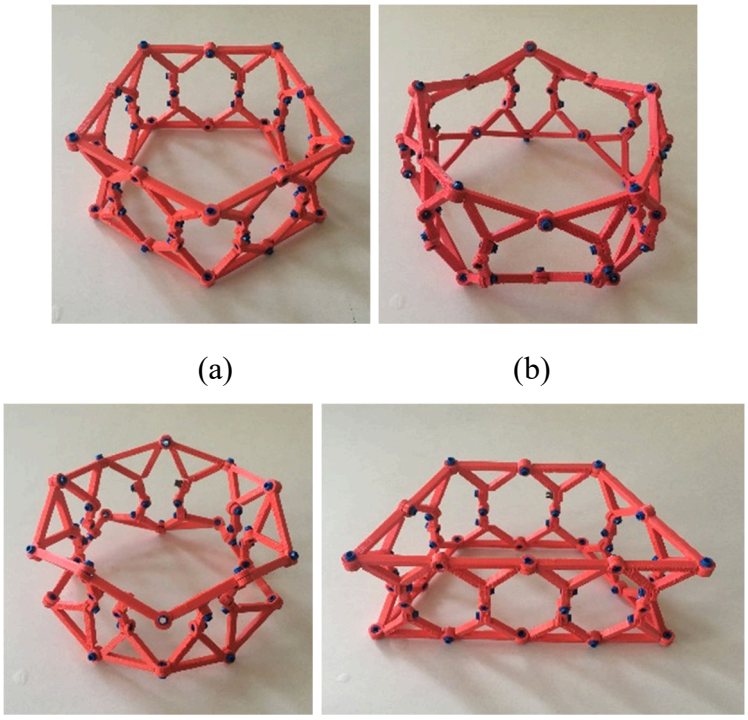

(a) (b)

(c) (d)

Fig. 5.14 Pentagonal prism mechanism constructed by 10R linkages using ten RRR chains: (a) initial posture; (b) outward deploying; (c) inward deploying; (d) planar 5R linkage mode

Using six 8R linkages and twenty-four RRR chains, a rhombohedron mechanism is assembled. Apart from the 1-DOF deploying mode [Figs. 5.15(b-c)], the mechanism has a 3-DOF parallelepiped mechanism mode [Fig. 5.15(d)]. The two modes can achieve transitions through the singular position, i.e., the initial state.

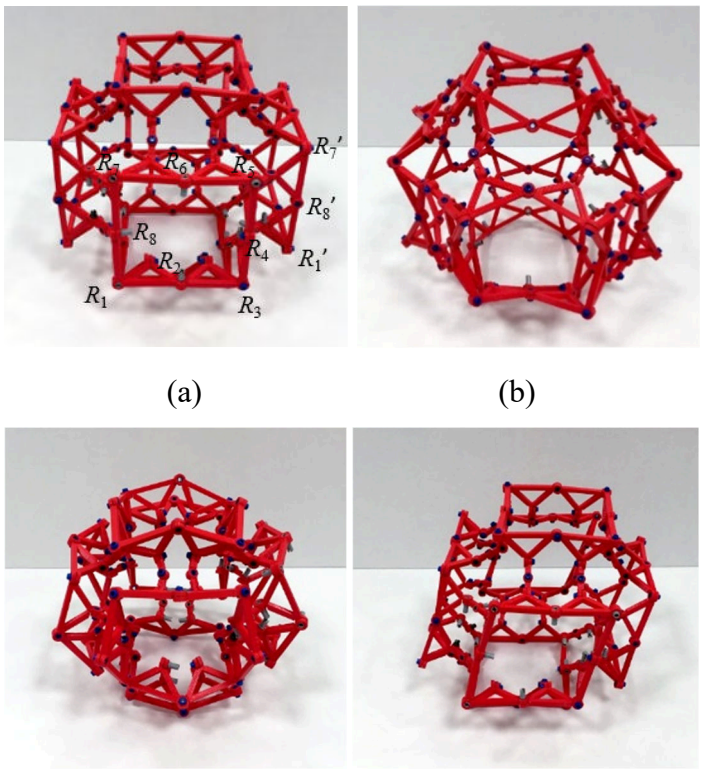

(a) (b)

(c) (d)

Fig. 5.15 Rhombohedron mechanism based on 8R linkages: (a) initial posture; (b) outward deploying; (c) inward deploying; (d) 3-DOF parallelepiped mechanism mode

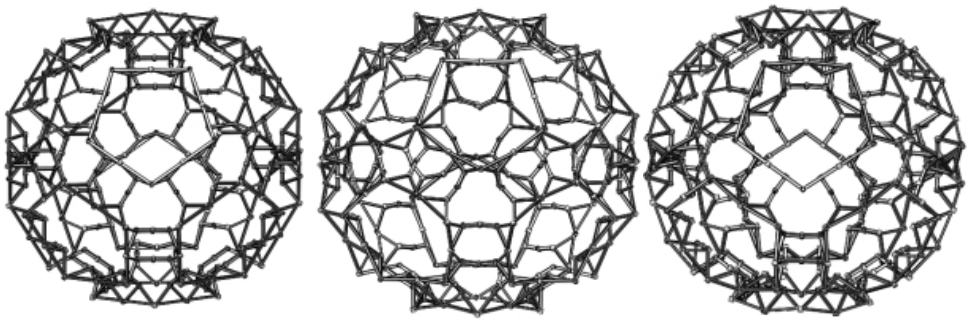

(a) (b) (c)

Fig. 5.16 Dodecahedron mechanism based on 10R linkages: (a) initial posture; (b) outward deploying; (c) inward deploying

A dodecahedron mechanism is also designed by connecting twelve 10R linkages, as shown in Fig. 5.16.

5.4 DPMs Connected Using Half the Number of RRR Chains

In this section, specific RRR chains of the prism mechanism in Section 5.2 (5.3) will be removed, and the mechanism obtains an additional rotation mode and has less interference.

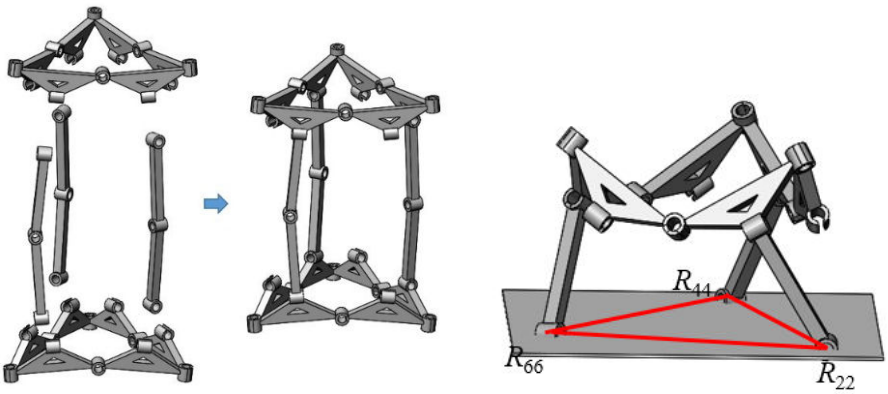

(a) (b)

Fig. 5.17 Prism mechanism connected by Bricard linkages using three RRR chains: (a) construction process; (b) the symmetry of the mechanism

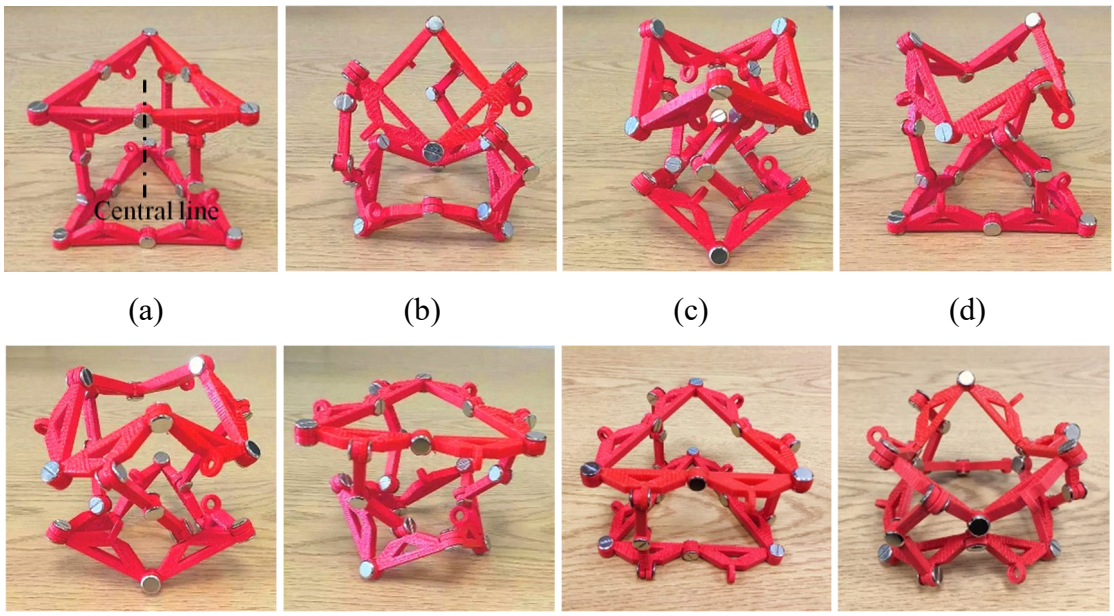

(a) (b) (c) (d)

(e) (f) (g) (h)

Fig. 5.18 Prism mechanism constructed by Bricard linkages using three RRR chains: (a) initial posture; (b) outward deploying; (c) inward deploying; (d-f) rotation mode; (g-h) folded posture

The mechanism constructed by two Bricard linkages using three RRR chains (removing chains 1, 3 and 5 in Fig. 5) is shown in Fig. 5.17(a). R_{22}, R_{44} and R_{66} are always on the same plane and form an equilateral triangle [Fig. 5.17(b)]. Apart from the deploying mode [Figs. 5.18(b-c)], the mechanism has a 1-DOF rotation mode, in which

the upper platform rotates around the central line of the mechanism while deploying, as shown in Fig. 5.18(d) (it is noted the lower Bricard linkage also deploys within a small range). In this case, the mechanism is not symmetric about the mirror plane anymore. The mechanism can further deform into the configurations shown in Figs. 5.18(e) and (f) by rotating the lower platform around the opposite direction. Since there is no interference between the adjacent RRR chains, the mechanism can be folded by deploying outward, as shown in Fig. 5.18(g). Then it can be further deployed into the posture in Fig. 5.18(h). To my best knowledge, among all the deployable mechanisms with multiple modes in the literature, this mechanism has the simplest structure. Besides, it is the first 1-DOF mechanism that is composed of Bricard linkages and has multiple modes.

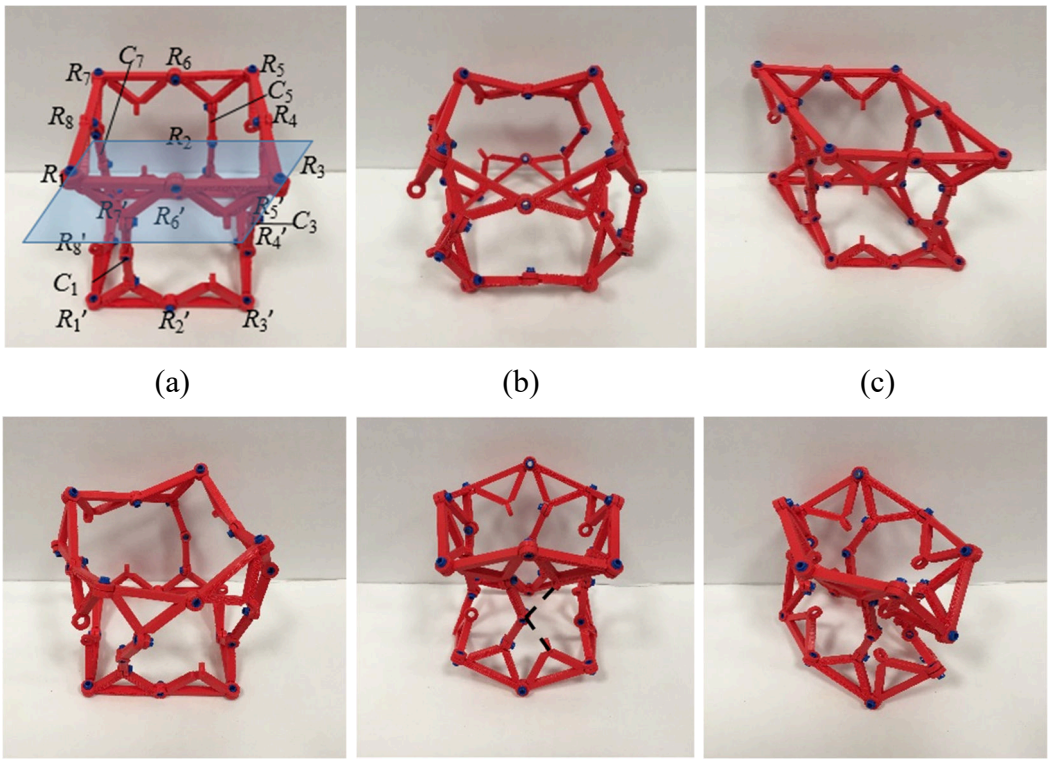

(a) (b) (c)

(d) (e) (f)

Fig. 5.19 Quadrangular prism mechanism constructed by 8R linkages using four RRR chains: (a) initial state; (b) deploying mode; (c) planar 4R linkage mode; (d) rotation mode; (e) deploying mode↔spherical 4R linkage mode; (f) spherical 4R linkage mode

Connecting two 8R linkages using four RRR chains, leads to a quadrangular prism mechanism with four motion modes. The same as the mechanism in Fig. 5.10, the mechanism with four RRR chains can also be deployed through two ways and has a planar 4R linkage mode [Figs. 5.19(b-c)]. Besides, it has an additional rotation mode, in which the two 8R linkages don't deploy synchronously [Fig. 5.19(d)]. In addition, during the

deploying process, the mechanism can turn into the configuration in Fig. 5.19(e). Through this position, the mechanism can switch into the spherical 4R mode, as shown in Fig. 5.19(f). The two 8R linkages move synchronously and both behave as spherical 4R linkages.

Similarly, connecting two 10R linkages with five RRR chains, as shown in Fig. 5.20, the pentagonal prism mechanism also obtains an additional 1-DOF rotation mode [Fig. 5.20(b)], apart from the deploying mode and the planar 5R linkage mode [Figs. 5.20(b-c)].

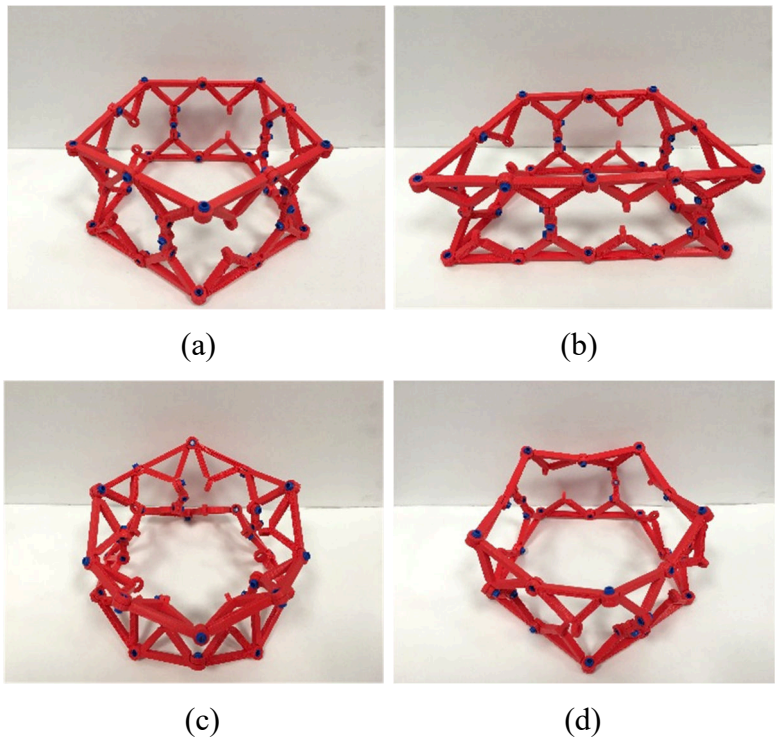

(a) (b)

(c) (d)

Fig. 5.20 Pentagonal prism mechanism constructed by 10R linkages using five RRR chains: (a) initial posture; (b) deploying mode; (c) planar 5R linkage mode; (d) rotation mode

When removing chains 2, 3 and 5 in Fig. 5.5, the prism mechanism obtained (Fig. 5.21) also has 1-DOF. Apart from the deployable mode [Fig. 5.21(b)], the mechanism has a bending mode, as shown in Figs. 5.21(c-d). The mechanism in this mode is symmetric about the mirror plane and is not line-symmetric. Similarly, removing chains 1, 2 and 3, results in another mechanism with 1-DOF deployable mode [Fig. 5.22(b)] and 1-DOF bending mode [Figs. 5.22(c-d)].

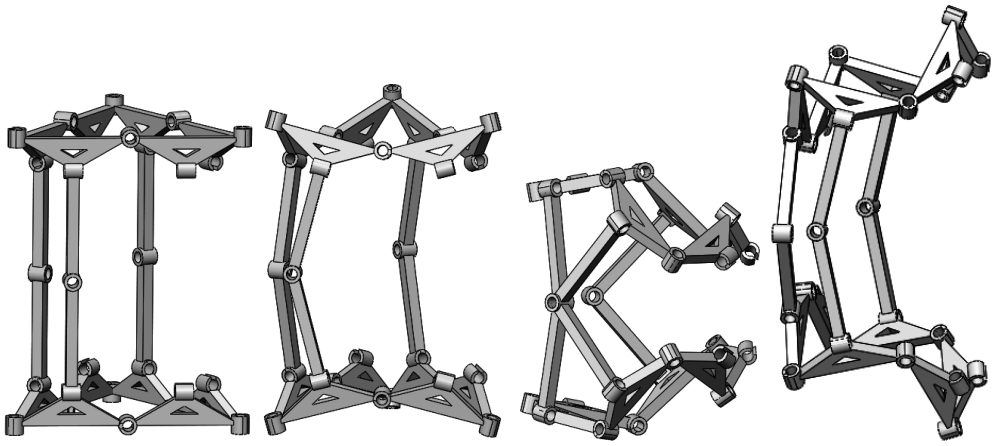

(a) (b) (c) (d)

Fig. 5.21 Variation of prism mechanism constructed by Bricard linkages using three symmetric RRR chains I: (a) initial posture; (b) deployable mode; (c-d) bending mode

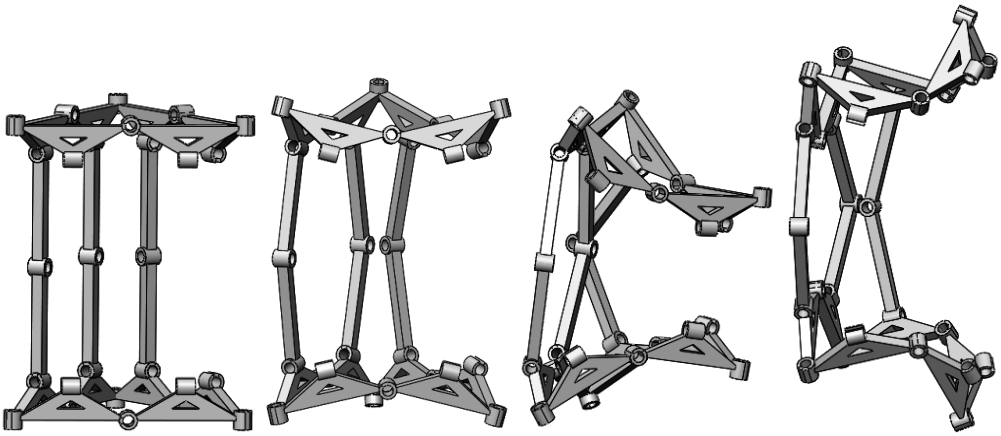

(a) (b) (c) (d)

Fig. 5.22 Variation of prism mechanism constructed by Bricard linkages using three symmetric RRR chains II: (a) initial posture; (b) deployable mode; (c-d) bending mode

5.5 Summary

In this chapter, a novel construction method has been proposed to construct DPMs with multiple modes. Using symmetric spatial RRR compositional units, single-loop linkages such as Bricard linkage, 8R linkage and 10R linkage are first built, and DPMs are then obtained by connecting these single-loop linkages using type II symmetric spatial RRR compositional units. The DPMs have only 1-DOF when deployed and can be deployed inward and outward. The mechanisms based on 8R and 10R linkages and the one constructed by connecting two Bricard linkages and three RRR chains have multiple modes and can switch modes through transition positions.

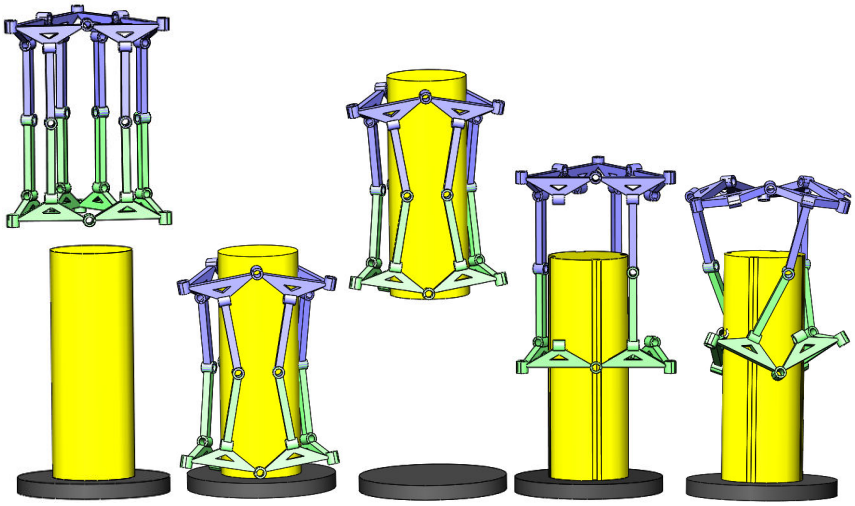

(a) (b) (c) (d) (e)

Fig. 5.23 Application of the multiple-layer prism mechanism-gripper

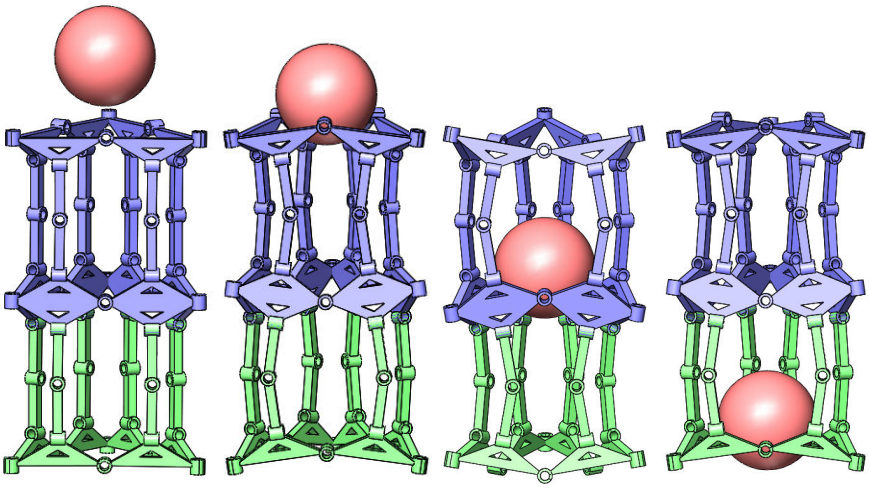

(a) (b) (c) (d)

Fig. 5.24 Application of the multiple-layer prism mechanism-fall protection system

The polyhedral mechanisms can be used in applications for decorations, entertainment and education. The prism mechanisms have potential applications on grippers, as shown in Fig. 5.23. Since there are two layers of grippers, they are more stable than the normal grippers [Fig. 5.23(a-c)]. Especially the prism mechanisms with half the number of RRR limbs, they can achieve 1-DOF rotation motions [Fig. 5.23(d-e)]. The one with multiple layers can be applied to the fall protection system (Fig. 5.24). When the upper prism mechanism deploys outward, the object is stuck in the first layer. When the upper prism mechanism deploys inward, the object falls into the second layer and is stuck again. It can also be used for the other types of transmission.

CHAPTER 6 – STATICALLY BALANCED DEPLOYABLE POLYHEDRAL MECHANISMS WITH MULTIPLE MODES

In Chapters 3, 4 and 5, deployable mechanisms with multiple modes have been designed. In this chapter, the mechanisms obtained will be developed into statically balanced mechanisms.

The static balancing methods, including the ones for planar 4R parallelograms, general planar mechanisms, spherical mechanisms and spatial mechanisms, and the approach by using optimization tools will be addressed first.

6.1 Static Balancing Methods of Planar 4R Parallelogram

The 4R parallelogram mechanism is defined as the 4-bar mechanism consisting of two cranks, with the same link lengths, connected by a coupler. It has been widely applied to the railway engine wheels and lifting mechanisms. In this section, the balancing conditions for a planar 4R parallelogram linkage will be derived using both an algebraic method and a geometric method. The aim of this design is to use as few springs as possible to reduce the interference. We start with the case in which at least three springs are needed. After achieving balancing using three springs, the stiffness of specific springs is set as zero to reduce the number of the springs. We assume all the springs are zero-free-length springs.

6.1.1 Algebraic Method for Balancing Using External Springs

6.1.1.1 Static balancing of 4R parallelogram mechanism with three springs

A planar 4R parallelogram linkage is shown in Fig. 6.1(a). The four R joints of the mechanism are denoted by R_1, R_2, R_3, and R_4. The length of links 1 and 3 are L, and the length of link 2 and the frame are L'. Link 2 remains horizontal during the motion. A coordinate system is fixed to the base with its z-axis pointing vertically upward and its origin located at R_1. x-axis is along R_4R_1 and y-axis can be obtained by the right-hand rule.

Let the position vectors of the CM of the i^{th} link ${}^{i}\boldsymbol{P}_i$ and the spring connecting point ${}^{i}\boldsymbol{A}_i$ expressed in the i^{th} local coordinate frame be

$$\begin{cases} {}^{\boldsymbol{i}}\boldsymbol{P}_{\boldsymbol{i}} = \{a_{pi} \quad b_{pi} \quad c_{pi}\}^T \\ {}^{\boldsymbol{i}}\boldsymbol{A}_{\boldsymbol{i}} = \{a_i \quad b_i \quad c_i\}^T \end{cases} \tag{6.1}$$

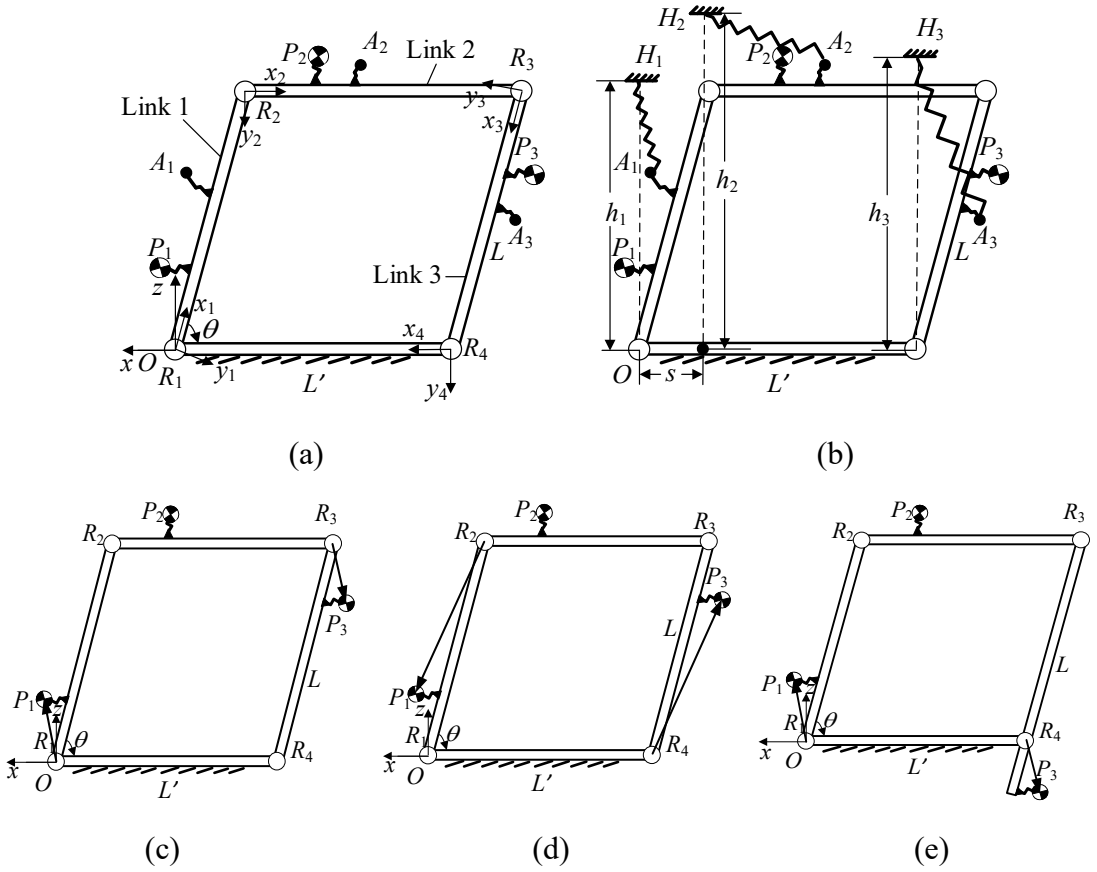

Fig. 6.1 Static balancing of planar 4R parallelogram linkage using three springs (algebraic method): (a) the sketch of the 4R parallelogram linkage; (b) the spring attachment point; (c) special case a; (d) special case b (e) special case c

The position vectors of the CMs of the links and the spring connecting points in the global coordinate frame are calculated as

$$\boldsymbol{P_1} = \left\{-\sqrt{{a_{p1}}^2 + {b_{p1}}^2}C(\theta + arctan\frac{-b_{p1}}{a_{p1}}) \quad -c_{p1} \quad \sqrt{{a_{p1}}^2 + {b_{p1}}^2}S(\theta + arctan\frac{-b_{p1}}{a_{p1}})\right\}^T$$
$$= \{-a_{p1}C\theta - b_{p1}S\theta \quad -c_{p1} \quad a_{p1}S\theta - b_{p1}C\theta\}^T \tag{6.2a}$$

$$\boldsymbol{P_2} = \boldsymbol{P_{R2}} + {}^{\boldsymbol{2}}\boldsymbol{P_2} = \{-LC\theta - a_{p2} \quad -c_{p2} \quad LS\theta - b_{p2}\}^T \tag{6.2b}$$

$$\boldsymbol{P_3} = \left\{\sqrt{(l-a_{p3})^2 + {b_{p3}}^2}C(\theta - \beta) - L' \quad -c_{p3} \quad \sqrt{(l-a_{p3})^2 + {b_{p3}}^2}S(\theta - \beta)\right\}^T$$
$$= \{-LC\theta - L' + a_{p3}C\theta + b_{p3}S\theta \quad -c_{p3} \quad LS\theta + b_{p3}C\theta - a_{p3}S\theta\}^T \tag{6.2c}$$

where

$$\beta = arctan\frac{-b_{p3}}{l - a_{p3}}$$

$$\boldsymbol{A_1} = \{-a_1C\theta - b_1S\theta \quad -c_1 \quad a_1S\theta - b_1C\theta\}^T \tag{6.2d}$$

$$\boldsymbol{A_2} = \{-LC\theta - a_2 \quad -c_2 \quad LS\theta - b_2\}^T \tag{6.2e}$$

$$\boldsymbol{A_3} = \{-LC\theta - L' + a_3C\theta + b_3S\theta \quad -c_3 \quad LS\theta + b_3C\theta - a_3S\theta\}^T \tag{6.2f}$$

According to [102, 104], the spring connecting points on the base, H_1 and H_3, for links 1 and 3, which are mounted on the base, should be right above the associated R joints [Fig. 6.1(b)]. Position vectors $\boldsymbol{H_1}$ and $\boldsymbol{H_3}$ are given by

$$\boldsymbol{H_1} = \{0 \quad 0 \quad h_1\}^T \tag{6.3}$$

$$\boldsymbol{H_3} = \{-L' \quad 0 \quad h_3\}^T \tag{6.4}$$

Suppose the position vector of the spring connecting point on the base, $\boldsymbol{H_2}$, for link 2 is

$$\boldsymbol{H_2} = \{s \quad 0 \quad h_2\}^T \tag{6.5}$$

The total potential energy is

$$\begin{aligned} V_{123} = {} & \frac{1}{2}k_1|\boldsymbol{A_1} - \boldsymbol{H_1}|^2 + \frac{1}{2}k_2|\boldsymbol{A_2} - \boldsymbol{H_2}|^2 + \frac{1}{2}k_3|\boldsymbol{A_3} - \boldsymbol{H_3}|^2 + m_1gP_{1z} + m_2gP_{2z} + \\ & m_3gP_{3z} = \frac{1}{2}\{(a_1^2 + b_1^2 + c_1^2 + h_1^2)k_1 + a_2^2k_2 + b_2^2k_2 + c_2^2k_2 + 2b_2k_2h_2 + h_2^2k_2 + \\ & k_2L^2 + k_3L^2 + k_3(a_3^2 + b_3^2 + c_3^2 + h_3^2 - 2La_3) - 2b_{p2}gm_2 + 2a_2k_2s + k_2s^2 + \\ & 2[b_1h_1k_1 - b_3h_3k_3 + m_3gb_{p3} - m_1gb_{p1} + k_2L(a_2 + s)]C\theta + 2\{a_1h_1k_1 - a_3h_3k_3 + \\ & L[h_3k_3 + (b_2 + h_2)k_2] - m_1ga_{p1} - m_2gL + m_3ga_{p3} - m_3gL\}S\theta\} \end{aligned} \tag{6.6}$$

where m_i is the mass of the i^{th} link, g is the gravitational acceleration, and k_i is the stiffness of the i^{th} spring.

In a statically balanced system, the potential energy of the system is constant, and the coefficients of the variable θ must vanish [117]. The conditions for the static balancing of the 4R linkage using three springs are obtained as:

$$\begin{cases} b_1h_1k_1 - b_3h_3k_3 + m_3gb_{p3} - m_1gb_{p1} + k_2L(a_2 + s) = 0 \\ a_1h_1k_1 - a_3h_3k_3 + L[h_3k_3 + (b_2 + h_2)k_2] - m_1ga_{p1} - m_2gL + m_3ga_{p3} - m_3gL = 0 \end{cases} \tag{6.7}$$

Equation (6.7) indicates that the balancing conditions for the 4R parallelogram linkage are independent of the length and the local position of the CM of link 2 (coupler), because a_{p2}, b_{p2} and L' have vanished.

In the following, we will discuss three specific cases:

Case a: $m_1a_{p1} = m_3a_{p3}$, $m_1b_{p1} = m_3b_{p3}$ [Fig. 6.1(c)]. In this case the balancing conditions are

$$\begin{cases} b_1h_1k_1 - b_3h_3k_3 + k_2L(a_2 + s) = 0 \\ a_1h_1k_1 - a_3h_3k_3 + L[h_3k_3 + (b_2 + h_2)k_2] - (m_2 + m_3)gL = 0 \end{cases} \tag{6.8}$$

The balancing conditions are only related to the weights of links 2 and 3.

Case b: m_1a_{p1} - m_1L = m_3a_{p3} - m_3L, m_1b_{p1} = m_3b_{p3} [Fig. 6.1(d)]. In this case, the balancing conditions are

$$\begin{cases} b_1h_1k_1 - b_3h_3k_3 + k_2L(a_2 + s) = 0 \\ a_1h_1k_1 - a_3h_3k_3 + L[h_3k_3 + (b_2 + h_2)k_2] - (m_1 + m_2)gL = 0 \end{cases} \tag{6.9}$$

The balancing conditions are only related to the weights of links 1 and 2.

Case 3: m_3a_{p3} - m_3L = m_1a_{p1}, m_1b_{p1} = m_3b_{p3} [Fig. 6.1(e)]. In this case the balancing conditions are

$$\begin{cases} b_1h_1k_1 - b_3h_3k_3 + k_2L(a_2 + s) = 0 \\ a_1h_1k_1 - a_3h_3k_3 + L[h_3k_3 + (b_2 + h_2)k_2] - m_2gL = 0 \end{cases} \tag{6.10}$$

Links 1 and 3 are balanced by each other, one only needs to balance link 2.

From Eqs. (6.8-6.10), it is observed that the balancing conditions for the 4R parallelogram linkage are independent of the positions of the CMs of the links in the above three cases (a_{p1}, a_{p3}, b_{p1} and b_{p3} have vanished). This is important, because it shows there is no need to consider the length of link 2 and the positions of CMs of the links when balancing these particular 4R parallelogram linkages. One can set $L' = L$ and $^{i}\boldsymbol{P_i} = \{0 \quad 0 \quad 0\}^T$ when analyzing the 4R parallelogram linkage, for the convenience of calculation.

6.1.1.2 Static balancing of 4R parallelogram mechanism with two springs

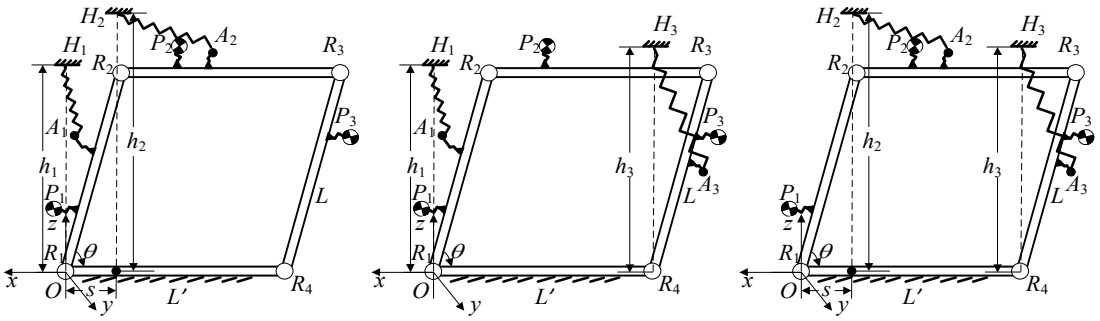

(a) (b) (c)

Fig. 6.2 Static balancing of planar 4R parallelogram linkage using two springs (algebraic method): (a) the springs are attached to links 1 and 2; (b) the springs are attached to links 1 and 3; (c) the springs are attached to links 2 and 3;

Now let us investigate how to balance the linkage using two springs. Let the stiffness of one of the three springs of the system in Fig. 6.1(b) be zero, the balancing conditions for the parallelogram with two springs are readily obtained.

If the planar 4R parallelogram linkage is statically balanced using two springs attached to links 1 and 2 respectively [Fig. 6.2(a)], the total potential energy of the system can be obtained from Eq. (6.6) by setting $k_3 = 0$ as:

$$V_{12} = \frac{1}{2}k_1|\boldsymbol{A_1} - \boldsymbol{H_1}|^2 + \frac{1}{2}k_2|\boldsymbol{A_2} - \boldsymbol{H_2}|^2 + m_1gP_{1z} + m_2gP_{2z} + m_3gP_{3z} = \frac{1}{2}\{(a_1^2 + b_1^2 + c_1^2 + h_1^2)k_1 + a_2^2k_2 + b_2^2k_2 + c_2^2k_2 + 2b_2k_2h_2 + h_2^2k_2 + k_2L^2 - 2b_{p2}gm_2 + 2a_2k_2s + k_2s^2 + 2[b_1h_1k_1 + m_3gb_{p3} - m_1gb_{p1} + k_2L(a_2 + s)]C\theta + 2[a_1h_1k_1 + L(b_2 + h_2)k_2 - m_1ga_{p1} - m_2gL + m_3ga_{p3} - m_3gL]S\theta\} \tag{6.11}$$

The balancing conditions are derived as:

$$\begin{cases} b_1h_1k_1 + m_3gb_{p3} - m_1gb_{p1} + k_2L(a_2 + s) = 0 \\ a_1h_1k_1 + L(b_2 + h_2)k_2 - m_1ga_{p1} - m_2gL + m_3ga_{p3} - m_3gL = 0 \end{cases} \tag{6.12}$$

If $m_1b_{p1} = m_3b_{p3}$ and $a_{p3} = L$, there is no need to balance link 3. Equation (6.12) becomes

$$\begin{cases} b_1h_1k_1 + k_2L(a_2 + s) = 0 \\ a_1h_1k_1 + L(b_2 + h_2)k_2 - m_1ga_{p1} - m_2gL = 0 \end{cases} \tag{6.13}$$

Let $k_2 = 0$ [in Eq. (6.6)], i.e., the two springs are connected to links 1 and 3 respectively [Fig. 6.2(b)]. The potential energy of the system and the balancing conditions are yielded as

$$V_{13} = \frac{1}{2}k_1|\boldsymbol{A_1} - \boldsymbol{H_1}|^2 + \frac{1}{2}k_3|\boldsymbol{A_3} - \boldsymbol{H_3}|^2 + m_1gP_{1z} + m_2gP_{2z} + m_3gP_{3z} = \frac{1}{2}\{(a_1^2 + b_1^2 + c_1^2 + h_1^2)k_1 + k_3L^2 + k_3(a_3^2 + b_3^2 + c_3^2 + h_3^2 - 2La_3) - 2b_{p2}gm_2 + 2(b_1h_1k_1 - b_3h_3k_3 + m_3gb_{p3} - m_1gb_{p1})C\theta + 2(a_1h_1k_1 - a_3h_3k_3 + Lh_3k_3 - m_1ga_{p1} - m_2gL + m_3ga_{p3} - m_3gL)S\theta\} \tag{6.14}$$

$$\begin{cases} b_1h_1k_1 - b_3h_3k_3 + m_3gb_{p3} - m_1gb_{p1} = 0 \\ a_1h_1k_1 - a_3h_3k_3 + Lh_3k_3 - m_1ga_{p1} - m_2gL + m_3ga_{p3} - m_3gL = 0 \end{cases} \tag{6.15}$$

Similarly, let $k_1 = 0$ [in Eq. (6.6)]. The springs are attached to links 2 and 3 respectively [Fig. 6.2(c)], the potential energy of the system and the balancing conditions are calculated as

$$V_{23} = \frac{1}{2}k_2|\boldsymbol{A_2} - \boldsymbol{H_2}|^2 + \frac{1}{2}k_3|\boldsymbol{A_3} - \boldsymbol{H_3}|^2 + m_1gP_{1z} + m_2gP_{2z} + m_3gP_{3z} = \frac{1}{2}\{a_2^2k_2 + b_2^2k_2 + c_2^2k_2 + 2b_2k_2h_2 + h_2^2k_2 + k_2L^2 + k_3L^2 + k_3(a_3^2 + b_3^2 + c_3^2 + h_3^2 - 2La_3) - 2b_{p2}gm_2 + 2a_2k_2s + k_2s^2 + 2[-b_3h_3k_3 + m_3gb_{p3} - m_1gb_{p1} + k_2L(a_2 + s)]C\theta + 2\{-a_3h_3k_3 + L[h_3k_3 + (b_2 + h_2)k_2] - m_1ga_{p1} - m_2gL + m_3ga_{p3} - m_3gL\}S\theta\} \tag{6.16}$$

$$\begin{cases} -b_3h_3k_3 + m_3gb_{p3} - m_1gb_{p1} + k_2L(a_2 + s) = 0 \\ -a_3h_3k_3 + L[h_3k_3 + (b_2 + h_2)k_2] - m_1ga_{p1} - m_2gL + m_3ga_{p3} - m_3gL = 0 \end{cases}$$

(6.17)

If $m_1 b_{p1} = m_3 b_{p3}$ and $a_{p1} = 0$, there is no need to balance link 1, as shown in Fig. 6.2(e). The balancing conditions become

$$\begin{cases} -b_3 h_3 k_3 + k_2 L(a_2 + s) = 0 \\ -a_3 h_3 k_3 + L[h_3 k_3 + (b_2 + h_2)k_2] - m_2 g L + m_3 g a_{p3} - m_3 g L = 0 \end{cases} \tag{6.18}$$

6.1.1.3 Static balancing of 4R parallelogram mechanism with one spring

Now it will be verified that the linkage can be balanced using one spring. The spring is attached to links 1, 2 or 3 respectively, as shown in Fig. 6.3.

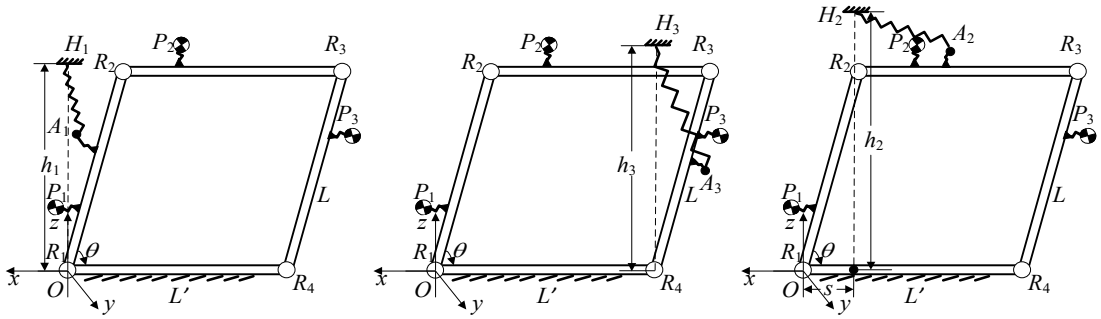

(a) (b) (c)

Fig. 6.3 Static balancing of planar 4R parallelogram linkage using one spring (algebraic method): (a) the spring is attached to link 1; (b) the spring is attached to link 3; (c) the spring is attached to link 2;

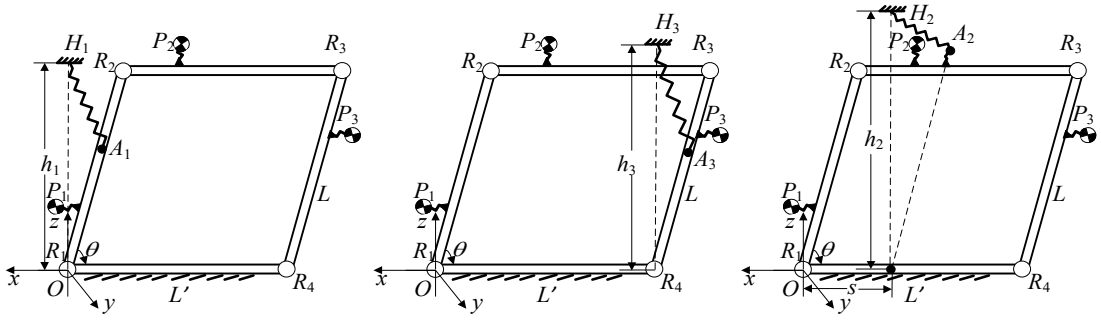

(a) (b) (c)

Fig. 6.4 The solutions of static balancing of planar 4R parallelogram linkage using one springs: (a) the spring is attached to link 1; (b) the spring is attached to link 3; (c) the spring is attached to link 2

Let $k_2 = k_3 = 0$ [in Eq. (6.6)], there is only one spring used to connect link 1 to balance the 4R parallelogram linkage. The total potential energy of the system is

$$V_1 = \frac{1}{2}k_1|\boldsymbol{A_1} - \boldsymbol{H_1}|^2 + m_1gP_{1z} + m_2gP_{2z} + m_3gP_{3z} = \frac{1}{2}[(a_1^2 + b_1^2 + c_1^2 + h_1^2)k_1 - 2b_{p2}gm_2 + 2(b_1h_1k_1 + m_3gb_{p3} - m_1gb_{p1})C\theta + 2(a_1h_1k_1 - m_1ga_{p1} - m_2gL + m_3ga_{p3} - m_3gL)S\theta]$$

(6.19)

The balancing conditions are derived as:

$$\begin{cases} b_1h_1k_1 + m_3gb_{p3} - m_1gb_{p1} = 0 \\ a_1h_1k_1 - m_1ga_{p1} - m_2gL + m_3ga_{p3} - m_3gL = 0 \end{cases} \quad (6.20)$$

If $m_1a_{p1} = m_3a_{p3}$ and $m_1b_{p1} = m_3b_{p3}$ [Fig. 6.1(c)], the balancing conditions are

$$\begin{cases} b_1 = 0 \\ a_1h_1k_1 - (m_2 + m_3)gL = 0 \end{cases} \quad (6.21)$$

Eq. (6.21) shows that the spring is attached to the line R_1R_2, as shown in Fig. 6.4(a).

Similarly, when the spring is attached to link 3, the potential energy of the system and the balancing conditions are obtained as

$$V_3 = \frac{1}{2}k_3|\boldsymbol{A_3} - \boldsymbol{H_3}|^2 + m_1gP_{1z} + m_2gP_{2z} + m_3gP_{3z} = \frac{1}{2}[k_3L^2 + k_3(a_3^2 + b_3^2 + c_3^2 + h_3^2 - 2La_3) - 2b_{p2}gm_2 + 2(-b_3h_3k_3 + m_3gb_{p3} - m_1gb_{p1})C\theta + 2(-a_3h_3k_3 + Lh_3k_3 - m_1ga_{p1} - m_2gL + m_3ga_{p3} - m_3gL)S\theta]$$

(6.22)

$$\begin{cases} -b_3h_3k_3 + m_3gb_{p3} - m_1gb_{p1} = 0 \\ -a_3h_3k_3 + Lh_3k_3 - m_1ga_{p1} - m_2gL + m_3ga_{p3} - m_3gL = 0 \end{cases} \quad (6.23)$$

When $m_1a_{p1} = m_3a_{p3}$, $m_1b_{p1} = m_3b_{p3}$ [Fig. 6.1(c)], the balancing conditions are

$$\begin{cases} b_3 = 0 \\ (L - a_3)h_3k_3 - Lg(m_2 + m_3) = 0 \end{cases} \quad (6.24)$$

The spring attachment point on the link should be on the line R_3R_4 [Fig. 6.4(b)].

When letting $k_1 = k_3 = 0$ [in Eq. (6.6)], namely, the spring is attached to link 2. The potential energy of the system is

$$V_2 = \frac{1}{2}k_2|\boldsymbol{A_2} - \boldsymbol{H_2}|^2 + m_1gP_{1z} + m_2gP_{2z} + m_3gP_{3z} = \frac{1}{2}\{a_2^2k_2 + b_2^2k_2 + c_2^2k_2 + 2b_2k_2h_2 + h_2^2k_2 + k_2L^2 - 2b_{p2}gm_2 + 2a_2k_2s + k_2s^2 + 2[m_3gb_{p3} - m_1gb_{p1} + k_2L(a_2 + s)]C\theta + 2[L(b_2 + h_2)k_2 - m_1ga_{p1} - m_2gL + m_3ga_{p3} - m_3gL]S\theta\}$$

(6.25)

The following balancing conditions are derived as

$$\begin{cases} m_3gb_{p3} - m_1gb_{p1} + k_2L(a_2 + s) = 0 \\ L(b_2 + h_2)k_2 - m_1ga_{p1} - m_2gL + m_3ga_{p3} - m_3gL = 0 \end{cases} \quad (6.26)$$

Let $m_1a_{p1} = m_3a_{p3}$, $m_1b_{p1} = m_3b_{p3}$ [Fig. 6.1(c)], the balancing conditions become

$$\begin{cases} a_2 + s = 0 \\ (b_2 + h_2)k_2 - (m_2 + m_3)g = 0 \end{cases} \quad (6.27)$$

It is observed from Eq. (6.27) that the x coordinate of the spring attachment point on the base in the global coordinate and that on link 2 in the local coordinate should be the same [Fig. 6.4(c)]. Besides, the sum of the z coordinate of the spring attachment point on the base in the global coordinate and that on link 2 in the local coordinate should be constant and is equal to $(m_2 + m_3)g/k_2$.

6.1.2 Algebraic Method for Balancing Using Internal Springs

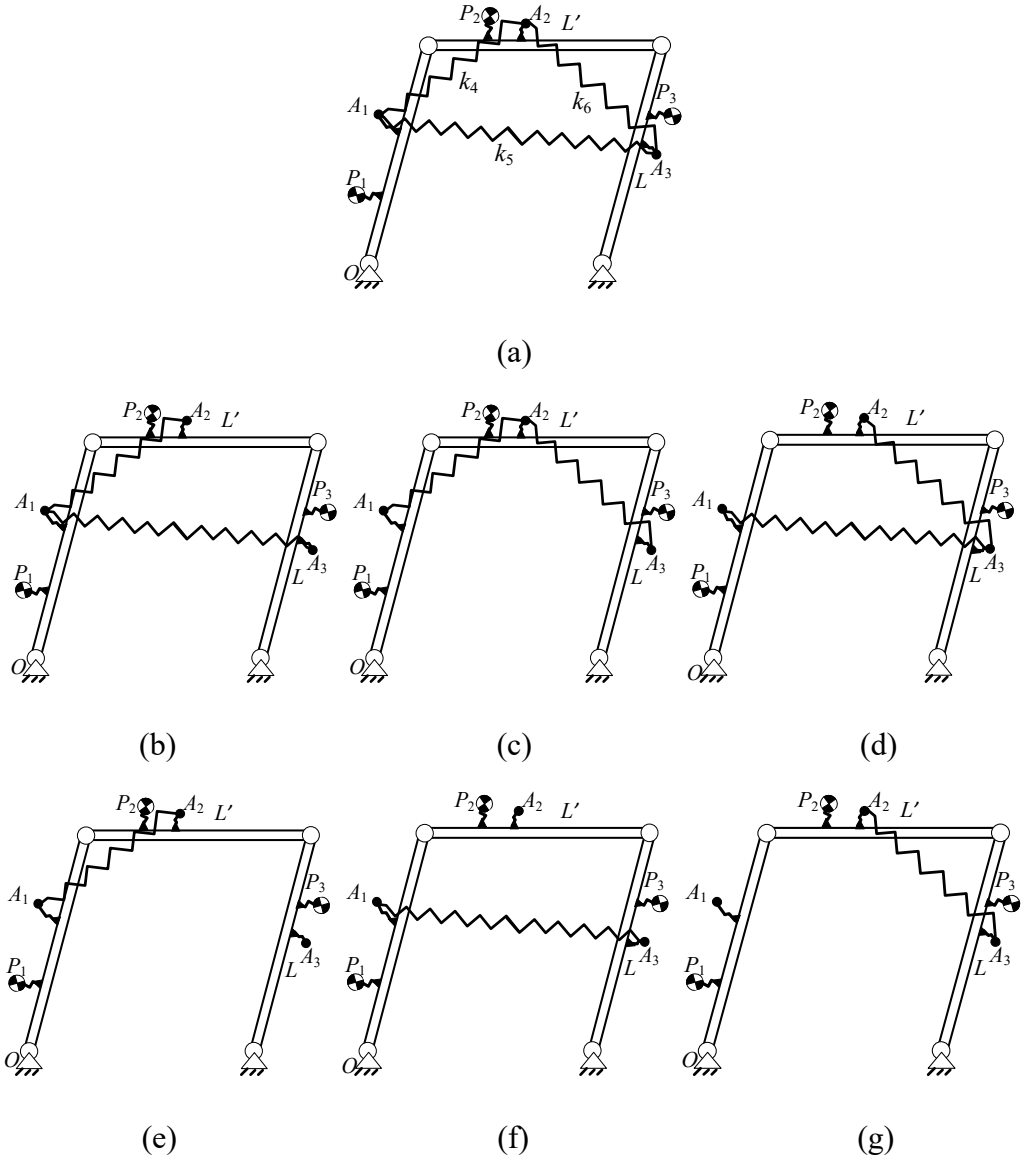

Fig. 6.5 Static balancing of planar 4R parallelogram mechanism using internal springs (algebraic method): (a) using three springs; (b-d) using two springs; (e-g) using one spring

In this section, the 4R parallelogram mechanism will be balanced using internal springs. First, three springs will be used to connect links 1 and 2, links 2 and 3, and links 1 and 3 respectively.

Let the stiffness of springs be k_4, k_5 and k_6, the total potential energy of the mechanism is obtained as

$$V_{456} = \frac{1}{2}\{b_1^2k_4 + b_2^2k_4 + c_1^2k_4 - 2c_1c_2k_4 + c_2^2k_4 + 2a_1a_3k_5 + b_1^2k_5 + 2b_1b_3k_5 + b_3^2k_5 + c_1^2k_5 - 2c_1c_3k_5 + c_3^2k_5 + a_1^2(k_4 + k_5) + b_2^2k_6 + b_3^2k_6 + c_2^2k_6 - 2c_2c_3k_6 + c_3^2k_6 + a_2^2(k_4 + k_6) + a_3^2(k_5 + k_6) - 2a_3k_5L - 2a_1(k_4 + k_5)L + k_4L^2 + k_5L^2 - 2a_2k_6L' + (k_5 + k_6)L'^2 - 2m_2gb_{p2} - 2\{a_1a_2k_4 + b_1b_2k_4 - a_2a_3k_6 - b_2b_3k_6 - a_2k_4L + [a_1k_5 + a_3(k_5 + k_6) - k_5L]L' + g(m_1gb_{p1} - m_3gb_{p3})\}C\theta - 2[-a_1b_2k_4 + a_3b_2k_6 + a_2(b_1k_4 - b_3k_6) + b_2k_4L + (b_1 + b_3)k_5L' + b_3k_6L' - m_1ga_{p1} - m_2gL + m_3ga_{p3} - m_3gL]S\theta\}$$

(6.28)

The following balancing conditions are derived as

$$\begin{cases} a_1a_2k_4 + b_1b_2k_4 - a_2a_3k_6 - b_2b_3k_6 - a_2k_4L + [a_1k_5 + a_3(k_5 + k_6) - k_5L]L' \\ +g(m_1gb_{p1} - m_3gb_{p3}) = 0 \\ -a_1b_2k_4 + a_3b_2k_6 + a_2(b_1k_4 - b_3k_6) + b_2k_4L + (b_1 + b_3)k_5L' + b_3k_6L' \\ -m_1ga_{p1} - m_2gL + m_3ga_{p3} - m_3gL = 0 \end{cases}$$

(6.29)

Let $k_6 = 0$, which means only two springs are used to connect links 1 and 2, and links 1 and 3, the potential energy of the mechanism is

$$V_{45} = \frac{1}{2}\{b_1^2k_4 + b_2^2k_4 + c_1^2k_4 - 2c_1c_2k_4 + c_2^2k_4 + 2a_1a_3k_5 + b_1^2k_5 + 2b_1b_3k_5 + b_3^2k_5 + c_1^2k_5 - 2c_1c_3k_5 + c_3^2k_5 + a_1^2(k_4 + k_5) + a_2^2k_4 + a_3^2k_5 - 2a_3k_5L - 2a_1(k_4 + k_5)L + k_4L^2 + k_5L^2 + k_5L'^2 - 2m_2gb_{p2} - 2[a_1a_2k_4 + b_1b_2k_4 - a_2k_4L + (a_1k_5 + a_3k_5 - k_5L)L' + g(m_1gb_{p1} - m_3gb_{p3})]C\theta - 2[-a_1b_2k_4 + a_2b_1k_4 + b_2k_4L + (b_1 + b_3)k_5L' - m_1ga_{p1} - m_2gL + m_3ga_{p3} - m_3gL]S\theta\}$$

(6.30)

The balancing conditions are

$$\begin{cases} a_1a_2k_4 + b_1b_2k_4 - a_2k_4L + (a_1k_5 + a_3k_5 - k_5L)L' + g(m_1gb_{p1} - m_3gb_{p3}) = 0 \\ -a_1b_2k_4 + a_2b_1k_4 + b_2k_4L + (b_1 + b_3)k_5L' - m_1ga_{p1} - m_2gL + m_3ga_{p3} - m_3gL = 0 \end{cases}$$

(6.31)

When two springs are adopted to connect links 1 and 2, and links 2 and 3, the potential energy is calculated as

$$V_{46} = \frac{1}{2}\{b_1^2k_4 + b_2^2k_4 + c_1^2k_4 - 2c_1c_2k_4 + c_2^2k_4 + a_1^2k_4 + b_2^2k_6 + b_3^2k_6 + c_2^2k_6 - 2c_2c_3k_6 + c_3^2k_6 + a_2^2(k_4 + k_6) + a_3^2k_6 - 2a_1k_4L + k_4L^2 - 2a_2k_6L' + k_6L'^2 - 2m_2gb_{p2} - 2[a_1a_2k_4 + b_1b_2k_4 - a_2a_3k_6 - b_2b_3k_6 - a_2k_4L + a_3k_6L' +$$

$$g(m_1gb_{p1} - m_3gb_{p3})]C\theta - 2[-a_1b_2k_4 + a_3b_2k_6 + a_2(b_1k_4 - b_3k_6) + b_2k_4L + b_3k_6L' - m_1ga_{p1} - m_2gL + m_3ga_{p3} - m_3gL]S\theta\}$$

(6.32)

The mechanism is balanced if

$$\begin{cases} a_1a_2k_4 + b_1b_2k_4 - a_2a_3k_6 - b_2b_3k_6 - a_2k_4L + a_3k_6L' + g(m_1gb_{p1} - m_3gb_{p3}) = 0 \\ -a_1b_2k_4 + a_3b_2k_6 + a_2(b_1k_4 - b_3k_6) + b_2k_4L + b_3k_6L' \\ -m_1ga_{p1} - m_2gL + m_3ga_{p3} - m_3gL = 0 \end{cases}$$

(6.33)

Similarly, if two springs are attached to links 1 and 3, and links 2 and 3 respectively, the potential energy is

$$V_{56} = \frac{1}{2}\{2a_1a_3k_5 + b_1^2k_5 + 2b_1b_3k_5 + b_3^2k_5 + c_1^2k_5 - 2c_1c_3k_5 + c_3^2k_5 + a_1^2k_5 + b_2^2k_6 + b_3^2k_6 + c_2^2k_6 - 2c_2c_3k_6 + c_3^2k_6 + a_2^2k_6) + a_3^2(k_5 + k_6) - 2a_3k_5L - 2a_1k_5L + k_5L^2 - 2a_2k_6L' + (k_5 + k_6)L'^2 - 2m_2gb_{p2} - 2\{-a_2a_3k_6 - b_2b_3k_6 + [a_1k_5 + a_3(k_5 + k_6) - k_5L]L' + g(m_1gb_{p1} - m_3gb_{p3})\}C\theta - 2[a_3b_2k_6 - a_2b_3k_6 + (b_1 + b_3)k_5L' + b_3k_6L' - m_1ga_{p1} - m_2gL + m_3ga_{p3} - m_3gL]S\theta\}$$

(6.34)

The balancing conditions are

$$\begin{cases} -a_2a_3k_6 - b_2b_3k_6 + [a_1k_5 + a_3(k_5 + k_6) - k_5L = 0 \\ a_3b_2k_6 - a_2b_3k_6 + (b_1 + b_3)k_5L' + b_3k_6L' - m_1ga_{p1} - m_2gL + m_3ga_{p3} - m_3gL = 0 \end{cases}$$

(6.35)

When only one spring is used to connect links 1 and 2, the potential energy is yielded as

$$V_4 = \frac{1}{2}k_4|\boldsymbol{A_1} - \boldsymbol{A_2}|^2 + m_1gP_{1z} + m_2gP_{2z} + m_3gP_{3z} = \frac{1}{2}\{k_4[a_2^2 + b_1^2 + b_2^2 + (c_1 - c_2)^2 + (a_1 - L)^2] - 2m_2gb_{p2} - 2(a_1a_2k_4 + b_1b_2k_4 - a_2k_4L + m_1gb_{p1} - m_3gb_{p3})C\theta + 2(-a_2b_1k_4 + a_1b_2k_4 - b_2k_4L + m_1ga_{p1} + m_2gL - m_3ga_{p3} + m_3gL)S\theta\}$$

(6.36)

The following balancing conditions are derived as

$$\begin{cases} a_1a_2k_4 + b_1b_2k_4 - a_2k_4L + m_1gb_{p1} - m_3gb_{p3} = 0 \\ -a_2b_1k_4 + a_1b_2k_4 - b_2k_4L + m_1ga_{p1} + m_2gL - m_3ga_{p3} + m_3gL = 0 \end{cases} \quad (6.37)$$

When the spring is attached to links 1 and 3, the potential energy is

$$V_5 = \frac{1}{2}k_5|\boldsymbol{A_1} - \boldsymbol{A_3}|^2 + m_1gP_{1z} + m_2gP_{2z} + m_3gP_{3z} = \frac{1}{2}\{k_5[(b_1 + b_3)^2 + (c_1 - c_3)^2 + (a_1 + a_3 - L)^2 + L_2^2] - 2m_2gb_{p2} - 2[k_5L_2(a_1 + a_3 - L) + m_1gb_{p1} - m_3gb_{p3}]C\theta + 2[-(b_1 + b_3)k_5L_2 + m_1ga_{p1} - m_3ga_{p3} + m_2gL + m_3gL]S\theta\}$$

(6.38)

The mechanism is statically balanced if

$$\begin{cases} k_5L_2(a_1+a_3-L)+m_1gb_{p1}-m_3gb_{p3}=0 \\ -(b_1+b_3)k_5L_2+m_1ga_{p1}-m_3ga_{p3}+m_2gL+m_3gL=0 \end{cases} \tag{6.39}$$

If the spring is attached to links 2 and 3, the potential energy is

$$\begin{aligned} V_6=\frac{1}{2}\{&b_2^2k_6+b_3^2k_6+c_2^2k_6-2c_2c_3k_6+c_3^2k_6+a_2^2k_6+a_3^2k_6-2a_2k_6L'+k_6L'^2- \\ &2m_2gb_{p2}-2[-a_2a_3k_6-b_2b_3k_6+a_3k_6L'+g(m_1gb_{p1}-m_3gb_{p3})]C\theta- \\ &2(a_3b_2k_6-a_2b_3k_6+b_3k_6L'-m_1ga_{p1}-m_2gL+m_3ga_{p3}-m_3gL)S\theta\} \end{aligned} \tag{6.40}$$

The balancing conditions are

$$\begin{cases} -a_2a_3k_6-b_2b_3k_6+a_3k_6L'+g(m_1gb_{p1}-m_3gb_{p3})=0 \\ a_3b_2k_6-a_2b_3k_6+b_3k_6L'-m_1ga_{p1}-m_2gL+m_3ga_{p3}-m_3gL=0 \end{cases} \tag{6.41}$$

6.1.3 Geometric Method for Balancing Using External Springs

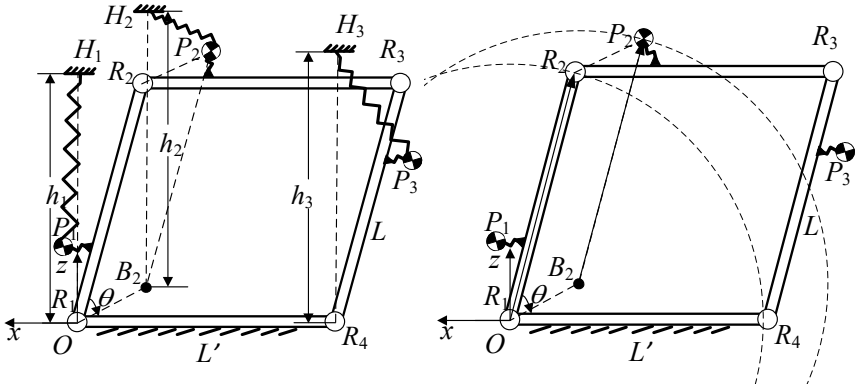

Fig. 6.6 Static balancing of planar 4R parallelogram linkage using three external springs (geometric method): (a) the balancing method; (b) the virtual rotation centre

First, the 4R parallelogram linkage is balanced using three external springs. Link 1(3) are readily balanced by connecting the CM of link 1(3) and the point right above R_1 (R_4) ($\boldsymbol{H_1}=\{0 \quad 0 \quad m_1g/k_1\}^T, \boldsymbol{H_3}=\{-L' \quad 0 \quad m_3g/k_3\}^T$) respectively [Fig. 6.6(a)].

To balance link 2, the concept of virtual rotation centre is introduced. Draw a parallelogram based on R_1, R_2 and P_2, and the fourth vertex of the parallelogram B_2 is the virtual rotation centre of P_2 [Fig. 6.6(b)]. P_2 always rotates around B_2, and the spring attachment point on the base for link 2 should be right above B_2. The position of B_2 is obtained as $\{-a_{p2} \quad -c_{p2} \quad -b_{p2}\}^T$, H_2 is right above B_2 and $\boldsymbol{H_2}=$

$\{-a_{p2} \quad -c_{p2} \quad m_2 g/k_2 - b_{p2}\}^T$. Link 2 is balanced by connecting H_2 and P_2. The parameters a_1, b_1, c_1, a_2, b_2, c_2, a_3, b_3, c_3, h_1, h_2 and h_3 obtained using the geometric method satisfy Eq. (6.7). This confirms that the results are correct.

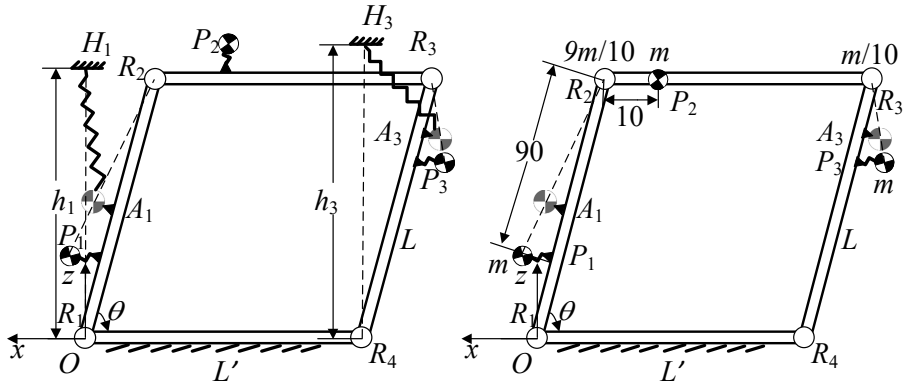

(a) (b)

Fig. 6.7 Static balancing of planar 4R parallelogram linkage using two external springs (geometric method): (a) the balancing method; (b) mass moment substitution of link 2

To balance the 4R parallelogram linkage using two springs, the mass of link 2 should be distributed to links 1 and 3 [Fig. 6.7(b)]. Since link 2 is always horizontal, the difference between the potential energies associated with the gravity of the CM of link 2 and an arbitrary point on the line R_2R_3 keeps constant (equal to m_2gb_{p2}), the balancer of link 2 experiences the mass as if it were fixed anywhere on the line R_2R_3. Suppose that the position vector of the CM of link 2 in the 2nd local coordinate frame is $\{a_{p2} \quad 0 \quad c_{p2}\}^T$. The position of the first equivalent mass on R_2 in the 2nd local coordinate frame is $\{0 \quad 0 \quad 0\}^T$, and that of the second equivalent mass on R_3 is $\{L' \quad 0 \quad t_2\}^T$. t_2 and the weights of the two equivalent masses satisfy the following conditions:

$$\begin{cases} m_{22} = m_2 a_{p2}/L' \\ m_{21} = m_2 - m_{22} \\ t_2 = m_2 c_{p2}/m_{22} \end{cases} \tag{6.42}$$

The positions vector of the CMs of the augmented links 1 and 3 in the local frames are obtained as

$$^1\boldsymbol{A_1} = {}^1\boldsymbol{P_1'} = \begin{Bmatrix} m_1 a_{p1} + m_{21} L/(m_1 + m_{21}) \\ m_1 b_{p1}/(m_1 + m_{21}) \\ m_1 c_{p1}/(m_1 + m_{21}) \end{Bmatrix} \tag{6.43}$$

$$^3\boldsymbol{A_3} = {}^3\boldsymbol{P_3'} = \begin{Bmatrix} m_3 a_{p3}/(m_3 + m_{22}) \\ m_3 b_{p3}/(m_3 + m_{22}) \\ (m_3 c_{p3} + m_{22} t_2)/(m_3 + m_{22}) \end{Bmatrix} \tag{6.44}$$

H_1 and H_3 are points right above R_1 and R_4 respectively, with heights of $h_1 = (m_1 + m_{21})g/k_1, h_3 = (m_3 + m_{22})g/k_3$.

The 4R parallelogram linkage is statically balanced by connecting points H_1 and A_1, and H_3 and A_3 using two springs respectively [Fig. 6.7(a)]

An example is now given to illustrate the balancing method. Let $m_1 = m_2 = m_3 = m$, $L' = L = 100mm$, the positions of the CMs of link 1 in the 1st local coordinate frame and link 3 in the 3rd local coordinate frame are $\{10 \quad 20 \quad 0\}^T$ and the CM of link 2 is on the line R_2R_3 and the position vector in 2nd local coordinate frame is $\{10 \quad 0 \quad 0\}^T$. The position vector, $^1\boldsymbol{A_1}$, of the CM of the augmented link 1 in the 1st local coordinate frame and the mass of the augmented link 1 are calculated as

$$^1\boldsymbol{A_1} = {}^1\boldsymbol{P_1'} = \{1000/19 \quad 200/19 \quad 0\}^T \tag{6.45}$$

$$m_1' = 19m/10 \tag{6.46}$$

Similarly, the position vector, $^3\boldsymbol{A_3}$, of the CM of the augmented link 3 in the 3rd local coordinate frame and the mass of the augmented link 3 are

$$^3\boldsymbol{A_3} = {}^3\boldsymbol{P_3'} = \{100/11 \quad 200/11 \quad 0\}^T \tag{6.47}$$

$$m_3' = 11m/10 \tag{6.48}$$

The heights of the spring attachment points on the base H_1 and H_3 are $h_1 = 19mg/10k_1, h_3 = 11mg/10k_3$. The obtained positions of the spring attachment points satisfy Eq. (6.15).This proves that the balancing conditions have nothing to do with the positions of CMs of the links when the mass moments of links 1 and 3 are equal.

When balancing the system using one spring, the masses of links 1 and 3 should be distributed onto the base and link 2 [Fig. 6.8(b)]. It is observed from Eqs. (6.2a) and (6.2c) that the sum of P_{1z} and P_{3z} is $LC\theta$ when $a_{p1} = a_{p3}$ and $b_{p1} = b_{p3}$, i.e., the total potential energy and the balancing condition of the system when $m_1 = m_3$ are independent of the values of a_{p1} (a_{p3}) and b_{p1} (b_{p3}). Suppose that $a_{p1} = a_{p3} = a$, $b_{p1} = b_{p3} = 0$ and $c_{p1} = c_{p3} = c$, i.e., the position vectors of the CMs of link 1 in 1st local coordinate frame and link 3 in 3rd local coordinate frame are $\{a \quad 0 \quad c\}^T$. The position of the equivalent mass on R_1 is $\{0 \quad 0 \quad 0\}^T$, and that of the equivalent mass on R_2 is $\{L \quad 0 \quad t_1\}^T$. t_1 and the weights of the two equivalent masses can be calculated as:

$$\begin{cases} m_{12} = m_1 a/L \\ m_{11} = m_1 - m_{12} \\ t_1 = m_1 c/m_{12} \end{cases} \tag{6.49}$$

Similarly, the parameters of link 3 can be obtained as

$$\begin{cases} m_{32} = m_3 a/L \\ m_{31} = m_3 - m_{32} \\ t_3 = m_3 c/m_{32} \end{cases} \tag{6.50}$$

The position vector, ${}^{2}\boldsymbol{A_2}$, of the CM of the augmented link 2 in the 2nd local frame is yielded as

$$ {}^{2}\boldsymbol{A_2} = {}^{2}\boldsymbol{P_2'} = \begin{Bmatrix} (m_2 a_{p2} + m_{31} L')/(m_2 + m_{12} + m_{31}) \\ m_2 b_{p2}/(m_2 + m_{12} + m_{31}) \\ m_2 c_{p2}/(m_2 + m_{12} + m_{31}) \end{Bmatrix} \tag{6.51} $$

Draw a parallelogram based on R_1, R_2 and A_2, and the fourth vertex of the parallelogram B_2 is the virtual rotation centre of A_2 [Fig. 6.8(a)]. The spring attachment point on the base for link 2 should be right above B_2, with a height of $h_2 = (m_2 + m_{12} + m_{31})g/k_2$.

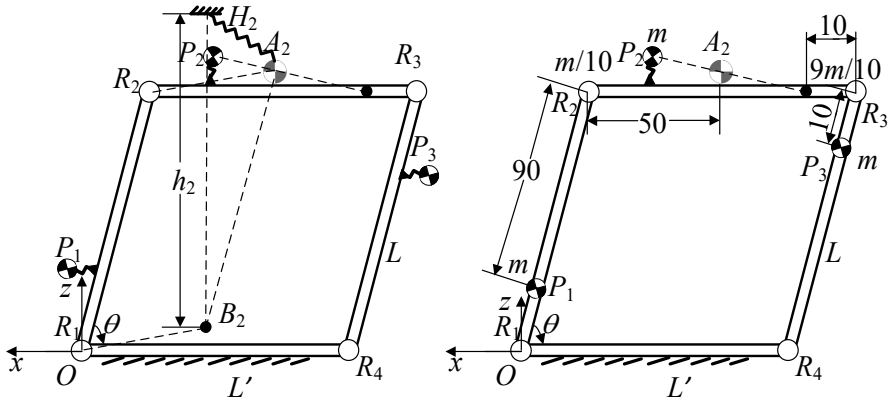

Fig. 6.8 Static balancing of planar 4R parallelogram linkage using one spring (geometric method): (a) the balancing method; (b) mass moment substitution of links 1 and 3

A numerical example is given as follows. Suppose the positions of CMs of the links 1 and 3 in local coordinate frames are $\{10 \quad 0 \quad 0\}^T$ and that of link 2 is $\{10 \quad 20 \quad 0\}^T$. The position vector, ${}^{2}\boldsymbol{A_2}$, of the CM of the augmented link 2 in the local coordinate frame and the mass of the augmented link 2 are calculated as

$$ {}^{2}\boldsymbol{A_2} = {}^{2}\boldsymbol{P_2'} = \{50 \quad 10 \quad 0\}^T \tag{6.52} $$

$$ m_2' = 2m \tag{6.53} $$

B_2, the position of virtual rotation centre of A_2, and H_2 (the point right above B_2) are calculated as

$$ \boldsymbol{B_2} = \{-a_{p2} \quad 0 \quad -b_{p2}\}^T = \{-50 \quad 0 \quad -10\}^T \tag{6.54} $$

$$ \boldsymbol{H_2} = \{-a_2 \quad 0 \quad 2mg/k_2 - b_2\}^T = \{-50 \quad 0 \quad 2mg/k_2 - 10\}^T \tag{6.55} $$

The 4R parallelogram linkage is statically balanced by connecting points H_2 and A_2 using one spring [Fig. 6.8(a)]. The obtained positions of the spring attachment points satisfy Eq. (6.27).

The algebraic method proposed above can also be applied to a general 4R linkage, which can be balanced using two or three springs. When balancing the general 4R linkage using the geometric method, the mass of the coupler can be distributed onto the two cranks. The mechanism is then equivalent to two 1-link manipulators with payloads. Each manipulator can be balanced by connecting a point right above the R joint and the point on the line defined by the R joint and the CM of the augmented manipulator. When distributing the masses of links 1 and 3 onto the base and link 2, the 4R parallelogram linkage turns into a 2-link manipulator (whose link masses are zero) with a payload. The manipulator then can be balanced using the method proposed in [104].

6.2 Static Balancing Method of Planar Manipulators

In this section, planar manipulators with links whose masses cannot be neglected will be balanced. This is different from the system in [102, 104] in which only the weight of the payload was considered, the weights of the links are considered in this thesis. Planar 1R, 2R and 3R manipulators are represented schematically in Fig. 6.9. For the sake of convenience, assume that the CM of each link is at the centroid of the link.

A global coordinate is attached to the ground, with the z-axis pointing in the direction opposite to the gravitational acceleration vector. The z-axis of the local coordinate frames are along the axes of the R joints and x-axis point from R_i to R_{i+1}. Let θ_1, θ_2, and θ_3 be the joint variables associated with the three R joints respectively and the link lengths are represented by L_i (i = 1, 2, 3…).

The positions of the CMs of the links P_i, and the R joints P_{Ri} are:

$$\boldsymbol{P_1} = \{L_1 C\theta_1/2 \quad 0 \quad L_1 S\theta_1/2\}^T \tag{6.56a}$$

$$\boldsymbol{P_{R2}} = \{L_1 C\theta_1 \quad 0 \quad L_1 S\theta_1\}^T \tag{6.56b}$$

$$\boldsymbol{P_2} = \{L_1 C\theta_1 + [L_2 C(\theta_1 + \theta_2)]/2 \quad 0 \quad L_1 S\theta_1 + [L_2 S(\theta_1 + \theta_2)]/2\}^T \tag{6.56c}$$

$$\boldsymbol{P_{R3}} = \{L_1 C\theta_1 + L_2 C(\theta_1 + \theta_2) \quad 0 \quad L_1 S\theta_1 + L_2 S(\theta_1 + \theta_2)\}^T \tag{6.56d}$$

$$\boldsymbol{P_3} = \{L_1 C\theta_1 + L_2 C(\theta_1 + \theta_2) + L_3[C(\theta_1 + \theta_2 + \theta_3]/2 \quad 0 \quad P_{3z}\}^T \tag{6.56e}$$

where

$$P_{3z} = L_1 S\,\theta_1 + L_2 S(\theta_1 + \theta_2) + L_3[S(\theta_1 + \theta_2 + \theta_3]/2$$

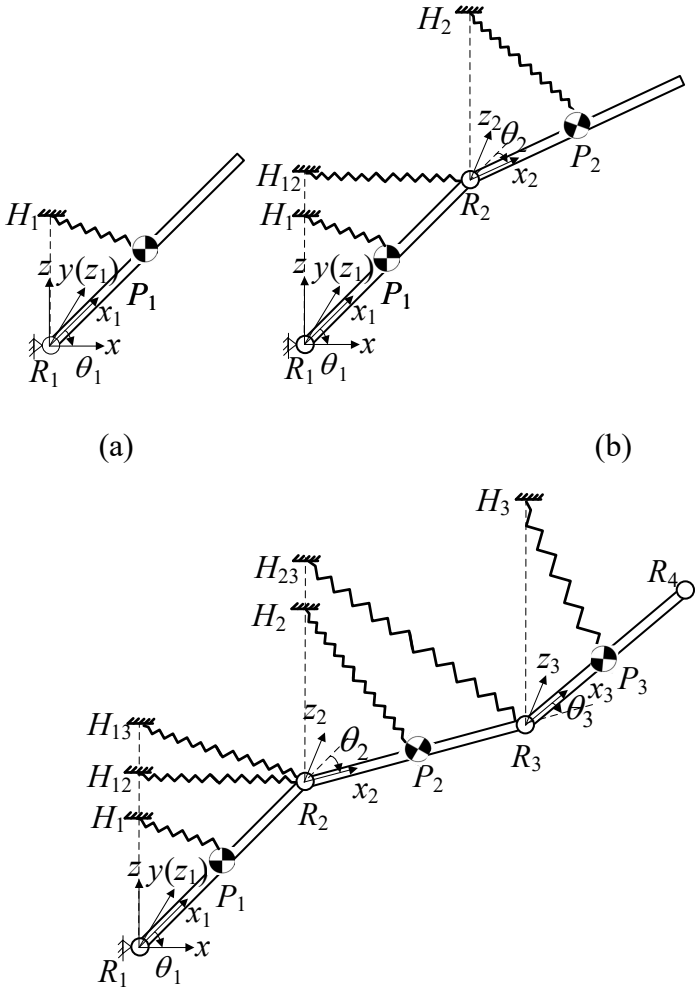

Fig. 6.9 Static balancing of planar manipulators: (a) manipulator with one link; (b) manipulator with two links; (c) manipulator with three links

According to [102, 104], a one-link manipulator mounted on R joint, U joint or S joint [117] can be balanced using one spring. One end of the spring is right above the joint and the other end should be on the line defined by the CM of the manipulator and the centre of the joint. It is noted that the spring attachment point on the base for the manipulator mounted on an R joint can be any point right above the axis of the R joint. The height of the spring connecting point on the base is $h = mg/k$, when attaching the spring to the CM of the manipulator directly. Hence, the first link of the manipulators can be readily balanced, by connecting the point right above R_1 and the CM of the first link using one spring [Fig. 6.9(a)]. Let the spring connecting point H_1 on the base be

$$\boldsymbol{H_1} = \{0 \quad 0 \quad m_1 g/k\}^T \tag{6.57}$$

The total potential energy is calculated as

$$V_1 = V_{s1} + V_{m1} = \frac{1}{2}k|\boldsymbol{P_1} - \boldsymbol{H_1}|^2 + mgP_{1z} = (L_1^2k^2 + 4m_1^2g^2)/8k \quad (6.58)$$

which is a constant value. The result implies that the one-link manipulator is gravity-compensated.

As in [174], one spring is adopted to balance the link 2, with one end fixed at a point right above R_2 and the other end attached to the CM of link 2 (or any other positions, as long as they meet the requirement of similar triangles [174]). The global coordinate frame is set at R_2 and the system is equal to a 1-link manipulator mounted on an R joint, which can be statically balanced using one spring. However, when attaching the global coordinate frame to R_1, link 2 with R_2 is not an independent unit anymore. The spring connecting point on the base H_2, which is a point right above R_2, is given by

$$\boldsymbol{H_2} = \{P_{R2x} \quad P_{R2y} \quad m_2g/k + P_{R2z}\}^T \quad (6.59)$$

The total potential energy of link 2 is calculated as

$$V_2 = V_{s2} + V_{m2} = \frac{1}{2}k|\boldsymbol{P_2} - \boldsymbol{H_2}|^2 + mgP_{2z} = (L_2^2k^2 + 4m_2^2g^2 + 8L_1km_2gS\theta_1)/8k \quad (6.60)$$

Similarly, H_3, which is a point right above R_3, and the potential energy of link 3 are yielded as:

$$\boldsymbol{H_3} = [P_{R3x} \quad P_{R3y} \quad m_3g/k + P_{R3z}]^T \quad (6.61)$$

$$\begin{aligned} V_3 = V_{s3} + V_{m3} &= \frac{1}{2}k|\boldsymbol{P_3} - \boldsymbol{H_3}|^2 + mgP_{3z} \\ &= [L_3^2k^2 + 4m_3^2g^2 + 8L_1km_3gS\theta_1 + 8L_2km_3gS(\theta_1 + \theta_2)]/8k \end{aligned} \quad (6.62)$$

Equations (6.60) and (6.62) imply that the potential energies of links 2 and 3 are not constants, which means the two links are not statically balanced.

Now let us observe the position vectors of links 2 and 3. The position of the second link contains two components, including the translation of R_2 and the rotation of link 2 with respect to the global coordinate frame. The latter term can be balanced using one spring as mentioned above and for the former one, which is a variation with respect to θ_1, an additional spring is needed. One end of the spring should be attached to H_{12} ($\{P_{R1x} \quad P_{R1y} \quad m_2g/k + P_{R1z}\}^T$) with the other end to R_2, as shown in Fig. 6.9(b). The potential energy of the link 2 is then calculated as:

$$\begin{aligned} V_2 = V_{s2} + V_{m2} &= \frac{1}{2}k|\boldsymbol{P_2} - \boldsymbol{H_2}|^2 + \frac{1}{2}k|\boldsymbol{P_{R2}} - \boldsymbol{H_{12}}|^2 + mgP_{2z} \\ &= (4L_1^2k^2 + L_2^2k^2 + 8m^2g^2)/8k \end{aligned} \quad (6.63)$$

which is a constant value. The position vector of link 3 is composed of the translation of R_3 (including the movement of R_3 with respect to R_2 and the movement of R_2 with respect to R_1) and the rotation of link 3. Two additional springs are added, which connect H_{13}

($\{P_{R1x} \quad P_{R1y} \quad m_3 g/k + P_{R1z}\}^T$) and R_2, and H_{23} ($\{P_{R2x} \quad P_{R2y} \quad m_3 g/k + P_{R2z}\}^T$) and R_3 respectively [Fig. 6.9(c)]. The total potential energy of link 3 is obtained as:

$$V_3 = V_{s3} + V_{m3} = \frac{1}{2}k|\boldsymbol{P_3} - \boldsymbol{H_3}|^2 + \frac{1}{2}k|\boldsymbol{P_{R3}} - \boldsymbol{H_{23}}|^2 + \frac{1}{2}k|\boldsymbol{P_{R2}} - \boldsymbol{H_{13}}|^2 + mgP_{3z}$$
$$= (4L_1^2k^2 + 4L_2^2k^2 + L_3^2k^2 + 12m_3^2g^2)/8k \qquad (6.64)$$

which is also a constant value. Equations (6.63-6.64) verify that the method proposed in this section is valid and the i^{th} link of the manipulators can be balanced using i springs. When adding the fourth link, another four springs are needed, which connect H_{14} ($\{P_{R1x} \quad P_{R1y} \quad m_4 g/k + P_{R1z}\}^T$) and one point on the axis of R_2, and H_{24} ($\{P_{R2x} \quad P_{R2y} \quad m_4 g/k + P_{R2z}\}^T$) and one point on the axis of R_3, H_{34} ($\{P_{R3x} \quad P_{R3y} \quad m_4 g/k + P_{R3z}\}^T$) and one point on the axis of R_4 and H_4 ($\{P_{R4x} \quad P_{R4y} \quad m_4 g/k + P_{R4z}\}^T$) and the CM of link 4 respectively.

6.3 Static Balancing Method of Spherical Manipulators

In this section, the conditions of the static balancing for the spherical manipulators will be derived. Spherical manipulators refer to the ones in which the axes of the R joints intersect at a point, and have RCM kinematics.

6.3.1 Static Balancing of Spherical Manipulators

Since all the links of spherical manipulators move around the point of intersection, which is equivalent to a virtual S joint, it is hypothesized that all the spherical manipulators composed of n moving links can be balanced using n [or (n-1)] springs. The general balancing method is: using one spring to balance each moving link of the manipulators. One end of the spring is attached right above the point of intersection, the other end is fixed on the CM of the link [Fig. 6.10]. It is noted that the connecting point on the base for the first link can be any point on the line right above the axis of the first R joint, as shown in Fig. 6.10.

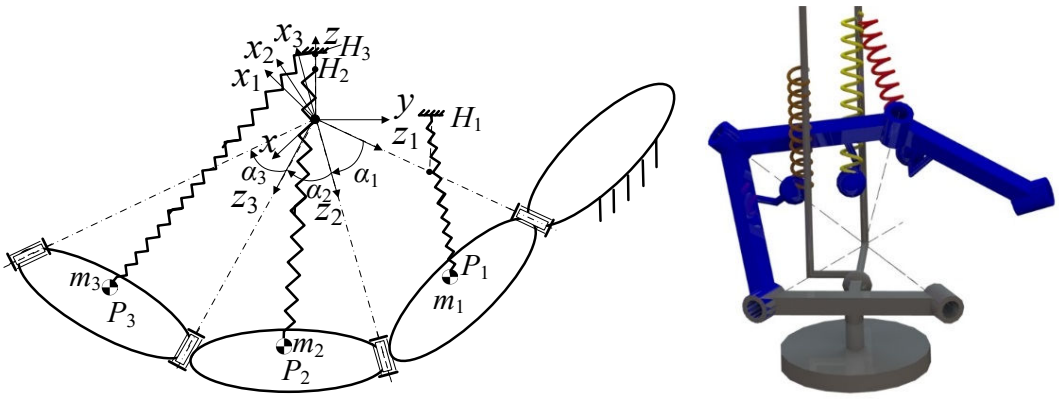

(a) (b)

Fig. 6.10 Static balancing of spherical manipulator: (a) the sketch of the manipulator; (b) the 3D model of the manipulator

A global coordinate system is fixed to the base with its z-axis pointing vertically upward and with its origin located at the intersection of the axes of the R joints. Suppose the position vector of the CM of the i^{th} link in the i^{th} local frame is represented by

$$^{i}\boldsymbol{P_i} = \{a_i \quad b_i \quad c_i\}^T \tag{6.65}$$

The link masses and joint twist angles of the manipulator are respectively noted as m_i and α_i (i = 1, 2, 3…). The position vectors of the CMs of the three links in the global coordinate system are yielded as

$$\begin{Bmatrix} \boldsymbol{P_1} \\ 1 \end{Bmatrix} = {}_1^0T \begin{Bmatrix} {}^{1}\boldsymbol{P_1} \\ 1 \end{Bmatrix} = \{-b_1S\theta_1 + a_1C\theta_1 \quad c_1 \quad -a_1S\theta_1 - b_1C\theta_1 \quad 1\}^T \tag{6.66a}$$

$$\begin{Bmatrix} \boldsymbol{P_2} \\ 1 \end{Bmatrix} = {}_1^0T\,{}_2^1T \begin{Bmatrix} {}^{2}\boldsymbol{P_2} \\ 1 \end{Bmatrix} = \{P_{2x} \quad (c_2C\alpha_1 - b_2S\alpha_1C\theta_2 - a_2S\alpha_1S\theta_2)/2 \quad P_{2z} \quad 1\}^T \tag{6.66b}$$

where

$$P_{2x} = [-S\theta_1(S\alpha_1c_2 + b_2C\alpha_1C\theta_2 + a_2C\alpha_1S\theta_2) + C\theta_1(a_2C\theta_2 - b_2S\theta_2)]/2$$

$$P_{2z} = [C\theta_1(-S\alpha_1c_2 + b_2C\alpha_1C\theta_2 + a_2C\alpha_1S\theta_2) + S\theta_1(-a_2C\theta_2 + b_2S\theta_2)]/2$$

$$\begin{Bmatrix} \boldsymbol{P_3} \\ 1 \end{Bmatrix} = {}_1^0T\,{}_2^1T\,{}_3^2T \begin{Bmatrix} {}^{3}\boldsymbol{P_3} \\ 1 \end{Bmatrix} = \{P_{3x} \quad P_{3y} \quad P_{3z} \quad 1\}^T \tag{6.66c}$$

where

$$P_{3x} = -C\theta_1[C\theta_2(-a_3C\theta_3 + b_3S\theta_3) + S\theta_2(b_3C\alpha_2C\theta_3 + c_3S\alpha_2 + a_3C\alpha_2S\theta_3)] - S\theta_1\{C\alpha_1[c_3C\theta_2S\alpha_2 + a_3C\theta_3S\theta_2 - b_3S\theta_2S\theta_3 + C\alpha_2C\theta_2(b_3C\theta_3 + a_3S\theta_3)] + S\alpha_1[c_3C\alpha_2 - S\alpha_2(b_3C\theta_3 + a_3S\theta_3)]\}$$

$$P_{3y} = -S\alpha_1[c_3C\theta_2S\alpha_2 + a_3C\theta_3S\theta_2 - b_3S\theta_2S\theta_3 + C\alpha_2C\theta_2(b_3C\theta_3 + a_3S\theta_3)] + C\alpha_1[c_3C\alpha_2 - S\alpha_2(b_3C\theta_3 + a_3S\theta_3)]$$

$$P_{3z} = c_3 S\alpha_2 S\theta_1 S\theta_2 + C\theta_1 S\alpha_1 S\alpha_2 (b_3 C\theta_3 + a_3 S\theta_3) + C\theta_2 S\theta_1 (-a_3 C\theta_3 + b_3 S\theta_3) - C\alpha_1 C\theta_1 [c_3 C\theta_2 S\alpha_2 + a_3 C\theta_3 S\theta_2 - b_3 S\theta_2 S\theta_3 + C\alpha_2 C\theta_2 (b_3 C\theta_3 + a_3 S\theta_3)] + C\alpha_2 [-c_3 C\theta_1 S\alpha_1 + S\theta_1 S\theta_2 (b_3 C\theta_3 + a_3 S\theta_3)]$$

${}^{i-1}_{i}T$ are provided in Appendix (C). The spring connecting points H_i on the base are all set to be

$$\boldsymbol{H_i} = \{0 \quad 0 \quad m_i g/k\}^T \qquad (i = 1,2,3) \tag{6.67}$$

The potential energy of each link can be obtained as

$$V1 = \frac{1}{2}k|\boldsymbol{P_1} - \boldsymbol{H_1}|^2 + m_1 g P_{1z} = (a_1^2 k^2 + b_1^2 k^2 + c_1^2 k^2 + g^2 m_1^2)/(2k) \tag{6.68}$$

$$V2 = \frac{1}{2}k|\boldsymbol{P_2} - \boldsymbol{H_2}|^2 + m_2 g P_{2z} = (a_2^2 k^2 + b_2^2 k^2 + c_2^2 k^2 + g^2 m_2^2)/(2k) \tag{6.69}$$

$$V3 = \frac{1}{2}k|\boldsymbol{P_3} - \boldsymbol{H_3}|^2 + m_3 g P_{3z} = (a_3^2 k^2 + b_3^2 k^2 + c_3^2 k^2 + g^2 m_3^2)/(2k) \tag{6.70}$$

Based on the results, one can conclude that the total potential energy is constant and the system designed is statically balanced.

6.3.2 Example 1: Static Balancing of Mechanisms Constructed Using Spherical Kinematic Chain Units

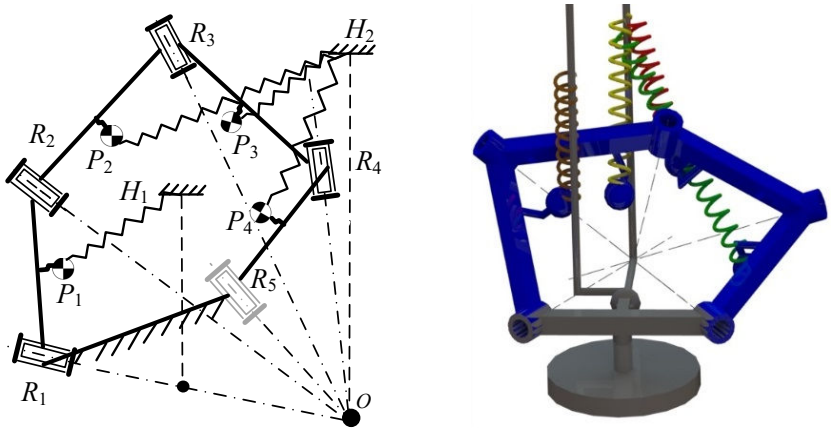

(a) (b)

Fig. 6.11 Static balancing of spherical 5R mechanism: (a) the sketch of the mechanism; (b) the 3D model of the mechanism

Based on Section 6.3.1, one can obtain that each link of the spherical manipulators can be balanced using one spring. Similarly, all the mechanisms constructed using spherical kinematic chain units can be balanced, by removing specific joints. Take the spherical 5R mechanism as an example. When removing R_5 [Fig. 6.11(a)], the mechanism turns into a spherical 4R manipulator, and each moving link of the mechanism is balanced using one spring. The spring connecting points on the base for link 1 can be any point right above

the joint axis of R_1, as shown in Fig. 6.11. One can also divide the spherical 5R linkage into two spherical chain units composed of R_1 and R_2, and R_5 and R_4 respectively by removing R_3.

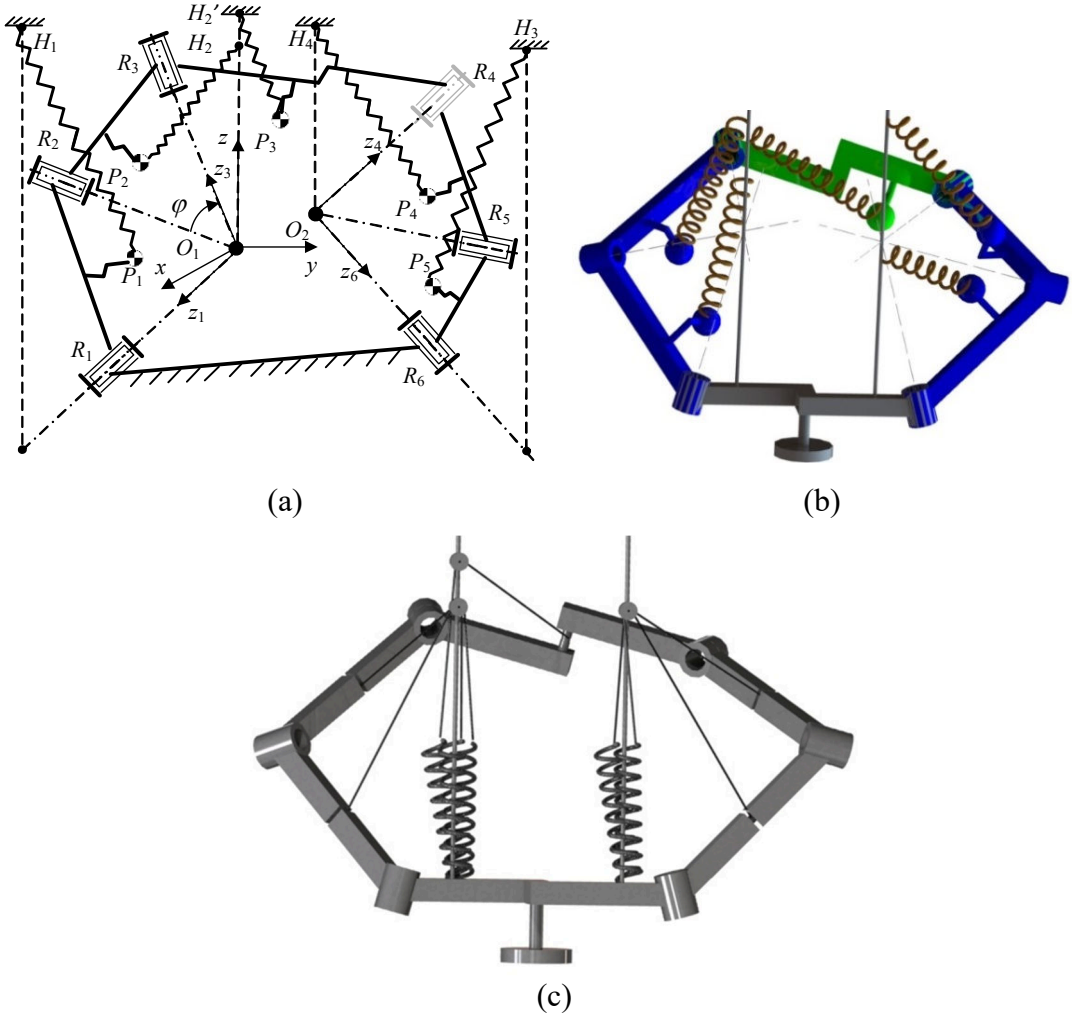

Fig. 6.12 Static balancing of Bennett 6R double-spherical mechanism: (a) the sketch of the mechanism; (b) the 3D model of the mechanism (the special case when the spring attachment points on the base for balancing links 1 and 5 are right above O_1 and O_2 respectively); (c) the practical design of the system

In fact, the above static balancing approach is not limited to spherical mechanisms in which the axes of all the R joints intersect at a point. For instance, in the 1-DOF Bennett 6R double-spherical mechanism (Fig. 6.12), the joint axes of R_1, R_2 and R_3 intersect at O_1, and the joint axes of R_4, R_5 and R_6 intersect at O_2 (double-RCM mechanism). The mechanism can be divided into two spherical kinematic chain units composed of R_1, R_2 and R_3, and R_6 and R_5 respectively by removing R_4 (or two spherical kinematic chain units composed of R_1 and R_2 and R_6, R_5 and R_4 respectively by removing R_3). H_1 is a point right

above the axis of R_1 and H_2 and H_2' are two points right above O_1. The masses of the links in the first spherical kinematic chain unit are balanced by connecting H_1 and the CM of link 1, H_2 and the CM of link 2, and H_2' and the CM of link 3 using three springs respectively. Similarly, the second spherical kinematic chain unit can also be balanced as shown in Fig. 6.12. Suppose the masses of links 1, 2, 4 and 5 are m and that of link 3 is m', and the CM of each link is in the middle of the links, a prototype is designed, as shown in Fig. 6.12(c). Rollers and cables are used to achieve zero-free-length springs. The heights of the attachment points $h_1 = h_2 = h_3 = h_4 = mg/k$ and $h_2' = m'g/k$.

If the two spherical kinematic chain units of the Bennett 6R double-spherical mechanism have the same parameters as the 3-DOF spherical manipulators in Section 2.3, fewer springs will be required for the static balancing.

6.3.3 Example 2: Static Balancing of Mechanisms Constructed Using Spherical Chain Units and Other Types of Chain Units

This section will focus on the mechanisms that are constructed using spherical chain units and other types of chain units. Take the Bennett plano-spherical hybrid linkage as an example (Fig. 6.13), the axes of joints R_1, R_2 and R_3 are parallel, and those of R_4, R_5 and R_6 intersect at a point. Links 1, 3, 4 and 5 can be easily balanced based on the proposed methods.

The mass of link 2 can be replaced by two point-masses on the joint axes of R_2 and R_3, then the mechanism is equivalent to two chain units with payloads, including one mounted on R_1, and one spherical chain unit composed of R_4, R_5 and R_6. H_1 is a point right above the axis of R_1, H_2 and H_2' are two points right above the intersection of the axes of R_4, R_5 and R_6 and H_3 is a point on the line right above R_6. Four springs are used, one is attached to H_1 and to the CM of the augmented link 1 (combining the mass of link 1 and the first point-mass of link 2); the other three are attached to H_2 and the CM of link 4, H_2' and the CM of the augmented link 3 (combining the mass of link 3 and the second point-mass of link 2), and H_3 and the CM of link 5 respectively.

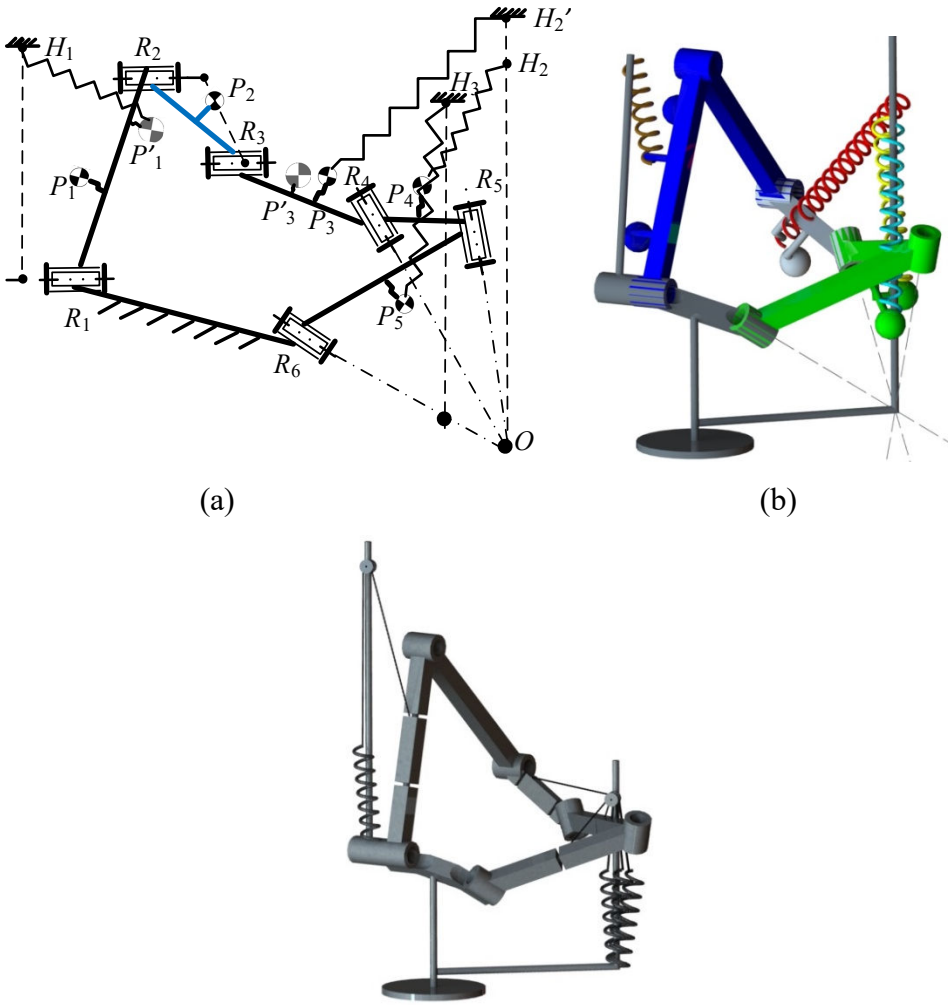

Fig. 6.13 Static balancing of Bennett plano-spherical hybrid linkage: (a) the sketch of the mechanism; (b) the 3D model of the mechanism (the special case when the spring attachment point for balancing link 5 is right above O); (c) the practical design of the system

Suppose the masses of links 1, 2, 4 and 5 are m and that of link 3 is $m/2$, and the CM of each link is in the middle of the link, a prototype is designed, as shown in Fig. 6.13(c). When distributing the mass of link 2 to link 1 and link 3, the spring attachment point on links 1 and 3 are at the top third of link 1 and top quarter of link 3 respectively. The masses of augmented links 1 and 3 are $3m/2$ and m respectively. $h_1 = 3mg/2k$ and $h_2 = h_2' = h_3 = mg/k$.

A 3-DOF 3-RRS spherical PM, composed of two platforms and three RRS chains [173], is shown in Fig. 6.14. The axes of two R joints in each chain intersect at a point. Different from the spherical mechanism in [117], the axes of the R joints have no common point and the mechanism has no fixed centre of rotation. The two links in each chain are easily

balanced by attaching the springs to the point right above the point of intersection and to the CM of the links. To balance the upper platform, the mass of the upper platform is replaced by three point-masses located at the three S joints on the platform. The mass and mass moment (about O) of the upper platform should be equal to those of the three point-masses [Fig. 6.14(a)].

$$\begin{cases} m_u = m_{u1} + m_{u2} + m_{u3} \\ m_{u1}g(0, r_1C\varphi_1, r_1S\varphi_1) + m_{u2}g(0, r_2C\varphi_2, r_2S\varphi_2) + m_{u3}g(0,0,-r_3) = 0 \end{cases} \tag{6.71}$$

which leads to

$$\begin{cases} m_{u1}r_1C\varphi_1 + m_{u2}r_2C\varphi_2 = 0 \\ m_{u1}r_1S\varphi_1 + m_{u2}r_2S\varphi_2 - m_{u3}r_3 = 0 \end{cases} \tag{6.72}$$

Since the mechanism is symmetrically distributed,

$$\begin{cases} r_1 = r_2 = r_3 \\ \varphi_1 + \varphi_2 = \pi \end{cases} \tag{6.73}$$

Substituting Eq. (6.73) into Eq. (6.71), it is obtained that $m_{u1} = m_{u2} = m_{u3} = m_u/3$. By replacing the mass of the upper platform with the three point-masses, the PM is equal to three 2R spherical chain units with payloads. The mass of the first chain unit is balanced by connecting H_{11} (the point right above the axes of R_{11}) and the CM of link 11 P_{11}, and H_{12} (the point right above the intersection of the axes of the two R joints) and the CM of the augmented link 12 P_{12}' (combining the masses of the upper platform and link 12) using two springs respectively [Fig. 6.14(b)]. Similarly, the other two chain units can also be balanced.

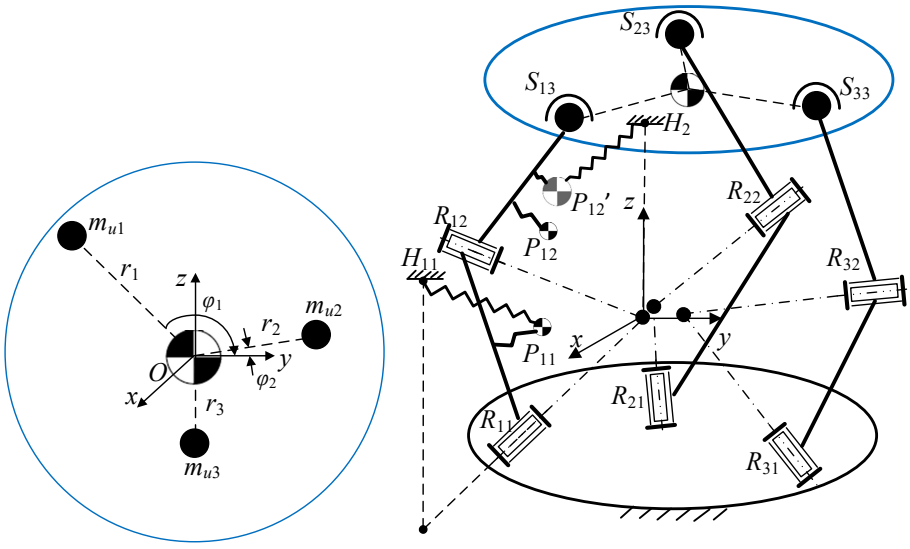

(a) (b)

Fig. 6.14 Static balancing of 3-RRS PM: (a) mass moment substitution of the upper platform; (b) the sketch of the mechanism

6.4 Static Balancing Method of Spatial Manipulators

In this section, the static balancing method of spatial manipulator will be addressed. In Section 6.2, the static balancing method for the planar manipulator has been proposed. Now the method will be extended and applied to spatial manipulators.

6.4.1 Static Balancing of Spatial Manipulators

The spatial manipulators are shown in Fig. 6.15. The spheres represent the positions of the CMs of the links.

Suppose the position vectors of the CM of the i^{th} link and R_i [a point that is the intersection of link (i-1) and link i] in the i^{th} local coordinate frame are represented by

$$^{\boldsymbol{i}}\boldsymbol{P_i} = \{a_i \quad b_i \quad c_i\}^T \tag{6.74a}$$

$$^{\boldsymbol{i}}\boldsymbol{P_{Ri}} = \{0 \quad 0 \quad 0\}^T \tag{6.74b}$$

Let

$$l_0 = 0,\ d_1 = 0 \tag{6.75}$$

The position vectors of the CMs of the links (P_i) and the R joints (P_{Ri}) expressed in the global coordinate frame are obtained as

$$\{\begin{matrix}\boldsymbol{P_1}\\1\end{matrix}\} = {}_1^0T\{\begin{matrix}^{\boldsymbol{1}}\boldsymbol{P_1}\\1\end{matrix}\} =$$

$$\{a_1C\theta_1 - b_1S\theta_1 \quad -c_1S\alpha_0 + C\alpha_0(b_1C\theta_1 + a_1S\theta_1) \quad c_1C\alpha_0 + S\alpha_0(b_1C\theta_1 + a_1S\theta_1)\ 1\}^T \tag{6.76a}$$

$$\{\begin{matrix}\boldsymbol{P_{R2}}\\1\end{matrix}\} = {}_1^0T\,{}_2^1T\{\begin{matrix}^{\boldsymbol{2}}\boldsymbol{P_{R2}}\\1\end{matrix}\}$$

$$\{L_1C\theta_1 + d_2S\theta_1S\alpha_1 \quad P_{R2y} \quad L_1S\alpha_0S\theta_1 + d_2C\alpha_1C\alpha_0 - d_2S\alpha_0S\alpha_1C\theta_1 \quad 1\}^T \tag{6.76b}$$

where $P_{R2y} = L_1C\alpha_0S\theta_1 - d_2C\alpha_1S\alpha_0 - d_2C\alpha_0S\alpha_1C\theta_1$

$$\left\{\begin{matrix}\boldsymbol{P_2}\\1\end{matrix}\right\} = {}_1^0T\,{}_2^1T\{\begin{matrix}^{\boldsymbol{2}}\boldsymbol{P_2}\\1\end{matrix}\} = \{P_{2x} \quad P_{2y} \quad P_{2z} \quad 1\}^T \tag{6.76c}$$

where

$$P_{2x} = \{S\theta_1[(c_2 + d_2)S\alpha_1 - C\alpha_1(b_2C\theta_2 + a_2S\theta_2)] + C\theta_1(L_1 + a_2C\theta_2 - b_2S\theta_2)\}$$

$$P_{2y} = -S\alpha_0[(c_2 + d_2)C\alpha_1 + S\alpha_1(b_2C\theta_2 + a_2S\theta_2)] + C\alpha_0[-(c_2 + d_2)C\theta_1S\alpha_1 + C\alpha_1C\theta_1(b_2C\theta_2 + a_2S\theta_2) + S\theta_1(L_1 + a_2C\theta_2 - b_2S\theta_2)]$$

$$P_{2z} = C\alpha_0[(c_2 + d_2)C\alpha_1 + S\alpha_1(b_2C\theta_2 + a_2S\theta_2)] + S\alpha_0[-(c_2 + d_2)C\theta_1S\alpha_1 + C\alpha_1C\theta_1(b_2C\theta_2 + a_2S\theta_2) + S\theta_1(L_1 + a_2C\theta_2 - b_2S\theta_2)]$$

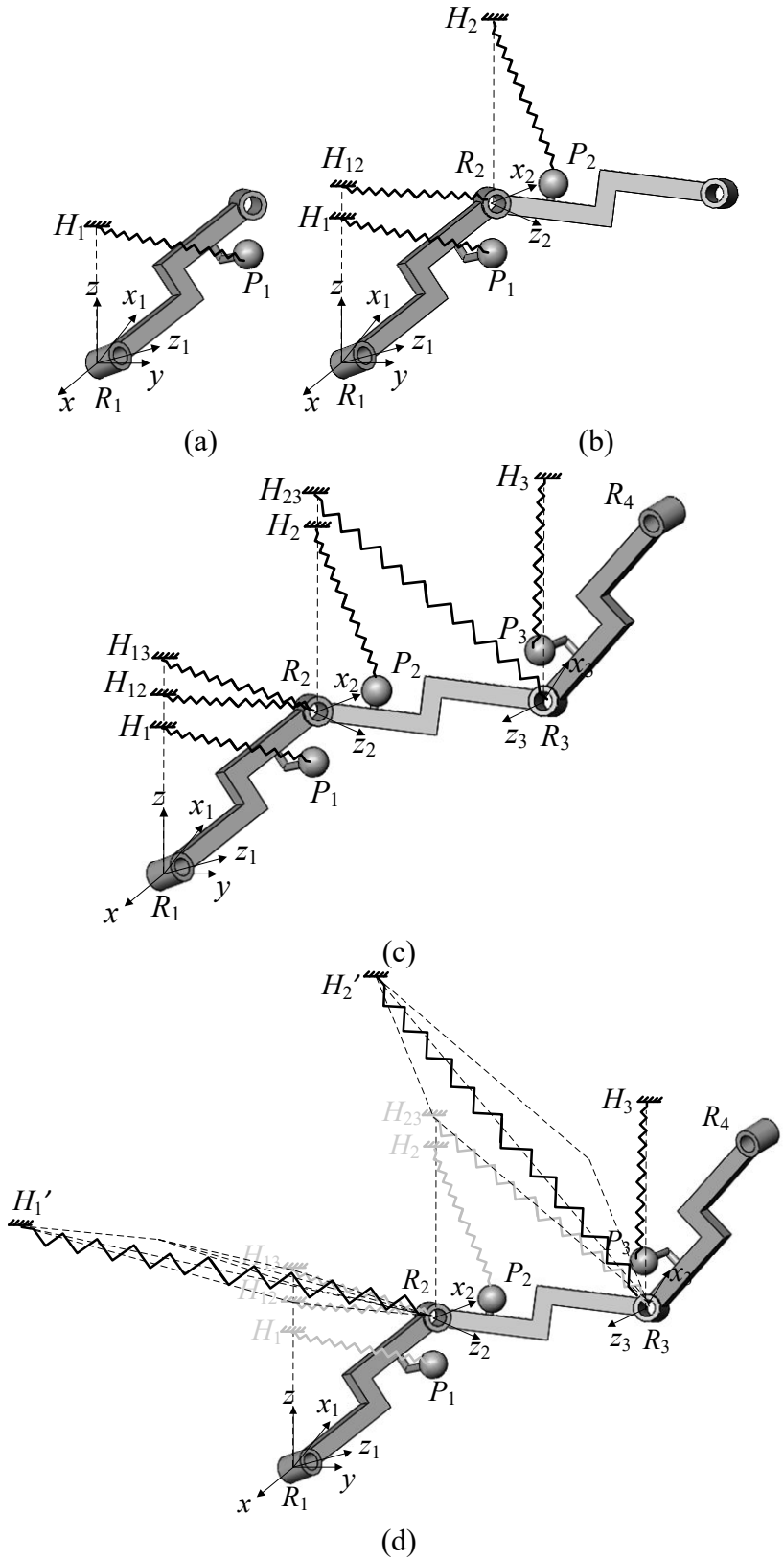

Fig. 6.15 Static balancing of spatial manipulators: (a) manipulator with one link; (b) manipulator with two links; (c) manipulator with three links; (d) the replacement of the springs through vector synthesis

$$\begin{Bmatrix} \boldsymbol{P_{R3}} \\ 1 \end{Bmatrix} = {}^{0}_{1}T\,{}^{1}_{2}T\,{}^{2}_{3}T\begin{Bmatrix} {}^{\mathbf{3}}\boldsymbol{P_{R3}} \\ 1 \end{Bmatrix} = \{P_{R3x} \quad P_{R3y} \quad P_{R3z} \quad 1\}^T \tag{6.76d}$$

where

$$P_{R3x} = C\theta_1(L_1 + L_2C\theta_2 + d_3S\alpha_2S\theta_2) + S\theta_1[(d_2 + d_3C\alpha_2)S\alpha_1 + C\alpha_1(d_3C\theta_2S\alpha_2 - L_2S\theta_2)]$$

$$P_{R3y} = S\alpha_0S\alpha_1(d_3C\theta_2S\alpha_2 - L_2S\theta_2) - C\alpha_1[(d_2 + d_3C\alpha_2)S\alpha_0 + C\alpha_0C\theta_1(d_3C\theta_2S\alpha_2 - L_2S\theta_2)] + C\alpha_0[-(d_2 + d_3C\alpha_2)C\theta_1S\alpha_1 + S\theta_1(L_1 + L_2C\theta_2 + d_3S\alpha_2S\theta_2)]$$

$$P_{R3z} = C\alpha_0[C\alpha_1(d_2 + d_3C\alpha_2) + S\alpha_1(d_3C\theta_2S\alpha_2 - L_2S\theta_2)] + S\alpha_0\{-C\theta_1[(d_2 + d_3C\alpha_2)S\alpha_1 + d_3C\theta_2S\alpha_2 - L_2S\theta_2] + S\theta_1(L_1 + L_2C\theta_2 + d_3S\alpha_2S\theta_2)\}$$

$$\begin{Bmatrix} \boldsymbol{P_3} \\ 1 \end{Bmatrix} = {}^{0}_{1}T\,{}^{1}_{2}T\,{}^{2}_{3}T\begin{Bmatrix} {}^{\mathbf{3}}\boldsymbol{P_3} \\ 1 \end{Bmatrix} = \{P_{3x} \quad P_{3y} \quad P_{3z} \quad 1\}^T \tag{6.76e}$$

where

$$P_{3x} = C\theta_1\{L_1 + C\theta_2(L_2 + a_3C\theta_3 - b_3S\theta_3) + S\theta_2[(c_3 + d_3)S\alpha_2 - C\alpha_2(b_3C\theta_3 + a_3S\theta_3)]\} + S\theta_1\{S\alpha_1[d_2 + (c_3 + d_3)C\alpha_2 + S\alpha_2(b_3C\theta_3 + a_3S\theta_3)] - C\alpha_1[-(c_3 + d_3)C\theta_2S\alpha_2 + C\alpha_2C\theta_2(b_3C\theta_3 + a_3S\theta_3) + S\theta_2(L_2 + a_3C\theta_3 - b_3S\theta_3)]\}$$

$$P_{3y} = C\alpha_0\{-C\theta_1S\alpha_1[d_2 + (c_3 + d_3)C\alpha_2 + S\alpha_2(b_3C\theta_3 + a_3S\theta_3)] + S\theta_1[L_1 + (c_3 + d_3)S\alpha_2S\theta_2 - C\alpha_2S\theta_2(b_3C\theta_3 + a_3S\theta_3) + C\theta_2(L_2 + a_3C\theta_3 - b_3S\theta_3)] + C\alpha_1C\theta_1[-(c_3 + d_3)C\theta_2S\alpha_2 + C\alpha_2C\theta_2(b_3C\theta_3 + a_3S\theta_3) + S\theta_2(L_2 + a_3C\theta_3 - b_3S\theta_3)]\} - S\alpha_0\{C\alpha_1[d_2 + (c_3 + d_3)C\alpha_2 + S\alpha_2(b_3C\theta_3 + a_3S\theta_3)] + S\alpha_1[-(c_3 + d_3)C\theta_2S\alpha_2 + C\alpha_2C\theta_2(b_3C\theta_3 + a_3S\theta_3) + S\theta_2(L_2 + a_3C\theta_3 - b_3S\theta_3)]\}$$

$$P_{3z} = S\alpha_0\{-C\theta_1S\alpha_1[d_2 + (c_3 + d_3)C\alpha_2 + S\alpha_2(b_3C\theta_3 + a_3S\theta_3)] + S\theta_1[L_1 + (c_3 + d_3)S\alpha_2S\theta_2 - C\alpha_2S\theta_2(b_3C\theta_3 + a_3S\theta_3) + C\theta_2(L_2 + a_3C\theta_3 - b_3S\theta_3)] + C\alpha_1C\theta_1[-(c_3 + d_3)C\theta_2S\alpha_2 + C\alpha_2C\theta_2(b_3C\theta_3 + a_3S\theta_3) + S\theta_2(L_2 + a_3C\theta_3 - b_3S\theta_3)]\} + C\alpha_0\{C\alpha_1[d_2 + (c_3 + d_3)C\alpha_2 + S\alpha_2(b_3C\theta_3 + a_3S\theta_3)] + S\alpha_1[-(c_3 + d_3)C\theta_2S\alpha_2 + C\alpha_2C\theta_2(b_3C\theta_3 + a_3S\theta_3) + S\theta_2(L_2 + a_3C\theta_3 - b_3S\theta_3)]\}$$

$$\begin{Bmatrix} \boldsymbol{P_{R4}} \\ 1 \end{Bmatrix} = {}^{0}_{1}T\,{}^{1}_{2}T\,{}^{2}_{3}T\,{}^{3}_{4}T\begin{Bmatrix} {}^{\mathbf{4}}\boldsymbol{P_{R4}} \\ 1 \end{Bmatrix} = \{P_{4x} \quad P_{4y} \quad P_{4z} \quad 1\}^T \tag{6.76f}$$

where

$$P_{R4x} = C\theta_1\{L_1 + C\theta_2(L_2 + L_3C\theta_3) + S\theta_2[(d_3 + d_4)S\alpha_2 - L_3C\alpha_2S\theta_3]\} + S\theta_1\{S\alpha_1[d_2 + (d_3 + d_4)C\alpha_2 + L_3S\alpha_2S\theta_3] + C\alpha_1\{-(L_2 + L_3C\theta_3)S\theta_2 + C\theta_2[(d_3 + d_4)S\alpha_2 - L_3C\alpha_2S\theta_3]\}\}$$

$$P_{R4y} = S\alpha_0S\alpha_1\{-(L_2 + L_3C\theta_3)S\theta_2 + C\theta_2[(d_3 + d_4)S\alpha_2 - L_3C\alpha_2S\theta_3]\} + C\alpha_0\{-C\theta_1S\alpha_1[d_2 + (d_3 + d_4)C\alpha_2 + L_3S\alpha_2S\theta_3] + S\theta_1[L_1 + C\theta_2(L_2 + L_3C\theta_3) + S\theta_2(d_3 + d_4)S\alpha_2 - L_3C\alpha_2S\theta_2S\theta_3]\} - C\alpha_1\{S\alpha_0[d_2 + (d_3 + d_4)C\alpha_2 + L_3S\alpha_2S\theta_3] + C\alpha_0C\theta_1\{-(L_2 + L_3C\theta_3)S\theta_2 + C\theta_2[(d_3 + d_4)S\alpha_2 - L_3C\alpha_2S\theta_3]\}\}$$

$$P_{R4z} = C\alpha_0\{C\alpha_1[d_2 + (d_3 + d_4)C\alpha_2 + L_3S\alpha_2S\theta_3] + S\alpha_1\{(L_2 + L_3C\theta_3)S\theta_2 + C\theta_2[(d_3 + d_4)S\alpha_2 - L_3C\alpha_2S\theta_3]\}\} + S\alpha_0\{S\theta_1\{L_1 + C\theta_2(L_2 + L_3C\theta_3) + S\theta_2[(d_3 + d_4)S\alpha_2 - L_3C\alpha_2S\theta_2S\theta_3]\} - C\theta_1\{S\alpha_1[d_2 + (d_3 + d_4)C\alpha_2 + L_3S\alpha_2S\theta_3] + C\alpha_1\{-(L_2 + L_3C\theta_3)S\theta_2 + C\theta_2[(d_3 + d_4)S\alpha_2 - L_3C\alpha_2S\theta_3]\}\}\}$$

${}^{i-1}_{i}T$ are provided in Appendix (D). The first link is readily balanced using one spring, the total potential energy of link 1 is computed as:

$$V_1 = V_{s1} + V_{m1} = \frac{1}{2}k|\boldsymbol{P_1} - \boldsymbol{H_1}|^2 + mgP_{1z} = (a_1^2k^2 + b_1^2k^2 + c_1^2k^2 + m_1^2g^2)/2k$$

(6.77)

Connecting H_{12} and one point on the axis of R_2, and H_2 and the CM of link 2 using two springs respectively, the second link is then statically balanced. It is noted that attaching the spring to the CM of the link is just an example to illustrate the method, the attachment point on the link can be any points on the line defined by a point on the axis of the R joint and the CM of the link. The potential energy of link 2 is

$$\begin{aligned} V_2 = V_{s2} + V_{m2} &= \frac{1}{2}k|\boldsymbol{P_2} - \boldsymbol{H_2}|^2 + \frac{1}{2}k|\boldsymbol{P_{R2}} - \boldsymbol{H_{12}}|^2 + m_2 g P_{2z} \\ &= (L_1^2k^2 + a_2^2k^2 + b_2^2k^2 + c_2^2k^2 + d_2^2k^2 + 2m_2^2g^2)/2k \end{aligned} \tag{6.78}$$

which is a constant. The third link can be balanced by connecting H_{13} and one point on the axis of R_2, H_{23} and one point on the axis of R_3, and H_3 and the CM of link 3 (or any points on the line defined by a point on the axis of the R joint and the CM of the link) using three springs respectively. The potential energy of link 3 is calculated as

$$\begin{aligned} V_3 = V_{s3} + V_{m3} &= \frac{1}{2}k|\boldsymbol{P_3} - \boldsymbol{H_3}|^2 + \frac{1}{2}k|\boldsymbol{P_{R3}} - \boldsymbol{H_{23}}|^2 + \frac{1}{2}k|\boldsymbol{P_{R2}} - \boldsymbol{H_{13}}|^2 + m_3 g P_{3z} \\ &= (L_1^2k^2 + L_2^2k^2 + a_3^2k^2 + b_3^2k^2 + c_3^2k^2 + d_2^2k^2 + d_3^2k^2 + 3m_3^2g^2)/2k \end{aligned} \tag{6.79}$$

Equations (6.78-6.79) infer that the method proposed above applies to any spatial manipulators, and the four parameters of the link, l, d, α and θ can be with arbitrary values. The total potential energy of the system is yielded as

$$\begin{aligned} V_t = V_1 + V_2 + V_3 = (&a_1^2k^2 + b_1^2k^2 + c_1^2k^2 + a_2^2k^2 + b_2^2k^2 + c_2^2k^2 + a_3^2k^2 + b_3^2k^2 + \\ &c_3^2k^2 + 2L_1^2k^2 + L_2^2k^2 + 2d_2^2k^2 + d_3^2k^2 + m_1^2g^2 + 2m_2^2g^2 + 3m_3^2g^2)/2k \end{aligned} \tag{6.80}$$

It is noted that the spring attachment positions H_i can be any points right above the axes of the R joint.

The total number of springs of the nR serial manipulator using the proposed geometric method is $n + (n - 1) + (n - 2) + \ldots + 2 + 1 = n\,(n + 1)/2$. It is noted that the number of springs can be reduced through vector synthesis. For example, the two springs connected to H_2 and P_2, and H_{23} and R_3 can be replaced by one spring connected to H_2' and R_3, as shown in Fig. 6.15(d). The three springs connected to H_1 and P_1, H_{12} and R_2 and H_{13} and R_2 can be replaced by one spring connected to H_1' and R_2.

When a payload is added at the end of the manipulator composed of n moving links, n springs are needed to balance the payload. One end of each spring is attached on $\boldsymbol{H_i}$, which is a point right above R_i, and the other end is to R_{i+1}, as shown in Fig. 6.16.

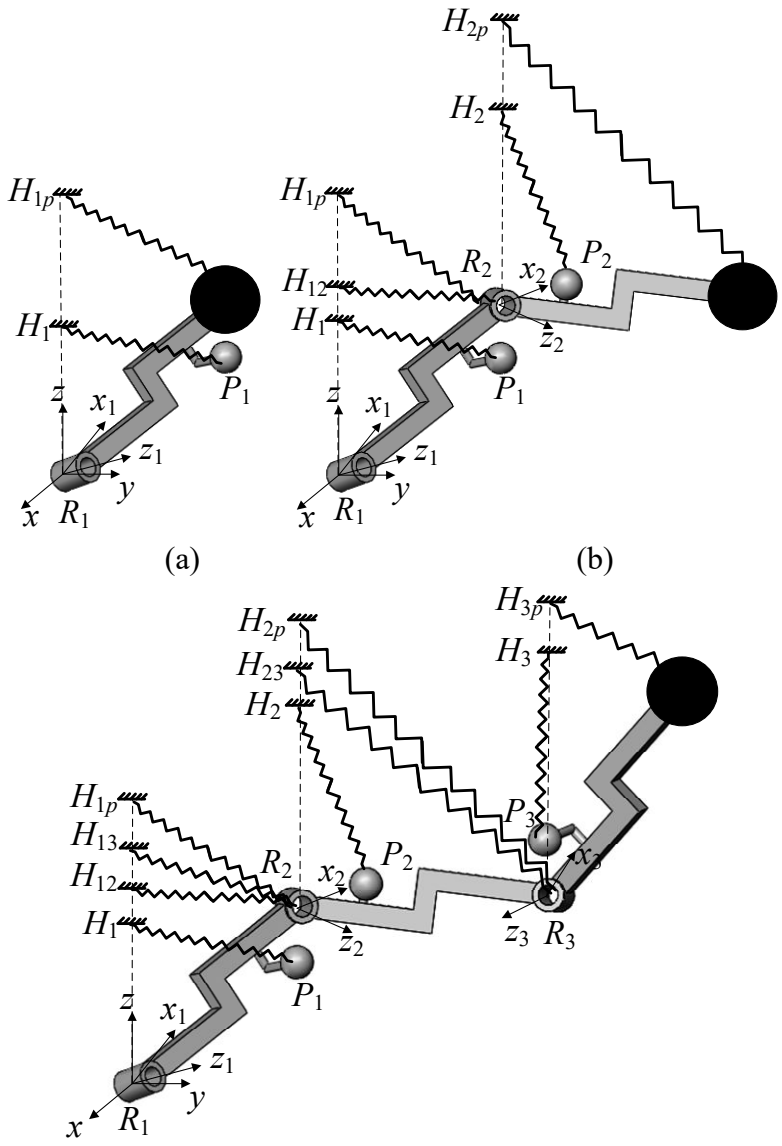

Fig. 6.16 Static balancing of spatial manipulators with payload: (a) manipulator with one link; (b) manipulator with two links; (c) manipulator with three links

The total potential energies of the 1-link manipulator, 2-link manipulator and 3-link manipulator with payloads are respectively computed as

$$V_{1p} = V_{s1p} + V_{m1p} + V_1 = \frac{1}{2}k\left|\boldsymbol{P_{R2}} - \boldsymbol{H_{1p}}\right|^2 + MgP_{R2z} + V_1 = (a_1^2k^2 + b_1^2k^2 + c_1^2k^2 + d_2^2k^2 + L_1^2k^2 + m_1^2g^2 + M^2g^2)/2k \tag{6.81}$$

$$V_{2p} = V_{s2p} + V_{m2p} + V_2 = \frac{1}{2}k\left|\boldsymbol{P_{R3}} - \boldsymbol{H_{2p}}\right|^2 + \frac{1}{2}k\left|\boldsymbol{P_{R2}} - \boldsymbol{H_{1p}}\right|^2 + MgP_{R3z} + V_2 = (2L_1^2k^2 + L_2^2k^2 + a_2^2k^2 + b_2^2k^2 + c_2^2k^2 + 2d_2^2k^2 + d_3^2k^2 + 2m_2^2g^2 + 2M^2g^2)/2k \tag{6.82}$$

$$V_{3p} = V_{s3p} + V_{m3p} + V_3 = \frac{1}{2}k\left|\boldsymbol{P_{R4}} - \boldsymbol{H_{3p}}\right|^2 + \frac{1}{2}k\left|\boldsymbol{P_{R3}} - \boldsymbol{H_{2p}}\right|^2 + \frac{1}{2}k\left|\boldsymbol{P_{R2}} - \boldsymbol{H_{1p}}\right|^2$$
$$+MgP_{R4z} + V_3 = (2L_1^2k^2 + 2L_2^2k^2 + L_3^2k^2 + a_3^2k^2 + b_3^2k^2 + c_3^2k^2$$
$$+2d_2^2k^2 + 2d_3^2k^2 + d_4^2k^2 + 3m_3^2g^2 + 3M^2g^2)/2k \tag{6.83}$$

which are constants.

6.4.2 3D Model of the Statically Balanced Spatial Manipulator

The positions of the spring connecting points on the base can be defined using additional linkages, such as RRRR linkages or RSRS linkages described in [104, 174]. We simply adopt an auxiliary serial mechanism with three translational DOFs for each link. The end-effectors have constant lengths of $m_i g/k$ (Fig. 6.17).

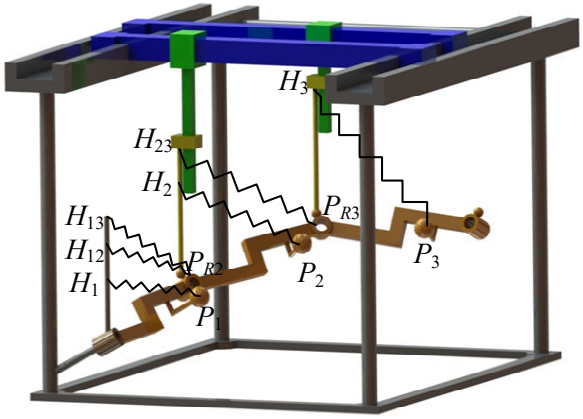

Fig. 6.17 3D model of the statically balanced spatial manipulator system

Each end-effector is connected to the R joint of the manipulator using an S joint. Hence, H_i are always right above the R joints with a distance of $m_i g/k$. Another method is to assemble one PM with three translation DOFs (such as Delta robot) above each R joint. The masses of the end-effectors of the auxiliary mechanism can be balanced using counterweights.

6.4.3 Static Balancing of a Mechanism with Multiple Modes

Figure 6.18 shows a 2-DOF 3-4R PM which has 14 2-DOF operation modes, including four spherical translation modes, six planar motion modes, and four sphere-on-sphere rolling modes [75]. Two approaches are adopted to balance the mechanism. In the first method, the mechanism is equal to three manipulators, including one limb with the upper

platform, which has four R joints, and another two limbs which contains three R joints each. Assume the mass of the link within the limbs is m and that of the platform is noted as M. The heights of H_i, which are the spring attaching points for the links within the chains, are $h_i = mg/k$ and the heights of H_{i2}, which are the spring connecting points for the platform, are $h_{i2} = Mg/k$. In the second method, the mass of the upper platform is replaced by three point-masses located at the three R joints on the platform. Then the mechanism is equal to three manipulators, each with three R joints and one payload at the end-effector. The heights of H_{i3}, which are the spring connecting points for the payloads, are $h_{i3} = Mg/3k$. The statically balanced systems using the two methods are respectively shown in Figs. 6.18(a) and (b).

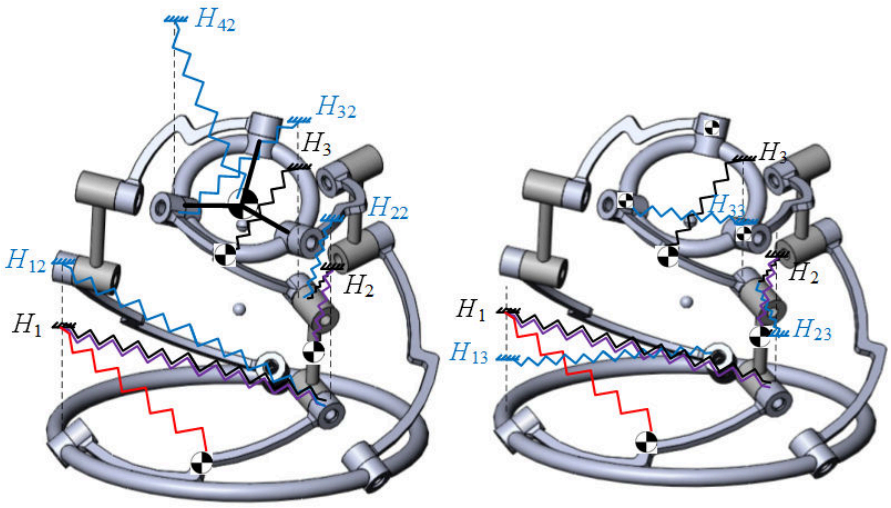

(a) (b)

Fig. 6.18 Static balancing of 3-4R PM with multiple modes [75]: (a) method I; (b) method II

6.5 Static Balancing Method Using Optimization Tools

In this section, a novel numerical optimization method will be proposed to derive the static balancing conditions.

6.5.1 Static Balancing of Planar 1-link Manipulator

In this section, a 1-link manipulator mounted on an R joint will be balanced to illustrate the optimization method.

The planar 1R manipulator is represented schematically in Fig. 6.19. In the literature (such as [102, 104]), it is stated that the manipulators can only be balanced by connecting the point right above the axis of the R joint and the point on the line defined by the joint and the CM of the link, as shown in Fig. 6.19(a). In this section, it will be shown that the position of spring attachment point has other approximate solutions. These solutions are also valid in the range of permitted errors. Suppose that P is the CM of the manipulator, O is a point on the axis of the R joint, the spring attachment points on the manipulator and the base are A and H respectively, B is a point at the same horizontal level as O and H is right above B. The lengths of OB, OP and BH are noted as s, L and h respectively. The position vector of A in the local coordinate frame is $\{a \quad b \quad c\}^T$.

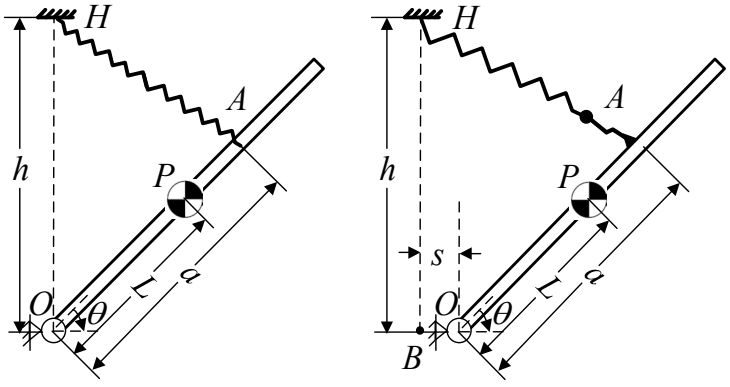

(a) (b)

Fig. 6.19 Static balancing of planar 1R manipulator: (a) the solution in the literature; (b) the solution in this thesis

The CMs of the positions of P and A are calculated as:

$$\boldsymbol{P} = \{LC\theta \quad 0 \quad LS\theta\}^T \tag{6.84a}$$

$$\boldsymbol{A} = \{aC\theta - bS\theta \quad -c \quad aS\theta + bC\theta\}^T \tag{6.84b}$$

Let the spring connecting point $\boldsymbol{H}$ on the base be

$$\boldsymbol{H} = \{s \quad 0 \quad h\}^T \tag{6.85}$$

The potential energy of the manipulator is expressed as

$$\begin{aligned} V = V_s + V_m &= \tfrac{1}{2}k|\boldsymbol{H} - \boldsymbol{A}|^2 + mgP_z \\ &= \{k[(s - aC\theta + bS\theta)^2 + (bC\theta - h + aS\theta)^2 + c^2]\}/2 + mgLS\theta \end{aligned} \tag{6.86}$$

The condition for the static balancing of the manipulator is the total potential energy is a constant. The sum of squared differences between two obtained potential energies when giving different values of variables should be as small as possible. The objective function is set as

$$Vs = \sum_{i=1}^{9}(V_{i+1} - V_i)^2 = f(a, b, s, h) \tag{6.87}$$

where V_i is the potential energy when $\theta = \theta_i$, θ_i are random values from 0° to 180°. The objective function is a formula related to a, b, s and h. It is noted that the variance of the total potential energy is independent of c. The optimization toolbox 'fmincon' of MATLAB is adopted to minimize the objective function.

$$[x, fval] = fmincon(fun, x0, [], [], [], [], lb, ub, nonlcon, options)$$

where x starts from $x0$ and attempts to find a minimizer x of the function. lb and ub are a set of lower and upper bounds on the design variable. For the 1-link manipulator, the lower and upper bound are set to be (the attachment points should be on the link)

$$\begin{aligned} lb &= [0,0,-100,0] \\ ub &= [100,100,100,100] \end{aligned} \tag{6.88}$$

Let $k = 0.1\ N/mm$, $l = 100mm$, $m = 0.1kg$ and $g = 9.8N/kg$. The optimization is regarded as successful if $fval\ (Vs) < 10^{-5}$. When giving different initial values in MATLAB, different sets of a, b, s and h can be obtained. Four sets of results are listed in Table 6.1 as examples.

Table 6.1 The optimization results of the 1-link manipulator

Initial values	Optimization results
30, 30, 30, 30	3.8138, 27.4887, -34.9777, 4.8528
50, 50, 50, 50	7.6918, 32.3854, -28.6447, 6.8034
10, 20, 20, 10	19.9761, 8.3321, -17.4301, 41.7884
90, 80, 80, 90	7.5853, 38.6085, -24.4396, 4.8016

The results in Table 6.1 show that different from the conclusions in the literature, the spring connecting point on the base can be away from the vertical line passing through the R joints, and that on the manipulator doesn't have to be on the line defined by the R joint and the CM of the link.

To verify the correctness of the result, one set of a, b, s and h (7.6918, 32.3854, -28.6447, and 6.8034) are substituted into the formula of the total potential energy of the manipulator. When giving different values of θ, the corresponding potential energies are obtained. Several examples are listed in Table 6.2. The plot of the potential energy of the system with respect to θ drawn by MATLAB is given in Fig. 6.20.

When θ varies from 0° to 180°, the values of the potential energy almost keeps constant. The results verify the proposed optimization method is valid and the obtained sets of results can be the spring attachment points of the statically balanced 1-link manipulator.

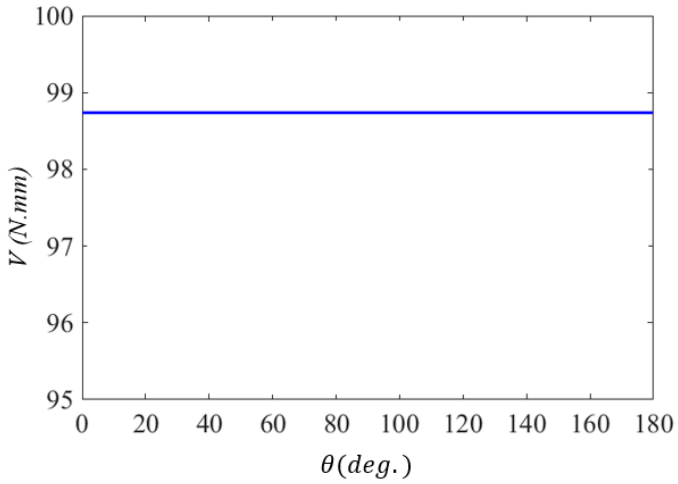

Fig. 6.20 The potential energy of the 1-link manipulator

Table 6.2 The values of the potential energy of the 1-link manipulator

θ	0	π/20	π /10	3π /20	π /5	π /4	3π /10
V	98.7390	98.7390	98.7390	98.7390	98.7390	98.7390	98.7391
θ	7π/20	2π/5	9π/20	π/2	11π/20	3π/5	13π/20
V	98.7390	98.7391	98.7391	98.7391	98.7391	98.7392	98.7392
θ	7π/10	3π/4	4π/5	17π/20	9π/10	19π/20	π
V	98.7392	98.7392	98.7392	98.7393	98.7393	98.7393	98.7393

6.5.2 Static Balancing of Spherical Manipulators

In this section, the proposed optimization method will be applied to spherical manipulators with links whose weights cannot be neglected.

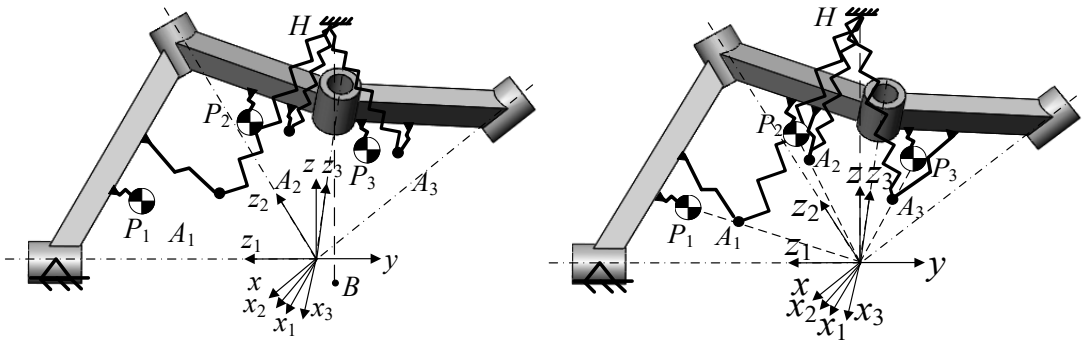

(a) (b)

Fig. 6.21 Static balancing of 3-link spherical manipulators: (a) the 3-link manipulator; (b) the results of the spring attachment points

The 3-link manipulator is shown in Fig. 6.21(a). A coordinate system is fixed to the base with its z-axis pointing vertically upward and with its origin located at the intersection of the axes of the R joints.

Suppose that the position vectors of the CM of the i^{th} link and the spring connecting point on the link in the i^{th} local coordinate frame are represented by

$$^{\boldsymbol{i}}\boldsymbol{P_i} = \{10 \quad 20 \quad 30\}^T \tag{6.89a}$$

$$^{\boldsymbol{i}}\boldsymbol{A_i} = \{a_n \quad b_n \quad c_n\}^T \tag{6.89b}$$

For the sake of conciseness, the joint twist angles of the manipulator are assumed to be equal, which is denoted as α, and $\alpha = 60°$. It is noted that the parameters of the links can be distinct, the manipulator with identical links is just an example to illustrate the optimization method. The position vectors of the CM of the i^{th} link and the spring connecting point on the link in the global coordinate frame are calculated as:

$$\begin{Bmatrix} \boldsymbol{P_1} \\ 1 \end{Bmatrix} = {}_1^0T\begin{Bmatrix} {}^{\boldsymbol{1}}\boldsymbol{P_1} \\ 1 \end{Bmatrix} = \{10C\theta_1 - 20S\theta_1 \quad 30 \quad -10S\theta_1 - 20C\theta_1 \quad 1\}^T \tag{6.90a}$$

$$\begin{Bmatrix} \boldsymbol{P_2} \\ 1 \end{Bmatrix} = {}_1^0T{}_2^1T\begin{Bmatrix} {}^{\boldsymbol{2}}\boldsymbol{P_2} \\ 1 \end{Bmatrix} = \{P_{2x} \quad P_{2y} \quad P_{2z} \quad 1\}^T \tag{6.90b}$$

where

$$P_{2x} = 5[2C\theta_1(C\theta_2 - 2S\theta_2) - S\theta_1(3\sqrt{3} + 2C\theta_2 + S\theta_2)]$$

$$P_{2y} = -5(-3 + 2\sqrt{3}C\theta_2 + \sqrt{3}S\theta_2)$$

$$P_{2z} = -5[2S\theta_1(C\theta_2 - 2S\theta_2) + C\theta_1(3\sqrt{3} + 2C\theta_2 + S\theta_2)]$$

$$\begin{Bmatrix} \boldsymbol{P_3} \\ 1 \end{Bmatrix} = {}_1^0T{}_2^1T{}_3^2T\begin{Bmatrix} {}^{\boldsymbol{3}}\boldsymbol{P_3} \\ 1 \end{Bmatrix} = \{P_{3x} \quad P_{3y} \quad P_{3z} \quad 1\}^T \tag{6.90c}$$

where

$$P_{3x} = -5\{C\theta_1[6\sqrt{3}S\theta_2 - 4C\theta_2(C\theta_3 - 2S\theta_3)] + S\theta_1[3\sqrt{3}(1 + C\theta_2) + (-3 + C\theta_2)(2C\theta_3 + S\theta_3)] + 2S\theta_2[2C(\theta_1 + \theta_3) + S(\theta_1 + \theta_3)]\}/2$$

$$P_{3y} = 5[3 - 9C\theta_2 - 2\sqrt{3}C\theta_3(1 + C\theta_2 + S\theta_2) - \sqrt{3}(1 + C\theta_2 - 4S\theta_2)S\theta_3]/2$$

$$P_{3z} = \{5C\theta_1[-3\sqrt{3}(1 + C\theta_2) - 2C\theta_3(-3 + C\theta_2 + S\theta_2) + (3 - C\theta_2 + 4S\theta_2)S\theta_3] + 10S\theta_1[-2C\theta_2(C\theta_3 - 2S\theta_3) + S\theta_2(3\sqrt{3} + 2C\theta_3 + S\theta_3)]\}/2$$

$$\begin{Bmatrix} \boldsymbol{A_1} \\ 1 \end{Bmatrix} = {}_1^0T\begin{Bmatrix} {}^{\boldsymbol{1}}\boldsymbol{A_1} \\ 1 \end{Bmatrix} = \{a_1C\theta_1 - b_1S\theta_1 \quad c_1 \quad -a_1S\theta_1 - b_1C\theta_1 \quad 1\}^T \tag{6.90d}$$

$$\begin{Bmatrix} \boldsymbol{A_2} \\ 1 \end{Bmatrix} = {}_1^0T{}_2^1T\begin{Bmatrix} {}^{\boldsymbol{2}}\boldsymbol{A_2} \\ 1 \end{Bmatrix} = \{A_{2x} \quad A_{2y} \quad A_{2z} \quad 1\}^T \tag{6.90e}$$

where

$$A_{2x} = -S\theta_1(\sqrt{3}c_2 + b_2C\theta_2 + a_2S\theta_2)/2 + C\theta_1(a_2C\theta_2 - b_2S\theta_2)$$

$$A_{2y} = [c_2 - \sqrt{3}(b_2C\theta_2 + a_2S\theta_2)]/2$$

$$A_{2z} = -C\theta_1(\sqrt{3}c_2 + b_2C\theta_2 + a_2S\theta_2)/2 + S\theta_1(-a_2C\theta_2 + b_2S\theta_2)$$

$$\begin{Bmatrix} \boldsymbol{A_3} \\ 1 \end{Bmatrix} = {}^0_1T\,{}^1_2T\,{}^2_3T\begin{Bmatrix} {}^{\boldsymbol{3}}\boldsymbol{A_3} \\ 1 \end{Bmatrix} = \{A_{3x} \quad A_{3y} \quad A_{3z} \quad 1\}^T \tag{6.90f}$$

where

$$A_{3x} = \{-S\theta_1[\sqrt{3}c_3(1 + C\theta_2) - 3b_3C\theta_3 + b_3C\theta_2C\theta_3 + 2a_3C\theta_3S\theta_2 - 3a_3S\theta_3 + a_3C\theta_2S\theta_3 - 2b_3S\theta_2S\theta_3] + C\theta_1[-2S\theta_2(\sqrt{3}c_3 + b_3C\theta_3 + a_3S\theta_3) + 4C\theta_2(a_3C\theta_3 - b_3S\theta_3)]\}/4$$

$$A_{3y} = -\{c_3 - 3c_3C\theta_2 - \sqrt{3}[C\theta_3(b_3 + b_3C\theta_2 + 2a_3S\theta_2) + (a_3 + a_3C\theta_2 - 2b_3S\theta_2)S\theta_3]\}/4$$

$$A_{3z} = \{4C\theta_2S\theta_1(-a_3C\theta_3 + b_3S\theta_3) - C\theta_1[\sqrt{3}c_3(1 + C\theta_2) + (-3 + C\theta_2)(b_3C\theta_3 + a_3S\theta_3)] + 2S\theta_2[-a_3C(\theta_1 + \theta_3) + \sqrt{3}c_3S\theta_1 + b_3S(\theta_1 + \theta_3)]\}/4$$

Since the links are identical, let

$$\begin{cases} a_1 = a_2 = a_3 = a \\ b_1 = b_2 = b_3 = b \\ c_1 = c_2 = c_3 = c \end{cases} \tag{6.91}$$

The spring connecting point on the base $\boldsymbol{H}$ is given by

$$\boldsymbol{H} = \{s \quad t \quad h\}^T \tag{6.92}$$

The total potential energy of the system is calculated as

$$V = \frac{1}{2}k|\boldsymbol{A_1} - \boldsymbol{H_1}|^2 + \frac{1}{2}k|\boldsymbol{A_2} - \boldsymbol{H_2}|^2 + \frac{1}{2}k|\boldsymbol{A_3} - \boldsymbol{H_3}|^2 + mgP_{1z} + mgP_{2z} + mgP_{3z} = \{k\{6(a^2 + b^2 + c^2 + h^2 + s^2) + 6t^2 + t\{c(-7 + 3C\theta_2) + \sqrt{3}\{2aS\theta_2 + C\theta_3(b + 2aS\theta_2) + (a - 2bS\theta_2)S\theta_3 + C\theta_2[b(2 + C\theta_3) + aS\theta_3]\}\}\} + S\theta_1\{4ahk - 40mg + 4bks + 3\sqrt{3}cks - 3ks(bC\theta_3 + aS\theta_3) + C\theta_2[4ahk - 40mg + 2bks + \sqrt{3}cks + (4ahk - 40mg + bks)C\theta_3 + (-4bhk + 80mg + aks)S\theta_3] - 2S\theta_2\{-10mg(4 + 3\sqrt{3} + 2C\theta_3 + S\theta_3) + k\{-as(1 + C\theta_3) + bsS\theta_3 + h[\sqrt{3}c + b(2 + C\theta_3) + aS\theta_3]\}\}\} + C\theta_1\{-10gm[8 + 9\sqrt{3} - 6C\theta_3 + 2S\theta_2(1 + C\theta_3 - 2S\theta_3) - 3S\theta_3 + C\theta_2(4 + 3\sqrt{3} + 2C\theta_3 + S\theta_3)] + k\{4bh + 3\sqrt{3}ch - 4as - 3h(bC\theta_3 + aS\theta_3) + 2S\theta_2\{s[\sqrt{3}c + b(2 + C\theta_3) + aS\theta_3] + h(a + aC\theta_3 - bS\theta_3)\} + C\theta_2\{h[\sqrt{3}c + b(2 + C\theta_3) + aS\theta_3] - 4s(a + aC\theta_3 - bS\theta_3)\}\}\}\}/4 \tag{6.93}$$

The objective function is a formula of *a*, *b*, *c*, *s*, *t* and *h*.

$$Vs = \sum_{i=1}^{9}(V_{i+1} - V_i)^2 = f(a, b, c, s, t, h) \tag{6.94}$$

When giving different initial values, the optimization results of the parameters are obtained, which are given in Table 6.3. From the results, it can be seen that *s* and *t* are always approximately equal to zero, which means the spring attachment point on the base

should always be right above the intersection of the R joints. Besides, $\{a \quad b \quad c\}^T$ and the position vector of the CM of each link in the local coordinate frame are always proportional, i.e., the spring attachment point on the link is on the line defined by the intersection of the R joints and the CM of the link [Fig. 6.21(b)].

Table 6.3 The optimization results of the 3-link spherical manipulator with three springs

Initial values	Optimization results
30, 30, 30, 30, 30, 30	1.6775, 3.3652, 5.0331, 0.0383, 0.0502, 58.3455
10, 20, 30, 40, 50, 60	2.1011, 4.3442, 6.3128, 0.3315, 0.4289, 45.9785
90, 80, 70, 60, 50, 40	23.2670, 46.8468, 69.8214, 0.0061, 0.0080, 4.2000
50, 40, 30, 30, 40, 50	7.2258, 14.4949, 21.6802, 0.0088, 0.0115, 13.5453

Now statically balanced 3-link manipulator with two springs will be designed. The two springs are attached to links 1 and 3 respectively [Fig. 6.22(a)].

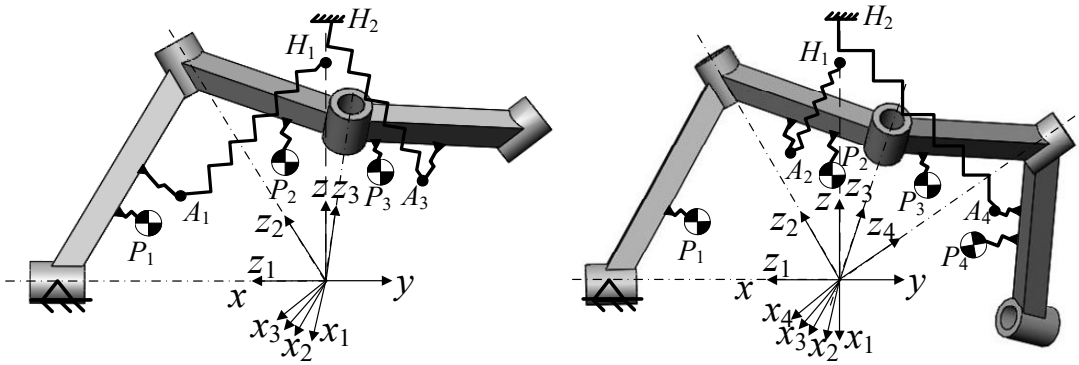

(a) (b)

Fig. 6.22 Static balancing of spherical manipulators with two springs: (a) 3-link manipulator; (b) 4-link manipulator

The spring connecting points on the base H_1 and H_2 are given by

$$\boldsymbol{H_1} = \{0 \quad 0 \quad h_1\}^T \tag{6.95}$$

$$\boldsymbol{H_2} = \{0 \quad 0 \quad h_2\}^T \tag{6.96}$$

The potential energy of the 3-link manipulator with two springs is obtained as:

$$V = \frac{1}{2}k|\boldsymbol{A_1} - \boldsymbol{H_1}|^2 + \frac{1}{2}k|\boldsymbol{A_3} - \boldsymbol{H_2}|^2 + mgP_{1z} + mgP_{2z} + mgP_{3z} = \{2(a_1^2 + a_3^2 +$$

$$b_1^2 + b_3^2 + c_1^2 + c_3^2 + h_1^2 + h_2^2)k + C\theta_1\{k\{4b_1h_1 + \sqrt{3}c_3h_2 + \sqrt{3}c_3h_2C\theta_2 +$$

$$h_2C\theta_3[b_3(-3 + C\theta_2) + 2a_3S\theta_2] + h_2[a_3(-3 + C\theta_2) - 2b_3S\theta_2]S\theta_3\} - 10mg[8 +$$

$$9\sqrt{3} - 6C\theta_3 + 2S\theta_2(1 + C\theta_3 - 2S\theta_3) - 3S\theta_3 + C\theta_2(4 + 3\sqrt{3} + 2C\theta_3 + S\theta_3)]\} -$$

$$2S\theta_1\{10mg[2+2C\theta_2(1+C\theta_3-2S\theta_3)-S\theta_2(4+3\sqrt{3}+2C\theta_3+S\theta_3)]+$$
$$k[-2a_1h_1+h_2S\theta_2(\sqrt{3}c_3+b_3C\theta_3+a_3S\theta_3)+2h_2C\theta_2(-a_3C\theta_3+b_3S\theta_3)]\}\}/4 \quad (6.97)$$

The objective function is in terms of a_1, b_1, a_3, b_3, c_3, h_1 and h_2.

$$Vs=\sum_{i=1}^{9}(V_{i+1}-V_i)^2=f(a_1,b_1,a_3,b_3,c_3,h_1,h_2) \quad (6.98)$$

Table 6.4 The optimization results of the 3-link spherical manipulator with two springs

Initial values	Optimization results
30, 30, 30, 30, 30, 30, 30	0.0024, 8.0239, 0.0045, 24.7639, 65.6994, 43.9671, 7.9186
50, 50, 50, 50, 50, 50, 50	0.0017, 5.7170, 0.0045, 24.9049, 66.0734, 61.7083, 7.8737
10, 20, 30, 40, 30, 20, 10	0.0032, 40.2335, 0.0007, 15.1062, 40.0956, 8.7653, 12.9765
90, 80, 70, 60, 70, 80, 90	0.0013, 19.7935, 0.0012, 28.8591, 76.6015, 17.8165, 6.7924

Table 6.5 The values of the potential energy of the 3-link spherical manipulator with two springs

θ	0, 0, 0	π/8, π/7, π/6	π/3, π/4, π/5
V	349.4992	349.5019	349.5039
θ	π/2, π/2, π/2	π, π, π	π/10, π/5, π/10
V	349.5079	349.4656	349.5024
θ	π/5, 2π/5, π/5	3π/10, 3π/5, 3π/10	2π/5, 4π/5, 2π/5
V	349.5038	349.5077	349.5134
θ	π/2, π, π/2	3π/5, 6π/5, 3π/5	7π/10, 7π/5, 7π/10
V	349.5128	349.5011	349.4846
θ	4π/5, 8π/5, 4π/5	9π/10, 9π/5, 9π/10	π, 2π, π
V	349.4751	349.4754	349.4768

When giving different initial values, seven parameters in Table 6.4 are obtained. The results show that a_1 and a_3 should be zero, namely, the spring attachment point for each link should be on the plane defined by the two R joints of the link. Substituting the first set of parameters (0.0024, 8.0239, 0.0045, 24.7639, 65.6994, 43.9671, and 7.9186) into Eq. (6.97), the potential energies are calculated, as shown in Table 6.5.

Let $\theta_2=2\theta_1$, the surface of potential energies of the system with respect to θ_1 and θ_3 is drawn in Fig. 6.23. Table 6.5 and Figure 6.23 show that the potential energy almost keeps constant and is approximately equal to 349.5 *N.mm*.

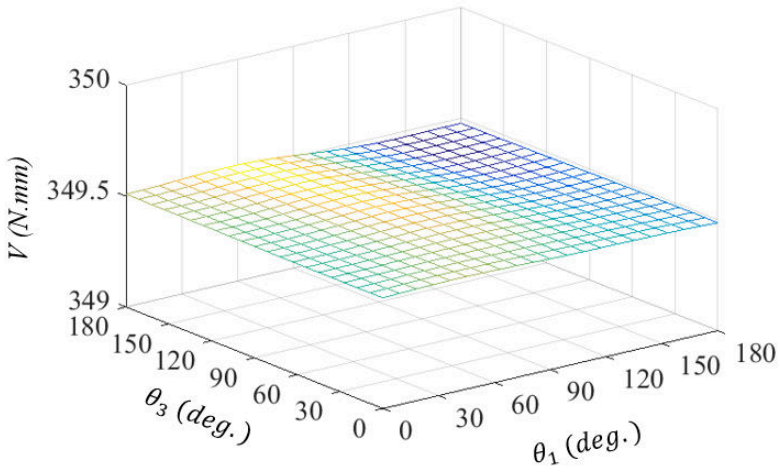

Fig. 6.23 The potential energy of the 3-link spherical manipulator with two springs

Then the statically balanced 4-link manipulator with two springs will be designed using the optimization method. The two springs are attached to links 2 and 4 respectively [Fig. 6.22(b)]. The position vectors of the CM of the 4th link, and the spring connecting point on link 4 and the total potential energy of the system are calculated as

$$\begin{Bmatrix} \boldsymbol{P_4} \\ 1 \end{Bmatrix} = {}^0_1T\,{}^1_2T\,{}^2_3T\,{}^3_4T\begin{Bmatrix} {}^{\boldsymbol{4}}\boldsymbol{P_4} \\ 1 \end{Bmatrix} = \{P_{4x} \quad P_{4y} \quad P_{4z} \quad 1\}^T \tag{6.99a}$$

where

$$P_{4x} = \{5S\theta_1\{-6\sqrt{3}[1 - 3C\theta_3 + C\theta_2(1 + C\theta_3) - 2S\theta_2S\theta_3] + 4C\theta_4[3 + C\theta_3(3 - 2S\theta_2) + (3 + 2S\theta_2)S\theta_3 - C\theta_2(-3 + C\theta_3 + S\theta_3)] + [6(1 + C\theta_2) - 2C\theta_3(-3 + C\theta_2 - 8S\theta_2) + 4(-6 + 2C\theta_2 + S\theta_2)S\theta_3]S\theta_4\}/2 - 10C\theta_1\{S\theta_2[\sqrt{3}(1 + C\theta_3) + 2C\theta_4(-3 + C\theta_3 + S\theta_3) + (-3 + C\theta_3 - 4S\theta_3)S\theta_4] + C\theta_2[-4C\theta_3(C\theta_4 - 2S\theta_4) + 2S\theta_3(3\sqrt{3} + 2C\theta_4 + S\theta_4)]\}\}/4$$

$$P_{4y} = 5\{(-1 + 3C\theta_2)(-3 + 2\sqrt{3}C\theta_4 + \sqrt{3}S\theta_4) + C\theta_3[-9(1 + C\theta_2) - 2\sqrt{3}C\theta_4(1 + C\theta_2 + 2S\theta_2) - \sqrt{3}(1 + C\theta_2 - 8S\theta_2)S\theta_4] + 2S\theta_3\{9S\theta_2 - \sqrt{3}\{C\theta_4 + C(\theta_2 + \theta_4) - 2[S\theta_4 + S(\theta_2 + \theta_4)]\}\}\}/4$$

$$P_{4z} = \{5C\theta_1\{-6\sqrt{3}[1 - 3C\theta_3 + C\theta_2(1 + C\theta_3) - 2S\theta_2S\theta_3] + 4C\theta_4[2S\theta_2(-C\theta_3 + S\theta_3) - C\theta_2(-3 + C\theta_3 + S\theta_3) + 3(1 + C\theta_3 + S\theta_3)] + [6(1 + C\theta_2) - 2C\theta_3(-3 + C\theta_2 - 8S\theta_2) + 4(-6 + 2C\theta_2 + S\theta_2)S\theta_3]S\theta_4\}/2 - 10S\theta_1\{S\theta_2[-3\sqrt{3}(1 + C\theta_3) - 2C\theta_4(-3 + C\theta_3 + S\theta_3) + (3 - C\theta_3 + 4S\theta_3)S\theta_4] + C\theta_2[4C\theta_3(C\theta_4 - 2S\theta_4) - 2S\theta_3(3\sqrt{3} + 2C\theta_4 + S\theta_4)]\}\}/4$$

$$\begin{Bmatrix} \boldsymbol{A_4} \\ 1 \end{Bmatrix} = {}^0_1T\,{}^1_2T\,{}^2_3T\,{}^3_4T\begin{Bmatrix} {}^{\boldsymbol{4}}\boldsymbol{A_4} \\ 1 \end{Bmatrix} = \{A_{4x} \quad A_{4y} \quad A_{4z} \quad 1\}^T \tag{6.99b}$$

where

$$A_{4x} = \{S\theta_1\{-2\sqrt{3}c_4[1 - 3C\theta_3 + C\theta_2(1 + C\theta_3) - 2S\theta_2 S\theta_3] + 2C\theta_4\{3b_4(1 + C\theta_2) - C\theta_3[b_4(-3 + C\theta_2) + 4a_4 S\theta_2] + 2(3a_4 - a_4 C\theta_2 + b_4 S\theta_2)S\theta_3\} + \{6a_4 + 6a_4 C\theta_2 + 2C\theta_3(3a_4 - a_4 C\theta_2 + 4b_4 S\theta_2) + 4[b_4(-3 + C\theta_2) + a_4 S\theta_2]S\theta_3\}S\theta_4\}/2 + C\theta_1\{-2S\theta_2[\sqrt{3}c_4(1 + C\theta_3) + (-3 + C\theta_3)(b_4 C\theta_4 + a_4 S\theta_4)] - 4C\theta_2[\sqrt{3}c_4 S\theta_3 + C\theta_3(-2a_4 C\theta_4 + 2b_4 S\theta_4)] - 4S\theta_3[b_4 C(\theta_2 + \theta_4) + a_4 S(\theta_2 + \theta_4)]\}\}/8$$

$$A_{4y} = \{c_4[2 - 6(1 + C\theta_2)C\theta_3 + 12S\theta_2 S\theta_3] - 2\sqrt{3}C\theta_4[b_4 + C\theta_3(b_4 + b_4 C\theta_2 + 4a_4 S\theta_2) + 2(a_4 + a_4 C\theta_2 - b_4 S\theta_2)S\theta_3] + \sqrt{3}\{-2a_4[1 + (1 + C\theta_2)C\theta_3] + 8b_4 C\theta_3 S\theta_2 + 4(b_4 + b_4 C\theta_2 + a_4 S\theta_2)S\theta_3\}S\theta_4 + 6C\theta_2[-c_4 + \sqrt{3}(b_4 C\theta_4 + a_4 S\theta_4)]\}/16$$

$$A_{4z} = \{[C(\theta_1 - \theta_2/2) - 3C(\theta_1 + \theta_2/2)]C(\theta_2/2)(\sqrt{3}c_4 - 3b_4 C\theta_4 - 3a_4 S\theta_4) + C\theta_3\{C\theta_1(-\sqrt{3}c_4(-3 + C\theta_2) - C\theta_4[b_4(-3 + C\theta_2) + 4a_4 S\theta_2] + (3a_4 - a_4 C\theta_2 + 4b_4 S\theta_2)S\theta_4\} + 2S\theta_1[S\theta_2(\sqrt{3}c4 + b_4 C\theta_4 + a_4 S\theta_4) + C\theta_2(-4a_4 C\theta_4 + 4b_4 S\theta_4)]) + S\theta_3\{a_4[3C(\theta_1 - \theta_4) + C(\theta_1 - \theta_2 - \theta_4) + 3C(\theta_1 + \theta_4) - 3C(\theta_1 + \theta_2 + \theta_4)] + 2\sqrt{3}c_4(2C\theta_2 S\theta_1 + C\theta_1 S\theta_2) + b_4[3S(\theta_1 - \theta_4) + S(\theta_1 - \theta_2 - \theta_4) - 3S(\theta_1 + \theta_4) + 3S(\theta_1 + \theta_2 + \theta_4)]\}\}/8$$

${}^{i-1}_{i}T$ are given in Appendix (C). The total potential energy of the 4-link manipulator with two springs are yielded as:

$$V = \frac{1}{2}k|\boldsymbol{A_2} - \boldsymbol{H_1}|^2 + \frac{1}{2}k|\boldsymbol{A_4} - \boldsymbol{H_2}|^2 + mgP_{1z} + mgP_{2z} + mgP_{3z} + mgP_{4z} = \{4(a_2^2 + a_4^2 + b_2^2 + b_4^2 + c_2^2 + c_4^2 + h_1^2 + h_2^2)k + C\theta_1\{\sqrt{3}(c_4 h_1 + 4c_2 h_2)k - 10(16 + 21\sqrt{3})gm - 3b_4 h_1 k C\theta_4 + 60gmC\theta_4 + 4a_2 h_2 k S\theta_2 - 40gmS\theta_2 - 3a_4 h_1 k S\theta_4 + 30gmS\theta_4 + C\theta_3\{-3\sqrt{3}c_4 h_1 k + 30(4 + 3\sqrt{3})gm - 40gmS\theta_2 + C\theta_4[-3b_4 h_1 k + 60gm + 4(a_4 h_1 k - 10gm)S\theta_2] + [-3a_4 h_1 k + 30gm + (-4b_4 h_1 k + 80gm)S\theta_2]S\theta_4\} + C\theta_2\{\sqrt{3}c_4 h_1 k + 4b_2 h_2 k - 10(8 + 9\sqrt{3})gm + \sqrt{3}c_4 h_1 k C\theta_3 - 40gmC\theta_3 - 30\sqrt{3}gmC\theta_3 - 20gmS\theta_3 + C\theta_4[(b_4 h_1 k - 20gm)(-3 + C\theta_3) + 2(a_4 h_1 k - 10gm)S\theta_3] + [(a_4 h_1 k - 10gm)(-3 + C\theta_3) - 2(b_4 h_1 k - 20gm)S\theta_3]S\theta_4\} + 2S\theta_3\{C\theta_4(-3a_4 h_1 k + 30gm - b_4 h_1 k S\theta_2 + 20gmS\theta_2) - h_1 k(\sqrt{3}c_4 S\theta_2 - 3b_4 S\theta_4 + a_4 S\theta_2 S\theta_4) + 10gm[3 - 6S\theta_4 + S\theta_2(4 + 3\sqrt{3} + S\theta_4)]\}\} - 2S\theta_1\{10gm\{4 + 4C\theta_2[1 + C\theta_3(1 + C\theta_4 - 2S\theta_4)] - 2C\theta_2 S\theta_3(4 + 3\sqrt{3} + 2C\theta_4 + S\theta_4) + S\theta_2[-8 - 9\sqrt{3} + 6C\theta_4 - 2S\theta_3(1 + C\theta_4 - 2S\theta_4) + 3S\theta_4 - C\theta_3(4 + 3\sqrt{3} + 2C\theta_4 + S\theta_4)]\} + k\{S\theta_2\{\sqrt{3}c_4 h_1 + 4b_2 h_2 + \sqrt{3}c_4 h_1 C\theta_3 + h_1 C\theta_4[b_4(-3 + C\theta_3) + 2a_4 S\theta_3] + h_1[a_4(-3 + C\theta_3) - 2b_4 S\theta_3]S\theta_4\} + 2C\theta_2[-2a_2 h_2 + h_1 S\theta_3(\sqrt{3}c_4 + b_4 C\theta_4 + a_4 S\theta_4) + 2h_1 C\theta_3(-a_4 C\theta_4 + b_4 S\theta_4)]\}\}/8$$

(6.100)

The objective function is in terms of a_2, b_2, c_2, a_4, b_4, c_4, h_1 and h_2.

$$Vs = \sum_{i=1}^{9}(V_{i+1} - V_i)^2 = f(a_2, b_2, c_2, a_4, b_4, c_4, h_1, h_2) \quad (6.101)$$

Table 6.6 The optimization results of the 4-link spherical manipulator with two springs

Initial values	Optimization results
30, 30, 30, 30, 30, 30, 30, 30	0.0036, 17.1379, 29.6707, 0.0010, 11.4028, 30.2685, 20.5805, 17.1901
10, 10, 10, 10, 10, 10, 10, 10	0.0015, 6.8826, 11.9157, 0.0006, 7.0988, 18.8437, 51.2464, 27.6121
10, 20, 30, 40, 40, 30, 20, 10	0.0025, 11.9307, 20.6555, 0.0021, 24.9150, 66.1365, 29.5629, 7.8673
10, 20, 30, 40, 40, 30, 20, 10	0.0013, 24.3884, 42.2374, 0.0001, 4.7615, 12.6402, 14.4591, 41.1640

The parameters when giving different initial values are listed in Table 6.6. Similar to the 3-link manipulator with two springs, a_2 and a_4 should be zero, namely, the spring attachment point for each link should be on the plane defined by the two R joints of the link. The potential energy yielded using the first set of obtained parameters (0.0036, 17.1379, 29.6707, 0.0010, 11.4028, 30.2685, 20.5805, and 17.1901) are given in Table 6.7. Let $\theta_2 = 2\theta_1$ and $\theta_4 = 2\theta_3$, the total potential energy of the manipulator associated with θ_1 and θ_3 is depicted in Fig. 6.24. Table 6.7 and Figure 6.24 show that the potential energy almost keeps constant and is approximately equal to 146.9 *N.mm*.

Table 6.7 The values of the potential energy of the 4-link spherical manipulator with two springs

θ	0, 0, 0, 0	π/9, π/8, π/7, π/6	π/3, π/4, π/5, π/6
V	146.9603	146.9624	146.9630
θ	π/2, π/2, π/2, π/2	π, π, π, π	π/10, π/5, π/10, π/5
V	146.9587	146.9807	146.9617
θ	π/5, 2π/5, π/5, 2π/5	3π/10, 3π/5, 3π/10, 3π/5	2π/5, 4π/5, 2π/5, 4π/5
V	146.9581	146.9546	146.9533
θ	π/2, π, π/2, π	3π/5, 6π/5, 3π/5, 6π/5	7π/10, 7π/5, 7π/10, 7π/5
V	146.9576	146.9701	146.9818
θ	4π/5, 8π/5, 4π/5, 8π/5	9π/10, 9π/5, 9π/10, 9π/5	π, 2π, π, 2π
V	146.9825	146.9761	146.9712

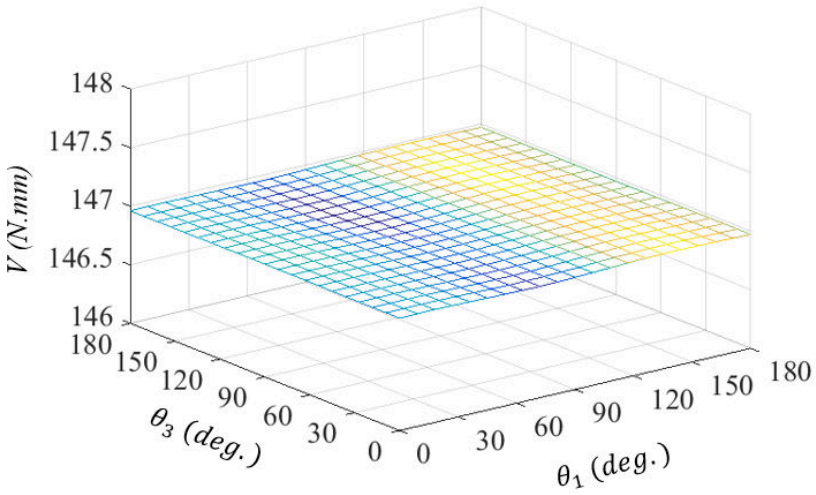

Fig. 6.24 The potential energy of the 4-link spherical manipulator with two springs

6.5.3 Static Balancing of Spatial Manipulators

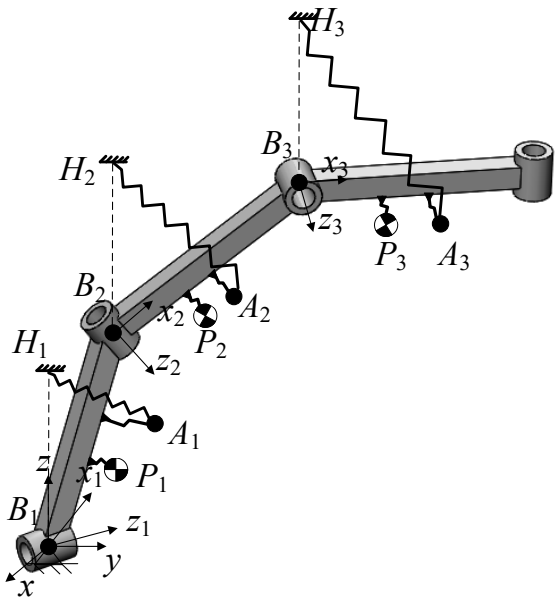

Fig. 6.25 Static balancing of 3-link spatial manipulators with three springs

Now statically balanced spatial manipulators will be designed using the proposed optimization method. A global coordinate is attached to the ground, with the z-axis pointing in the direction opposite to the gravitational acceleration vector. Let θ_1, θ_2, and θ_3 be the joint variables associated with the three revolute joints respectively and the link lengths are represented as l. It is obtained above that the i^{th} link of the n-link manipulator, in which the masses of the links cannot be neglected, can be balanced using i springs. In this section, each link will be balanced using only one spring. One end of each spring is

attached to H_i, which is a point right above R_i, and the other end is attached to A_i, as shown in Fig. 6.25.

Suppose the position vectors of the CM, the spring attachment point of the i^{th} link, and R_i in the i^{th} local coordinate frame are represented by

$$^{i}\boldsymbol{P_i} = \{10 \quad 20 \quad 30\}^T \tag{6.102a}$$

$$^{i}\boldsymbol{A_i} = \{a_n \quad b_n \quad c_n\}^T \tag{6.102b}$$

$$^{i}\boldsymbol{B_i} = \{0 \quad 0 \quad 0\}^T \tag{6.102c}$$

It is noted that the parameters of the links can be distinct, the manipulator with identical links is just an example to illustrate the optimization method. The spring connecting point on the base H_i, which is a point right above the B_i, is given by

$$\boldsymbol{H_i} = \{\boldsymbol{B_{ix}} \quad \boldsymbol{B_{iy}} \quad h + \boldsymbol{B_{iz}}\}^T \tag{6.103}$$

The heights of H_i are all set to be h to facilitate the design of the system. One can also give different values of h_i. Let

$$l_0 = 0, l_1 = l_2 = l \tag{6.104a}$$

$$\alpha_0 = 30^o, \alpha_1 = 60^o, \alpha_2 = 90^o \tag{6.104b}$$

$$d_1 = \ d_2 = d_3 = 0 \tag{6.104c}$$

The position vectors of the CMs of the links (P_i), the spring attachment points on the links and the R joints (B_i) expressed in the global coordinate frame are obtained as

$$\begin{Bmatrix} \boldsymbol{P_1} \\ 1 \end{Bmatrix} = {}_1^0T \begin{Bmatrix} {}^{1}\boldsymbol{P_1} \\ 1 \end{Bmatrix}$$

$$= \left\{10C\theta_1 - 20S\theta_1 \quad 10\sqrt{3}C\theta_1 - 15 + 5\sqrt{3}a_1S\theta_1 \quad 15\sqrt{3} + 10C\theta_1 + 5S\theta_1 \quad 1\right\}^T \tag{6.105a}$$

$$\begin{Bmatrix} \boldsymbol{P_2} \\ 1 \end{Bmatrix} = {}_1^0T\,{}_2^1T \begin{Bmatrix} {}^{2}\boldsymbol{P_2} \\ 1 \end{Bmatrix} = \{A_{2x} \quad A_{2y} \quad A_{2z} \quad 1\}^T \tag{6.105b}$$

where

$$P_{2x} = C\theta_1(l + 10C\theta_2 - 20S\theta_2) + 5S\theta_1(3\sqrt{3} - 2C\theta_2 - S\theta_2)$$

$$P_{2y} = [-15 - 45C\theta_1 + \sqrt{3}lS\theta_1 + 10\sqrt{3}C\theta_2(-1 + C\theta_1 + S\theta_1) + 5\sqrt{3}(-1 + C\theta_1 - 4S\theta_1)S\theta_2]/2$$

$$P_{2z} = [10C\theta_2(3 + S\theta_1) + S\theta_1(l - 20S\theta_2) + 15(\sqrt{3} + S\theta_2) + 5C\theta_1(-3\sqrt{3} + 2C\theta_2 + S\theta_2)]/2$$

$$\begin{Bmatrix} \boldsymbol{P_3} \\ 1 \end{Bmatrix} = {}_1^0T\,{}_2^1T \begin{Bmatrix} {}^{2}\boldsymbol{P_3} \\ 1 \end{Bmatrix} = \{A_{3x} \quad A_{3y} \quad A_{3z} \quad 1\}^T \tag{6.105c}$$

where

$$P_{2x} = C\theta_1[l + 30S\theta_2 + C\theta_2(l + 10C\theta_3 - 20S\theta_3)] + S\theta_1[30C\theta_2 - S\theta_2(l + 10C\theta_3 - 20S\theta_3) + 10\sqrt{3}(2C\theta_3 + S\theta_3)]/2$$

$$P_{2y} = \{2\sqrt{3}lS\theta_1 + \sqrt{3}l(-1 + C\theta_1)S\theta_2 + 2\sqrt{3}C\theta_2[15 - 15C\theta_1 + S\theta_1(l + 10C\theta_3 - 20S\theta_3)] - 10(2C\theta_3 + S\theta_3) - 30C\theta_1(2C\theta_3 + S\theta_3) + 10\sqrt{3}S\theta_2[(-1 + C\theta_1)C\theta_3 + 6S\theta_1 - 2(-1 + C\theta_1)S\theta_3]\}/4$$

$$P_{2z} = \{2lS\theta_1 + C\theta_2[-90 - 30C\theta_1 + 2S\theta_1(l + 10C\theta_3 - 20S\theta_3)] - 10\sqrt{3}(-1 + C\theta_1)(2C\theta_3 + S\theta_3) + S\theta_2[3l + lC\theta_1 + 10(3 + C\theta_1)C\theta_3 + 60S\theta_1 - 20(3 + C\theta_1)S\theta_3]\}/4$$

$$\{\begin{matrix}\boldsymbol{A_1}\\1\end{matrix}\} = {}^0_1T\{\begin{matrix}\boldsymbol{^1A_1}\\1\end{matrix}\}$$

$$= \{a_1C\theta_1 - b_1S\theta_1 \quad (\sqrt{3}b_1C\theta_1)/2 - c_1/2 + (\sqrt{3}a_1S\theta_1)/2 \quad A_{1z} \quad 1\} \tag{6.104d}$$

where

$$A_{1z} = (\sqrt{3}c_1)/2 + (b_1C\theta_1)/2 + (a_1S\theta_1)/2$$

$$\{\begin{matrix}\boldsymbol{A_2}\\1\end{matrix}\} = {}^0_1T\,{}^1_2T\{\begin{matrix}\boldsymbol{^2A_2}\\1\end{matrix}\} = \{A_{2x} \quad A_{2y} \quad A_{2z} \quad 1\}^T \tag{6.105e}$$

where

$$A_{2x} = lC\theta_1 + a_2(C\theta_1C\theta_2 - S\theta_1S\theta_2/2) - b_2(C\theta_1S\theta_2 + C\theta_2S\theta_1/2) + (\sqrt{3}c_2S\theta_1)/2$$

$$A_{2y} = \{-c_2 + C\theta_1[-3c_2 + \sqrt{3}(b_2C\theta_2 + a_2S\theta_2)] - \sqrt{3}[b_2C\theta_2 + a_2S\theta_2 - 2S\theta_1(l + a_2C\theta_2 - b_2S\theta_2)]\}/4$$

$$A_{2z} = [-\sqrt{3}c_2(-1 + C\theta_1) + 3b_2C\theta_2 + b_2C\theta_1C\theta_2 + 2lS\theta_1 + 2a_2C\theta_2S\theta_1 + 3a_2S\theta_2 + a_2C\theta_1S\theta_2 - 2b_2S\theta_1S\theta_2]/4$$

$$\{\begin{matrix}\boldsymbol{A_3}\\1\end{matrix}\} = {}^0_1T\,{}^1_2T\,{}^2_3T\{\begin{matrix}\boldsymbol{^3A_3}\\1\end{matrix}\} = \{A_{3x} \quad A_{3y} \quad A_{3z} \quad 1\}^T \tag{6.105f}$$

where

$$A_{3x} = \{2C\theta_1[l + c_3S\theta_2 + C\theta_2(l + a_3C\theta_3 - b_3S\theta_3)] + S\theta_1[c_3C\theta_2 + \sqrt{3}(b_3C\theta_3 + a_3S\theta_3) - S\theta_2(l + a_3C\theta_3 - b_3S\theta_3)]\}/2$$

$$A_{3y} = \{2\sqrt{3}c_3S\theta_1S\theta_2 + \sqrt{3}l[2S\theta_1 + (-1 + C\theta_1)S\theta_2] - C\theta_3[b_3 + 3b_3C\theta_1 + 2\sqrt{3}a_3S^2(\theta_1/2)S\theta_2] - a_3S\theta_3 - 3a_3C\theta_1S\theta_3 + \sqrt{3}b_3S\theta_2S\theta_3 - \sqrt{3}b_3C\theta_1S\theta_2S\theta_3 + \sqrt{3}C\theta_2[c_3 - c_3C\theta_1 + 2S\theta_1(l + a_3C\theta_3 - b_3S\theta_3)]\}/4$$

$$A_{3z} = \{l(2S\theta_1 + 3S\theta_2) - \sqrt{3}(-1 + C\theta_1)(b_3C\theta_3 + a_3S\theta_3) + S\theta_2[lC\theta_1 + a_3(3 + C\theta_1)C\theta_3 + 2c_3S\theta_1 - b_3(3 + C\theta_1)S\theta_3] - C\theta_2[3c_3 + c_3C\theta_1 - 2S\theta_1(l + a_3C\theta_3 - b_3S\theta_3)]\}/4$$

$$\{\begin{matrix}\boldsymbol{B_1}\\1\end{matrix}\} = {}^0_1T\{\begin{matrix}\boldsymbol{^1B_1}\\1\end{matrix}\} = \{0 \quad 0 \quad 0 \quad 1\}^T \tag{6.105g}$$

$$\{\begin{matrix}\boldsymbol{B_2}\\1\end{matrix}\} = {}^0_1T\,{}^1_2T\{\begin{matrix}\boldsymbol{^2B_2}\\1\end{matrix}\} = \{lC\theta_1 \quad \sqrt{3}lS\theta_1/2 \quad lS\theta_1/2 \quad 1\}^T \tag{6.105h}$$

$$\{\begin{matrix}\boldsymbol{B_3}\\1\end{matrix}\} = {}^0_1T\,{}^1_2T\,{}^2_3T\{\begin{matrix}\boldsymbol{^3B_3}\\1\end{matrix}\} = \{B_{3x} \quad B_{3y} \quad B_{3z} \quad 1\}^T \tag{6.105i}$$

where

$$B_{3x} = lC\theta_1 + l(C\theta_1 C\theta_2 - S\theta_1 S\theta_2/2)$$

$$B_{3y} = l(\sqrt{3}C\theta_1 S\theta_2/4 - \sqrt{3}S\theta_2/4 + \sqrt{3}C\theta_2 S\theta_1/2) + \sqrt{3}lS\theta_1/2$$

$$B_{3z} = l(3S\theta_2/4 + C\theta_1 S\theta_2/4 + C\theta_2 S\theta_1/2) + lS\theta_1/2$$

${}^{i-1}_{i}T$ are provided in Appendix (D). The total potential energy of the system is yielded as

$$V = V_s + V_m = \frac{1}{2}k|\boldsymbol{A_1} - \boldsymbol{H_1}|^2 + \frac{1}{2}k|\boldsymbol{A_2} - \boldsymbol{H_2}|^2 + \frac{1}{2}k|\boldsymbol{A_3} - \boldsymbol{H_3}|^2 + mgP_{1z} + mgP_{2z} + mgP_{3z} = \{mg\{4(5+l)S\theta_1 + 2C\theta_2[-15 + S\theta_1(10 + l + 10C\theta_3 - 20S\theta_3)] + S\theta_2(30 + 3l + 30C\theta_3 + 20S\theta_1 - 60S\theta_3) + 10\sqrt{3}(9 + 2C\theta_3 + S\theta_3)\} + C\theta_1\{gm[-10C\theta_2 + S\theta_2(10 + l + 10C\theta_3 - 20S\theta_3) - 10(-4 + 3\sqrt{3} + 2\sqrt{3}C\theta_3 + \sqrt{3}S\theta_3)] + hk[-2b_1 + (-b_2 + c_3)C\theta_2 + C\theta_3(\sqrt{3}b_3 - a_3S\theta_2) + \sqrt{3}(c_2 + a_3S\theta_3) + S\theta_2(-a_2 + b_3S\theta_3)]\} + k\{2{a_1}^2 + 2{a_2}^2 + 2{a_3}^2 + 2{b_1}^2 + 2{b_2}^2 + 2{b_3}^2 + 2{c_1}^2 + 2{c_2}^2 + 2{c_3}^2 - 2\sqrt{3}c_1h - \sqrt{3}c_2h + 6h^2 + h\{-2a_1S\theta_1 - \sqrt{3}(b_3C\theta_3 + a_3S\theta_3) + S\theta_2[-3a_2 - 3a_3C\theta_3 + 2(b_2 - c_3)S\theta_1 + 3b_3S\theta_3] + C\theta_2[-3b_2 + 3c_3 - 2S\theta_1(a_2 + a_3C\theta_3 - b_3S\theta_3)]\}\}\}/4 \tag{6.106}$$

The objective function is in terms of a_1, b_1, c_1, a_2, b_2, c_2, a_3, b_3, c_3 and h.

$$Vs = \sum_{i=1}^{9}(V_{i+1} - V_i)^2 = f(a_1, b_1, c_1, a_2, b_2, c_2, a_3, b_3, c_3, h) \tag{6.107}$$

Table 6.8 The optimization results of the 3-link spatial manipulator

Initial values	Optimization results
30, 30, 30, 30, 30, 30, 30, 30, 30, 30	76.5880, 34.6767, 45.3864, 40.1175, 27.9223, 42.5598, 3.6471, 7.2941, 31.5694, 26.8711
50, 50, 50, 50, 50, 50, 50, 50, 50, 50	78.0471, 44.9043, 50.0000, 40.8819, 48.1032, 54.4176, 3.7165, 7.4331, 51.8198, 26.3687
10, 20, 30, 10, 20, 30, 10, 20, 30, 10	82.3028, 22.5867, 30.3838, 43.1109, 23.6953, 28.7874, 3.9192, 7.8384, 27.6145, 25.0052
10, 20, 30, 40, 50, 50, 40, 30, 20, 10	76.2961, 40.0464, 41.6901, 39.9646, 41.7102, 48.7505, 3.6332, 7.2663, 45.3433, 26.9739

When giving different initial values, ten parameters in Table 6.8 are obtained. Substituting the first set of parameters (76.5880, 34.6767, 45.3864, 40.1175, 27.9223, 42.5598, 3.6471, 7.2941, 31.5694, and 26.8711) into Eq. (6.106), the potential energy is calculated, as shown in Table 6.9. Let $\theta_2 = 2\theta_1$, the plot of the potential energy of the system with respect to θ_1 and θ_3 is given in Fig. 6.26. The obtained potential energy in

Table 6.9 and Figure 6.26 show that the potential energy varies in a small range, which can be neglected.

Table 6.9 The values of the potential energy of the 3-link spatial manipulator

θ	π, π, π	π /2, π /2, π /2	π /3, π /4, π /5
V	710.9435	710.9431	710.9431
θ	π /9, π /8, π /7	0, 0, 0	π/10, π/5, π/10
V	710.9434	710.9436	710.9433
θ	π/5, 2π/5, π/5	3π/10, 3π/5, 3π/10	2π/5, 4π/5, 2π/5
V	710.9431	710.9431	710.9431
θ	π/2, π, π/2	3π/5, 6π/5, 3π/5	7π/10, 7π/5, 7π/10
V	710.9432	710.9433	710.9434
θ	4π/5, 8π/5, 4π/5	9π/10, 9π/5, 9π/10	π, 2π, π
V	710.9435	710.9436	710.9437

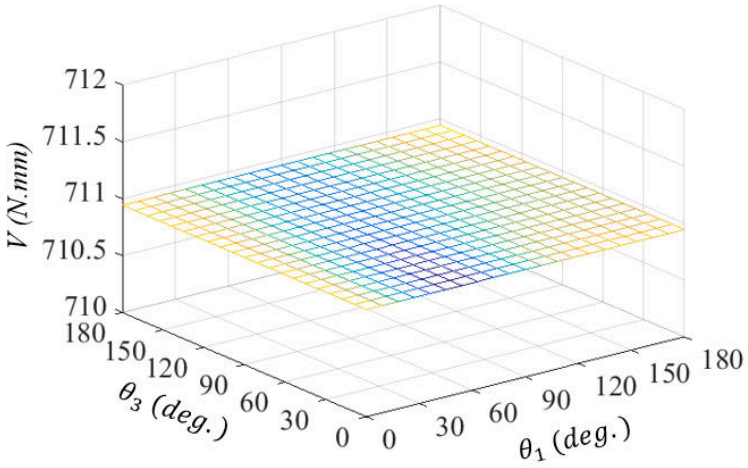

Fig. 6.26 The potential energy of the 3-link spatial manipulator

6.6 Statically Balanced Deployable Mechanisms with Multiple Modes

In this section, deployable mechanisms with multiple modes will be balanced based on the static balancing methods proposed in the previous sections. These mechanisms will be statically balanced using springs with and without auxiliary links.

6.6.1 Static Balancing of Single-loop 8R Linkages

First, statically balanced deployable 8R linkages will be addressed.

a) Statically Balanced 8R Linkage using only springs.

The static balancing method of spatial manipulators in Section 6.4 will be adopted to balance the 8R linkage. Link 8 is fixed on the ground, and R_8 is perpendicular to the ground plane. Hence, link 7 always moves on the ground, and has no need to balance (Fig. 6.27). The linkage is then equal to two manipulators, including the one composed of links 1, 2 and 3, and the one with links 6, 5 and 4. Each manipulator can be balanced using the proposed static balancing method of spatial manipulators in Section 6.4. Suppose that H_1, H_2, H_3, H_4, H_5 and H_6 are points right above joint R_1, R_2, R_3, R_5, R_6 and R_7 respectively. All the links are assumed to be the same, with the mass of m, and the heights of the spring connecting points on the base are $h = mg/k$. It is noted that R_7, the first R joint of the second manipulator moves on the ground, which has no influence on the balancing condition of the system, since the height of the CM of the manipulator is constant during the translational motion on the plane perpendicular to the direction of gravity. Link 1 is balanced by connecting H_1 and P_1 using one spring; link 2 is balanced by connecting H_2 and P_2, and H_1 and R_2; Link 3 is statically balanced by connecting H_3 and P_3, H_1 and R_2, H_2 and R_3. Similarly, link 4 can be balanced using three springs, link 5 is balanced using two springs and link 6 is balanced using one spring. The resulting 8R linkage with multiple modes is fully compensated for gravity in any modes.

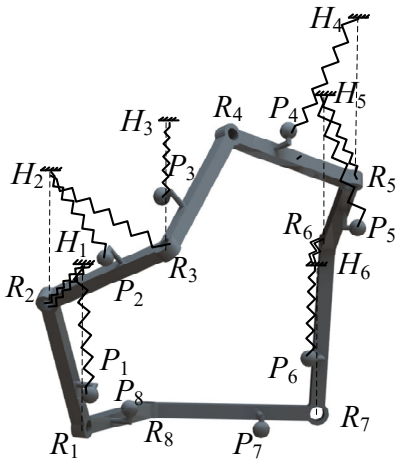

Fig. 6.27 Statically balanced 8R linkage with multiple modes

b) Statically Balanced 8R Linkage using Auxiliary Links

Now the static balancing method using auxiliary parallelograms will be designed. Special auxiliary parallelograms are adopted to identify the CM of the spatial manipulator, and then the CM is mounted on an S joint. The method is similar to the principal vectors proposed by Fischer [125] but is easier to achieve. Since the CMs of the manipulators are

fixed, the mechanisms are statically balanced. A two-link manipulator is shown in Fig. 6.28(a), in which the R joints of the auxiliary parallelogram are parallel with the second R joint of the manipulator. The method applies to manipulators with arbitrary links, as long as the links and the identical auxiliary links that are used as counterweights are arranged symmetrically about the centre of the parallelogram. The two additional links in the middle are used to define the CM of the augmented manipulator.

In the 3-link manipulator [Fig. 6.28(b)], the CM of the first two links are identified using the method above. Then an additional auxiliary parallelogram is used to connect the CM of the two-link manipulator and the CM of the third link using two S joints. Suppose the weight of the two-link manipulator is n times of the weight of the third link, the position of the intersection of the two links in the middle to define the CM is set at n out of (n+1) point.

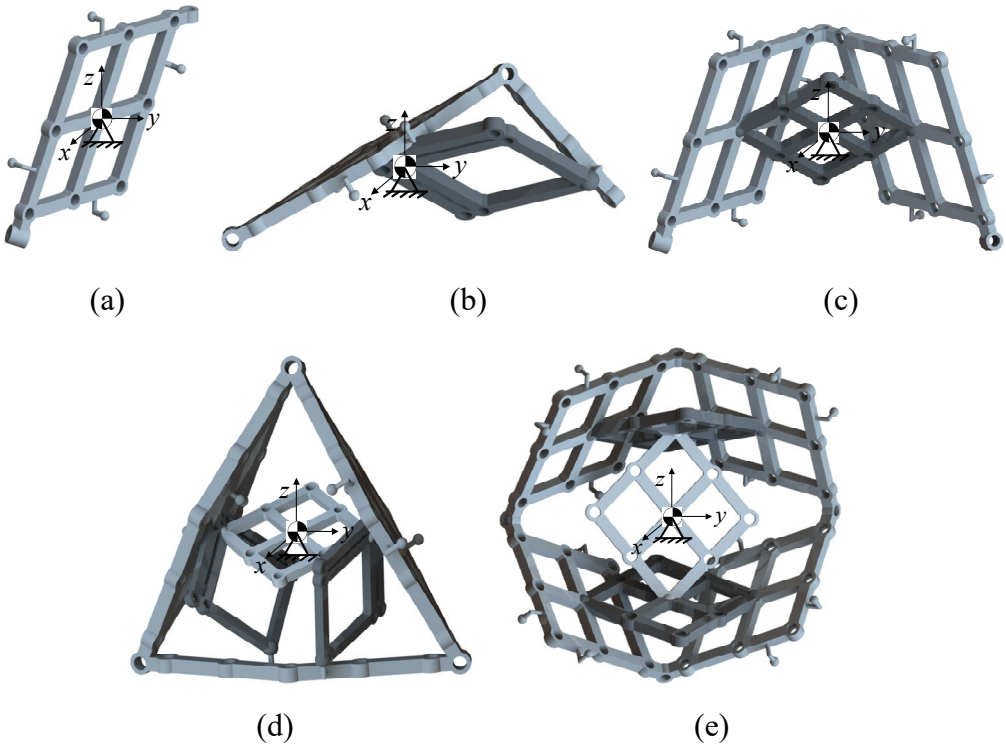

Fig. 6.28 Statically balanced manipulators using auxiliary parallelograms: (a) 2-link manipulator; (b) 3-link manipulator; (b) 4-link manipulator; (e) Bricard linkage; (f) 8R linkage

Based on the 2-link manipulator and the 3-link manipulator modular, countless statically balanced mechanisms can be constructed. For instance, when connecting two 2-link manipulators, and adding an additional parallelogram to connect the two CMs of the two 2-link manipulators, a statically balanced 4-DOF manipulator is then obtained

[Fig. 6.28(c)]. When adopting the additional parallelogram to connect two balanced 3-link manipulators, a statically balanced Bricard linkage is constructed [Fig. 6.28(d)]. Similarly, a statically balanced 8R linkage is designed, as shown in Fig. 6.28(e). It is noted the mechanisms using the auxiliary parallelogram may have the limited range of motions due to the interference of the parallelograms.

c) Statically Balanced 8R Linkage Using Springs and Auxiliary Links I

This section uses springs and auxiliary links to balance the manipulators. The 2-link manipulator with identical links and perpendicular joint axes is taken as an example to illustrate the approach. To let the local position of the CM of the manipulator be fixed, the auxiliary links with identical parameters of the links of the manipulator are adopted as counterweights, as shown in Fig. 6.29(a). As a result, the CM of the manipulator is located at the second R joint of the manipulator (*P*). The manipulator is then equivalent to a payload mounted on an R joint. One end of the spring is attached on *H*, which is a point right above the first R joint, the other end is fixed on *P*. It can be readily proved the manipulator is statically balanced.

Suppose the mass of the link of the manipulator is m, the point of attachment of the springs on the base is

$$\boldsymbol{H} = \{0 \quad 0 \quad 4mg/k\}^T \tag{6.108}$$

The position of the CM of the manipulator *P* and the potential energy are yielded as

$$\boldsymbol{P} = \{lC\theta \quad 0 \quad lS\theta\}^T \tag{6.109}$$

$$\boldsymbol{V} = V_s + V_m = \frac{1}{2}k|\boldsymbol{P} - \boldsymbol{H}|^2 + mgP_z = (l^2k^2 + 16m^2g^2)/2k \tag{6.110}$$

Eq. (6.109) verifies the system is statically balanced. By connecting the 2-link manipulators above, deployable single-loop linkages are obtained. The R joints used to connect the 2-link manipulators all intersect at a point. As described in Section 4, the DOF of the constrained linkages are all one during the deploying process, if R_i (i = 2, 4, 6…) are constrained on the same plane.

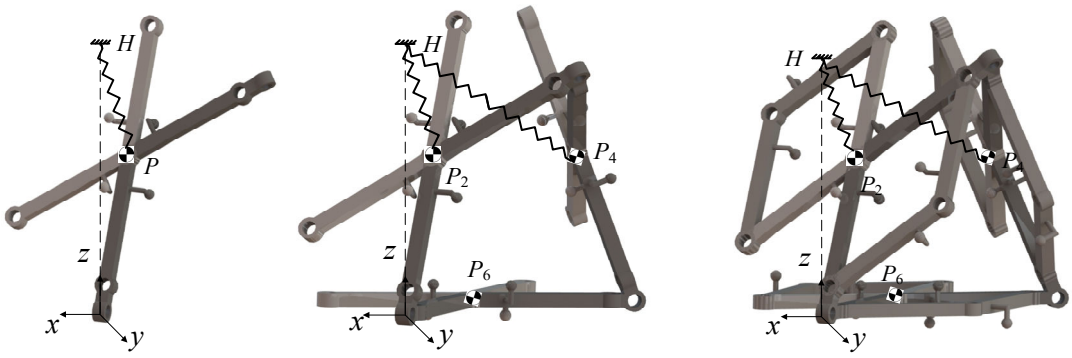

(a) (b) (c)

Fig. 6.29 Statically balanced mechanisms using auxiliary links and springs: (a) 2-DOF manipulator; (b) Bricard linkage; (c) extension of Bricard linkage

The static balancing of Bricard linkage is then discussed. The position vectors of R_i (i = 2, 4, 6) are calculated as

$$\boldsymbol{P_2} = \{lC\theta \quad 0 \quad lS\theta\}^T \tag{6.111a}$$

$$\boldsymbol{P_4} = \{l(C\theta - 1) \quad l(C\theta + 1)\sqrt{\frac{2C\theta+1}{(C\theta+1)^2}} \quad lS\theta\}^T \tag{6.111b}$$

$$\boldsymbol{P_6} = \{-l \quad 0 \quad 0\}^T \tag{6.111c}$$

Links 1 and 2 (of the first 2-link manipulator) are already balanced. The potential energy is calculated as

$$V_2 = V_{s2} + V_{m2} = \frac{1}{2}k|\boldsymbol{P_2} - \boldsymbol{H}|^2 + mgP_{2z} = (l^2k^2 + 16m^2g^2)/2k \tag{6.112}$$

Links 5 and 6 (of the third 2-link manipulator) always lie on the ground and do not need to balance. Now it will be verified that links 3 and 4 (of the second manipulator) are balanced, by connecting H and P_4 using one spring. The potential energy is computed as

$$V_4 = V_{s4} + V_{m4} = \frac{1}{2}k|\boldsymbol{P_4} - \boldsymbol{H}|^2 + mgP_{4z} = (3l^2k^2 + 16m^2g^2)/2k \tag{6.113}$$

Eq. (6.113) infers that the second 2-link manipulator is also balanced. Eqs. (6.112-6.113) imply that the static balancing method is valid by connecting R_2 (R_4), and the point right above R_1. The extension of the Bricard linkage in Fig. 6.29(c) is also balanced.

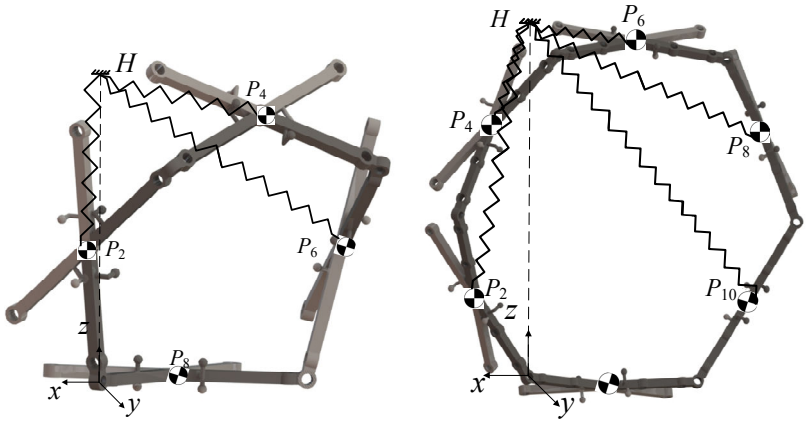

(a) (b)

Fig. 6.30 Statically balanced 8R linkage and 12R linkage using auxiliary links and springs: (a) 8R linkage; (b) 12R linkage

Now the static balancing of 8R linkage will be addressed. When connecting four statically balanced 2-link manipulators, a balanced 8R linkage is obtained, as shown in Fig. 6.30(a). Three springs are used to connect H and P_2, P_4 and P_6 respectively. The position vectors of R_i (i = 2, 4, 6, 8) in the global frame were obtained in Section 4 as

$$\boldsymbol{P_2} = \{lC\theta \quad 0 \quad lS\theta\}^T \tag{6.114a}$$

$$\boldsymbol{P_4} = \{l(2C\theta - 1) \quad 2l(C\theta + 1)\sqrt{(C\theta/(C\theta + 1)^2)} \quad 2lS\theta\}^T \tag{6.114b}$$

$$\boldsymbol{P_6} = \{l(C\theta - 2) \quad 2l(C\theta + 1)\sqrt{(C\theta/(C\theta + 1)^2)} \quad lS\theta\}^T \tag{6.114c}$$

$$\boldsymbol{P_8} = \{-l \quad 0 \quad 0\}^T \tag{6.114d}$$

The potential energies are given by

$$V_2 = V_{s2} + V_{m2} = \frac{1}{2}k|\boldsymbol{P_2} - \boldsymbol{H}|^2 + mgP_{2z} = (l^2k^2 + 16m^2g^2)/2k \tag{6.115}$$

$$V_4 = V_{s4} + V_{m4} = \frac{1}{2}k|\boldsymbol{P_4} - \boldsymbol{H}|^2 + mgP_{4z} = (5l^2k^2 + 16m^2g^2)/2k \tag{6.116}$$

$$V_6 = V_{s6} + V_{m6} = \frac{1}{2}k|\boldsymbol{P_6} - \boldsymbol{H}|^2 + mgP_{6z} = (5l^2k^2 + 16m^2g^2)/2k \tag{6.117}$$

Eqs. (6.115-6.117) imply that the 8R linkage is also balanced using the static balancing method. It is noted that the method is only valid when the 8R linkage is in the constrained configuration. Similarly, all the deployable single-loop linkages in the constrained configuration, such as the 12R linkage in Fig. 6.30(b), can be balanced. In a 12R linkage,

$$\varphi = arccos[(2 - C\theta)/(C\theta + 1)] \tag{6.118}$$

The potential energies of the system are yielded as

$$V_2 = (l^2k^2 + 16m^2g^2)/2k \tag{6.119}$$

$$V_4 = V_{10} = (7l^2k^2 + 16m^2g^2)/2k \tag{6.120}$$

$$V_6 = V_8 = (13l^2k^2 + 16m^2g^2)/2k \tag{6.121}$$

which are also constants.

d) Statically Balanced 8R Linkage Using Springs and Auxiliary Links II

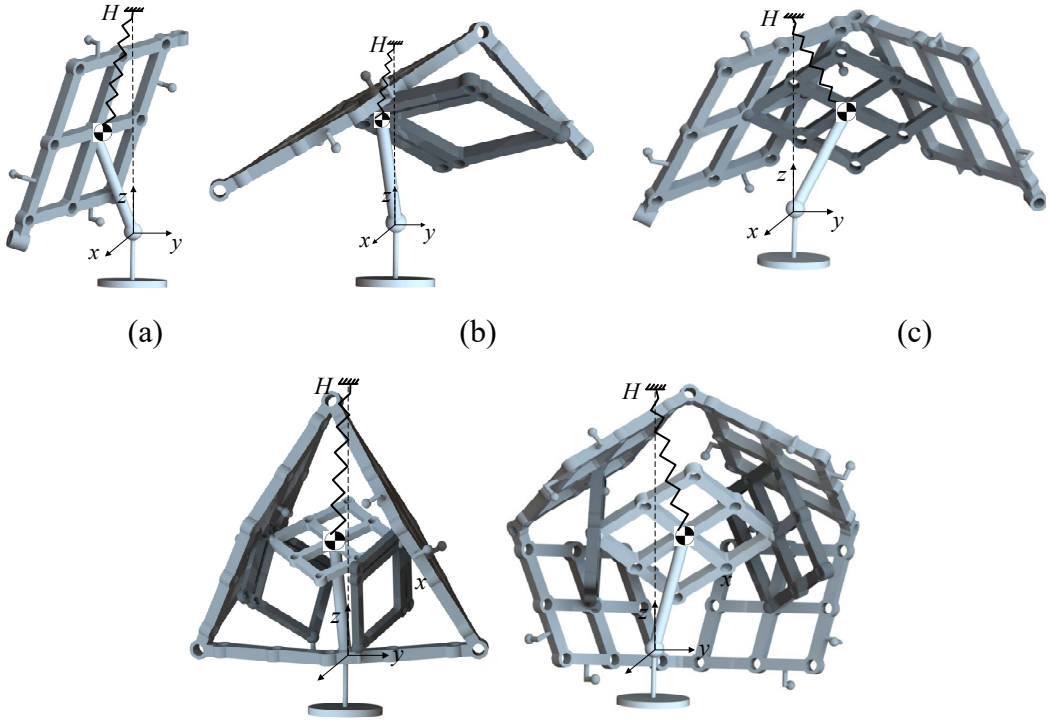

Fig. 6.31 Statically balanced manipulators using auxiliary parallelograms and springs: (a) 2-DOF manipulator; (b) 3-DOF manipulator; (c) 4-DOF manipulator; (d) Bricard linkage; (e) 8R linkage

We connect the manipulator with auxiliary links in b) to a link, which mounted on an S joint, using another S joint. The manipulator can be balanced by connecting the point right above the S joint on the base and the CM of the manipulator using one spring. The statically balanced 2-link, 3-link and 4-link manipulators, Bricard linkage and 8R linkage are provided in Fig. 6.31.

6.6.2 Static Balancing of DPMs

The DPMs proposed in Chapters 4 and 5 will be balanced in this section.

a) Statically Balanced DPMs using a Special 1-DOF Mechanism

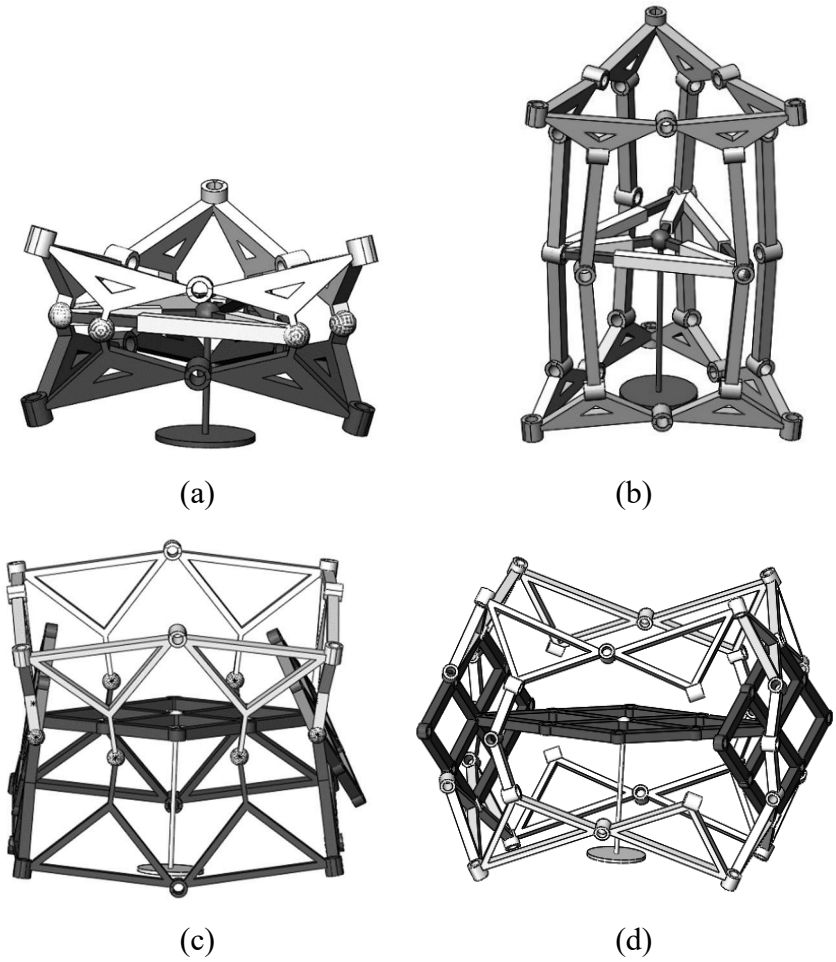

Fig. 6.32 Statically balanced DPMs: (a-b) the prism mechanisms based on Bricard linkages; (c-d) the prism mechanisms based on 8R linkages

DPMs can be developed into the statically balanced mechanisms using a special 1-DOF mechanism. The first mechanism discussed is the prism mechanism based on Bricard linkages using S joints. Since the mechanism is always plane-symmetric about the mirror plane and axisymmetric about the line defined by the intersection of R_2, R_4 and R_6 and that of R_2', R_4' and R_6', the CM of the mechanism is always at the centre of the triangle defined by the three interval S joints. A 1-DOF triangle mechanism composed of prismatic joints is attached to the S joints to identify the CM of the mechanism, as shown in Fig. 6.32(a). When mounting the CM of the mechanism on the base through an S joint, the mechanism becomes statically balanced, and can keep its postures during the deploying process. Similarly, the prism based on Bricard linkages using RRR chains can also be balanced. For the deployable prism mechanism based on 8R linkages using S joints or half the number of RRR chains, a parallelogram is added, instead of the triangle mechanism. The CM of the DPM and that of the parallelogram are coincident. Mounting the CM of the mechanism on an S joint, then the statically balanced deployable

mechanism based on 8R linkages with multiple modes is obtained. It is noted that the method is not valid when the DPMs are in the rotation modes, since the mechanisms in these modes are not symmetric about the mirror plane.

b) Statically Balanced DPMs using springs

In this section, only springs will be used to balance the DPMs proposed in Chapters 4 and 5. Since the prism mechanisms are always symmetric about the mirror plane, the mechanisms are cut in half to facilitate balancing. We start from the DPM based on 8R linkages using S joints, as shown in Fig. 6.33(a). All the S joints keep on the plane (the plane is fixed on the ground) and have 3-DOF rotations. Hence, each link can be balanced by connecting the CM of the link and the point right above the S joint using one spring, as shown in Fig. 6.33(b).

Then the statically balanced DPM based on 8R linkages using RRR chains [Fig. 6.34(a)] will be addressed. When cutting in half, the DPM is equivalent to the linkage composed of eight 2-link 2R manipulators in Fig. 6.34(b). The first link in each manipulator has a 1-DOF rotation on the plane and can be balanced by connecting the CM of the first link and the point right above the first R joint using one spring. As obtained in Section 6.4, the second link of the manipulator can be balanced using two springs which connect the CM of the second link and the point right above the second R joint, and the second R joint and the point right above the first R joint respectively.

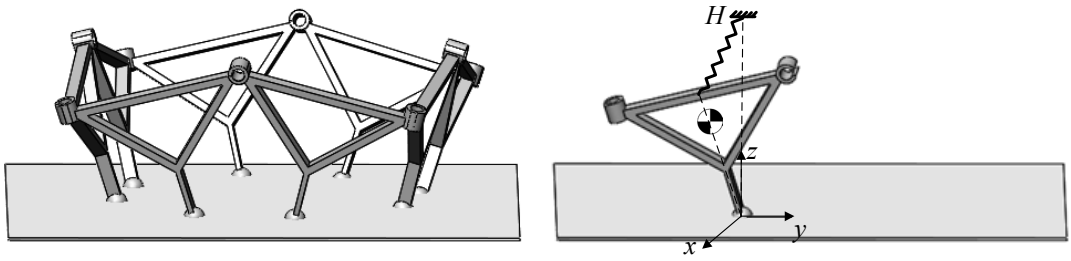

(a) (b)

Fig. 6.33 Statically balanced DPM based on 8R linkages using S joints

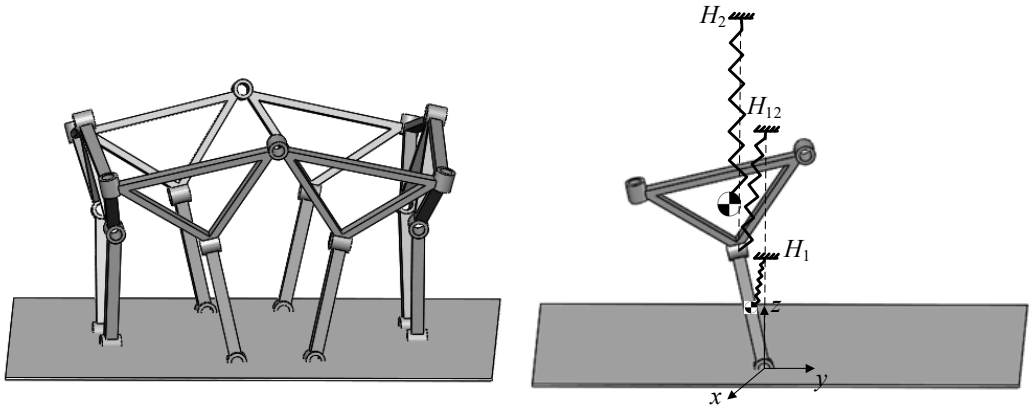

(a) (b)

Fig. 6.34 Statically balanced DPM based on 8R linkages using eight RRR chains

When connecting two 8R linkages using four RRR chains, the linkage constrained on the mirror plane is equivalent to the linkage comprised of four 3-link 3R manipulators [Fig. 6.35(b)]. The first link can be balanced by connecting the CM of the first link and the point right above the first R joint using one spring. The second link of the manipulator can be balanced using two springs which connect the CM of the second link and the point right above the second R joint, and the second R joint and the point right above the first R joint respectively. When connecting the CM of the third link and the point right above the third R joint, the third R joint and the point right above the second R joint, and the second R joint and the point right above the first R joint respectively, the third link is then statically balanced.

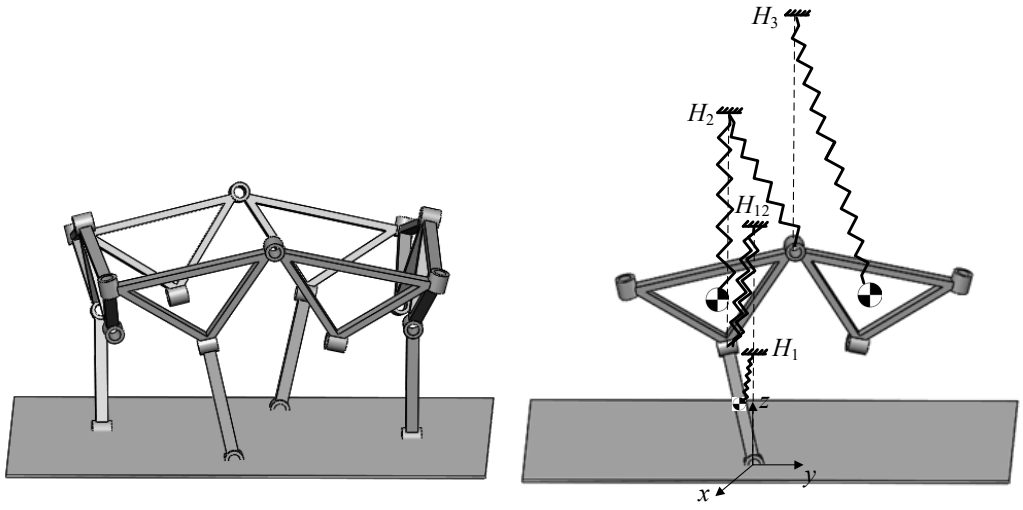

(a) (b)

Fig. 6.35 Statically balanced DPM based on 8R linkages using four RRR chains

This method applies to any prism mechanisms in any modes, except for the rotation mode of the mechanisms with half the number of the RRR chains.

6.7 Summary

This chapter is to develop the deployable mechanisms proposed in Chapters 3, 4 and 5 into the statically balanced mechanisms. First, the static balancing method of the planar 4R parallelogram, planar manipulators, spherical mechanisms and spatial mechanisms have been proposed, with almost no calculation. In addition, a numerical optimization approach has also been addressed to obtain the balancing conditions of the mechanisms. The sum of squared differences of the potential energies of the system is set as the objective function to obtain the spring attachment points. Then the proposed static balancing methods have been applied to the deployable mechanisms, including the ones with multiple modes. Statically balanced DPMs using only springs, auxiliary links and the combination of auxiliary links and springs have also been designed.

CHAPTER 7 – CONCLUSIONS

7.1 General Conclusions

This thesis has addressed the type synthesis and static balancing of a class of deployable mechanisms with multiple modes. First, the existing single-loop linkages, the deployable/foldable mechanisms and mechanisms with multiple modes have been reviewed. The statically balanced mechanisms using springs, counterweights and other approaches have also been presented.

Chapter 2 has discussed the theoretical tools used in this thesis, including DOF analysis, kinematic analysis and optimization tools, and the fundamentals of static balancing.

In Chapter 3, the construction method for foldable single-loop 8R linkages with multiple modes has been proposed. Planar 4R linkages and spherical 4R linkages were used to build spatial 8R linkages. The links are thick panels and the joints are offset to allow folding. There are two types of 8R linkages involved, including the one constructed using two spherical 4R linkages and the one connected using one planar 4R linkage and one spherical 4R linkage. The mechanisms have multiple modes, including an 8R linkage mode, a 6R linkage mode and 4R linkage modes. Besides, the mechanisms can be spread onto a plane and be folded into two or four layers.

Using a spatial triad, single-loop linkages have been connected in Chapters 4 and 5. Then the single-loop linkages were inserted to faces of polyhedrons to obtain DPMs. Two types of DPMs were designed, including the ones constructed using S joints and the ones using RRR chains. The DPMs have only 1-DOF when deployed. Several mechanisms have multiple modes and can switch among different modes through transition positions. Prototypes have been fabricated, using rigid or flexible joints. The ones with rigid joints have precise movement and the ones with compliant joints have a larger deploying ratio and can recover to the initial state after deploying.

In Chapter 6, static balancing methods for planar mechanisms, spherical mechanisms and spatial mechanisms have been addressed. All the mechanisms in this thesis are composed of links whose weights cannot be disregarded. Both an algebraic method and a geometric method have been adopted to design statically balanced 4R parallelogram. The 4R parallelogram can be balanced using three, two or one springs. The spherical manipulators and spatial manipulators are balanced using a geometric method readily, with almost no calculation. A novel numerical optimization method has also been

proposed, by setting the sum of squared differences of potential energies as the objective function. Using the proposed static balancing method, the deployable 8R linkage and DPMs have been developed into the ones that are statically balanced.

7.2 Main Contributions

The main contributions of this thesis are:

1) A novel construction method for deployable mechanisms using single-loop linkages has been presented. DPMs with multiple modes are obtained using this method. The mechanisms have simple structures and few DOFs. It has been revealed that by connecting single-loop linkages using half the number of the RRR chains, the mechanisms obtain an additional rotation mode.
2) A novel construction method for foldable single-loop 8R linkages with multiple modes is proposed. Instead of connecting consecutively as in the literature, the compositional 4R linkages are staggered to obtain the 8R linkages.
3) The general method for the static balancing of the spherical and spatial manipulators has been proposed. Using this method, any manipulators, including the ones with multiple modes, can be readily balanced with almost no calculation.
4) The 4R parallelogram linkage has been balanced using only one external spring. The concept of virtual rotation centre is first introduced in the design of the statically balanced system using a geometric method.
5) A novel numerical optimization method is proposed, which is suitable for the statically balanced systems using springs. More possible solutions can be found using this method, than the current methods in the literature.

7.3 Future Work

In the future, the work can be developed in the following aspects. First, deployable mechanisms with multiple modes have been designed in this thesis. However, there is still a lack of detailed DOF analysis and kinematic analysis for these mechanisms. In the future, the set of equations for each mechanism will be derived and then solved to obtain all the possible motion modes of the mechanisms. The application of these mechanisms also needs explorations. They may apply in the fields of entertainment, education and aerospace. Prototypes with better quality will be built and a control method will be used to actuate the mechanisms.

Secondly, the static balancing conditions for planar, spherical and spatial manipulators have been obtained using a geometric method, with almost no calculation. However, the number of springs can be reduced through mass moment substitution and vector synthesis. The interference between springs and links should be avoided.

Thirdly, the statically balanced system designed in this thesis all have constant payloads. In the cases that the payloads of the manipulators change, for example, picking up or dropping off objects, the system should be adjusted. Therefore, the devices with variable payloads deserve further explorations. In addition, springs and counterweights will be combined to balance the mechanisms. Constant force springs, gears and cams may also be adopted.

Finally, the static balancing methods have only been theoretically verified by calculating the total potential energy of the system. It would be better to design and fabricate practical prototypes to verify the feasibility and sensibility of the statically balanced mechanisms. Rollers and pulleys will be used to achieve the zero-free-length springs.

APPENDIX THE TRANSFER MATRIXES OF THE MECHANISMS

A The Transfer Matrixes of the Bricard Linkage.

The transfer matrixes of the Bricard linkage are

$$ {}_1^6T = {}_3^2T = {}_5^4T = \begin{bmatrix} C\theta & -S\theta & 0 & l \\ 0 & 0 & 1 & 0 \\ -S\theta & -C\theta & 0 & 0 \\ 0 & 0 & 0 & 1 \end{bmatrix} \tag{A1} $$

$$ {}_2^1T = {}_4^3T = {}_6^5T = \begin{bmatrix} -C\theta/(C\theta+1) & -\sqrt{1-C^2\theta/(C\theta+1)^2} & 0 & l \\ 0 & 0 & -1 & 0 \\ \sqrt{1-C^2\theta/(C\theta+1)^2} & -C\theta/(C\theta+1) & 0 & 0 \\ 0 & 0 & 0 & 1 \end{bmatrix} \tag{A2} $$

B The Transfer Matrixes of the 8R Linkage

The transfer matrixes of the 8R linkage are

$$ {}_1^8T = {}_3^2T = {}_5^4T = {}_7^6T = \begin{bmatrix} C\theta & -S\theta & 0 & l \\ 0 & 0 & 1 & 0 \\ -S\theta & -C\theta & 0 & 0 \\ 0 & 0 & 0 & 1 \end{bmatrix} \tag{B1} $$

$$ {}_2^1T = {}_6^5T = \begin{bmatrix} C\varphi & -S\varphi & 0 & l \\ 0 & 0 & -1 & 0 \\ S\varphi & C\varphi & 0 & 0 \\ 0 & 0 & 0 & 1 \end{bmatrix} \tag{B2} $$

$$ {}_4^3T = {}_8^7T = \begin{bmatrix} C\varphi_2 & -S\varphi_2 & 0 & l \\ 0 & 0 & -1 & 0 \\ S\varphi_2 & C\varphi_2 & 0 & 0 \\ 0 & 0 & 0 & 1 \end{bmatrix} \tag{B3} $$

C The Transfer Matrixes of the Spherical Manipulator

The transfer matrixes of the spherical manipulator are

$$ {}_1^0T = \begin{bmatrix} C\theta_1 & -S\theta_1 & 0 & 0 \\ 0 & 0 & 1 & 0 \\ -S\theta_1 & -C\theta_1 & 0 & 0 \\ 0 & 0 & 0 & 1 \end{bmatrix} \tag{C1} $$

$$
{}^{1}_{2}T = \begin{bmatrix} C\theta_2 & -S\theta_2 & 0 & 0 \\ C\alpha_1 S\theta_2 & C\alpha_1 C\theta_2 & S\alpha_1 & 0 \\ -S\alpha_1 S\theta_2 & -S\alpha_1 C\theta_2 & C\alpha_1 & 0 \\ 0 & 0 & 0 & 1 \end{bmatrix} \tag{C2}
$$

$$
{}^{2}_{3}T = \begin{bmatrix} C\theta_3 & -S\theta_3 & 0 & 0 \\ C\alpha_2 S\theta_3 & C\alpha_2 C\theta_3 & S\alpha_2 & 0 \\ -S\alpha_2 S\theta_3 & -S\alpha_2 C\theta_3 & C\alpha_2 & 0 \\ 0 & 0 & 0 & 1 \end{bmatrix} \tag{C3}
$$

$$
{}^{3}_{4}T = \begin{bmatrix} C\theta_4 & -S\theta_4 & 0 & 0 \\ C\alpha_3 S\theta_4 & C\alpha_3 C\theta_4 & S\alpha_3 & 0 \\ -S\alpha_3 S\theta_4 & -S\alpha_3 C\theta_4 & C\alpha_3 & 0 \\ 0 & 0 & 0 & 1 \end{bmatrix} \tag{C4}
$$

D The Transfer Matrixes of the Spatial Manipulator

The transfer matrixes of the spatial manipulator are

$$
{}^{0}_{1}T = \begin{bmatrix} C\theta_1 & -S\theta_1 & 0 & 0 \\ C\alpha_0 S\theta_1 & C\alpha_0 C\theta_1 & S\alpha_0 & 0 \\ S\alpha_0 S\theta_1 & S\alpha_0 C\theta_1 & C\alpha_0 & 0 \\ 0 & 0 & 0 & 1 \end{bmatrix} \tag{D1}
$$

$$
{}^{1}_{2}T = \begin{bmatrix} C\theta_2 & -S\theta_2 & 0 & L_1 \\ C\alpha_1 S\theta_2 & C\alpha_1 C\theta_2 & -S\alpha_1 & -d_2 S\alpha_1 \\ S\alpha_1 S\theta_2 & S\alpha_1 C\theta_2 & C\alpha_1 & d_2 C\alpha_1 \\ 0 & 0 & 0 & 1 \end{bmatrix} \tag{D2}
$$

$$
{}^{2}_{3}T = \begin{bmatrix} C\theta_3 & -S\theta_3 & 0 & L_2 \\ C\alpha_2 S\theta_3 & C\alpha_2 C\theta_3 & -S\alpha_2 & -d_3 S\alpha_2 \\ S\alpha_2 S\theta_3 & S\alpha_2 C\theta_3 & C\alpha_2 & d_3 C\alpha_2 \\ 0 & 0 & 0 & 1 \end{bmatrix} \tag{D3}
$$

REFERENCES

[1] Stewart, D., 1965. A platform with six degrees of freedom. Proceedings of the institution of mechanical engineers, 180(1), pp.371-386.

[2] Bennett, G.T., 1903. A new mechanism. Engineering, 76, p.777.

[3] Bennett, G.T., 1914. The skew isogram mechanism. Proceedings of the London Mathematical Society, 2(1), pp.151-173.

[4] Myard, F.E., 1931. Contribution à la géométrie des systèmes articulés. Bulletin de la Société Mathématique de France, 59, pp.183-210.

[5] Goldberg, M., 1943. New five-bar and six-bar linkages in three dimensions. Transactions of ASME, 65, pp.649-661.

[6] Huang, C., Kong, X. and Ou, T., 2009, January. Position analysis of a Bennett-based multiple-mode 7R linkage. In ASME 2009 International design engineering technical conferences and computers and information in engineering conference (pp. 1231-1236). American Society of Mechanical Engineers.

[7] Sarrus, P.T., 1853. Note sur la transformation des mouvements rectilignes alternatifs, en mouvements circulaires, et reciproquement, comptes. rendus. acad. Sci., Paris, 36, p.1036.

[8] Bricard, R., 1897. Mémoire sur la théorie de l'octaèdre articulé. Journal de Mathématiques pures et appliquées, 3, pp.113-148.

[9] Baker, J.E., 1980. An analysis of the Bricard linkages. Mechanism and Machine Theory, 15(4), pp.267-286.

[10] Bennett, G.T, 1905. The parallel motion of Sarrus and some allied mechanisms. Philosophy Magazine, 9, pp. 803-810.

[11] Waldron, K.J., 1967. A family of overconstrained linkages. Journal of Mechanisms, 2(2), pp.201-211.

[12] Chen, Y., 2003. Design of structural mechanisms, PhD thesis, University of Oxford.

[13] Chen, Y., You, Z. and Tarnai, T., 2005. Threefold-symmetric Bricard linkages for deployable structures. International journal of solids and structures, 42(8), pp.2287-2301.

[14] Chen, Y. and You, Z., 2009. Two-fold symmetrical 6R foldable frame and its bifurcations. International Journal of Solids and Structures, 46(25-26), pp.4504-4514.

[15] Chen, Y. and You, Z., 2008. An extended Myard linkage and its derived 6R linkage. Journal of Mechanical Design, 130(5), p.052301.

[16] Deng, Z., Huang, H., Li, B. and Liu, R., 2011. Synthesis of deployable/foldable single loop mechanisms with revolute joints. Journal of Mechanisms and Robotics, 3(3), p.031006.

[17] Li, B., Huang, H. and Deng, Z., 2016. Mobility analysis of symmetric deployable mechanisms involved in a coplanar 2-twist screw system. Journal of Mechanisms and Robotics, 8(1), p.011007.

[18] Li, B., Qi, X., Huang, H. and Xu, W., 2016. Modeling and analysis of deployment dynamics for a novel ring mechanism. Acta Astronautica, 120, pp.59-74.

[19] Li, B., Kong, W. and Qi, X., 2016. Modeling and design on modular deployable antenna. In Advances in Reconfigurable Mechanisms and Robots II (pp. 1037-1048). Springer, Cham.

[20] Qi, X., Deng, Z., Li, B., Liu, R. and Guo, H., 2013. Design and optimization of large deployable mechanism constructed by Myard linkages. CEAS Space Journal, 5(3-4), pp.147-155.

[21] Huang, H., Li, B., Deng, Z. and Liu, R., 2013. Randomized multi-objective optimal design of a novel deployable truss. Proceedings of the Institution of Mechanical Engineers, Part G: Journal of Aerospace Engineering, 227(11), pp.1720-1736.

[22] Huang, H., Li, B., Zhu, J. and Qi, X., 2016. A new family of Bricard-derived deployable mechanisms. Journal of Mechanisms and Robotics, 8(3), p.034503.

[23] Cui, J., Huang, H., Li, B. and Deng, Z., 2012. A novel surface deployable antenna structure based on special form of Bricard linkages. In Advances in Reconfigurable Mechanisms and Robots I (pp. 783-792). Springer, London.

[24] Gantes, C., 1991. A design methodology for deployable structures, PhD thesis, Massachusetts Institute of Technology.

[25] Lu, S., Zlatanov, D., Ding, X. and Molfino, R., 2014. A new family of deployable mechanisms based on the Hoekens linkage. Mechanism and Machine Theory, 73, pp.130-153.

[26] Miura, K., Furuya, H. and Suzuki, K., 1985. Variable geometry truss and its application to deployable truss and space crane arm. Acta Astronautica, 12(7-8), pp.599-607.

[27] Tibert, G., 2002. Deployable tensegrity structures for space applications, PhD thesis, Royal Institute of Technology.

[28] Lu, S., Zlatanov, D., Ding, X., Molfino, R. and Zoppi, M., 2013, August. A novel deployable mechanism with two decoupled degrees of freedom. In ASME 2013 International Design Engineering Technical Conferences and Computers and Information in Engineering Conference (pp. V06BT07A014-V06BT07A014). American Society of Mechanical Engineers.

[29] Guest, S.D. and Pellegrino, S., 1996. A new concept for solid surface deployable antennas. Acta Astronautica, 38(2), pp.103-113.

[30] Chen, Y., Peng, R. and You, Z., 2015. Origami of thick panels. Science, 349(6246), pp.396-400.

[31] Hoberman, C., 2010. Folding structures made of thick hinged sheets. U.S. Patent 7,794,019.

[32] Morgan, J., Magleby, S.P. and Howell, L.L., 2016. An approach to designing origami-adapted aerospace mechanisms. Journal of Mechanical Design, 138(5), p.052301.

[33] Kang, L. and Yi, B.J., 2016. Design of two foldable mechanisms without parasitic motion. IEEE Robotics and Automation Letters, 1(2), pp.930-937.

[34] Zhao, T.S., Wang, C., Liu, X., Bian, H. and Zhao, Y.Z., 2016. Stiffness and singularity analysis of foldable parallel mechanism for ship-based stabilized platform. Robotica, 34(4), pp.913-924.

[35] Jacobsen, J.O., Winder, B.G., Howell, L.L. and Magleby, S.P., 2010. Lamina emergent mechanisms and their basic elements. Journal of Mechanisms and Robotics, 2(1), p.011003.

[36] Albrechtsen, N.B., Magleby, S.P. and Howell, L.L., 2011, January. Using lamina emergent mechanisms to develop credit-card-sized products. In ASME 2011 International Design Engineering Technical Conferences and Computers and Information in Engineering Conference (pp. 223-231). American Society of Mechanical Engineers.

[37] Albrechtsen, N.B., Magleby, S.P. and Howell, L.L., 2010, January. Identifying potential applications for lamina emergent mechanisms using technology push product development. In ASME 2010 International Design Engineering Technical Conferences and Computers and Information in Engineering Conference (pp. 513-521). American Society of Mechanical Engineers.

[38] Lang, R.J. and Howell, L., 2018. Rigidly foldable quadrilateral meshes from angle arrays. Journal of Mechanisms and Robotics, 10(2), p.021004.

[39] Lang, R.J., Magleby, S. and Howell, L., 2016. Single degree-of-freedom rigidly foldable cut origami flashers. Journal of Mechanisms and Robotics, 8(3), p.031005.

[40] Nelson, T.G., Lang, R.J., Pehrson, N.A., Magleby, S.P. and Howell, L.L., 2016. Facilitating deployable mechanisms and structures via developable lamina emergent arrays. Journal of Mechanisms and Robotics, 8(3), p.031006.

[41] Hanna, B.H., Lund, J.M., Lang, R.J., Magleby, S.P. and Howell, L.L., 2014. Waterbomb base: a symmetric single-vertex bistable origami mechanism. Smart Materials and Structures, 23(9), p.094009.

[42] Chen, G., Magleby, S.P. and Howell, L.L., 2018. Membrane-enhanced lamina emergent torsional joints for surrogate folds. Journal of Mechanical Design, 140(6), p.062303.
[43] Hoberman, C., 2001. Reversibly expandable structures having polygon links. U.S. Patent 6,219,974.
[44] Hoberman, C., 1990. Reversibly expandable doubly-curved truss structure. U.S. Patent 4,942,700.
[45] Hoberman, C., 2008. Geared expanding structures. U.S. Patent 7,464,503.
[46] Wei, G., Ding, X. and Dai, J.S., 2009, January. Geometric and kinematic analysis of the Hoberman switch-pitch ball and its variant. In ASME 2009 International Design Engineering Technical Conferences and Computers and Information in Engineering Conference (pp. 1245-1254). American Society of Mechanical Engineers.
[47] Wei, G. and Dai, J.S., 2014. A spatial eight-bar linkage and its association with the deployable platonic mechanisms. Journal of Mechanisms and Robotics, 6(2), p.021010.
[48] Kiper, G. and Söylemez, E., 2013. Polyhedral linkages obtained as assemblies of planar link groups. Frontiers of Mechanical Engineering, 8(1), pp.3-9.
[49] St-Onge, D. and Gosselin, C., 2016. Synthesis and design of a one degree-of-freedom planar deployable mechanism with a large expansion ratio. Journal of Mechanisms and Robotics, 8(2), p.021025.
[50] Kiper, G., 2011, Design methods for planar and spatial deployable structures, PhD thesis, Middle East Technical University.
[51] Chen, Y., Yang, F. and You, Z., 2018. Transformation of polyhedrons. International Journal of Solids and Structures, 138, pp.193-204.
[52] Yim, M., Shen, W.M., Salemi, B., Rus, D., Moll, M., Lipson, H., Klavins, E. and Chirikjian, G.S., 2007. Modular self-reconfigurable robot systems [grand challenges of robotics]. IEEE Robotics & Automation Magazine, 14(1), pp.43-52.
[53] Murata, S., Yoshida, E., Kamimura, A., Kurokawa, H., Tomita, K. and Kokaji, S., 2002. M-TRAN: Self-reconfigurable modular robotic system. IEEE/ASME transactions on mechatronics, 7(4), pp.431-441.
[54] Pamecha, A., Chiang, C.J., Stein, D. and Chirikjian, G., 1996, August. Design and implementation of metamorphic robots. In Proceedings of the 1996 ASME Design Engineering Technical Conference and Computers in Engineering Conference (Vol. 10). Irvine, California, USA: ASME.
[55] Dai, J.S. and Jones, J.R., 1999. Mobility in metamorphic mechanisms of foldable/erectable kinds. Journal of mechanical design, 121(3), pp.375-382.

[56] Dai, J.S. and Wang, D., 2007. Geometric analysis and synthesis of the metamorphic robotic hand. Journal of mechanical design, 129(11), pp.1191-1197.
[57] Gao, Z., Wei, G. and Dai, J.S., 2015. Inverse kinematics and workspace analysis of the metamorphic hand. Proceedings of the Institution of Mechanical Engineers, Part C: Journal of Mechanical Engineering Science, 229(5), pp.965-975.
[58] Zhang, K., Dai, J.S. and Fang, Y., 2009, June. A new metamorphic mechanism with ability for platform orientation switch and mobility change. In Reconfigurable Mechanisms and Robots, 2009. ReMAR 2009. ASME/IFToMM International Conference on (pp. 596-602). IEEE.
[59] Gan, D., Dai, J.S. and Liao, Q., 2009. Mobility change in two types of metamorphic parallel mechanisms. Journal of Mechanisms and Robotics, 1(4), p.041007.
[60] Ye, W., Fang, Y. and Guo, S., 2014. Reconfigurable parallel mechanisms with planar five-bar metamorphic linkages. Science China Technological Sciences, 57(1), pp.210-218.
[61] Lee, C.C. and Hervé, J.M., 2007, June. Discontinuously movable 8R mechanisms with an infinity of bifurcations. In 12th IFToMM World Congress, Besançon (France).
[62] Lee, C.C. and Hervé, J.M., 2002, January. Discontinuous mobility of one family of spatial 6R mechanisms through the group algebraic structure of displacement set. In ASME 2002 International Design Engineering Technical Conferences and Computers and Information in Engineering Conference (pp. 645-653). American Society of Mechanical Engineers.
[63] Lee, C.C. and Hervé, J.M., 2005. Discontinuously movable seven-link mechanisms via group-algebraic approach. Proceedings of the Institution of Mechanical Engineers, Part C: Journal of Mechanical Engineering Science, 219(6), pp.577-587.
[64] Galletti, C. and Fanghella, P., 2001. Single-loop kinematotropic mechanisms. Mechanism and Machine Theory, 36(6), pp.743-761.
[65] Galletti, C. and Giannotti, E., 2002, January. Multiloop kinematotropic mechanisms. In ASME 2002 International Design Engineering Technical Conferences and Computers and Information in Engineering Conference (pp. 455-460). American Society of Mechanical Engineers.
[66] Wohlhart, K., 1996. Kinematotropic linkages. In Recent Advances in Robot Kinematics (pp. 359-368). Springer, Dordrecht.
[67] Ye, W., Fang, Y., Zhang, K. and Guo, S., 2014. A new family of reconfigurable parallel mechanisms with diamond kinematotropic chain. Mechanism and Machine Theory, 74, pp.1-9.

[68] Kong, X., 2018. A variable-DOF single-loop 7R spatial mechanism with five motion modes. Mechanism and Machine Theory, 120, pp.239-249.

[69] Kong, X. and Huang, C., 2009, June. Type synthesis of single-DOF single-loop mechanisms with two operation modes. In Reconfigurable Mechanisms and Robots, 2009. ASME/IFToMM International Conference on ReMAR (pp. 136-141). IEEE.

[70] Huang, C., Kong, X. and Ou, T., 2009, January. Position analysis of a Bennett-based multiple-mode 7R linkage. In ASME 2009 International design engineering technical conferences and computers and information in engineering conference (pp. 1231-1236). American Society of Mechanical Engineers.

[71] Kong, X., Wang, J., Yu, J. and Li, D., 2018, Jun. Reconfiguration analysis of a variable degrees-of-freedom multi-mode parallel mechanism. In Proceedings of the 4th IEEE/IFToMM Int. Conf. on Reconfigurable Mechanisms and Robots.

[72] Kong, X., Gosselin, C.M. and Richard, P.L., 2007. Type synthesis of parallel mechanisms with multiple operation modes. Journal of Mechanical Design, 129(6), pp.595-601.

[73] Kong, X. and Gosselin, C.M., 2007. Type synthesis of parallel mechanisms (Vol. 33). Springer.

[74] Kong, X. and Jin, Y., 2016. Type synthesis of 3-DOF multi-mode translational/spherical parallel mechanisms with lockable joints. Mechanism and Machine Theory, 96, pp.323-333.

[75] Kong, X., 2014. Reconfiguration analysis of a 3-DOF parallel mechanism using Euler parameter quaternions and algebraic geometry method. Mechanism and Machine Theory, 74, pp.188-201.

[76] Kong, X., 2016. Reconfiguration analysis of a 4-DOF 3-RER parallel mechanism with equilateral triangular base and moving platform. Mechanism and Machine Theory, 98, pp.180-189.

[77] Kiper, G., Gürcü, F., Korkmaz, K. and Söylemez, E., 2015. Kinematic design of a reconfigurable deployable canopy. In New Trends in Mechanism and Machine Science (pp. 167-174). Springer, Cham.

[78] Wei, G. and Dai, J.S., 2014. Reconfigurable and deployable platonic mechanisms with a variable revolute joint. In Advances in Robot Kinematics (pp. 485-495). Springer International Publishing.

[79] Zhao, J.S., Yan, Z.F. and Chu, F.L., 2012. A reconfigurable linkage and its applications in lift mechanism. In Advances in Reconfigurable Mechanisms and Robots I (pp. 815-829). Springer, London.

[80] Tian, Y., Yao, Y.A. and Wang, J., 2015. A rolling 8-bar linkage mechanism. Journal of Mechanisms and Robotics, 7(4), p.041002.

[81] Wang, J., Yao, Y. and Kong, X., 2016. A rolling mechanism with two modes of planar and spherical linkages. Proceedings of the Institution of Mechanical Engineers, Part C: Journal of Mechanical Engineering Science, 230(12), pp.2110-2123.

[82] Li, R., Yao, Y.A. and Kong, X., 2017. Reconfigurable deployable polyhedral mechanism based on extended parallelogram mechanism. Mechanism and Machine Theory, 116, pp.467-480.

[83] Li, R., Yao, Y.A. and Kong, X., 2016. A method for constructing reconfigurable deployable polyhedral mechanism. In Advances in Reconfigurable Mechanisms and Robots II (pp. 1023-1035). Springer, Cham.

[84] Stephens, B.J. and Atkeson, C.G., 2010, October. Dynamic balance force control for compliant humanoid robots. In Intelligent Robots and Systems (IROS), 2010 IEEE/RSJ International Conference on (pp. 1248-1255). IEEE.

[85] Ott, C., Roa, M.A. and Hirzinger, G., 2011, October. Posture and balance control for biped robots based on contact force optimization. In Humanoid Robots (Humanoids), 2011 11th IEEE-RAS International Conference on (pp. 26-33). IEEE.

[86] Okabe, S. and Ishii, T., 2000. Elevator system. U.S. Patent 6,062,344.

[87] https://en.wikipedia.org/wiki/Counterweight.

[88] George, C., 1937. Equipoising mechanism. U.S. Patent 2,090,439.

[89] French, M.J. and Widden, M.B., 2000. The spring-and-lever balancing mechanism, George Carwardine and the Anglepoise lamp. Proceedings of the Institution of Mechanical Engineers, Part C: Journal of Mechanical Engineering Science, 214(3), pp.501-508.

[90] Carwardine, G., 1940. Elastic force and equipoising mechanism. U.S. Patent 2,204,301.

[91] Bell, W. R., Coon, D. C., and Peterson, T. M., 2001. Support arm or surgical light apparatus. U.S. Patent No. 6,328,458.

[92] Fisher, K.J., 1992. Designer's case file: counterbalance mechanism positions a light with surgical precision. Mechanical Engineering, 114(5), pp.76-80.

[93] Saluja, R. and Nagare, A.T., 1991. Counterbalanced arm for a lighthead. U.S. Patent 5,025,359.

[94] Van Dorsser, W.D., Barents, R., Wisse, B.M. and Herder, J.L., 2007. Gravity-balanced arm support with energy-free adjustment. Journal of medical devices, 1(2), pp.151-158.
[95] Herder, J.L., 2005, June. Development of a statically balanced arm support: ARMON. In Rehabilitation Robotics, 2005. ICORR 2005. 9th International Conference on (pp. 281-286). IEEE.
[96] Smith, R.L., Lobo-Prat, J., Van der Kooij, H. and Stienen, A.H., 2013, June. Design of a perfect balance system for active upper-extremity exoskeletons. In Rehabilitation Robotics (ICORR), 2013 IEEE International Conference on (pp. 1-6). IEEE.
[97] Fattah, A., Agrawal, S.K., Catlin, G. and Hamnett, J., 2006. Design of a passive gravity-balanced assistive device for sit-to-stand tasks. Journal of Mechanical Design, 128(5), pp.1122-1129.
[98] Banala, S.K., Agrawal, S.K., Fattah, A., Krishnamoorthy, V., Hsu, W.L., Scholz, J. and Rudolph, K., 2006. Gravity-balancing leg orthosis and its performance evaluation. IEEE Transactions on robotics, 22(6), pp.1228-1239.
[99] Vrijlandt, N. and Herder, J., 2004. Seating unit for supporting a body or part of a body. U.S. Patent Application 10/479,391.
[100] Kuo, C.H. and Lai, S.J., 2016. Design of a novel statically balanced mechanism for laparoscope holders with decoupled positioning and orientating manipulation. Journal of Mechanisms and Robotics, 8(1), p.015001.
[101] Steinthorsson, A.T., Aguirre, M.E., Dunning, G. and Herder, J.L., 2015, August. Review, Categorization and Comparison of 1 DOF Static Balancers. In ASME 2015 International Design Engineering Technical Conferences and Computers and Information in Engineering Conference (pp. V05AT08A018-V05AT08A018). American Society of Mechanical Engineers.
[102] Nathan, R.H., 1985. A constant force generation mechanism. Journal of Mechanisms, Transmissions, and Automation in Design, 107(4), pp.508-512.
[103] Wongratanaphisan, T. and Cole, M.O., 2008. Analysis of a gravity compensated four-bar linkage mechanism with linear spring suspension. Journal of Mechanical Design, 130(1), p.011006.
[104] Herder, J.L., 2001. Energy-free Systems. Theory, conception and design of statically balanced spring mechanisms, PhD thesis, Delft University of Technology.
[105] Lin, P.Y., Shieh, W.B. and Chen, D.Z., 2009. Design of perfectly statically balanced one-DOF planar linkages with revolute joints only. Journal of Mechanical Design, 131(5), p.051004.

[106] Lin, P.Y., 2012. Design of statically balanced spatial mechanisms with spring suspensions. Journal of Mechanisms and Robotics, 4(2), p.021015.
[107] Dunning, A.G. and Herder, J.L., 2015, August. A close-to-body 3-spring configuration for gravity balancing of the arm. In Rehabilitation Robotics (ICORR), 2015 IEEE International Conference on (pp. 464-469). IEEE.
[108] Lustig, M. P., Dunning, A. G., & Herder, J. L., 2015, November. Parameter analysis for the design of statically balanced serial linkages using a stiffness matrix approach with Cartesian coordinates. In Proceedings of the 14th IFToMM World Congress (pp. 122-129).
[109] Walsh, G.J., Streit, D.A. and Gilmore, B.J., 1991. Spatial spring equilibrator theory. Mechanism and Machine Theory, 26(2), pp.155-170.
[110] Robertson, P.D., Herder, J. L., and Kuo, C., 2018. The static balancing of single-loop reconfigurable mechanisms. In Proceedings of the 4th IEEE/IFToMM Int. Conf. on Reconfigurable Mechanisms and Robots.
[111] Rahman, T., Ramanathan, R., Seliktar, R. and Harwin, W., 1995. A simple technique to passively gravity-balance articulated mechanisms. Journal of Mechanical Design, 117(4), pp.655-658.
[112] Agrawal, A. and Agrawal, S.K., 2005. Design of gravity balancing leg orthosis using non-zero-free-length springs. Mechanism and machine theory, 40(6), pp.693-709.
[113] Laliberté, T., Gosselin, C.M. and Jean, M., 1999. Static balancing of 3-DOF planar parallel mechanisms. IEEE/ASME transactions on mechatronics, 4(4), pp.363-377.
[114] Wang, J. and Gosselin, C.M., 1999. Static balancing of spatial three-degree-of-freedom parallel mechanisms. Mechanism and Machine Theory, 34(3), pp.437-452.
[115] Wang, J. and Gosselin, C.M., 2000. Static balancing of spatial four-degree-of-freedom parallel mechanisms. Mechanism and machine theory, 35(4), pp.563-592.
[116] Gosselin, C.M. and Wang, J., 2000. Static balancing of spatial six-degree-of-freedom parallel mechanisms with revolute actuators. Journal of Robotic Systems, 17(3), pp.159-170.
[117] Gosselin, C.M., 1999. Static balancing of spherical 3-DOF parallel mechanisms and manipulators. The International Journal of Robotics Research, 18(8), pp.819-829.
[118] Agrawal, S.K. and Fattah, A., 2004. Gravity-balancing of spatial robotic manipulators. Mechanism and machine theory, 39(12), pp.1331-1344.
[119] Xi, F. and Sinatra, R., 1997. Effect of dynamic balancing on four-bar linkage vibrations. Mechanism and Machine Theory, 32(6), pp.715-728.
[120] Ouyang, P.R. and Zhang, W.J., 2005. Force balancing of robotic mechanisms based on adjustment of kinematic parameters. Journal of Mechanical Design, 127(3), pp.433-440.

[121] Van der Wijk, V., 2014. Methodology for analysis and synthesis of inherently force and moment-balanced mechanisms, PhD thesis, University of Twente.
[122] Russo, A., Sinatra, R. and Xi, F., 2005. Static balancing of parallel robots. Mechanism and Machine Theory, 40(2), pp.191-202.
[123] Van der Wijk, V., Zhang, K. and Dai, J.S., 2016, August. Force balance of a spatial metamorphic 6R closed-chain linkage with specific kinematic conditions. In ASME 2016 International Design Engineering Technical Conferences and Computers and Information in Engineering Conference (pp. V05BT07A058-V05BT07A058). American Society of Mechanical Engineers.
[124] Kuo, C., Nguyen-Vu, L., and Chou, L., 2018. Static balancing of a reconfigurable linkage with switchable mobility by using a single counterweight. In Proceedings of the 4th IEEE/IFToMM Int. Conf. on Reconfigurable Mechanisms and Robots.
[125] Fischer, O., 1906. Theoretische grundlagen für eine mechanik der lebenden körper. Teubner, Leipzig.
[126] Agrawal, S.K. and Fattah, A., 2004. Reactionless space and ground robots: novel designs and concept studies. Mechanism and Machine theory, 39(1), pp.25-40.
[127] Yao, Y.A. and Yan, H.S., 2003. A new method for torque balancing of planar linkages using non-circular gears. Proceedings of the Institution of Mechanical Engineers, Part C: Journal of Mechanical Engineering Science, 217(5), pp.495-503.
[128] Gallego, J.A. and Herder, J.L., 2011. Buckling as a new perspective on static balancing of mechanisms. In 13th World Congress in Mechanism and Machine Science. Guanajuato, Mexico.
[129] Rijff, B.L., Herder, J.L. and Radaelli, G., 2011, January. An energy approach to the design of single degree of freedom gravity balancers with compliant joints. In ASME 2011 International Design Engineering Technical Conferences and Computers and Information in Engineering Conference (pp. 137-148). American Society of Mechanical Engineers.
[130] Radaelli, G., Gallego, J.A. and Herder, J.L., 2011. An energy approach to static balancing of systems with torsion stiffness. Journal of Mechanical Design, 133(9), p.091006.
[131] Boisclair, J., Richard, P.L., Laliberté, T. and Gosselin, C., 2017. Gravity compensation of robotic manipulators using cylindrical halbach arrays. IEEE/ASME Transactions on Mechatronics, 22(1), pp.457-464.
[132] Simionescu, I. and Ciupitu, L., 2000. The static balancing of the industrial robot arms: Part I: Discrete balancing. Mechanism and machine theory, 35(9), pp.1287-1298.

[133] Simionescu, I. and Ciupitu, L., 2000. The static balancing of the industrial robot arms: Part II: Continuous balancing. Mechanism and machine theory, 35(9), pp.1299-1311.
[134] Koser, K., 2009. A cam mechanism for gravity-balancing. Mechanics Research Communications, 36(4), pp.523-530.
[135] Van der Wijk, V. and Herder, J.L., 2009. Synthesis of dynamically balanced mechanisms by using counter-rotary countermass balanced double pendula. Journal of mechanical design, 131(11), p.111003.
[136] Acevedo, M., 2016. Design of reactionless mechanisms with counter-rotary counter-masses. In Dynamic Balancing of Mechanisms and Synthesizing of Parallel Robots (pp. 83-111). Springer, Cham.
[137] Arakelian, V.H. and Smith, M.R., 2005. Shaking force and shaking moment balancing of mechanisms: a historical review with new examples. Journal of Mechanical Design, 127(2), pp.334-339.
[138] Cho, C., Lee, W., Lee, J. and Kang, S., 2012. A 2-dof gravity compensator with bevel gears. Journal of mechanical science and technology, 26(9), pp.2913-2919.
[139] Kim, S.H. and Cho, C.H., 2015. Incomplete gravity compensator for a 4-DOF manipulator. Journal of Mechanical Science and Technology, 29(10), pp.4417-4426.
[140] Bijlsma, B.G., Radaelli, G. and Herder, J.L., 2017. Design of a compact gravity equilibrator with an unlimited range of motion. Journal of Mechanisms and Robotics, 9(6), p.061003.
[141] De Jong, J.J. and Herder, J.L., 2015, October. A comparison between five principle strategies for adapting shaking force balance during varying payload. In 14th IFToMM World Congress in Mechanism and Machine Science 2015.
[142] Chu, Y.L. and Kuo, C.H., 2017. A single-degree-of-freedom self-regulated gravity balancer for adjustable payload. Journal of Mechanisms and Robotics, 9(2), p.021006.
[143] Van Dorsser, W.D., Barents, R., Wisse, B.M., Schenk, M. and Herder, J.L., 2008. Energy-free adjustment of gravity equilibrators by adjusting the spring stiffness. Proceedings of the Institution of Mechanical Engineers, Part C: Journal of Mechanical Engineering Science, 222(9), pp.1839-1846.
[144] Wisse, B.M., Van Dorsser, W.D., Barents, R. and Herder, J.L., 2007, June. Energy-free adjustment of gravity equilibrators using the virtual spring concept. In Rehabilitation Robotics, 2007. ICORR 2007. IEEE 10th International Conference on (pp. 742-750). IEEE.

[145] Barents, R., Schenk, M., Van Dorsser, W.D., Wisse, B.M. and Herder, J.L., 2011. Spring-to-spring balancing as energy-free adjustment method in gravity equilibrators. Journal of Mechanical Design, 133(6), p.061010.
[146] Briot, S. and Arakelian, V., 2015, October. A new energy-free gravity-compensation adaptive system for balancing of 4-dof robot manipulators with variable payloads. In Proceedings of the Fourteenth International Federation for the Promotion of Mechanism and Machine Science World Congress (2015 IFToMM World Congress). Taipei, Taiwan.
[147] Yang, Z.W. and Lan, C.C., 2015. An adjustable gravity-balancing mechanism using planar extension and compression springs. Mechanism and Machine Theory, 92, pp.314-329.
[148] Chiang, W.H. and Chen, D.Z., 2017. Design of planar variable-payload balanced articulated manipulators with actuated linear ground-adjacent adjustment. Mechanism and Machine Theory, 109, pp.296-312.
[149] Lin, P.Y., Shieh, W.B. and Chen, D.Z., 2010. A stiffness matrix approach for the design of statically balanced planar articulated manipulators. Mechanism and Machine Theory, 45(12), pp.1877-1891.
[150] De Jong, J., Van Dijk, J. and Herder, J., 2018. A screw-based dynamic balancing approach, applied to a 5-bar mechanism. In Advances in Robot Kinematics 2016 (pp. 33-41). Springer, Cham.
[151] Moore, B. and Schicho, J., 2009. Two methods for force balancing of Bennett linkages. In Computational Kinematics (pp. 241-248). Springer, Berlin, Heidelberg.
[152] Lessard, S., Bonev, I.A., Bigras, P., Briot, S. and Arakelyan, V., 2007, June. Optimum static balancing of the parallel robot for medical 3D-ultrasound imaging. In IFTOMM 2007: 12th World Congress in Mechanism and Machine Science.
[153] Haines, R.S., 1981. Minimum rms shaking moment or driving torque of a force-balanced 4-bar linkage using feasible counterweights. Mechanism and Machine Theory, 16(3), pp.185-195.
[154] Chaudhary, H. and Saha, S.K., 2007. Balancing of four-bar linkages using maximum recursive dynamic algorithm. Mechanism and Machine Theory, 42(2), pp.216-232.
[155] Chaudhary, K. and Chaudhary, H., 2015. Optimal dynamic balancing and shape synthesis of links in planar mechanisms. Mechanism and Machine Theory, 93, pp.127-146.
[156] Soong, R.C. and Hsu, K.S., 2007. A design combining kinematic and dynamic balancing considerations with bi-material links for four-bar linkages. Journal of Information and Optimization Sciences, 28(4), pp.663-686.

[157] Soong, R.C. and Yan, H.S., 2007. Simultaneous minimization of shaking moment, driving torque, and bearing reactions of complete force balanced linkages. J. Chin. Soc. Mech. Eng, 28(3), pp.243-254.
[158] Alici, G. and Shirinzadeh, B., 2006. Optimum dynamic balancing of planar parallel mechanisms based on sensitivity analysis. Mechanism and Machine Theory, 41(12), pp.1520-1532.
[159] Alici, G. and Shirinzadeh, B., 2004. Optimum synthesis of planar parallel mechanisms based on kinematic isotropy and force balancing. Robotica, 22(1), pp.97-108.
[160] Segla, S., Kalker-Kalkman, C.M. and Schwab, A.L., 1998. Statical balancing of a robot mechanism with the aid of a genetic algorithm. Mechanism and machine theory, 33(1-2), pp.163-174.
[161] Schwarzfischer, F., Hüsing, M. and Corves, B., 2017, October. The dynamic synthesis of an energy-efficient Watt-II-mechanism. In International Symposiu on Multibody Systems and Mechatronics (pp. 213-222). Springer, Cham.
[162] Hunt, K.H., 1978. Kinematic geometry of mechanisms (Vol. 7). Oxford University Press, USA.
[163] Gogu, G., 2005. Mobility of mechanisms: a critical review. Mechanism and Machine Theory, 40(9), pp.1068-1097.
[164] Huang, Z. and Li, Q., 2003. Type synthesis of symmetrical lower-mobility parallel mechanisms using the constraint-synthesis method. The International Journal of Robotics Research, 22(1), pp.59-79.
[165] Denavit, J., Hartenberg, R.S., 1955. A kinematic notation for lower-pair mechanisms based on matrices. Transactions of the ASME, Journal of Applied Mechanics. 22(2), pp.215-221.
[166] Yang, T., 1996. Basic theory of mechanical system: structure, kinematic, and dynamic analysis. China Machine Press.
[167] Kong, X., 1997. Complete shaking force balancing of spherical mechanisms using mass moment substitution. Machine design (in Chinese), 14(8), pp.5-7.
[168] Kong, X., and Yang, T., 1997. A mass moment substitution method for complete shaking force balancing of spatial linkages involving R and P pairs (I). Mechanical Science and Technology (in Chinese), 16(4), pp.575-580.
[169] Kong, X., and Yang, T., 1998. Extensions to the mass moment substitution method for complete shaking force balancing of spatial linkages. In Proceedings of 1998 ASME Design Engineering Technical Conferences, USA, 1998, DETC98/MECH-5846.

[170] Wu, Y., 2003, Synthesis and analysis of reactionless spatial parallel mechanisms, PhD Thesis, Université Laval.
[171] Laliberté, T. and Gosselin, C.M., 2007, June. Polyhedra with articulated faces. In Proceedings of the 12th IFToMM World Congress Besancon, France, June (pp. 17-21).
[172] Kong, X., He, X. and Li, D., 2018. A double-faced 6R single-loop overconstrained spatial mechanism. Journal of Mechanisms and Robotics, 10(3), p.031013.
[173] Di Gregorio, R., 2004. The 3-RRS wrist: a new, simple and non-overconstrained spherical parallel manipulator. Journal of Mechanical Design, 126(5), pp.850-855.
[174] Lin, P.Y., Shieh, W.B. and Chen, D.Z., 2010. Design of a gravity-balanced general spatial serial-type manipulator. Journal of Mechanisms and Robotics, 2(3), p.031003.